

HEAT AND MASS TRANSFER TO DECELERATING FINELY-ATOMIZED SPRAYS

A  
THESIS

BY  
WILLIAM P. MANNING, B. Eng.

Chemical Engineering Laboratory - McGill University

Under Supervision of Dr. W.H. Gauvin

Submitted to the Faculty of Graduate Studies  
and Research of McGill University in partial  
fulfillment of the requirements for  
the degree of Doctor of Philosophy

McGill University

April 14th, 1958

### ABSTRACT

The transfer of heat, mass and momentum in the nozzle zone of sprays produced by internal-mixing, pneumatic and hollow-cone, pressure nozzles was determined for both co-current and cross-current drying air flow patterns. The Nusselt Numbers for the evaporating drops were correlated by means of the equation proposed by Ranz and Marshall for stationary drops in a moving air flow. Values of the drag coefficients for the decelerating drops, over a range of Reynolds Numbers of 1 to 100, were approximately one tenth of those predicted by the standard curve for spheres, and a dependence on the drop diameter was observed. Methods of measuring the physical properties of the water-air system were developed and tested with special attention devoted to the determination of drop velocities and air humidity.

## ACKNOWLEDGEMENTS

The author wishes to express his thanks to all those who in various ways have contributed to this work. He is particularly indebted to:

The faculty and graduate students of the Chemical Engineering Department, for their contributions and suggestions.

The Pulp and Paper Research Institute of Canada, for the loan of equipment.

His wife and brother, for their assistance in the experimental work and preparation of the thesis.

The National Research Council of Canada, for the award of a Bursary and two Studentships.

## TABLE OF CONTENTS

ABSTRACT	i
ACKNOWLEDGEMENTS	ii
TABLE OF CONTENTS	iii
LIST OF ILLUSTRATIONS	vii
LIST OF TABLES	x
INTRODUCTION	1
A. HISTORICAL REVIEW	
I. ATOMIZATION	
1. THEORY OF ATOMIZATION	6
a) Method of Small Disturbances	7
b) Method of Dimensional Analysis	11
c) Mechanics of Atomization	15
d) Gas Atomization	18
2. ATOMIZING NOZZLES	19
a) Pressure Nozzles	20
b) Spinning-Disk Nozzles	25
c) Pneumatic Nozzles	29
3. DROP SIZE DISTRIBUTION OF SPRAYS	32
a) Mean Diameters	33
b) Drop Size Distribution Functions	36
i. The Rosin-Rammler Equation	36
ii. The Nukiyama-Tanasawa Equation	37
iii. The Log-Probability Equation	38
iv. The Modified Probability Equation	39
c) Drop-Size Measuring Techniques	40
II. EVAPORATION FROM SPRAYS	43
1. HEAT AND MASS TRANSFER TO SINGLE DROPS	43
2. HEAT AND MASS TRANSFER TO SPRAYS	59
III. FLUID MECHANICS OF SPRAYS	71

1. THEORY OF JETS	71
a) Transport Equations for Turbulent Flow	72
b) Turbulence Theories Applied to Free Jets	76
i. Boussinesq's Hypothesis	76
ii. Prandtl's Theory	77
iii. Taylor's Theory	79
iv. Reichardt's Theory	80
c) Extension for Special Cases	82
i. Jet Discharging into Coaxial Duct	82
ii. Jet Discharging at Right Angles to Main Stream	86
2. FLUID MECHANICS OF SPRAY DROPS	87
a) Boundary Layer around Spheres	88
b) Drag Coefficients for Spheres	90
c) Application to Sprays	93
i. Turbulence	93
ii. The Effect of Particle Concentration	94
iii. Drop Rotation	95
iv. Droplet Deformation	96
d) The Effect of Acceleration on the Drag Coefficient	97
B. EXPERIMENTAL SECTION	
INTRODUCTION	105
I. MEASUREMENTS OF SPRAY PROPERTIES	108
1. SPRAY DROP SIZE DISTRIBUTION	108
a) Equipment	108
b) Procedure	110
c) Sources of Error	113
2. SPRAY DROP VELOCITIES	114
a) Photography of Spray Drops	114
b) Determination of Drop Velocities	118
c) Calculation of Drag Coefficients	130
3. SPRAY DROP TEMPERATURES	131
4. EVAPORATION FROM SPRAYS	134
a) Determination of Colour Intensity	134
b) Sources of Error	135
5. AIR VELOCITY IN SPRAYS	136

6. AIR TEMPERATURE IN SPRAY	137
a) Cross-Current Air Flow	139
b) Co-Current Drying Air Flow	140
c) Sources of Error	140
7. DETERMINATION OF THE AIR HUMIDITY	141
a) The Gravimetric Method	142
i. Equipment	142
ii. Procedure	143
b) The Volumetric Method	145
i. Equipment	145
ii. Procedure	148
c) The Dew Point Method	149
d) The Wet and Dry Bulb Method	151
e) Comparison of Methods	153
f) Sampling Techniques	156
i. Cross-Current Drying Air Flow	158
II. EVAPORATION WITH CROSS-CURRENT FLOW	159
1. EQUIPMENT	159
a) The Spray Chamber	160
b) Drying Air Circuit	163
c) Atomizing Nozzle Circuits	166
2. PROCEDURE	167
a) Adjustment of the Operating Conditions	167
b) Collection of the Experimental Data	168
3. CALCULATIONS	170
a) Analysis of the Flow Pattern	170
b) Material and Enthalpy Balances	173
c) Heat Transfer Coefficients and Nusselt Numbers	174
d) Mass Transfer Coefficients and Modified Nusselt Numbers	175
e) Incremental Drop Size Analysis	177
4. RESULTS	179
5. DISCUSSION OF RESULTS	180
a) Heat and Material Balances	189
b) Nozzle Characteristics	190
c) Heat and Mass Transfer	190
d) Drag Coefficients	193
e) Incremental Analysis of Evaporation Rates	194

III. EVAPORATION WITH CO-CURRENT FLOW	196
1. EQUIPMENT	197
a) The Spray Chamber	197
b) The Drying Air Circuit	204
c) The Atomizing Stream Circuits	205
2. PROCEDURE	207
a) Adjustment of Equipment	207
b) Collection of Experimental Data	208
c) Spray Drop Velocities	210
d) Flashing Tests	210
3. CALCULATIONS	211
a) Analysis of the Flow Pattern	211
b) Material and Enthalpy Balances	212
c) Transfer Coefficients and Nusselt Numbers	213
4. RESULTS	214
5. DISCUSSION OF RESULTS	222
a) Heat and Material Balances	222
b) Nozzle Characteristics	229
c) Heat and Mass Transfer	230
d) Effect of Feed Temperature	232
CONCLUSIONS	234
SUMMARY AND CONTRIBUTION TO KNOWLEDGE	243
NOMENCLATURE	245
BIBLIOGRAPHY	253
C. APPENDICES	
APPENDIX I SPRAY DROP VELOCITIES	A 1
APPENDIX II DRAG COEFFICIENT OF SPRAY DROPS	A11
APPENDIX III ASSESSMENT OF HUMIDITY MEASUREMENT METHODS	A14
APPENDIX IV CROSS-CURRENT EVAPORATION RUNS	A16
APPENDIX V CO-CURRENT EVAPORATION RUNS	A32
APPENDIX VI RESULTS OF INCREMENTAL DROF SIZE ANALYSIS	A52

LIST OF ILLUSTRATIONS

<u>Fig. No.</u>		<u>page</u>
1	Drag Coefficient for Spheres, Disks, and Cylinders	92
2	Comparison of the Data of Hanson and Ingebo	101
3	Sampling Devices and Thermometer Shields	111
4	Equipment for Determining Drop Velocities	117
5	Drop Velocities for Pneumatic Nozzle 1/4 JN No. 12 (Low Atomizing Pressures)	121
6	Drop Velocities for Pneumatic Nozzle 1/4 JN No. 12 (Low Atomizing Pressures)	122
7	Drop Velocities for Pneumatic Nozzle 1/4 JN No. 12 (Mixed Atomizing Pressures)	123
8	Drop Velocities for Pneumatic Nozzle 1/4 JN No. 12 (High Atomizing Pressures)	124
9	Drop Velocities for Pneumatic Nozzle 1/4 JN No. 12 (High Atomizing Pressures)	125
10	Drop Velocities for Pneumatic Nozzle 1/4 JN No. 22B	126
11	Drop Velocities for Pressure Nozzle 1/4 LNNSS No. 1	127
12	Drop Velocities for Pressure Nozzle 1/4 LN No. 1	128
13	Drop Velocities for Pressure Nozzle 1/4 LN No. 1 (Superheated Feed)	129
14	Drag Coefficients for Decelerating Spray Drops	132
15	Calibration Curve for Dye Concentration	135A
16	Probes for Measuring Air Velocities	138

<u>Fig. No.</u>		<u>page</u>
17	Schematic Diagram of the Gravimetric Method of Humidity Measurements	144
18	The Volumetric Method of Humidity Measurements	147
19	The Dew Point Method of Humidity Measurements	150
20	The Wet- and Dry-Bulb Method of Humidity Measurements	152
21	Sampling Devices for Humidity Measurements	157
22	The Cross-Current Flow Equipment	161
23	Schematic Diagram of the Cross-Current Flow Equipment	162
24	Schematic Diagram of Flow Patterns in any Section of the Cross-Current Spray Chamber	171
25	Heat Transfer Data for Runs 1 - 12	181
26	Mass Transfer Data for Runs 1 - 12	182
27	Heat Transfer Data for Runs 13-20	183
28	Mass Transfer Data for Runs 13-20	184
29	Typical Microphotographs of the Spray Drops in Cross-Current Flow Equipment	185
30	Changes in Spray Properties for Pneumatic Nozzle Runs	186
31	Changes in Spray Properties for Pressure Nozzle Runs	187
32	Application of Incremental Analysis to Cross-Current Flow Runs	188
33	The Co-Current Flow Equipment	198
34	Schematic Diagram of the Co-Current Flow Equipment	199
35	The Co-Current Flow Equipment (Nozzle Section)	200
36	Schematic Diagram of the Co-Current Flow Equipment (Nozzle Section)	201

<u>Fig. No.</u>		<u>page</u>
37	The Control Panel of the Co-Current Flow Equipment	202
38	Typical Microphotographs of the Spray Drops in Co-Current Flow Equipment	216
39	Changes in Spray and Air Properties for Run 29	217
40	Spray Evaporation - Distance from Nozzle Data	218
41	Air and Spray Temperature - Distance from Nozzle Data	219
42	Sauter Mean Drop Diameter - Distance from Nozzle Data	220
43	Effect of Feed Temperature on Evaporation	221
44	Heat Transfer Data for Runs 21-30	223
45	Mass Transfer Data for Runs 21-30	224
46	Heat and Mass Transfer Data for Runs 31-34	225
47	Heat and Mass Transfer Data for Runs 35 to 39	226
48	Initial Air Velocity Profile in Nozzle Section	227
49	Application of Incremental Analysis to Co-Current Flow Runs	228

LIST OF TABLES

<u>Table No.</u>		<u>page</u>
I	Mean Statistical Diameters	35
II	Generalized Variables	74
III	Nozzle Operating Conditions	120
IV	Comparison of Humidity-Measurement Methods	155
V	Comparison of Spray Chambers	164
VI	Drop Velocity - Drop Diameter Data	A1
VII	Drop Velocity - Drop Diameter Data	A3
VIII	Drop Velocity - Drop Diameter Data	A4
IX	Drop Velocity - Drop Diameter Data	A5
X	Drop Velocity - Drop Diameter Data	A6
XI	Drop Velocity - Drop Diameter Data	A7
XII	Drop Velocity - Drop Diameter Data	A8
XIII	Drop Velocity - Drop Diameter Data	A9
XIV	Drop Velocity - Drop Diameter Data	A10
XV	Drag Coefficient - Reynolds Number Data	A11
XVI	Drag Coefficient - Reynolds Number Data	A12
XVII	Drag Coefficient - Reynolds Number Data	A13
XVIII	Comparison Tests Using Synthetic Air	A14
XIX	Comparison Tests Using CO <sub>2</sub> -Free Saturated Air	A15
XX	Comparison Tests Using Room Air	A15
XXI	Run No. 1 - Table of Results	A16
XXII	Run No. 2 - Table of Results	A17
XXIII	Run No. 3 - Table of Results	A18

<u>Table No.</u>		<u>page</u>
XXIV	Run No. 4 - Table of Results	A19
XXV	Run No. 5 - Table of Results	A20
XXVI	Run No. 6 - Table of Results	A21
XXVII	Run No. 7 - Table of Results	A22
XXVIII	Run No. 8 - Table of Results	A23
XXIX	Run No. 9 - Table of Results	A24
XXX	Run No. 10 - Table of Results	A25
XXXI	Run No. 11 - Table of Results	A26
XXXII	Run No. 12 - Table of Results	A27
XXXIII	Run No. 13 and 14 - Table of Results	A28
XXXIV	Run No. 15 and 16 - Table of Results	A29
XXXV	Run No. 17 and 18 - Table of Results	A30
XXXVI	Run No. 19 and 20 - Table of Results	A31
XXXVII	Run No. 21 - Table of Results	A32
XXXVIII	Run No. 22 - Table of Results	A33
XXXIX	Run No. 23 - Table of Results	A34
XL	Run No. 24 - Table of Results	A35
XLI	Run No. 25 - Table of Results	A36
XLII	Run No. 26 - Table of Results	A37
XLIII	Run No. 27 - Table of Results	A38
XLIV	Run No. 28 - Table of Results	A39
XLV	Run No. 29 - Table of Results	A40
XLVI	Run No. 30 - Table of Results	A41
XLVII	Run No. 31 - Table of Results	A42
XLVIII	Run No. 32 - Table of Results	A43

<u>Table No.</u>		<u>page</u>
XLIX	Run No. 33 - Table of Results	A44
L	Run No. 34 - Table of Results	A45
LI	Run No. 35 - Table of Results	A46
LII	Run No. 36 - Table of Results	A47
LIII	Run No. 37 - Table of Results	A48
LIV	Run No. 38 - Table of Results	A49
LV	Run No. 39 - Table of Results	A50
LVI	Effect of Feed Temperature on Evaporation	A51
LVII	Sample Calculation for Run No. 6 Section 3	A52
LVIII	Results for Cross-Current Runs	A53
LIX	Results for Co-Current Runs	A54

## INTRODUCTION

Atomization may be defined as the production of finely-divided liquid drops dispersed in a gaseous medium by means of gas inertial forces, while a spray refers to the resulting dispersion in contrast to mists and fogs which are formed by other means. This operation has been known since the middle of the nineteenth century, but it was only during the last twenty-five years that it has achieved widespread industrial use. Nowadays, atomization finds application in an increasing number of physical and chemical processes, especially those where high heat and mass transfer rates are advantageous. This growing interest constitutes additional proof of the existence of a new and powerful trend in modern chemical technology towards the use of highly subdivided matter to create ever increasing surface areas for heat transfer, mass transfer, and chemical reactions.

An indication of the rate at which the industrial use of sprays is expanding can be readily obtained by reviewing the patent literature published since 1930. The following is a list of some of the more common unit operations involving the use of atomization:

Absorption and Desorption;

Humidification and Dehumidification;

Extraction in packed towers;

Flash Cooling;

Spray Drying;

Gas Scrubbing;

Fire-fighting;  
Venturi and Cyclone Evaporation;  
Spray Painting.

A recent development incorporating the use of atomization is the Atomized Suspension Technique (67). In this process the liquid feed is atomized at the top of a tower, the walls of which are maintained at an elevated temperature. A spray dispersed in its own vapour is thus produced, and it can be passed through successive zones of evaporation, drying and solid-gas reactions while flowing slowly down the tower.

Atomization also finds application in agriculture for the spraying of liquid chemicals, e.g., insecticides, herbicides, fungicides and defoliant; and in combustion for the mixing of liquid fuels with air in furnaces, internal combustion engines, jet engines and rocket engines.

One of the most important of these applications is spray drying, which may be defined as the drying of an atomized solution or slurry in contact with a stream of hot gases, under conditions which provide for the recovery of the dried product. The advantages of spray drying have been thoroughly reviewed in the literature (40, 112, 145). The rapid rate of drying combined with the fact that the droplets remain at the wet-bulb temperature of the drying air during most of the operation makes this process particularly advantageous for drying heat sensitive materials. Thus foodstuffs such as powdered eggs, milk, instant coffee and chocolate extracts are best dried by this method.

Also, soaps, detergents and many pharmaceuticals such as thermobile, blood plasma and penicillin are commonly spray dried.

Spray drying has been the object of considerable research in the Chemical Engineering Laboratories of McGill University for well over a decade because of the fundamental nature of the problems of heat and mass transfer which are involved. Owing to the experimental difficulties in taking accurate measurements in the so-called nozzle zone of the spray, i.e., the region where the newly-atomized drops rapidly decelerate to their terminal velocities, all of the previous investigations were concerned with the behaviour of the spray subsequent to that period, i.e., in the freely falling zone.

The present study constitutes the first attempt to investigate the rates of heat and mass transfer in the nozzle zone of the spray. It has been made possible by the use of high speed cinematography, and by the development of new techniques for sampling and measuring the properties of the spray. In order to broaden the scope of the investigation, the range of operating conditions, the patterns of flow, and the types of atomizing nozzles were selected in such a manner as to make the experimental information applicable not only to spray drying, but also to other processes in which atomization is involved.

The mechanism of atomization and the behaviour of sprays present complex problems in fluid mechanics, particle dynamics, and boundary layer theory. Owing to the large number of variables involved, the present knowledge of the momentum transfer aspects is quite limited and

only permits the formulation of conclusions which are largely qualitative. There is a distinct need for accurate values of the drag coefficient of drops in turbulent air streams under decelerating conditions. These aspects are currently receiving considerable attention and will undoubtedly become better understood with time.

In the following literature review an attempt has been made to present in a logical manner the great body of experimental data which has been accumulated during recent years on the many different aspects of spray formation and evaporation. Because of the controlling influence exerted by the initial average drop diameter and size distribution on all subsequent phenomena, such as evaporation and drying, the principles of atomization are thoroughly reviewed in the first section. The operating characteristics of the various types of spray nozzles are also discussed. Special emphasis has been placed on the experimental methods of drop size measurement and on the various distribution correlations which have been proposed.

In the second section, the theory of evaporation from sprays is considered. The development of the correlations expressing the rate of evaporation from a single drop is presented, together with their extension and application to clouds of drops undergoing deceleration with respect to the surrounding air.

The final section is devoted to the more recent concepts of fluid mechanics. Fluid flow in the vicinity of a pneumatic nozzle closely resembles that of a jet penetrating a stagnant gas, but complications

arise if the surrounding medium is confined or set in motion. In order to explain the phenomena occurring during pneumatic atomization, the theories of transport of heat, mass and momentum in jets are presented. This is followed by an analysis of the published data and of the theories which have been proposed to predict the drag coefficients of small drops undergoing a change in motion with respect to the surrounding medium.

A. HISTORICAL REVIEW

## I. ATOMIZATION

The importance of the degree of atomization achieved on the rate of heat and mass transfer to the resulting droplets cannot be over emphasized. A comparison of the evaporation rate of a bulk mass of liquid with that of an atomized spray reveals that an increase by a factor of one million is easily obtainable. This is due to the fact that both the individual transfer coefficients and the specific area available for transfer are indirectly proportional to the mean droplet diameter. Thus the overall transfer rate is proportional to the reciprocal of the square of the mean diameter.

### 1. THEORY OF ATOMIZATION

In order to create a spray of large surface area from a liquid mass, the latter must first be forced to assume an unstable free-liquid configuration with an even larger surface area than that of the final spray. This is usually accomplished by imparting to the liquid, as it flows through an atomizing nozzle, the kinetic energy required for the production of filaments or sheets of liquid. Friction with the gaseous phase in turn generates ripples and other disturbances on the liquid surface. The unstable configuration undergoes random disturbances, some of which occur at a greater rate and more frequently than others, followed by disintegration into separate drops. The formation of the intermediate state and the subsequent break-up usually occurs in time intervals of the order of one millionth of a second. High speed

photography has undoubtedly helped in the general understanding of the mechanism of drop formation, but the process is too rapid for the presently-known photographic and recording techniques to be of more than limited assistance.

The various theories of atomization advanced by many workers in the field (12, 88, 166, 192, 193, 243, 250, 259) over the last century can be divided into two main lines of approach, known as the method of small disturbances and the method of dimensional analysis.

a) Method of Small Disturbances

In this theory, it is considered that a small disturbance is imposed on the surface of the liquid jet; and its growth and the resulting break-up of the jet are then determined by applying the laws of conservation of energy. The equation for this arbitrary disturbance,  $\gamma$ , is:

$$\gamma = \gamma_0 (\exp \alpha \theta) \cos(\xi x/r_0) \quad \dots(1)$$

where  $\gamma_0$  - initial amplitude of the disturbance\*;

$\alpha$  - rate of growth of the amplitude;

$\theta$  - arbitrary time;

$\xi$  - number of waves per unit length of jet circumference;

---

\*Throughout this thesis symbols are defined only when they first occur in the text. A complete list may be found in the Nomenclature.

$x$  - axial distance from the source of the jet;  
 $r_0$  - initial radius of the jet.

The wave length,  $\lambda$ , of the disturbance is defined by the equation:

$$\lambda = 2\pi r_0 / \xi \quad \dots(2)$$

If all of the disturbances act randomly and have the same initial amplitude, then the wave length of the particular disturbance that grows most rapidly will determine the distance between the breaks in the jet.

The first application of this theory to jet disintegration was due to Rayleigh (192), who considered that capillary forces were of major importance. He derived the following equation for the potential energy,  $E_P$ , of the unstable configuration based on the assumption that the jet could be considered to be varicose, i.e., with straight axis and rotationally symmetric:

$$E_P = - (\sigma_L \pi \gamma^2 / 2r_0) (1 - \xi^2) \quad \dots(3)$$

where  $\sigma_L$  - surface tension of the liquid.

For this system, the rate of growth of the amplitude of the disturbance was given by the expression:

$$\alpha^2 = (\sigma_L / \rho_L r_0^3) (1 - \xi^2) i \xi J_0'(i \xi) / J_0(i \xi) \quad \dots(4)$$

where  $\rho_L$  - density of liquid;

$J_0$  - Bessel function of the first kind and zero order;  
 $J_0'$  - derivative of  $J_0$  with respect to the argument;  
 $i$  - imaginary unit.

By defining a new dimensionless rate of growth,  $\nu$  by the expression  $\alpha(\rho_L r_0^3 / \sigma_L)^{1/2}$ , equation (4) was rewritten as:

$$\nu^2 = (1 - \zeta^2) i \zeta J_0'(i \zeta) / J_0(i \zeta) \quad \dots(5)$$

Equations 2 and 5 were used to calculate the wave length of the most rapidly growing disturbances, and it was found to be nine times the initial radius of the jet. This was later shown to correspond to a mean drop diameter of nearly twice the initial diameter of the jet.

Rayleigh (193) extended his analysis to include the effect of the liquid viscosity on the mechanism of jet break-up, and obtained a very complicated expression for  $\nu$  which could only be evaluated for the limiting case when the viscosity became infinite:

$$\nu = (1 - \zeta^2) / Z \zeta^2 [(J_0'^2 / J_0^2) + 1 + 1/\zeta^2] \quad \dots(7)$$

where  $Z$  - Ohnesorge Number

$$= \mu_L / (2 \rho_L r_0 \sigma_L)^{1/2} \quad \dots(8)$$

$\mu_L$  - absolute viscosity of the liquid.

Here  $\nu$  reaches a maximum value when  $\zeta = 0$ , which means that the disturbance wave length will be very large.

Weber (259) considered the same system as Rayleigh's last

analysis and by assuming  $\zeta < 1$ , showed that  $\nu$  could be expressed in terms of  $Z$  and  $\zeta$ . He obtained the following explicit equation for the wave length of the most rapidly growing disturbance:

$$\lambda = 2\pi r_0 \sqrt{2(3Z + 1)} \quad \dots(9)$$

For inviscid liquids, the wave length was calculated to be  $8.88 r_0$ , while an infinite value was obtained when  $Z$  was very large. This is in accordance with Rayleigh's data.

In 1933 Tyler (250) measured the frequency of formation of drops from the jet,  $N_f$ , and correlated this in terms of the velocity of the liquid jet,  $V_L$ , by means of the equation:

$$V_L = N_f \lambda \quad \dots(10)$$

Equating the volumes of the drops produced to that of the jet, he obtained:

$$V_L/2N_f r_0 = \lambda/2r_0 = (1/12)(d/r_0)^3 \quad \dots(11)$$

where  $d$  - drop diameter.

Tyler obtained experimental values of the wave length by three different methods and found an average  $\lambda$  of  $9.38 r_0$ .

The most recent theoretical analysis using the method of small disturbances is due to Tomotika (243), who assumed that for relatively low liquid injection velocities the viscosity ratio of the liquid jet to that of the surrounding medium is the controlling factor. The resulting solution, although exceedingly complex, can best be interpreted by

computing numerical values of the wave length of the most rapidly growing disturbance, which was found to approach a minimum value of  $11 r_0$  when the fluid viscosities were almost equal, and gave infinite values for either infinite or zero viscosity ratios. This behaviour is in qualitative agreement with the analyses of Rayleigh (193) and Weber (259).

Reviewing the hypotheses mentioned above, it is evident that although Rayleigh's analysis is the basis for all jet disintegration theories, only Weber has succeeded in deriving a theory that includes the effects of liquid viscosity, velocity, surface tension, and density. It is also apparent that there is little hope of formulating a single theory that would enable accurate predictions of mean drop size and drop size distribution for all cases. The various attempts were based on over-simplified models and are consequently inadequate. However, these theories are of value as they suggest a logical method of correlating data and choosing dimensionless variables, and this has been of great assistance to the workers who have used the method of dimensional analysis.

#### b) Method of Dimensional Analysis

One of the most extensive analyses using this method was due to Holroyd (88), who assumed that the turbulent motion of the liquid jet was the major factor in the jet disintegration. The oscillatory motion of the surface of the liquid jet produces a centrifugal force which is opposed by that due to surface tension, and the following equation is derived by equating these forces.

$$d = k(\sigma_L / \rho_L \omega^2)^{1/3} \quad \dots(12)$$

where  $\omega$  - the mean angular velocity of the jet;

k - constant.

Holroyd used dimensional analysis to predict that:

$$\omega = (V_L / r_o) \text{fn}(\text{Re}) \quad \dots(13)$$

$$\text{where Re} = \text{Reynolds Number} = 2r_o \rho_L V_L / \mu_L \quad \dots(14)$$

Equations 12 and 13 lead to:

$$d/2r_o = \text{fn}(\text{Re})/\text{We} \quad \dots(15)$$

where We - Weber Number =

$$V_L (2 \rho_L r_o / \sigma_L)^{1/2} \quad \dots(16)$$

The substitution of Tyler's value of the drop diameter (eq. 11) enabled a linear correlation to be obtained:

$$d/2r_o = (23.5 + 0.000395\text{Re}) / (\text{We})^{2/3} \quad \dots(17)$$

Equation 17 was used to compare Kuehn's (120) data with that of Tyler and good agreement was found. However, an increase in the density of the surrounding medium has been shown to lead to the production of much smaller drops (66, 130, 267), a behaviour which is not predicted by equation 17.

Ohnesorge (166) used the method of dimensional analysis to determine the relative importance of the inertial, gravitational, capillary and viscous forces on jet disintegration. He correlated the experimental

data of Haenlein (77) in terms of a graph with the Reynolds and Weber Numbers as coordinates. From this graphical correlation Ohnesorge classified jet break-up into four different mechanisms, and the transition conditions have been reported by various workers (145, 159, 184, 197).

1 - Slow dripping or dribble without jet formation:

$$\left( \rho_L V_L^2 r / \sigma_L g_c \right) < 4 \quad \dots(18)$$

where  $g_c$  - dimensional constant, to convert the absolute system of dimensions to the gravitational system.

2 - Rayleigh or varicose break-up when:

$$\rho_L V_L^2 r / \sigma_L g_c > 4 \quad \text{and} \quad \rho_G V_L^2 r / \sigma_L g_c < 0.2 \quad \dots(19)$$

3 - Simuous break-up when:

$$0.2 < \rho_G V_L^2 r / \sigma_L g_c < 6.5 \quad \dots(20)$$

4 - Atomization when:

$$\rho_G V_L^2 r / \sigma_L g_c > 6.5 \quad \dots(21)$$

Baron (12) also applied dimensional analysis to jet break-up using the same initial assumptions as Holroyd. By including a dimensionless break-up length  $L/2r_o$ , he obtained the equation:

$$\text{fn}(L/2r_o, \text{We}, \text{Re}) = 0 \quad \dots(22)$$

where  $L$  - break-up length of liquid jet.

The break-up length has been shown to be directly proportional to the jet velocity by both analytical and experimental analyses (205, 259).

Using this fact and assuming that the effects of viscosity could be represented by a function of the Reynolds Number, Baron simplified equation 22 to:

$$L/2r_o = We \text{ fn}(Re) \quad \dots(23)$$

Equation 23 suggests that a correlation of jet break-up can be obtained by plotting a graph with  $(L/2r_o)We$  and  $Re$  as coordinates. This has been done, but the scatter of the experimental points makes any interpretation difficult (159). However, the following correlation was presented:

$$L/2r_o = 1.7 We (Re/10^4)^{-5/8} \quad \dots(24)$$

The relation between the undisturbed jet length and the velocity and viscosity of the jet has been investigated (221, 251, 252). These studies showed that Rayleigh's theory was only applicable to those cases where the viscous forces are small.

More recently Duffie and Marshall (45) proposed the following correlation for the calculation of the geometric mean diameter of the spray drops,  $d_g$ :

$$d_g = 72(r_o)^{0.56}/(Re)^{0.10} \quad \dots(25)$$

As has been mentioned previously, the complexity of the phenomena of liquid jet disintegration is such that no simple theory is possible. However, several qualitative conclusions can be made, and these have been summarized by Marshall (145) as follows:

- 1 - If the jet is turbulent throughout, it will break-up without the application of any external force, i.e. disintegration will occur in a

vacuum;

2 - If the liquid jet is in semiturbulent flow, that is, with a laminar layer surrounding a turbulent core, then disintegration of the jet will occur after it leaves the nozzle, but only when the turbulent core forges ahead of the laminar flow;

3 - If the jet is in laminar flow, some external disturbance or vibration is required for disintegration;

4 - Regardless of the type of flow, disintegration is favoured by air friction;

5 - The higher the viscosity of the liquid, the longer will be the break-up distance of the jet;

6 - As the pressure increases the break-up distance decreases;

7 - The break-up of a jet is influenced by non-uniform roughness of the orifice and by any other factor affecting the general turbulence conditions of the liquid and the smoothness of the liquid surface.

### c) Mechanics of Atomization

The mechanics of ideal atomization, that is, the production of drops of uniform size, can be used to elucidate the phenomena occurring during actual atomization. Edeling (46) showed that if the viscosity effects are negligible, the following separate effects of surface tension can be enumerated:

1 - Surface tension tends to reduce the liquid surface to a minimum possible area and so ensures the production of spherical drops;

2 - Surface tension resists change in area of the droplet surface; and the work required for a change in area is given by the equation:

$$dW_A = \sigma_L dA \quad \dots(26)$$

where  $W_A$  - work of surface formation;

$A$  - surface area of drop.

3 - Consider the cross section of a drop upon which the internal vapour pressure,  $p_s$ , of the liquid is acting. The counteracting force is that due to the surface tension acting along the circumference, and by equating these forces the following equation is obtained:

$$p_s = 4 \sigma_L / d \quad \dots(27)$$

Equation 27 indicates that the smaller a drop becomes the larger will be its pressure.

The external dynamic pressure,  $p_o$ , acting on the drop is given by the equation:

$$p_o = \rho_L V_R^2 / 2g_c \quad \dots(28)$$

where  $V_R$  = velocity of drop relative to the fluid.

During atomization, if the external pressure is greater than the internal pressure, the drop will split into smaller droplets until,

theoretically, the two pressures are equalized. This corresponds to a drop diameter of:

$$d = 8g_c \sigma_L / \rho_L V_R^2 \quad \dots(29)$$

This is, as was mentioned previously, an ideal case. However it has been shown that the drop diameter varies approximately as  $1/V_R$  to  $1/V_R^{3/2}$  (184).

Equation 26 can be used to calculate the energy,  $E_A$ , required for atomization:

$$E_A = \sigma_L S_w = 6 \sigma_L / \rho_L d \quad \dots(30)$$

where  $S_w = 6 / \rho_L d$  - area per unit mass of atomized liquid.

Conversion of the area term to that produced per unit time changes the energy term into the power requirement for atomization. The efficiencies of energy consumption so computed for atomizing nozzles are exceedingly low, below 1% (145). This is due to the fact that in actual atomization the following additional energy requirements must be met:

- 1 - The energy required to overcome the viscous forces during the deformation of the liquid. This is not easily calculated, but is probably of considerable magnitude due to the high rates of deformation encountered;
- 2 - The energy needed to prevent the atomized drops from recombining when they are some distance from the nozzle;

3 - The energy required by the expansion of the spray from the nozzle and the entrainment of the surrounding fluid. This term is equal to the initial kinetic energy of the spray;

4 - Losses due to inefficient application of energy.

d) Gas Atomization

Atomization produced by the impaction of a gaseous stream on a liquid jet results in the formation of the smallest drops. Considerable work has been done in determining the mechanism of pneumatic atomization (25, 68, 84, 120, 131, 134, 165, 189, 203, 207, 210, 260), and three different types of drop formation have been recorded. At low Weber Numbers, that is for low velocities, dropwise atomization occurs (145, 184). Ripples and bead-like swellings are induced in the liquid stream and the amplitude of these disturbances increases until filaments are formed. Atomization of these filaments follows Rayleigh's theory.

In the range of the first critical Weber Number, circa  $We = 6$ , the liquid drops become flattened and the atomizing gas blows the drops into a balloon shaped film surrounded by a liquid torus (85, 123, 184, 186). Rupture of this unstable configuration is rapid, with the film forming smaller drops than those produced by the surrounding torus.

When the Weber Number reaches thirty, a second critical region is attained. Here, the shape of the deformed configuration changes considerably and a lens-shaped form is obtained. This is convex when

viewed from the side of the air blast. Filaments of liquid are ripped off the edges and these atomize according to Rayleigh's theory (85, 123, 184, 186). The difference in the shape of the deformed configuration is due to the fact that shearing forces of the air blast are strong enough to disintegrate the drop before the impact stresses have succeeded in accelerating the heavier central part into the previous balloon shape.

## 2. ATOMIZING NOZZLES

The function of any atomizing nozzle is twofold: to atomize the liquid feed into drops of the required size, and to distribute and mix these drops with the surrounding gas.

Nozzles may be conveniently classified into several distinct types by considering the manner in which the energy required for atomization is supplied. The types of nozzles which are used most widely in industry are:

- 1 - Pressure nozzles, in which pressure energy is used to impart a high rotational velocity to the liquid before discharge from an orifice;
- 2 - Spinning-disk or centrifugal nozzles, in which atomization is effected by discharging the liquid from the periphery of a rapidly rotating wheel;
- 3 - Pneumatic nozzles in which the liquid jet is disintegrated due to impaction by a high velocity gas stream.

Other methods of atomization have been developed and they include the impingement of liquid jets, supersonic and subsonic vibrations, and high-voltage electrical impulses. However, these are of minor industrial importance. Excellent reviews on the mechanism and characteristics of atomizers are available in the literature (55, 68, 145, 173), and so only the salient features of the operation are presented. Considerations of the initial drop size produced by pressure, spinning-disk and pneumatic nozzles have, however, been included.

a) Pressure Nozzles

In this type of nozzle, atomization is achieved by imparting a swirling or rotary motion to the liquid jet prior to discharge from the nozzle orifice. This motion, which breaks the jet into the ligaments from which the drops are formed, may be accomplished in a swirl chamber with either a fixed spiral or a tangential inlet. The spray pattern produced is usually in the form of a hollow cone, but solid cone sprays can be obtained by incorporating some liquid flow through an axial orifice. Variations in the shape of the spray may be obtained by changing the shape of the nozzle orifice, e.g., flat or fan sprays can be produced by means of elliptical orifices.

Both the liquid flow rate and the initial drop size are functions of the liquid properties, nozzle orifice diameter, atomizing pressure and the geometry of the swirl chamber. Hence, independent control of the feed rate and drop size is impossible and this inflexibility partially offsets the main advantages of this type of atomizer, namely

simplicity of operation and uniformity of drop size distribution. Due to the high pressures required, considerable erosion occurs and the orifice must be fabricated from hard alloys. Even so maintenance is a problem, as good atomization cannot be obtained if the nozzle orifice becomes scratched, distorted or partially plugged by foreign matter. As both the capacity and spray characteristics are extremely sensitive to changes in atomizing pressure, multiple nozzles are often used in industrial equipment where large capacities are required (55).

Dorman (42) used the method of dimensional analysis in obtaining a correlation for the initial particle diameters in terms of the spray characteristics. The following equations are based on the assumptions that the effect of the liquid viscosity is negligible and that the surface tension appears to the one third power as indicated previously (193):

$$d_{vs} = 4.4(q_L/\theta)^{1/3} \sigma_L^{1/3} \rho_L^{1/6} P_L^{-1/2} \quad \dots(31)$$

$$d_{99.99} = 12(q_L/\theta)^{1/3} \sigma_L^{1/3} \rho_L^{1/6} P_L^{-1/2} \quad \dots(32)$$

where  $d_{vs}$  - Sauter mean diameter, (cm.);\*

$d_{99.99}$  - diameter of drop such that 99.99% of spray drops have diameter less than it, (cm.);

$q_L$  - liquid flow rate, (cm.<sup>3</sup>)/(sec.);

---

\* In this section the symbols have been changed to conform with those defined in the Nomenclature, but the units used by the original authors have been retained, as most of their equations are semi-empirical.

- $\theta$  - angle of spray, (radians);  
 $\sigma_L$  - surface tension, (dynes)/(cm.);  
 $\rho_L$  - density of the liquid, (gm.)/(cm.<sup>3</sup>);  
 $P_L$  - atomizing pressure, (dynes)/(cm.<sup>2</sup>).

Dorman obtained good results for both water and kerosene, and a similar correlation was obtained by Straus (227) for water only. Evaluation of the applicability of this work is difficult owing to the limited quantity of experimental data available.

Fraser et al. (55) found that the statistical drop diameter was inversely proportional to the cube root of the atomizing pressure. They modified equations 31 and 32 and experimentally determined the effect of viscosity on the drop diameter which was found to be proportional to the 0.2 power for hollow cone nozzles, and the 0.1 power for fan nozzles.

Tate and Marshall (235), while investigating the characteristics of pressure nozzles, obtained the following equation for the Sauter mean diameter of the spray in terms of the diameter of the nozzle orifice and the velocity components of the liquid jet leaving the nozzle:

$$d_{vs} = 286(d_{or} + 0.17)\exp(13/V_V - 0.0094V_T) \quad \dots(33)$$

where  $d_{vs}$  - mean Sauter diameter, microns;

$d_{or}$  - orifice diameter, in.;

$V_V$  - vertical component of the liquid velocity,  $V_L$ , (ft.)/(sec.);

$V_T$  - tangential component of the liquid velocity,  $V_L$ ,  
(ft.)/(sec.).

Equations for these velocity components were presented in terms of the flow rate and nozzle geometry, and the experimental verification was confined to water for several different nozzles.

Turner and Moulton (248) obtained the following correlations for the arithmetic mean diameter of organic liquid sprays produced by two hollow cone, grooved-core, pressure nozzles:

$$d_a = 16.6 d_{or}^{1.52} q_L^{-0.44} \sigma_L^{0.71} \mu_L^{0.16} \quad \dots(34)$$

$$d_a = 41.4 d_{or}^{1.59} q_L^{-0.54} \sigma_L^{0.59} \mu_L^{0.22} \quad \dots(35)$$

where  $d_a$  - arithmetic mean diameter, microns;

$d_{or}$  - nozzle orifice diameter, (mm.);

$q_L$  - flow rate, (gm.)/(sec.);

$\sigma_L$  - liquid surface tension, (dynes)/(cm.);

$\mu_L$  - liquid viscosity, centipoises.

Consiglio and Sliepcevich (32) determined the effect of the physical properties and the feed rate on the specific surface area of the spray. Their correlations can be written in terms of dimensionless groups.

$$(S_w d_{or}^2 \sigma_L \rho_L^2 / \mu_L^2) = (2.91)(10^{-4})(q_L \rho_L / d_{or} \mu_L)^{2.4} \quad \dots(36)$$

$$(d_{or} P_L \rho_L / \mu_L^2) = 0.28 (q_L \rho_L / d_{or} \mu_L)^{2.4} \quad \dots(37)$$

where  $S_w$  - specific surface area of spray, (cm.<sup>2</sup>)/(gm.);

$d_{or}$  - orifice diameter, (cm.);

$P_L$  - atomizing pressure, (p.s.i.a.);

$\delta_L$  - surface tension of liquid, (dynes)/(cm.);

$\rho_L$  - density of liquid, (gm.)/(cm.<sup>3</sup>);

$q_L$  - liquid feed rate, (cm.<sup>3</sup>)/(sec.);

$\mu_L$  - liquid viscosity, poise.

Equations 36 and 37 were tested for water and several organic liquids with the same nozzle. Good agreement was obtained and the authors noted that the effect of the volume flow rate on the specific surface area of the spray appeared to be greater for their particular nozzle than that reported by previous investigators. The data of Rupe (201), Lloyd (136), Tate and Marshall (235) indicate exponents ranging from 0.3 to 0.80 on the flow rate group compared with the exponent of 2.4 in the above equations.

This brief review indicates that correlations relating the drop size or specific surface area of the spray to the spray characteristics of a particular nozzle are possible. However, any general correlation which would include the effect of nozzle design would lead to additional complexity. For swirl chamber nozzles of the grooved-core type, the construction of the swirl chamber and nozzle orifice would have to be considered. The lack of geometric similarity between commercial nozzles of the same type makes the formulation of any such correlation extremely doubtful.

### b) Spinning-Disk Nozzles

Atomization in this type of nozzle is accomplished by first spreading the liquid feed into a thin sheet and then discharging this sheet from the periphery of a rapidly-rotating, specially designed disk. The feed is pumped at low pressure and introduced at the centre of the spinning-disk, which may be of various forms, with or without vanes, and of any practical size. Spray patterns from spinning-disk nozzles are usually umbrella shaped, but when very fine atomization is accomplished the flow pattern resembles a dispersed cloud. In fact, spinning-disk nozzles may be considered to be the extreme case of a pressure nozzle in which the liquid jet is discharged with tangential velocity only and a cone angle of 180 degrees.

The main advantage of this type of nozzle is its extreme flexibility of operation. The nozzle capacity and the drop size are both functions of the rate of rotation of the disk, but can be varied independently to obtain a wide range of capacities and mean drop sizes. In addition, any liquid that can be pumped may be atomized by this method. However, the wide spray angle limits the choice of the air flow patterns and usually only co-current flow and its auxiliaries (high-frequency motors, drive, forced lubrication systems, etc.) can be used. The high initial cost of spinning-disk atomizers is not completely compensated by their high capacity and flexibility and their use is therefore confined to cases where pressure nozzles are impractical.

Walter and Prewett (258) showed that the formation of drops

from the edge of a spinning disk is analogous in many ways to the well known case of drop formation from a stationary tip. Liquid flows to the edge of the disk and accumulates until the centrifugal force on the collected mass is greater than the retaining force due to surface tension. These authors assumed therefore, that a proportionality existed between the product of surface tension, drop diameter and the accelerating force, and derived the following equation:

$$d_a \omega (D_d \rho_L)^{1/2} / \sigma_L^{1/2} = k \quad \dots(38)$$

where  $d_a$  - arithmetic mean drop diameter, (cm.);

$\omega$  - angular velocity, (radians)/(sec.);

$D_d$  - diameter of disk, (cm.);

$\rho_L$  - density of liquid feed, (gm.)/(cm.<sup>3</sup>);

$k$  - constant.

The constant  $k$  was experimentally evaluated and was found to lie between 2.7 and 6.5, with an average value of 3.8. For high rotation rates (50,000 to 100,000 r.p.m.) Walton and Prewett obtained very uniform drop sizes and reported that the shape of the edge of the disk had very little effect on the mean drop diameter.

Friedman et al. (59) investigated the effect of disk speed, disk diameter, feed rate and liquid properties on the drop size distribution obtained from vaned-disk atomizers. They did not definitely establish the effect due to disk diameter, but nevertheless presented the following equation for the Sauter mean diameter in terms of various groups of the variables involved:

$$d_{vs}/R_d = 0.4(q_L/w \rho_L R_d^2)^{0.6} (\mu_L/q_L)^{0.2} (\sigma_L \rho_L L_v/q_L)^{0.1} \dots(39)$$

where  $R_d$  - radius of the disk, (ft.);  
 $d_{vs}$  - mean Sauter diameter, (ft.);  
 $q_L$  - feed rate of liquid atomized, based on wetted periphery, (lb.)/(min.)(ft.);  
 $\rho_L$  - density of feed, (lb.)/(cu.ft.);  
 $w$  - angular velocity of disk, (r.p.m.);  
 $\mu_L$  - viscosity of feed, (lb.)/(ft.)(min.);  
 $\sigma_L$  - surface tension of feed, (lb.)/(min.<sup>2</sup>);  
 $L_v$  - wetted periphery of disk, (ft.).

Differences between equations 38 and 39 may be attributed to the fact that different types of nozzles were used and that Friedman et al. obtained a wider drop size distribution.

Fraser and Eisenklam (54) determined the drop sizes of sprays produced by a square-edged, spinning-disk atomizer. They used the equation of Harkins and Brown (81) to determine the surface tension during drop formation due to gravitational forces as a basis for correlating their results. Their correlation involves the entity  $d_M$ , which was defined as the arithmetic mean diameter of largest majority of the drop size spectrum. Drops of smaller diameters occurred as peaks in the frequency curve but these were neglected as they constituted only a relatively small percentage volume of the spray.

$$d_M = 360,000 (\sigma_L/D_d \rho_L)^{1/2}/w \dots(40)$$

where  $d_M$  - diameter of the main drop formed, microns;  
 $\sigma_L$  - liquid surface tension, (dynes)/(cm.);  
 $D_d$  - diameter of the disk, (cm.);  
 $\rho_L$  - density of the liquid, (gm.)/(cm.<sup>3</sup>);  
 $\omega$  - angular velocity of disk, (r.p.m.).

Equation 40 agrees very closely with equation 39. Unfortunately, it is only valid for low feed rates and is not applicable when flooding of the disk occurs.

The work of Adler and Marshall (2) and Friedman et al. (59) was reviewed and extended by Herring and Marshall (83), who measured the drop sizes obtained from twelve different spinning-disk atomizers. They found that the following equation could be used to predict the probability of a certain drop size occurring in water sprays:

$$y = d(\omega D_d)^{0.83} (n_v b)^{0.12} / (q_L)^{0.24} \quad \dots(41)$$

where  $y$  - ordinate value on the probability plot;  
 $d$  - drop diameter, microns;  
 $\omega$  - angular velocity of disk, (r.p.m.);  
 $D_d$  - disk diameter, (in.);  
 $n_v$  - number of vanes for a disk;  
 $b$  - vane height, (in.);  
 $q_L$  - liquid feed rate, (lb.)/(min.).

In contrast to the correlations previously presented for drop sizes from pressure nozzles, the main omission in the theory of atomization from spinning disks appears to be the failure to include data

for liquids other than water. This seriously reduces the applicability and usefulness of the above equations.

c) Pneumatic Nozzles

In this type of nozzle a gas stream is used to disintegrate the liquid jet. The feed at low pressure is atomized by the gas at a higher pressure, acting either internally or externally. In the external-mixing nozzles, the feed can be introduced by suction or gravity head and the necessity of pumping is therefore eliminated. However, a more uniform drop size distribution is usually obtained when an internal-mixing nozzle is used. Among the advantages of pneumatic nozzles are the relatively low pressures required for operation, the flexibility due to the independence of the drop size on the capacity, and the ability to achieve very fine atomization. Unfortunately, these advantages are offset to a certain degree by irregular drop sizes and high power consumption for gas compression. A comparison of the cone angles of sprays from pneumatic nozzles with those obtained from pressure nozzles reveals that much narrower sprays are usually produced. Also pneumatic atomization invariably produces a solid cone spray in contrast with the hollow cone sprays obtained from most pressure nozzles.

Due to their relative inefficiencies, pneumatic nozzles are used principally for the production of test sprays and in special cases where the gas stream is required, i.e., the spraying of soap with steam as the atomizing fluid. Other applications include such low capacity devices as paint spray-guns, perfume atomizers, carburettors and small-scale spray

dryers. However, the demand for larger-capacity models seems to be increasing, and semi-commercial nozzles have recently become available.

Relatively few correlations on the drop sizes produced by pneumatic nozzles are available in the literature. A spray with extremely uniform drops was obtained by Rasbash (190), who used a battery of hypodermic needles surrounded by a stream of low-pressure air. The capacity of a unit consisting of 169 needles could be varied from 20 to 160 gallons per minute. As particle sizes lower than 200 microns were not obtained, this performance can only be considered to be of limited applicability.

Nukiyama and Tanasawa (165) determined the drop size distribution produced by small pneumatic nozzles using mixtures of alcohol and glycerine, with air as the atomizing gas. They developed the following empirical equation which correlates the Sauter mean diameter in terms of the operating variables:

$$d_{vs} = (585/V_R) (\sigma_L/\rho_L)^{0.5} + 597 \left[ \mu_L/(\rho_L \sigma_L)^{0.5} \right]^{0.45} (1000q_L/q_A)^{1.5} \quad \dots(42)$$

where  $d_{vs}$  - Sauter mean diameter, microns;

$V_R$  - relative velocity between liquid and air stream,  
(m.)/(sec.);

$\sigma_L$  - surface tension of liquid, (dynes)/(cm.);

$\rho_L$  - density of the liquid, (gm.)/(cm.<sup>3</sup>);

$\mu_L$  - viscosity of the liquid, poises;

$q_L$  - volumetric flow rate of the liquid, (cm.<sup>3</sup>)/(sec.);

$q_A$  - volumetric flow rate of the air, (cm.<sup>3</sup>)/(sec.).

This equation is not dimensionally consistent, but is nevertheless applicable to air atomization of liquids of density 0.7 to 1.2 gm./cm.<sup>3</sup>, surface tension 19 to 75 dynes per cm., and viscosity 0.3 to 50 c.p. The applicability has been extended by Briton (19) to include supersonic air velocities and by Lewis et al. (131) who showed from tests with ethylene and nitrogen that the drop size is proportional to the gas viscosity and practically independent of the gas density. Examination of equation 42 also reveals that the second term becomes negligibly small and hence can be omitted when the ratio  $q_A/q_L$  is greater than 10,000.

Wetzel and Marshall (261) studied the atomization of liquid jets in high velocity gas streams and developed the following expression for the geometric mean diameter of the drop:

$$d_g = (4.2)(10)^6 (V_R)^{-1.68} d_{or}^{0.35} \quad \dots(43)$$

where  $d_g$  - geometric mean diameter, microns;

$V_R$  - relative velocity between air and liquid, (ft./sec.);

$d_{or}$  - diameter of nozzle orifice, in.

Wetzel and Marshall found that in all instances the drop size distribution data obeyed the log-normal distribution law. This equation differs most significantly from equation 42 in the exponent of the velocity term. Marshall (145) has attributed this difference to the difference in the size of the respective nozzles. The very complexity of pneumatic atomization makes it extremely unlikely that any correlation capable of predicting drop size distributions in terms of the physical

properties of the fluids and the nozzle design will be developed.

### 3. DROP SIZE DISTRIBUTION OF SPRAYS

The drop size distribution is one of the most important and fundamental characteristics of a spray, as any calculation of the evaporation rate requires a detailed knowledge of the size-frequency parameters. The drop size distribution of a spray can be represented mathematically by a distribution function involving two parameters, one of which is usually a mean diameter and the other a measure of the dispersion or deviation of the spray drops from the mean diameter. In some cases it may prove more convenient to introduce other parameters, e.g., the maximum and minimum drop sizes occurring in the spray. A graph with the number of drops of a given size and the drop diameter as coordinates is, in effect, a frequency distribution curve representing the drop size distribution. If the ordinate of this graph were changed to the fraction of the total number of drops in the spray, then the area under the frequency curve is unity provided that all the drops are of the same shape. This is referred to as a normalized distribution function and can be expressed mathematically as:

$$\int_0^{\infty} f(d) d(d) = 1 \quad \dots(44)$$

where  $f(d)$  - normalized distribution function;

$d$  - drop diameter.

Another informative method of representing a distribution function involves the cumulative distribution curve. Actually, this is

merely the integral of the frequency distribution curve and the ordinate represents the percentage or fraction of the total number of drops in the spray with diameters less than a given particle size. As sprays must exhibit a maximum drop size, the curve intersects the maximum drop size abscissa at the 100% ordinate value. The cumulative distribution function  $F(d)$  is defined as:

$$F(d) = \int_0^d f(d) d(d) \quad \dots(45)$$

It should be noted that other distribution functions based on the surface area or volume fraction of the total spray contained by a particular drop size can be defined.

#### a) Mean Diameters

In many engineering studies, it is desirable to work only with average diameters instead of considering the various drop-size increments individually. This has led to the formulation of various kinds of mean diameters each of which possesses an individual physical meaning and field of application. Mugele and Evans (163) have developed the following general analytical expression for determining the mean diameters of a continuous distribution function:

$$(d_{qp})^{q-p} = \int_{d_0}^{d_m} d^q f(d) d(d) / \int_{d_0}^{d_m} f(d) d(d) \quad \dots(46)$$

where  $d_{qp}$  - generalized mean statistical diameter;

$p, q$  - integers characteristic of the particular mean diameter;

$d_m$  - diameter of the largest drop in spray;

$d_o$  - diameter of the smallest drop in spray.

The more commonly-used mean diameters together with their fields of application and mathematical definitions are given in Table I on page 35. As can be seen, these diameters are mathematically defined by introducing various values of the integers  $p$  and  $q$  in the general expression, (equation 46).

In addition to these, the number and volume median diameters and the geometric mean diameter are of common use. The number median diameter is the diameter of a drop such that half the total number of drops have diameters greater than it. Mathematically it may be defined by:

$$\int_{d_o}^{d_{nm}} f(d) d(d) = \frac{1}{2} \int_{d_o}^{d_m} f(d) d(d) = \frac{1}{2} \quad \dots(47)$$

where  $d_{nm}$  - number median diameter.

Similarly the volume median diameter can be defined by:

$$\int_{d_o}^{d_{vm}} d^3 f(d) d(d) = \frac{1}{2} \int_{d_o}^{d_m} d^3 f(d) d(d) = (d_v)^3/2 \quad \dots(48)$$

where  $d_{vm}$  - volume median diameter;

$d_v$  - volume mean diameter, defined in Table I.

The geometric mean diameter,  $d_g$ , used in the theory of comminution by grinding and in general statistical correlations, is defined by:

$$\ln(d_g) = \int_{d_o}^{d_m} \ln(d) f(d) d(d) / \int_{d_o}^{d_m} f(d) d(d) \quad \dots(49)$$

TABLE I

MEAN STATISTICAL DIAMETERS

<u>Mean Diameter</u>	<u>Symbol</u>	<u>p</u>	<u>q</u>	<u>Field of Application</u>	<u>Definition</u>
Linear or Arithmetic	$d_a$	0	1	Comparisons, evaporation, spraying.	$d_a = \frac{\int_{d_0}^{d_m} d f(d) d(d)}{\int_{d_0}^{d_m} f(d) d(d)}$
Surface	$d_s$	0	2	Surface area controlling, absorption and extraction.	$(d_s)^2 = \frac{\int_{d_0}^{d_m} d^2 f(d) d(d)}{\int_{d_0}^{d_m} f(d) d d}$
Volume	$d_v$	0	3	Volume controlling, hydrology, comparison of mass distribution.	$(d_v)^3 = \frac{\int_{d_0}^{d_m} d^3 f(d) d(d)}{\int_{d_0}^{d_m} f(d) d(d)}$
Surface-diameter	$d_{sd}$	1	2	Adsorption.	$d_{sd} = \frac{\int_{d_0}^{d_m} d^2 f(d) d(d)}{\int_{d_0}^{d_m} d f(d) d(d)} = \frac{(d_s)^2}{d_a}$
Volume-diameter	$d_{vd}$	1	3	Evaporation, molecular diffusion.	$(d_{vd})^2 = \frac{\int_{d_0}^{d_m} d^3 f(d) d(d)}{\int_{d_0}^{d_m} d f(d) d(d)} = \frac{(d_v)^3}{d_a}$
Volume-surface or Sauter	$d_{vs}$	2	3	Efficiencies studies, mass transfer, reaction.	$d_{vs} = \frac{\int_{d_0}^{d_m} d^3 f(d) d(d)}{\int_{d_0}^{d_m} d^3 f(d) d(d)} = \frac{(d_v)^3}{(d_s)^2}$

## b) Drop Size Distribution Functions

Drop size distribution functions are essentially mathematical expressions used to represent the frequency distribution curve. These functions should be as simple as possible, i.e., easy to manipulate mathematically, consistent with the occurring phenomena and possessing the least number of arbitrary constants. The constants characterize the distribution of the particular system and must be determined experimentally. The lack of good reliable data on sprays in the literature is responsible for the scarcity of critical analyses of the distribution functions reviewed below.

### i. The Rosin-Rammler Equation

This equation was presented in 1933 (198), and although it was originally designed for application to powdered materials, it has been applied to sprays. The distribution function is usually expressed in the cumulative form as:

$$V_f = 1 - \exp -(d/\bar{d})^\delta \quad \dots(50)$$

where  $V_f$  - cumulative volume fraction, i.e., volume fraction of material with diameter less than  $d$ ;

$\bar{d}$  - size parameter;

$\delta$  - distribution parameter.

From this expression an equation for the mean statistical diameter can be derived in terms of the volume median diameter,  $d_{vm}$ , previously defined:

$$d_{qp}^{(q-p)} = d_{vm}^{(q-p)} \Gamma[(q-3)/\delta + 1] / \Gamma[(p-3)/\delta + 1] \quad \dots(51)$$

where  $\Gamma$  - gamma function.

In particular the Sauter mean diameter is:

$$d_{vs} = d_{vm} / \Gamma(1 + 1/\delta) \quad \dots(52)$$

There is very little experimental evidence in favour of the Rosin-Rammler equation and its main weakness was stated by Mugele and Evans (163) to be the assumption of an infinite range of  $d$  values. This makes the equation particularly unreliable for high diameter comparisons.

#### ii. The Nukiyama-Tanasawa Equation

This is a completely empirical equation designed to fit the drop size distribution obtained by pneumatic atomization (165). It is generally expressed as:

$$dn_d/d(d) = k(d)^2 \exp-b(d)^\delta \quad \dots(53)$$

where  $n_d$  - number of drops with diameters between zero and  $d$   
in the entire sample;

$k$  - constant;

$b, \delta$  - parameters.

The constant  $k$  has the dimensions  $d^{-\delta}$ , and hence equation 53 may be rewritten as:

$$dn_d/d(d) = [\delta b^{3/\delta} / \Gamma(3/\delta)] d^2 \exp-bd^\delta \quad \dots(54)$$

From this the generalized expression for the mean statistical diameter can be written as:

$$d_{qp}^{(q-p)} = b^{-(q-p)} \Gamma[(q+3)/\delta] / \Gamma[(p+3)/\delta] \quad \dots(55)$$

This distribution function suffers from the defect that it predicts the existence of drop sizes much larger than the maximum size actually found. Lewis et al. (131) offered an explanation for this phenomenon but in general the Nukiyama-Tanasawa equation is not regarded as reliable (163).

### iii. The Log-Probability Equation

In this equation, statistical analysis is used to limit the distribution of the variables, and the frequency curve may be written as:

$$dV_p/dy = (\delta/\pi^{1/2}) \exp - \delta^2 y^2 \quad \dots(56)$$

$$\text{where } y - \text{function of } d = - \ln(d/d_{vm}) \quad \dots(57)$$

$\delta$  - parameter.

Expressions for the mean statistical diameter, and in particular the Sauter mean diameter can be derived:

$$d_{pq} = d_{vm} \exp(p + q - 6)/4 \delta^2) \quad \dots(58)$$

$$d_{vs} = d_{vm} \exp(1/4 \delta^2) \quad \dots(59)$$

This function has been applied to the drop size distribution data of sprays with some success (14, 33, 124, 163). It is generally considered to be superior to the functions of Rosin and Rammeler and Nukiyama and Tanasawa.

iv. The Modified Probability Equation

It is sometimes desirable to emphasize the existence of a maximum drop diameter rather than to consider large drops having very low frequencies. A new function for  $y$  in equation 56 is needed, and its requirements were summarized by Mugele and Evans (163) as:

1. As  $y$  varies from  $-\infty$  to  $+\infty$ ,  $x$  should vary from  $d_0$  to  $d_m$ ;
2. Qualitatively, the function should be capable of interpretation in terms of fundamental mechanics, i.e., no predictions contrary to reasonably well established trends should be obtained;
3. The resulting equations should satisfy the existing data within the accuracy of measurement;
4. Mathematical simplicity is required in order to permit evaluation of the distribution parameters.

The function observed to be best suited was defined as follows:

$$y = \ln \left[ \frac{(d_m - d_{vm})}{(d_{vm})} \right] d^\delta / (d_m^\delta - d^\delta) \quad \dots(60)$$

It should be noted that equation 56 is still valid, even though  $y$  has been redefined. Mugele and Evans obtained the following expression for the Sauter mean diameter:

$$d_{vs} = d_m \left[ 1 + \frac{(d_m - d_{vm})}{d_{vm}} \exp(1/4 \delta^2) \right] \quad \dots(61)$$

This function was found to give the most accurate predictions of the drop size distribution in sprays (163). In addition, the Sauter mean diameter so calculated agreed closely with that computed from the

experimental data.

c) Drop-Size Measuring Techniques

Due to the wide field of application, several methods of determining the size of spray drops have been developed, and critical analyses of these techniques are available in the literature (40, 73, 145, 184, 231). The main difficulty appears to reside in the sampling method. When a droplet-laden fluid impinges on a sampling device, the fluid is deflected around the body while the drops, by virtue of their greater inertia, tend to impinge on the body. The target efficiency represents the fraction of drops in the fluid volume swept by the body which will impinge in the body. This efficiency has been found to increase with an increase in drop velocity, and fluid velocity, and to decrease with an increase in the size of the sampling device (172).

The most common and accurate method is to collect a sample of the spray in a very small immersion cell filled with an immiscible solvent. The bottom of the cell is usually made of optical glass coated with an anti-wetting agent so that the spray drops remain spherical. Measurement of the drop sizes is generally accomplished by photography with the aid of a microscope. The method which was developed by DeJuhasz et al. (39) was carefully analysed by Rupe (201), and many investigators (2, 40, 41, 46, 82, 149, 231, 235) have used it with considerable success.

A modification of this method is to use a glass slide covered with an immiscible solvent or grease instead of the immersion cell (71,

165, 174, 175). Corrections for flattening of the drops on the slide have to be made. Two serious drawbacks are the threat of evaporation occurring before the photograph can be taken and the poor target efficiency of small drops on the relatively large slide. This makes the method unsuitable for very volatile sprays.

Direct photography of the spray has been reported by York and Stubbs (268) and others (91, 99, 153, 225). The most obvious advantage of this system is the elimination of a sampling device with the inherent error due to target efficiency. However, there are several objections to this method and the principal ones are the high initial cost and difficulty of calibration. The depth of focus of the cameras used is small and as the camera is usually directed at right angles to the spray axis representative samples cannot be obtained. Another consequence of the narrow depth of focus is the small sample numbers obtained.

A permanent sample of the spray can be obtained by atomizing a molten wax which solidifies almost instantly in the surrounding medium. Joyce (105) and others (248, 261) have used this method and reported good results. The drop sizes were determined by photography or sieving and so a large sample number could be analysed. However, this method is decidedly limited in application.

One of the simplest methods involves the impaction of the drops on slides of magnesium oxide, and carbon black (9, 166, 126, 130, 131, 150, 165, 189, 228, 232). Relations between the size of the hole made in the coat and the drop diameter have been developed by Stoker (228). The main

objection to this approach is the extreme calibration that would have to be performed before the method could be used. A modification of this method is to cover the glass slide with blotting paper or other absorbent material and to measure the size of the stain produced by the drop microscopically. It is, again necessary to establish the relation between the drop size and the stain diameter using drops produced by micropipettes. The method is both laborious and time consuming and is only applicable to relatively sparse sprays.

Sedimentation studies have received considerable attention (82, 168, 236) and the usual procedure involves the collection of the spray in a bath that is sufficiently cold to freeze the spray drops. The drop size distribution can be computed from the settling rate assuming the validity of Stokes Law. Complexity of equipment and sampling difficulties have limited the application of this method (89, 137).

Optical absorption by the spray drops provides a method of determining the mean drop size (32, 203, 207, 219, 241). The intensity of a Tyndall beam is approximately proportional to the reciprocal of the mean diameter. Application of this method is limited, as the drop size distribution cannot be obtained from the data. For very finely divided sprays light scattering has been used (74, 183, 204, 216), but the accuracy obtained was poor. Other methods using impaction, interception on fine wires, electrical and thermal precipitators have been investigated. Of these, the thermal precipitator appears to be most promising and its use is slowly increasing.

## II. EVAPORATION FROM SPRAYS

Evaporation from sprays is of fundamental importance in a great many industrial processes and has therefore been the object of a large number of investigations. Most of the work was however concerned with the study of the rates of heat and mass transfer to single drops, almost invariably in a stationary condition. The evaluation of these transfer coefficients in the case of spray drops is considerably more difficult and consequently relatively few investigations have appeared in the literature.

When the relative velocity between the spray drops and the drying air is changing, elaborate precautions must be taken in order to measure the physical properties of the drying air; similarly, determinations of the spray drop sizes and drop velocities are exceedingly difficult. A survey of the literature on the evaporation of sprays can be conveniently divided into two sections: in the first, the literature on the determination of the heat and mass transfer coefficients to single drops is reviewed, while in the second section the extension to clouds of drops is considered.

### 1. HEAT AND MASS TRANSFER TO SINGLE DROPS

Evaporation from a liquid drop is a boundary layer problem. The evaporating drop is considered to be surrounded by a film of vapour and the surrounding gaseous medium. In this concept, the diffusing vapour leaves the surface of the drop and is dissipated in the surrounding gas, while the heat required for evaporation reaches the drop by conduction,

convection and radiation through the boundary layer. Also, the partial pressure of the diffusing vapour decreases from the saturated value at the drop surface to that prevailing in the gaseous medium, while the temperature in the boundary layer rises from the drop temperature to that of the surrounding gas. When steady state is attained, the temperature of the drop surface and consequently the vapour concentration reach constant values for which the transfer rates of heat and mass are balanced. Stefan (226) and Maxwell (148) were the first to realize that this condition enabled evaporation from drops to be considered as a diffusional problem.

In 1910, Morse (162) determined the evaporation rates from small spheres of iodine placed on the pan of an accurate balance, and showed that the rate of evaporation was directly proportional to the diameter of the sphere rather than the surface area or square of the diameter. It was not until 1918 that Langmuir (125) presented the first correlation for the evaporation rate in terms of the partial pressure of the diffusing vapours and the geometry of the drop. His equation resulted from an analysis of Morse's data, and was based on an analogy to heat transfer by natural convection:

$$dm/d\Theta = -S_f \int D_v d(\rho_v) \quad \dots(62)$$

where  $dm/d\Theta$  - evaporation rate of drop, (lb.)/(hr.);

$D_v$  - diffusivity of the diffusing vapour, (ft.<sup>2</sup>)/(hr.);

$\rho_v$  - density of the diffusing vapour, (lb.)/(ft.<sup>3</sup>);

$S_f$  - shape factor =  $(2\pi Dd)/(D - d)$  ... (63)

$D$  - diameter of surrounding gas film, (ft.).

Equation 62 was modified by assuming that the diameter of the drop is negligible compared with that of the gas film, and that the diffusivity and vapour density are independent:

$$dm/d\theta = - (2 r d D_v M / RT) p_s \quad \dots(64)$$

where  $M$  - molecular weight of diffusing vapour, (lb.)/lb.-mol.);

$T$  - absolute temperature of drop, °R.;

$p_s$  - vapour pressure of drop at  $T$  °R., (lb. force)/(ft.<sup>2</sup>);

$R$  - gas constant, 1543 (ft.-lb.-force)/(lb.-mol.)(°R.).

An inherent assumption in this equation is that the partial pressure of the diffusing vapours is zero at a large distance from the drop. Equation 64 is a specific expression for the more general equation of mass transfer on a molar basis, given by:

$$dm'/d\theta = -k_G A p_s \quad \dots(65)$$

where  $dm'/d\theta$  - diffusion or evaporation rate, (lb.-mol.)/(hr.);

$k_G$  - mass transfer coefficient, (lb.-mol.)/(hr.)(ft.<sup>2</sup>)( $\Delta p$ );

$A$  - area available for transfer usually taken as total area of drop surface, (ft.<sup>2</sup>).

The modified Nusselt Number for mass transfer,  $Nu^*$ , can be evaluated for the evaporating drop where there is no relative velocity between the drop and the surrounding medium, by combining equations 64 and 65:

$$Nu^* = k_G M_m dp_f / D_v \rho_f = k_G d RT / D_v = 2 \quad \dots(66)$$

where  $M_m$  - average molecular weight of gases in the surrounding

film, (lb.)/(lb.-mol.);

$p_f$  - average partial pressure of the surrounding medium  
in the gas film, (lb.-force)/(ft.<sup>2</sup>);

$\rho_f$  - average density of the gas film, (lb.)/(ft.<sup>3</sup>).

Due to the analogy between heat and mass transfer, a similar expression can be written for the Nusselt Number:

$$\text{Nu} = hd/k_f = 2.0 \quad \dots(67)$$

where  $h$  - heat transfer coefficient, (B.t.u.)/(hr.)(ft.<sup>2</sup>)(°F.);

$k_f$  - average thermal conductivity of the gas film, (B.t.u.)/(hr.)  
(ft.)(°F.).

Equations 64, 65, 67 are interdependent and their validity has been verified by many workers (61, 72, 91, 96, 97, 104, 139, 188, 234, 245). Minor modifications to Langmuir's equation were made by Bradley et al. (18) for very low pressures and very small drops, i.e., below one micron in diameter. Also Kyte et al. (122) added a correction factor for heat conduction due to free molecular motion at very low pressures. Shereshefsky and Steckler (213) have added a correction for the presence of a finite concentration of the diffusing vapours in the surrounding gas.

In 1934, Fuchs (62) obtained the same equation as Shereshefsky and Steckler for the evaporation of small liquid drops:

$$dm/d\theta = -(2\tilde{n}dD_v M/RT)(p_s - p_a) \quad \dots(68)$$

where  $p_a$  - partial pressure of diffusing component in the surrounding medium, (lb.-force)/(ft.<sup>2</sup>).

This equation was the result of a theoretical analysis based on the following assumptions:

- 1 - The drop is spherical;
- 2 - No relative motion between the drop and surrounding gas occurs;
- 3 - The surrounding gas extends infinitely in all directions;
- 4 - The temperature and pressure of the surrounding gas remain constant;
- 5 - The drop temperature remains constant;
- 6 - The boundary layer is saturated with the diffusing vapour at the surface of the drop;
- 7 - The vapour pressure of the drop is negligible compared with the total pressure;
- 8 - The evaporation process is constant with time, and Fick's law of diffusion is applicable.

In 1936 Takahasi (233) performed a series of experiments on the evaporation of water drops of diameter 0.4 to 2.0 mm. and with relative air velocities of 1 to 6 metres/sec. He correlated his data and offered an equation of the form:

$$dm/d\theta = - (2 \pi d D_v M/RT)(p_s - p_a) [1 - k(Re)^{1/2}] \quad \dots(69)$$

where  $k$  - constant for a particular system.

This was the first appearance of a correction factor for relative motion between the drop and the surrounding gas. No theoretical explanation was

offered until 1938 when Nils Froessling (61) presented his classical paper "Über die Verdunstung fallender Tropfen". A brief resumé of his work is now presented.

Froessling based his analysis on the assumption that Langmuir's equation could be modified for use with relative motion between the drop and the surrounding medium by means of a friction or wind factor "f":

$$dm/d\Theta = - (2\pi r d \frac{M}{V} / RT) p_s f \quad \dots(70)$$

Froessling considered the drop to be located at the origin of the coordinate axes (x, y, z), and applied the Navier-Stokes equations, the equation of continuity, the material balance on the diffusing vapours in the boundary layer and Fick's Law of diffusion. These equations are:

The Navier Stokes equations, assuming steady motion:

$$u(\partial u/\partial x) + v(\partial u/\partial y) + w(\partial u/\partial z) = -(1/\rho_f) (\partial P/\partial x) + \mu_f/\rho_f (\partial^2 u/\partial x^2 + \partial^2 u/\partial y^2 + \partial^2 u/\partial z^2) \quad \dots(71)$$

$$u(\partial v/\partial x) + v(\partial v/\partial y) + w(\partial v/\partial z) = -(1/\rho_f) (\partial P/\partial y) + \mu_f/\rho_f (\partial^2 v/\partial x^2 + \partial^2 v/\partial y^2 + \partial^2 v/\partial z^2) \quad \dots(72)$$

$$u(\partial w/\partial x) + v(\partial w/\partial y) + w(\partial w/\partial z) = -(1/\rho_f) (\partial P/\partial z) + \mu_f/\rho_f (\partial^2 w/\partial x^2 + \partial^2 w/\partial y^2 + \partial^2 w/\partial z^2) \quad \dots(73)$$

where u, v, w - velocity components in boundary layer, in directions x, y, z:

P - total pressure in the boundary layer;

$\mu_f$  - average absolute viscosity of the gas film,  
(lb.)/(ft.)(hr.).

The equation of continuity:

$$\partial u / \partial x + \partial v / \partial y + \partial w / \partial z = 0 \quad \dots(74)$$

Equation for the diffusion of the volatile component:

$$\begin{aligned} & u(\partial c / \partial x) + v(\partial c / \partial y) + w(\partial c / \partial z) \\ & = D_v (\partial^2 c / \partial x^2 + \partial^2 c / \partial y^2 + \partial^2 c / \partial z^2) \end{aligned} \quad \dots(75)$$

where  $c$  - concentration of diffusing vapour in the boundary layer.

Fick's Law of diffusion:

$$dm/d\theta = -D_v \int_A (\partial c / \partial n)_A dA \quad \dots(76)$$

where  $n$  - distance from surface of drop, along normal;

$(\partial c / \partial n)_A$  - concentration gradient normal to drop surface.

Certain boundary conditions can be stated:

1 - for large  $x$ ,  $y$ , or  $z$ ;  $u = V_R$ ,  $v = w = 0$ , and  $c = 0$ .

2 - for  $x^2 + y^2 + z^2 = d^2/4$ ;  $u = v = w = 0$ , and  $c = c_m$ .

where  $c_m$  - concentration of diffusing vapour at the drop surface.

These non-linear, second-order, partial differential equations are insoluble by known mathematical techniques. Froessling obtained an approximate solution, however, by defining the following dimensionless quantities:

$$\begin{aligned} x &= x_1 d & u &= u_1 V_R & P &= P_1 V_R^2 \rho_f \\ y &= y_1 d & v &= v_1 V_R & c &= c_1 c_m \\ z &= z_1 d & w &= w_1 V_R & A &= A_1 d^2 \\ n &= n_1 d & & & & \dots(77) \end{aligned}$$

where the subscript 1 refers to the new dimensionless quantity.

The Reynolds and Schmidt Numbers may be defined by:

$$\text{Re} = dV_R \rho_f / \mu_f \quad \dots(78)$$

$$\text{Sc} = \mu_f / \rho_f D_v \quad \dots(79)$$

and, 
$$D_v / dV_R = 1 / (\text{Re})(\text{Sc}) \quad \dots(80)$$

These dimensionless quantities permitted equation 76 to be rewritten as:

$$dm/d\theta = -D_v c_m d \int_{A_1} (\partial c_1 / \partial n_1)_A dA_1 \quad \dots(81)$$

From the above it is evident that the terms  $u_1$ ,  $v_1$ ,  $w_1$ , and  $P_1$  are functions of  $\text{Re}$ ,  $x_1$ ,  $y_1$ ,  $z_1$ , and so from equation 75 it may be deduced that  $c_1$  is a function of  $\text{Re}$ ,  $\text{Sc}$ ,  $x_1$ ,  $y_1$ , and  $z_1$ .

The concentration of the diffusing vapour at the drop surface can be calculated from the formula:

$$c_m = p_s M / RT \quad \dots(82)$$

Equation 82 and the foregoing statements enable equation 81 to be converted to the following form:

$$dm/d\theta = -(dD_v M / RT) p_s f_n(\text{Re}, \text{Sc}) \quad \dots(83)$$

A comparison of equations 70 and 83 shows that the correction factor  $f$  for relative motion is:

$$f = f_n(\text{Re}, \text{Sc}) \quad \dots(84)$$

Since for any given system the Schmidt Number is constant, the friction factor is therefore a function of the Reynolds Number only.

Froessling continued his analysis in order to determine the form

of this friction factor. He considered the front part of the sphere where the boundary layer exists separately from the rear which is complicated by the formation of turbulent vortices. The analysis may be summarized in the following steps:

- 1 - Application of Boltze's equation (15) for the velocity in boundary layer before the point of separation to the sphere, and conversion to polar coordinates;
- 2 - Rearrangement of equation 75 to polar coordinates;
- 3 - Substitution of boundary conditions as before;
- 4 - Simplification by assuming that the thickness of the boundary layer is negligible when compared with the radius of the sphere;
- 5 - Definition of new dimensionless quantities.

At this stage, Froessling had an equation for the rate of evaporation from the frontal part of the sphere. Experimental data on the sublimation of naphthalene spheres indicated that 80% of the total evaporation occurred before the point of separation. Therefore Froessling assumed that the rate of evaporation after the point of separation could be considered to occur in the same manner as in the frontal boundary layer. In fact, the only effect of such an assumption would be a small change in the numerical coefficient. This assumption enabled Froessling to integrate the expression for the rate of evaporation in the boundary layer over the whole surface of the drop. The result may be expressed mathematically as:

$$dm/d\theta = -(2\tilde{n} dD_V M/RT)p_s [k(Re)^{1/2} fn(Sc)] \quad \dots(85)$$

where  $k$  - constant.

Polhausen (176) and Kronjiline (119) calculated the heat transfer rates from plates and cylinders respectively, and by analogy to their work, Froessling predicted that the function of the Schmidt Number was approximately the cube root i.e.:

$$dm/d\theta = -(2\tilde{n} dD_V M/RT)p_s [k(Re)^{1/2}(Sc)^{1/3}] \quad \dots(86).$$

This analysis cannot be considered as a proof of the dependence of the Nusselt Number or the square root of the Reynold's Number, as Froessling introduced the factor  $(Re)^{1/2}$  into the definitions of the second set of dimensionless quantities.

However, Froessling obtained considerable experimental data in order to evaluate the constant in equation 86. The experimental procedure involved the suspension of liquid drops on a thermocouple in a stream of hot air and measurement of the change in size by shadow photography. Elaborate precautions were taken to ensure that the air flow would not cause deformation of the suspended drops. From tests on the evaporation rate of water, aniline, and nitrobenzene drops for Reynolds Numbers from 0 to 1000, Froessling presented the following correlation:

$$dm/d\theta = -(2\tilde{n} dD_V M/RT)(p_s - p_a)[1 + 0.276(Re)^{1/2}(Sc)^{1/3}] \quad \dots(87).$$

This equation can be rewritten in terms of the modified Nusselt Number:

$$Nu' = 2.0 + 0.552(Re)^{1/2}(Sc)^{1/3} \quad \dots(88)$$

The overall heat transfer coefficient to small spheres in a forced flow of air, water and oil for Reynolds Numbers of 0 to 100,000 was measured by Kramers (113) who correlated his data by means of the following equation:

$$\text{Nu} = 2.0 + 1.3 (\text{Pr})^{0.15} + 0.66(\text{Pr})^{0.31}(\text{Re})^{1/2} \quad \dots(89)$$

$$\text{where Pr - Prandtl Number} = (C_p \mu_f / k_f) \quad \dots(90)$$

$C_p$  - specific heat at constant pressure of gas film,  
(B.t.u.)/(lb.)(°F.).

Higher values for the Nusselt Number are obtained using this equation, especially for low Reynolds Numbers. Still higher heat and mass transfer rates were reported by Friedlander (56). This increase has been attributed to forced convection (188).

Kronig and Bruijsten (118) used a perturbation method in obtaining a mathematical solution for the evaporation from drops in the laminar region. Their correlation is based on the assumption that the velocity streams are symmetrical around the drop and that the boundary layer does not break away from the surface of the drop:

$$\text{Nu} = 2 + 1/2(\text{Pr})(\text{Re}) + (581/1921)(\text{Pr})^2(\text{Re})^2 \quad \dots(91)$$

Ingebo (96) determined the rate of evaporation of nine different liquids under evaporation conditions similar to those encountered in aircraft engines. He obtained an equation analogous to that of Froessling but with the inclusion of a ratio factor of the thermal conductivities of surrounding medium,  $k_g$ , and the diffusing vapour,  $k_v$ :

$$Nu' = 2.0 + 0.303 (Re Sc)^{0.6} (k_a/k_v)^{0.5} \quad \dots(92)$$

This equation was later modified by Ingebo (97, 98) to include a correction factor for the mean free path of the diffusing vapour molecules:

$$Nu' = 2.56 10^6 (Re)(Sc)(gl/\bar{c}^2)^{0.6} (k_a/k_v)^{0.5} \quad \dots(93)$$

where  $g$  - acceleration due to gravity, (ft.)/(sec.<sup>2</sup>);  
 $l$  - mean free path of diffusing molecules, (ft.);  
 $\bar{c}$  - root mean square velocity of diffusing molecules,  
(ft.)/(sec.).

It should be noted that for iso-octane drops evaporating in air the following equation was obtained for the Nusselt Number:

$$Nu = 2.0 + 0.39(Re)^{0.6} \quad \dots(94)$$

This is in good agreement with Froessling's equation.

In 1951, Kinzer and Gunn (110) studied the evaporation rates of freely falling water drops in air and concluded that three different regions existed for evaporation:

- 1 - For  $Re$  0 to 7, the air velocity is slow enough to reduce the evaporation rate to that of a drop at rest;
- 2 - For  $Re$  7 to 2000, a transition range occurs where the evaporation rate is a function of the Reynolds Number;
- 3 - For  $Re$  over 2000, deformation and flattening of the drops occur, thus making any analytical solution extremely complex and difficult.

They derived an equation for the evaporation rate on the assumption that the temperature in the boundary layer could be expressed in terms of a complementary error function. Their final equation can be rearranged and expressed in the form:

$$\text{Nu} = 2.0 + 0.48 \text{F}(\text{Re})^{1/2} \quad \dots(95)$$

where F is a function of the Reynolds Number.

The evaporation rate, drop temperature, relative velocity and air temperature were measured experimentally by three different techniques. These techniques were: freely falling drops, drops supported by a vertical air flow, and drops floated in a tapered tube by vertical air flow. The term F was experimentally evaluated and proved to be approximately unity for water diffusing into air over a large range of Reynolds Numbers.

A deviation from unity in the value of F was reported for low Reynolds Numbers, i.e., in the range commonly encountered in spray drying. However the contribution to the relative motion is small and so the Nusselt Numbers obtained agreed with those calculated by Froessling's equation.

An extensive investigation of the factors influencing the rates of evaporation of pure liquid drops was performed by Ranz and Marshall (188) whose experimental conditions were very similar to those of Froessling. The drops were suspended from a glass capillary which was connected to a micro-burette graduated in  $10^{-5}$ -ml. divisions. This permitted the measurement of the rate of feed required to maintain the size of the drop constant. Tests were also performed on drops with

decreasing diameter and here a projection microscope and camera were used to record changes in the diameter. Considerable precautions were taken to ensure that the flow of the drying air was uniform around the drop. This was accomplished by means of a converging nozzle, the aperture of which was covered with a 140 mesh copper wire screen.

The results of studies on water and benzene drops evaporating in air confirmed the analogy between heat and mass transfer. Their data were correlated by means of the equations:

$$\text{Nu} = 2.0 + 0.6(\text{Re})^{1/2}(\text{Pr})^{1/3} \quad \dots(96)$$

$$\text{Nu}' = 2.0 + 0.6(\text{Re})^{1/2}(\text{Sc})^{1/3} \quad \dots(97)$$

Comparison of equation 88 with equations 96 and 97 shows the excellent agreement with Froessling's work, especially at low Reynolds Numbers. An analysis of the data of other investigators (49, 113, 114, 157, 265) revealed that equations 96 and 97 could be extrapolated with remarkable accuracy five times beyond the experimental range of Reynolds Numbers (0 to 200).

Equations 96 and 97 are consistent with the fact that for conditions of no relative velocity the Nusselt Numbers must be equal to two. This assumes that the heat transfer proceeds by simple conduction and the mass transfer by simple diffusion. In practice, however, the density gradients around the evaporating drop set up motion of the fluid and so Ranz and Marshall (188) proposed the following equations to account for this phenomenon:

$$\text{Nu} = 2.0 + 0.6(\text{Gr})^{1/4}(\text{Pr})^{1/3} \quad \dots(98)$$

$$Nu' = 2.0 + 0.6(Gr)^{1/4}(Sc)^{1/3} \quad \dots(99)$$

$$\text{where } Gr - \text{Grashof Number} = (d^3 \rho_f^2 g_c \beta \Delta T) / \mu_f^2 \quad \dots(100)$$

$\beta$  - coefficient of volume expansion of gas film,  $1/T$ , ( $^{\circ}R.$ ) ;

$T$  - temperature difference across gas film,  $^{\circ}F.$

These equations, although only verified experimentally to a limited extent, are consistent with the standard correlations for heat transfer by free convection (151).

The correlations of Froessling (61) and Ranz and Marshall (188) must be modified where very high surrounding gas temperatures are encountered. Their equations were based on the assumption that all the sensible heat transported to the drop surface was converted to latent heat of evaporation. For high drying temperatures and consequently rapid evaporation, consideration must be given to the heat required to increase the temperature of the diffusing vapours to that of the surrounding medium.

Investigation of the rates of evaporation for burning fuel drops have led to the development of several correlations for high-temperature evaporation. The differential equation governing the phenomenon of heat conduction through the film surrounding the drop with simultaneous vapour diffusion is:

$$d^2 T_f / dr^2 + (2/r - B/r^2) (dT_f / dr) = 0 \quad \dots(101)$$

where  $T_f$  - absolute temperature of surrounding gas film;

$r$  - distance from drop centre to point in gas film;

$B$  - is defined by  $(dm/d\theta)(C_p / 4\pi k_f)$  ... (102)

The ratio of the Nusselt Number for high-temperature evaporation to that where no evaporation is occurring can be obtained by integration of equation 101 and subsequent rearrangement (69, 145, 185, 202).

$$\text{Nu}/(\text{Nu})_{B=0} = B(1/r - 1/R)/[\exp B(1/r - 1/R) - 1] \dots(103)$$

where R - radius of gas film.

Mirsky (161) developed the following equation using the boundary layer theory presented by Goldstein (70):

$$\text{Nu} = \chi [2.0 + k(\text{Re})^{1/2}(\text{Pr})^{1/3}] \dots(104)$$

where k - constant;

$\chi$  - defined by:

$$\chi = h_{fg}/C_p(T_f - T) \ln[1 - C_p(T_f - T)/h_{fg}] \dots(105)$$

where  $h_{fg}$  - latent heat of vapourization of liquid, (B.t.u.)/(lb.).

When the temperature difference is small compared to the latent heat, equation 103 reduces to that of Ranz and Marshall, equation 96.

Mirsky correlated his data by means of the expression:

$$d_2^n = d_1^n - \lambda \theta \dots(106)$$

where  $d_1$  - initial diameter of drop;

$d_2$  - diameter of drop at time  $\theta$ ;

$$\lambda = (8k_f/\rho_f C_p) [D/(D - d)] \ln[1 + C_p(T_f - T)/h_{fg}] \dots(107)$$

The exponent n was found to be a function of the relative air velocity, and values of 1.88 to 1.50 were obtained for velocities of 0 to 9 metres/sec.

## 2. HEAT AND MASS TRANSFER TO SPRAYS

When efforts are made to extend the correlations expressing the rates of evaporation of single drops to sprays, several complications arise:

- 1 - The size of the individual drops which constitute the spray are usually very much smaller than those used in the determination of the rates of evaporation of single drops;
- 2 - The complexity of the drying air patterns and the turbulence generated make the establishment of an accurate relative velocity very difficult. This is especially true for regions in the immediate vicinity of pneumatic nozzles, inlet air ducts and other sources of fluid flow;
- 3 - The rapid rate of evaporation usually has the effect of altering the driving forces, i.e., the temperature differential for heat transfer, and the humidity or the partial pressure of the diffusing vapours for mass transfer;
- 4 - Industrial sprays are rarely comprised of pure liquids, and the presence of dissolved solids affects the partial pressure of the drop and consequently the rate of evaporation;
- 5 - The analytical functions used to express the drop size distribution of sprays in terms of a mean drop diameter are nearly always non-linear. This makes mathematical manipulation rather difficult.

In spite of these complications, several informative studies on sprays have appeared in the literature. Analogies with the transport of solid particles by gas streams have been made, and the rates of heat transfer were determined (103, 135, 167). Johnstone et al. (103) and Ljachowski (135) determined the heat transfer to clouds of small particles falling through a heated air zone. The rise in temperature of the particles was measured calorimetrically and the results of both investigations, although showing a considerable spread, are in agreement with Froessling's correlation. Oktay (167) studied the effect of particle size, concentration and velocity on the heat transfer to clouds of small particles settling in still air. A correction for radiant heat from the walls of the container was included. He developed an empirical equation for the heat transfer which exhibited the same trend as the correlations proposed for single particles.

The application of the correlations of Froessling, and Ranz and Marshall to turbulent gas streams is not valid from the theoretical point of view as their experimental data were obtained using elaborate precautions for maintaining a laminar velocity field. Before the work performed in turbulent gas streams can be considered, the following properties of turbulent flow fields should be noted.

In the study of turbulent systems it is convenient to consider that the fluctuating variable is composed of a mean component which remains constant with time and fluctuating component which oscillates about this mean value. These components are denoted by a bar and prime respectively. The velocity,  $V$ , in the turbulent field can be represented by:

$$V = \bar{V} + V' \quad \dots(108)$$

$$\text{where } \bar{V} \text{ - time-mean component, } = \lim_{\theta \rightarrow \infty} (1/\theta) \int_{\theta_0}^{\theta + \theta_0} V d\theta \dots(109)$$

$V'$  - fluctuating component.

Two important and measurable characteristics of the turbulent flow are the intensity of turbulence and the scale of turbulence. The former which is a measure of the degree of the fluctuations is usually defined by the following equation.

$$\text{Intensity of turbulence} = (1/3)(\bar{u}'^2 + \bar{v}'^2 + \bar{w}'^2)^{1/2}/\bar{V} \quad \dots(110)$$

$$\text{where } \bar{u}'^2 = \lim_{\theta \rightarrow \infty} (1/\theta) \int_{\theta_0}^{\theta + \theta_0} (u')^2 d\theta \quad \dots(111)$$

$\bar{v}'^2$ ,  $\bar{w}'^2$  - similarly defined;

$u'$ ,  $v'$ ,  $w'$  - fluctuating components of the velocity components in x, y, z directions.

For isotropic turbulence:

$$\bar{u}'^2 = \bar{v}'^2 = \bar{w}'^2 \quad \dots(112)$$

$$\text{and so the intensity of turbulence} = (\bar{u}'^2)^{1/2}/\bar{V} \quad \dots(113)$$

The scale of turbulence is a measure of the magnitude of the turbulent eddies and may be defined in terms of a characteristic length, L.

$$L = \int_0^{\infty} R(y) dy \quad \dots(114)$$

where  $R(y)$  - correlation coefficient

$$= \overline{u_1' u_2'} / (\overline{u_1'^2})^{1/2} (\overline{u_2'^2})^{1/2} \quad \dots(115)$$

$u_1^f, u_2^f$  - fluctuating component of velocities at two points whose transverse distance is  $y$ .

Studies of the dispersion of solid and liquid particles in turbulent gas streams have led to a better understanding of the contributing variables (5, 28, 133, 138, 222). A detailed analysis of statistical properties of momentum transfer in two-phase flow was presented by Soo (222) who based his analysis on the following assumptions:

- 1 - The turbulence of the fluid is isotropic and non-decaying;
- 2 - The relative velocity between the solid particles and the air stream is small, and consequently, the Reynolds Number is less than unity;
- 3 - Interaction of one solid particle on the nearest particle can be neglected;
- 4 - The average velocity of the solid particles can be taken as equal to that of the air stream;
- 5 - Effects due to acceleration or deceleration are negligible.

From this study several important conclusions concerning the mechanism of solid dispersion were formulated:

- 1 - The characteristics of turbulence of one phase can be determined from that of the other phase;
- 2 - The fundamental parameters affecting the transfer of momentum are the Reynolds Number based on the root mean square of the fluctuating

component of the air stream velocity, the ratio of the particle diameter to the Lagrangian scale of turbulence of the stream, and the ratio of the densities of the particle and air stream;

3 - The scale of turbulence of the particle is greater than that of the air stream and the intensity of turbulence of the particles is less than that of the stream;

4 - The eddy diffusivity of the particles is greater than that of the air stream but approaches the value of the air stream for small particles and low turbulence intensities.

The results of other workers (5, 28, 133, 138) agree closely with the conclusions presented by Soo for particle diffusion.

In particular Longwell and Weiss (138) studied the mixing and distribution of liquids sprayed into high velocity air streams. The transport of material within the stream was almost exclusively a result of eddy diffusion. The distribution of the liquid drops in the gas stream was found to be a function of the type of nozzle, the distance from the nozzle, gas velocity, air flow patterns, and the intensity of turbulence. It was noted that uniform distributions were obtained for low gas velocities and small intensities of turbulence.

Perhaps the most conclusive results are those of Kesler (108) who determined the drop and vapour concentration profiles, air temperature, and drop size distribution in a co-current spray dryer. The equipment consisted of a 6-in. i.d. cylindrical column, 44-ft. long, where the top

24 ft. were used to establish a pattern of normal pipe turbulence in the air stream prior to the introduction of the spray. Measurements were made through seven pairs of ports spaced logarithmically over a distance of 17.5 ft. The drop size distribution obtained for water and alcohol sprays did not agree with that predicted by the Nukiyama - Tanasawa equation. Kesler expressed his results in terms of a dimensionless diffusion coefficient,  $\beta$ , defined by the equation:

$$\beta = \epsilon / R_D V_G \quad \dots(116)$$

where  $R_D$  - radius of the column, (ft.);

$V_G$  - mean velocity of the air stream, (ft.)/(sec.);

$\epsilon$  - eddy diffusivity defined by the equation:

$$(w/A_D) = - \epsilon \rho_G (\partial c / \partial x) \quad \dots(117)$$

where  $(w/A_D)$  - mass velocity of the spray, (lb.)/(hr.)(ft.<sup>2</sup>);

$\partial c / \partial x$  - concentration gradient of spray expressed in pounds of diffusing material per lb. of air per ft. of path.

Numerical values of 0.005 and 0.007 for the diffusion coefficients were obtained for alcohol and water sprays respectively with air velocities from 20 to 90 ft./sec. and for mean drop sizes of 14 to 30 microns. These diffusion coefficients correspond to eddy diffusivities of 0.11 to 0.15 ft.<sup>2</sup>/sec., and are in excellent agreement with the correlation of Sherwood and Woertz (215):

$$\beta = 0.08 f_F \quad \dots(118)$$

where  $f_F$  - Fanning friction factor.

The evaporation rates for alcohol sprays were also determined. The results indicated that the correlations of the rate of evaporation to stationary, single drops could be applied. From this data, Kesler concluded that the relative velocity between the drops and air stream was zero and consequently the eddy diffusivities of the spray drops and turbulent air stream were identical.

The results of Longwell and Weiss (138) and Kesler (108) were confirmed by Friedlander (57), who reported that practically all of the heat and mass transfer from liquid drops to the surrounding air occurred by eddy diffusion. When steady state conditions were obtained, the eddy diffusion of the small particles was found to vary slightly with air velocity.

Direct studies on the rates of evaporation of spray drops are somewhat rare, (28, 40, 79, 99, 108, 147, 175). Attempts to apply the drop distribution functions have generally been unsuccessful (11, 51, 182) and only the work of Probert (182) is discussed here. For conditions of no relative velocity, Probert made a mathematical analysis of the change in the drop size distribution of sprays which was assumed to follow the Rosin-Rammler equation. Equations for the variation in the volume median diameter with time for various conditions of spray uniformity were developed. These expressions predicted that a spray with a narrow size distribution would evaporate completely more quickly than one of the same mean diameter and with a wider size distribution even though the initial rate would be lower.

Pinder (175) determined the variation in drop size, air temperature and air humidity accompanying the evaporation of a water spray with an arithmetic mean diameter of 14 microns. He calculated the heat and mass transfer coefficients, which were found to vary inversely with the drop diameter. Consequently the Nusselt Number remained constant over a wide range of drop sizes. Its numerical value was, however, quite low.

A similar, though more extensive study was performed by Dlouhy (40), who determined the heat and mass transfer coefficients during the evaporation of water sprays in a vertical, co-current spray dryer 8-in. i.d. and 14-ft. long. For a range of Sauter mean drop diameters of 11 to 39 microns, drying air velocities of 3 to 15 ft./sec. and air temperatures of 100 to 250°F., the transfer coefficients were found to be essentially the same as those for single drops evaporating under stagnant conditions, i.e.,  $Nu = Nu' = 2.0$ . This was in agreement with the results of Kesler, and so Dlouhy concluded that the eddy diffusivities of the spray drops and the air stream were equal.

In an analysis of the evaporation of sprays, Marshall (147) recommended the adoption of a step-wise procedure for the calculation of the time required for complete evaporation. Once the initial drop size distribution is known, the spray is divided into several increments of drop size and a suitable time interval selected. The evaporation occurring in this time interval is then calculated, using equation 97, and assuming that the driving potential, i.e., partial pressure or temperature difference, remains constant for each individual drop size increment. When the

diameters of the increments are modified to account for this evaporation a new drop size distribution is obtained and the above procedure is repeated. Marshall recommended that the time interval should be such that the smallest drop size increment is completely evaporated. An analogous procedure was used independently by Dlouhy (40) for the calculation of the drying time of a colloidal solution of calcium ligno-sulphonate.

A recent extensive mathematical analysis of the factors affecting the drop size distribution of a moving spray undergoing evaporation was presented by Shapiro and Erickson (211). They derived the following differential equation for the number of drops per unit volume,  $n_V$ , in terms of the drop diameter, drop velocity and time for unidimensional flow in a duct of uniform cross-sectional area:

$$\begin{aligned} d\theta &= dx/V_D = d(d)/(Dd/D\theta) \\ &= d[dn_V/d(d)]/[dn_V/d(d)] [\partial V_D/\partial x + \partial(Dd/D\theta)/\partial(d)] \dots(119) \end{aligned}$$

where D - substantial derivative.

The solution of this equation is possible only when the variables can be separated. Application to a cloud undergoing evaporation in an infinite medium produced some interesting results. It was found that, when molecular transfer was the controlling factor, the mean volume diameter remained practically constant over a period of time. Consequently the proposal to replace the conventional concept of an evaporating spray as being a diminution in size of a fixed number of drops, by a decrease in number of drops of uniform size was presented. This new concept was

tested experimentally and the new model was shown to represent the evaporation rates more accurately than the conventional approach. A serious drawback to this method is that an infinite time is required for complete evaporation of the drops to occur. However the time for complete evaporation can be obtained by considering the largest size of drops separately.

Introduction of a change in the relative velocity between the spray drops and the air stream adds complexity to the problem. An increase in the relative velocity increases the heat and mass transfer rates but also reduces the time available for evaporation. Edeling (46) in an analysis of the fundamentals of spray drying assumed that the time required for the spray to decelerate to the terminal velocity of the individual drops in the drying air was too short for appreciable evaporation to occur. On the other hand, several more recent articles have shown that under certain conditions considerable evaporation can occur during the period of deceleration (28, 79, 99, 175).

Sjenitzer (217) presented a mathematical analysis for the evaporation of a drop undergoing deceleration. His calculations were based on Froessling's equation for the evaporation rates and Lapple and Shepherd's correlations for the drag coefficients in terms of the Reynolds Number. The result was an equation showing the fraction of the total evaporation occurring which was due to the relative motion between the drop and the surrounding medium. This fraction is a function of the Reynolds Number, i.e., dependent on both the drop diameter and velocity, and so it is difficult to interpret his results. The analysis is further weakened by

the absence of accurate values of the drag coefficient for a decelerating body.

Hanson (79) assumed that the evaporation rate equation of Froessling could be applied to a spray of drops and used this in the determination of the drag coefficients of fuel sprays. Appreciable evaporation occurred during the acceleration of the sprays by the high velocity air stream. A dependence on the air velocity was found. Typical results were 30, 37, and 45 per cent evaporation at a distance of 10 in. from the nozzle for air velocities of 50, 60 and 75 ft./sec.; and 60, 67, 75 per cent evaporation at a distance of 25 in. for the same air velocities. Fledderman and Hanson (51) determined the effect of air turbulence on the evaporation rate of the fuel spray in the above system. At a distance of 18 in. from the nozzle the evaporation of the spray increased from 52% to 64%, when the intensity of turbulence increased from 2.2% to 7.4%. This corresponds to the results obtained by Maisel and Sherwood (144), for single spheres.

Coldren (28, 30) developed a pneumatic thermometer and hygrometer to measure changes in temperature and humidity during the evaporation of a water spray. This instrument relies on the changes in pressure and temperature as a sample of air is passed through an orifice. The dryer consisted of a two-fluid atomizer with hot air at 400°F. as the atomizing fluid. The spray was discharged into a second co-current stream of hot air at 280°F. and travelling at 30 ft./sec. Complete evaporation in the first 30 inches of the 6 in. diameter duct was reported. The air velocity, humidity, temperature as well as the water temperature and

concentration were measured at six different distances from the nozzle. The data were analyzed according to Reichardt's theory of turbulence, and the momentum, heat and mass fluxes in the dryer were calculated. Coldren did not measure the spray velocity and so was unable to calculate the heat or mass transfer coefficients for the spray drops.

Ingebo (99) measured the vaporization rates of iso-octane sprays at distances of 1, 5, 14 and 18 inches downstream from the point of injection into a high velocity air stream. The method of spray formation consisted of discharge counter-currently to the drying air stream from a 0.041-in. orifice located one inch from the sealed end of 0.25-in. Inconel tube which was installed at right angles to the air stream. Other data recorded included the air velocity, wet-bulb temperature and the drying air temperature. Ingebo stated several important conclusions:

- 1 - Drop size distributions obtained from the experimental data agreed with the Nukiyama-Tanasawa and the log-probability equations;
- 2 - The vaporization rate of the iso-octane spray based on the mean surface diameter was found to be in good agreement with the expression for the evaporation of single drops (see equation 94);
- 3 - The relative velocity between the spray and the air was found to have a considerable effect on the drying time, and approximately 50% of the spray was evaporated during the acceleration period.

### III. FLUID MECHANICS OF SPRAYS

Several complex phenomena occur simultaneously in the region of a spray where the liquid drops are decelerating with respect to the surrounding fluid. These phenomena are: the deceleration of the liquid drops, the expansion and mixing of the jet with the surrounding fluid, and the evaporation of the liquid drops. The rate of evaporation depends on the relative velocity of the drops with respect to the surrounding fluid, which is a function of the drag force, and on the existing temperature differential. This temperature difference in turn depends on the degree of mixing of the jet with the surrounding gas. In analyzing this complex, interdependent system it is convenient to consider the theory of jet mixing and turbulent transport of momentum, heat and mass before investigating the effect of deceleration on the drag coefficient.

#### 1 - THEORY OF JETS

The discharge of a fluid from a nozzle into the surrounding fluid medium results in the formation of a jet and this is invariably accompanied by an increase in the rate of dissipation of energy due to the production of turbulence. The form or structure of the jet is dependent on the nozzle design, the physical properties of the discharged fluid and the velocity of discharge. Entrainment of the surrounding medium by the action of the jet is of the utmost importance, and the availability and the physical properties of the surrounding medium control

to a large extent the shape of the jet. The formation of a turbulent zone where the jet mixes rapidly with the surrounding medium inevitably occurs. Relative intensities of turbulence of as high as 20% have been recorded in this region (36). When the radial profiles of the velocity distribution become similar at successive sections taken perpendicular to the main flow direction, i.e. the nozzle axis, the turbulence is considered to be fully developed. Various mathematical functions including the power series, the trigonometric series and the probability function, have been proposed to represent the velocity profile in this turbulent region. But, before these functions can be investigated the fundamental concepts of turbulent transport, which form the basis of the semi-empirical theories of turbulence, must be considered.

#### a) Transport Equations for Turbulent Flow

The rate of accumulation of mass, heat or momentum in a given volume,  $\tau$ , is equal to the sum of the generation in that volume and the transport to the volume through the enclosing surface,  $\sigma$ . Both molecular motion and bulk fluid motion are included in the transport term. The rate of accumulation can be expressed mathematically by means of a generalized differential equation involving the generalized variables of concentration,  $\psi$ , rate of generation for unit volume,  $Q$ , molecular diffusion constant,  $D$ , and molecular transport potential,  $\phi$ .

$$\partial \left( \int_{\tau} \psi d\tau \right) / \partial \theta = \int_{\tau} Q d\tau + \int_{\sigma} DV \phi \cdot Nd\sigma - \int_{\sigma} \psi V \cdot Nd\sigma \dots (120)$$

where  $\nabla$  - vector differential operator;

$V$  - velocity vector (components  $u, v, w$ );

$N$  - unit vector directed outward normal to surface.

Here, the first term on the right denotes the rate of generation within the volume, while the second and third terms denote the rate of transport across the surface by molecular diffusion and bulk fluid respectively. Expressions for the generalized variables have been summarized by Alexander et al. (4) and are given in Table II.

Gauss' divergence theorem can be applied to equation 120 provided that the volume is small enough for the flow parameters to be considered constant and at the same time large enough for statistical averages to be meaningful. By converting surface integrals to volume integrals and equating the integrand to zero, the following expression is obtained:

$$\partial\psi/\partial\theta = Q + \nabla \cdot D\nabla\phi - \nabla \cdot \psi V \quad \dots(121)$$

This equation can be rearranged to the more familiar Navier Stokes equation, by considering momentum flux and expressing the generalized variables by the expression given in Table II. The following assumptions must be made before further simplification is possible:

- 1 - The mean pressure throughout the flow field is constant;
- 2 - There are no chemical reactions or heat release due to a change of phase;
- 3 - Sensible heat changes due to kinetic energy dissipation are negligibly small;

TABLE II  
GENERALIZED VARIABLES

<u>Flux</u>	<u><math>\psi</math></u>	<u><math>Q</math></u>	<u><math>D</math></u>	<u><math>\phi</math></u>
Mass Flux	$\rho_G c_i$	$Q_i$	$D_v$	$\rho_G c_i$
Heat Flux	$\rho_G C_p t$	$Q_h$	$k_a$	$t$
Momentum Flux	$\rho_G V \cdot S$	$-\nabla P \cdot S$	$\mu_G$	$V \cdot S$

where  $c_i$  - concentration of the  $i$ -th component in fluid, (lb.)/(lb. fluid);

$Q_i$  - local rate of generation of  $i$ -th component of fluid, (lb.)/(unit volume)(hr.);

$Q_h$  - local rate of generation of sensible heat, (B.t.u.)/(unit volume)(hr.);

$S$  - unit vector in any given direction.

4 - The molecular transport term can be neglected;

5 - The jet and ambient fluids are incompressible and have the same density and temperature throughout.

$$\text{Hence } - \overline{\nabla \cdot \psi \mathbf{V}} = 0 \quad \dots(122)$$

where the bar denotes the operation of time-averaging, e.g.

$$\bar{Y} = \lim_{\theta \rightarrow \infty} (1/\theta) \int_{\theta_0}^{\theta + \theta_0} Y d\theta \quad \dots(123)$$

where Y - any fluctuating variable.

It is also assumed that  $\bar{Y}$  is independent of the arbitrary reference time  $\theta_0$ . By applying the concept of resolving the flow parameters into time-mean and fluctuating components equation 122 can be written as:

$$- \overline{\nabla \cdot (\psi + \psi')(\mathbf{V} + \mathbf{V}')} = 0 \quad \dots(124)$$

and expanding:

$$\overline{\nabla \cdot \bar{\psi} \bar{\mathbf{V}}} + \overline{\nabla \cdot \bar{\psi} \mathbf{V}'} + \overline{\nabla \cdot \psi' \bar{\mathbf{V}}} + \overline{\nabla \cdot \psi' \mathbf{V}'} = 0 \quad \dots(125)$$

The second and third terms disappear as the time-average of the fluctuating component is by definition zero. The first term can be expanded as follows:

$$\overline{\nabla \cdot \bar{\psi} \bar{\mathbf{V}}} = \bar{\mathbf{V}} \cdot \nabla \bar{\psi} + \psi \nabla \cdot \bar{\mathbf{V}} \quad \dots(126)$$

where the last term is zero as the fluid is considered to be incompressible. Combination of equations 125 and 126 yields:

$$\bar{\mathbf{V}} \cdot \nabla \bar{\psi} = -\nabla \cdot \overline{\psi' \mathbf{V}'} \quad \dots(127)$$

This equation forms the basis of all the semi-empirical turbulence theories. Further assumptions are required in order to evaluate  $\overline{u'v'}$ , and the various hypotheses advanced merely state methods of relating this product to the flow parameters and their derivatives. All of the assumptions made in deriving equation 127 are valid for an isothermal, turbulent, free jet of air discharging at subsonic velocities into stagnant air. Consequently, free jets have been widely used in testing the applicability of the theories of turbulence (27, 36, 87, 121, 256).

#### b) Turbulence Theories Applied to Free Jets

In order to simplify this treatment, only the momentum directed along the x axis of a free jet discharging along the latter is considered. For cylindrical co-ordinates  $(x, r, \phi)$ , equation 127 can be reduced to:

$$\bar{V} \cdot \nabla \bar{u} = -\nabla \cdot \overline{u'v'} \quad \dots(128)$$

##### (i) Boussinesq's Hypothesis

In 1877 Boussinesq (16) correlated the product  $\overline{u'v'}$  obtained by expanding equation 128 in terms of the transverse gradient of the mean velocity by defining an exchange coefficient which was later named the eddy kinematic viscosity,  $\epsilon$  :

$$\overline{u'v'} = -\epsilon (d\bar{u}/dy) \quad \dots(129)$$

Application of this to free jets by substitution in equation 128 yields:

$$\bar{V} \cdot \nabla \bar{u} = -\nabla \cdot (\overline{u'^2})_i - \epsilon (\partial \bar{u} / \partial r)_j - \overline{u'w'}_k \quad \dots(130)$$

where  $i, j, k$ , - unit vectors in the  $x, y, z$ , directions for Cartesian coordinates or  $x, r, \phi$ , for cylindrical coordinates.

The fact that further assumptions are required to evaluate  $\epsilon$  and that these assumptions change with the system under consideration seriously reduce the applicability of Boussinesq's hypothesis. However Hinze and van der Hegge Zijnen (87) applied equation 130 to free jets by assuming that the eddy viscosity was:

- 1 - A function of the velocity along the axis of flow;
- 2 - A function of distance from an equivalent point-source jet;
- 3 - Constant for a given cross-section of the jet.

They developed equations for the transport of momentum and heat but achieved only limited success, as the equations failed to correlate data obtained at an appreciable distance from the nozzle axis.

#### (ii) Prandtl's Theory

In 1925 Prandtl (180) proposed his mixing length concept in order to establish a relationship between the product  $\overline{u' \psi'}$  and the mean flow parameters. Considering only the transport of momentum, a certain quantity of the turbulent fluid is assumed to move with unchanged momentum along a vector path, which can be considered as the analogue of the mean free path in the kinetic theory of gases. When this quantity of fluid has travelled along this path, which need not be in the same direction as the main fluid velocity, it mixes completely with the

surrounding fluid. As the fluid velocities at the ends of this path are seldom identical, the packet of fluid has a momentum different to that of the surrounding fluid prior to mixing. The change in the mean velocity of the surrounding fluid is proportional to this difference in momentum. The concentration of heat and mass can be similarly considered to be conserved over corresponding mixing lengths, and so the general case can be expressed by the equation:

$$\psi' = \Delta \bar{\Psi} \quad \dots(131)$$

The increment  $\Delta \bar{\Psi}$  can be evaluated in terms of the mixing length using Taylor's series. Only the first term is appreciable as the mixing length,  $L\psi$ , is small:

$$\Delta \bar{\Psi} = -L\psi \cdot \nabla \bar{\Psi} = \psi' \quad \dots(132)$$

Combining equations 127 and 132:

$$\bar{V} \cdot \nabla \bar{\psi} = \nabla \cdot (\overline{L\psi \cdot \nabla \psi}) \bar{V}' \quad \dots(133)$$

Considering the x-directed momentum only, equation 133 can be reduced to:

$$\bar{V} \cdot \nabla \bar{u} = \nabla \cdot (\overline{L_u \cdot \nabla u}) \bar{V}' \quad \dots(134)$$

where  $L_u$  - vector mixing length for x-directed momentum.

The eddy viscosity,  $\ell$ , is defined in terms of the scalar components of the mixing length,  $l_x$ ,  $l_r$ ,  $l_\phi$ , and the fluctuating components of the velocity.

$$\ell = \overline{l_x u'} = \overline{l_r v'} = \overline{l_\phi w'} \quad \dots(135)$$

Equation 134 can now be rewritten in terms of the eddy viscosity.

$$\bar{v} \cdot \bar{v}_u = \nu \cdot \epsilon \nabla u \quad \dots(136)$$

No solution of equation 136 is possible until a relation between the eddy viscosity and the flow parameters is obtained. Prandtl (180) used a correlation coefficient,  $l_{pu}$ , to obtain a definition of the eddy viscosity in terms of a more easily measured mixing length:

$$\epsilon = l_{pu}^2 |\nabla \bar{u}| \quad \dots(137)$$

For free jets where the change in axial velocity with respect to  $x$  and  $\phi$  can be neglected, equations 136 and 137 can be expressed as:

$$\bar{v} \cdot \bar{v}_u = (1/r) \partial [ r l_{pu}^2 |(\partial u / \partial r)| (\partial u / \partial r) ] / \partial r \quad \dots(138)$$

where  $|(\partial u / \partial r)|$  - absolute value of  $(\partial u / \partial r)$  irrespective of sign.

Prandtl (180) and Tollmien (242) have applied equation 138 to free jets by making various assumptions for the mixing length, e.g.,  $l_{pu}$  is proportional to the breadth of the mixing zone and independent of  $r$ . Their correlations were in general unsatisfactory. The work of Tollmien (242), Hinze and van der Hegge Zijnen (87), Kuethe (121), Howarth (92), has been reviewed by Alexander et al. (4) who attributed the discrepancies between theory and experimental results to the multiplicity of assumptions made in the derivations of the correlations used.

### (iii) Taylor's Theory

This theory is analogous to that of Prandtl where momentum was considered to be conserved during transport. Taylor (238) made the additional assumption that vorticity or the moment of momentum is also

conserved. Howarth (92) made assumptions similar to those used in deriving equation 138 and obtained the following equation which is analogous to that of Prandtl.

$$\bar{v} \cdot \nabla \bar{u} = -l_T^2 (\partial \bar{u} / \partial r) (1/r) \partial [r (\partial \bar{u} / \partial r)] / \partial r \quad \dots(139)$$

$$\text{where } \varepsilon = l_T^2 |\nabla \bar{u}| \quad \dots(140)$$

Here the eddy viscosity,  $\varepsilon$ , is identical to that used by Prandtl (equation 137). Howarth obtained a solution for equation 140, but the velocity distribution did not agree satisfactorily with experimental results.

It should be noted that Taylor's Theory cannot be applied directly to heat or mass transport as both temperature and concentration are scalar quantities. However, Howarth assumed that equation 140 could be extended to include heat or mass transport by replacing  $u$  by  $\psi$ .

$$\bar{v} \cdot \nabla \psi = -l_T^2 (\partial \psi / \partial r) (1/r) \partial [r (\partial \psi / \partial r)] / \partial r \quad \dots(141)$$

This is a drastic assumption, and has not been confirmed by experimental results.

#### (iv) Reichardt's Theory

Reichardt (194, 195) found from the measurements of momentum in regions of turbulent mixing that an analogy existed between the processes of turbulent and molecular transfer. From these measurements Reichardt introduced an inductive theory of free turbulence in which he assumed that the longitudinal mean velocity distribution could be represented by probability or error functions which closely agreed with the experimental

results. For instance, the velocity distribution in a free jet may be expressed by the equation:

$$u^2 = (k/b^2)\exp-(r/b)^2 \quad \dots(142)$$

where  $k$  - constant

$b$  - function of  $x$  only.

The  $x$ -directed momentum equation of the mean flow for an axially-symmetrical jet can be obtained from equation 122.

$$\partial u^2 / \partial x + (1/r) \partial (r \bar{uv}) / \partial r = 0 \quad \dots(143)$$

Equation 142 is a solution of equation 143 if:

$$\bar{uv} = -\Lambda \partial u^2 / \partial r \quad \dots(144)$$

$$\text{where } \Lambda = (b/2)(db/dx) \quad \dots(145)$$

The above inductive theory can be generalized for the transfer of heat and mass (194). The main weakness of this theory is that it is based on mean velocities only, and as such it can hardly be expected to predict an accurate distribution of turbulent fluctuations. However recent workers (4, 6, 7) have achieved some success in applying Reichardt's Theory to jets. In particular, Alexander et al. (4) reported the development of an extension of Reichardt's Theory to free isothermal jets based on the equations of motion and continuity. They were successful in transforming the non-linear flow equations to linear differential equations. The solution obtained was in two parts, one for radial distribution and the other for axial change. The former which was found to agree closely with experimental results may be written as:

$$(\overline{\rho_G u^2})_{x,r} / (\overline{\rho_G u^2})_{x,0} = \exp 0.693(r/r_{1/2})^2 \quad \dots(146)$$

where  $r_{1/2}$  - radial distance at which the flow momentum is one-half the value at the axis.

subscripts  $x, r$ ;  $x, 0$  refer to points  $r$  distant from the axis and on the axis respectively.

The correlation expressing the change in flow variable with axial distance may be written as:

$$(\overline{\rho u^2})_{x,0} / (\overline{\rho u^2})_{0,0} = 1 - \exp - (r/C_m x)^2 \quad \dots(147)$$

where  $C_m = 0.075$  - spreading coefficient.

Equation 147 reduces to the widely used parabolic law for momentum distribution when  $r/C_m x$  is small (3, 35, 195, 239, 242). Although the agreement with the experimental results was not as good as was obtained for equation 146, nevertheless the experimental error was seldom greater than 10%.

### c) Extension for Special Cases

The application of the turbulent theories for jet mixing is now extended to include those cases which were investigated experimentally, i.e., discharge of a jet into a coaxial duct, and into an air stream where the mean velocity was perpendicular to the jet axis.

#### (i) Jet Discharging into Coaxial Duct

Due to the powerful suction produced by the expanding jet, wide-

spread industrial use has developed where large volumes of gas or vapour can be entrained by the jet and discharged at low pressures. Among these operations are: exhausting fumes or air, vacuum evaporation, distillation, crystallization, drying, and air conditioning.

When a fluid is discharged from a nozzle or orifice the issuing stream can be considered to act as a jet pump for moving the surrounding fluid. At least four different processes have been reported to occur during mixing (7, 106, 114, 116, 249):

- 1 - Acceleration of the particles of the surrounding fluid (induced fluid) by impact of the particles from the nozzle fluid (motive fluid);
- 2 - Entrainment of the induced fluid by viscous friction at the periphery of the jet;
- 3 - Overexpansion of the jet to a pressure below that of the induced fluid, with consequent flow of the latter toward the axis of the jet;
- 4 - Change of phase with large volume change due to flashing, condensation or rapid evaporation.

The theoretical analysis of a jet in which several of these processes occur simultaneously becomes extremely complicated, and drastic assumptions have been made in order to obtain solutions. Flugel (52) assigned average velocities to the high-velocity core and the low-velocity annulus at any cross-section, and evaluated an empirical drag coefficient by calculating the drag force between the two streams. This analysis

satisfies momentum considerations but does not represent the mechanics of mixing.

Victorein (255) considered only that the part of the jet which is close enough to the nozzle for the spreading of the jet to be unaffected by the duct walls and at the same time far enough away for the jet to be treated as a point of momentum and mass. In addition he assumed that the pressure remained constant in the duct and that Prandtl's mixing length was uniform at any cross-section and proportional to the width of the jet. These assumptions are incompatible with the observed phenomena of mixing in a duct and no correlation for the length required for complete mixing was given.

Alexander et al. (7) assumed that the molecular transport, boundary layer formation, radial pressure gradients, and heat losses at the duct wall could be neglected. Using Reichardt's Theory of turbulence, they derived the following equation for the momentum flux in the duct:

$$(M - M_{\infty}) / (M_{jav} - M_{iav}) = \sum_{n=1}^{\infty} A_n J_0(a_n 2r/D_d) \exp \int_0^x (4a_n^2 \Lambda / D_d^2) dx \quad \dots (148)$$

$$\text{where } M - \text{total momentum flux } (P_{gc} + \rho_G u^2) \quad \dots (149)$$

$J_1$  - Bessel function of the first kind and first order;

$J_0$  - Bessel function of the first kind and zero order;

$A_n$  - arbitrary coefficient of nth term in series of  $J_0$ ;

$a_n$  - nth root of  $J_1$ ;

$D_d$  - diameter of duct;

$\Lambda$  - proportionality function (equation 131, 132);

av - subscript denoting average;

i - subscript denoting induced stream conditions at plane of nozzle;

j - subscript denoting jet stream condition at plane of nozzle;

$\infty$  - subscript denoting conditions at point of complete mixing.

Several qualitative conclusions on the phenomenon of jet mixing in a duct can be drawn from the data available in the literature (5, 6, 7, 28, 107, 116, 154, 240).

1 - The changes in the radial velocity profiles with distance from the nozzle have been determined by several workers (5, 6, 7, 28). Initially, a high velocity core surrounded by a slower moving annulus exists. The velocity of this core decreases as it expands in area; and eventually a uniform velocity profile is obtained. Equation 148, which has been reported to represent the momentum flux at any point in the duct (7), is indicative of the velocity profiles obtained;

2 - The transfer of heat is more rapid than that of mass or momentum;

3 - Complete mixing of the two streams occurs from four to ten duct diameters along the nozzle axis (107, 116, 154). It should be noted that the velocity profile becomes practically uniform before complete mixing has occurred;

4 - The static pressure in the duct decreases initially and gradually recovers as the velocity profile becomes uniform;

5 - The mass velocity past any given cross-section of the duct remains practically constant especially for high induction ratios, (the induction ratio is defined as the ratio of the weight of the induced fluid to that of the motive fluid);

6 - The turbulence level decreases from that of free jets, circa 20% to that of fully developed turbulent pipe flow, circa 3%, (7).

(ii) Jet discharging at Right Angles to the Main Stream

The mathematical representation of this phenomenon is extremely ponderous and difficult and loses significance due to the large numbers of assumptions involved. However, several qualitative conclusions can be drawn from the experimental data reported in the literature (22, 47, 53):

1 - The pressure forces of the main fluid stream deform the jet, and displacement in the direction of the main stream occurs;

2 - During this deformation, the jet is flattened and spreads out in a direction at right angles to the main stream;

3 - The penetration of the jet into the main stream is limited by the deflection due to the pressure forces. However there is a second, slower penetration due to turbulent mixing;

4 - Penetration can be increased by using a jet that is elongated or elliptical in the stream direction. The presence of another jet or form of fluid disturbance upstream has a similar effect;

5 - If the jet discharges into a narrow chamber, considerable contact with the walls occurs due to the flattening effect described above and venturi action.

## 2. FLUID MECHANICS OF SPRAY DROPS

Fluid flow is considered to be divided into two distinct types or classes depending on the manner in which the flow occurs. These types are known as laminar flow where the velocity is unidirectional and flow occurs in laminae or streamlines, and turbulent flow where a random fluctuating velocity is superimposed on the main flow velocity and the flow proceeds with considerable mixing. The change from one flow type to the other is gradual and the period over which this change occurs is known as the transition range. For the case of a sphere or drop moving with respect to the surrounding gaseous medium, the flow type can be determined from a modified Reynold's Number which is defined as:

$$Re = dV_R \rho_G / \mu_G \quad \dots(150)$$

As in the case of pipe flow, this dimensionless group is a ratio of the inertia reaction per unit volume,  $\rho_G V_R^2 / d$ , and the viscous force,  $V_R \mu_G / d^2$ . From the above, it is evident that the greater the Reynolds' Number becomes the less will be the effect of the viscous forces. The transition from laminar flow to the transition range is the subject of considerable contention, but is generally considered to occur at a Reynolds Number of 1 to 2 (70, 129). Fully developed turbulence exists only for Reynolds Numbers greater than 500 (70, 129).

a) Boundary Layer around Spheres

The resistance of the fluid to the motion of spherical particles can be qualitatively understood by visualizing the fluid flow patterns around the sphere. Accordingly a brief review of the formation of the boundary layer around spheres is now presented. In order to facilitate the explanation, the sphere is considered to be divided into two equal segments by an equatorial line at right angles to the direction of fluid flow. Prandtl's Boundary Layer Theory (179) stated that the velocity of the fluid in contact with the surface of the sphere was zero, and that the velocity increased with increase in the distance from the surface until the velocity of the surrounding medium was attained. This envelope of retarded fluid is known as the boundary layer. These views are now universally accepted. The fluid impinging on the frontal hemisphere is divided symmetrically about the centre of the surface and accelerated sideways towards the equator. For laminar flow the fluid in the boundary layer adheres to the surface and closes up behind the sphere in a manner similar to the division on the frontal surface. Before this concept can be extended to turbulent flow, the forces acting on the fluid in the boundary layer must be considered.

The acceleration of the fluid towards the equator on the frontal surface produces a negative pressure gradient in the boundary layer in the direction of flow. Also, the velocity of the fluid just outside the boundary layer tends to decrease when the fluid has passed the equator and a positive pressure gradient is established. This force together with the viscous force of the surrounding layer of fluid and the frictional force

at the surface determines the movement of this part of the boundary layer. This pressure gradient increases with increase in the Reynolds Number and it eventually overcomes the streamline flow past the sphere. Consequently the fluid in the boundary layer is brought to rest with respect to the surface of the sphere and a back flow in the direction of the pressure gradient may occur. The boundary layer is then forced to leave the surface and the point at which this occurs is known as the point of separation. The occurrence of this phenomenon coincides with the development of turbulence, i.e.,  $Re > 500$ .

During the transition from viscous to turbulent flow several interesting phenomena occur behind the sphere. At the beginning of the transition range, when the boundary layer begins to separate, a stationary ring or vortex forms close to the surface. This vortex appears as two eddies when cut by a plane passing through the axis of motion. Nisi and Porter (164) noted that this vortex increased and was thrown off at a Reynolds Number of fifty while Schmidt (206) noticed the appearance of a second vortex. Lunnon (141) felt that a succession of rings or vortices formed and slipped away behind the spheres and that a definite periodicity depending on the velocity was established. At higher Reynolds Numbers, the vortex ring ceases to be distinguishable and a turbulent wake is formed. Under these conditions, the width and strength of the wake behind the sphere and the position on the sphere of the circle at which the wake envelope leaves it are the factors which determine the resistance to motion. It should be noted that these phenomena are accompanied by strict axial symmetry.

## b) Drag Coefficients for Spheres

From the previous section, it may be seen that any mathematical formulation for fluid resistance is exceedingly difficult due to the complexity of the fluid motion and it was only for the viscous range that some success was achieved. In 1850 Stokes (230) formulated the following law for the resistance of the fluid to the fall of a sphere:

$$R_D = 3 \pi \mu_G d V_R \quad \dots(151)$$

This equation was verified by Page (169) who showed that this resistance was the sum of two separate factors. The first was a frictional effect or shearing stress exerted by the fluid on the surface of the sphere. This is known as skin drag and constitutes two-thirds of the resistance in the viscous range. The second was a pressure effect due to differences in pressure on the front and back of the sphere. This is referred to as the form drag. However as the Reynolds Number increases, the contribution of the skin drag rapidly decreases and at  $Re = 1000$  becomes negligibly small compared with the form drag.

Mathematical analysis in the turbulent range failed and the solution of the problem lay in the fact that the resistance to flow could be correlated in terms of a graph whose coordinates were the modified Reynolds Number and the drag coefficient. The drag coefficient  $C_D$  was defined as:

$$C_D = 2R_D / (\rho_G V_R^2 A_f) \quad \dots(152)$$

where  $R_D$  - drag force;

$$A_f - \text{cross-sectional area opposed to flow} = \pi d^2 / 4 \quad \dots(153)$$

The realization that a single graph could be used for spheres of all sizes and densities and for fluids of all densities and viscosities was due to Rayleigh (193). Rayleigh's original graph was for laminar flow, but the range of the graph has been extended (8, 24, 181, 199, 212, 223, 262, 269). Lapple and Shepherd (129) collected the data available and presented a graph of the drag coefficients for spheres, cylinders and disks for Reynolds Numbers of 0.0001 to 1,000,000. This curve is shown in Fig. 1. Their curve for spheres is referred to as the standard curve but it is valid only for constant velocity conditions and in the absence of wall effects and other forms of fluid disturbances. The following correlations have been proposed for the evaluation of the drag coefficient in terms of the Reynolds Number (70, 129).

$$\begin{aligned}
 \text{When } Re < 2, \quad C_D &= 24/Re \\
 2 < Re < 500, \quad C_D &= 0.4 + 40/Re \\
 Re > 500, \quad C_D &= 0.44 \qquad \dots(154)
 \end{aligned}$$

With the aid of these equations Lapple and Shepherd (129) calculated the trajectories of spheres under the influence of gravitational and centrifugal forces, with or without initial velocities. Their method may be divided into three steps:

1 - A force balance on the particle with the resultant force equated to the product of the mass and the time derivative of the velocity in the direction of the force;

2 - Substitution of the drag coefficient and the velocity in terms of the Reynolds Number. If a change in the type of flow occurred

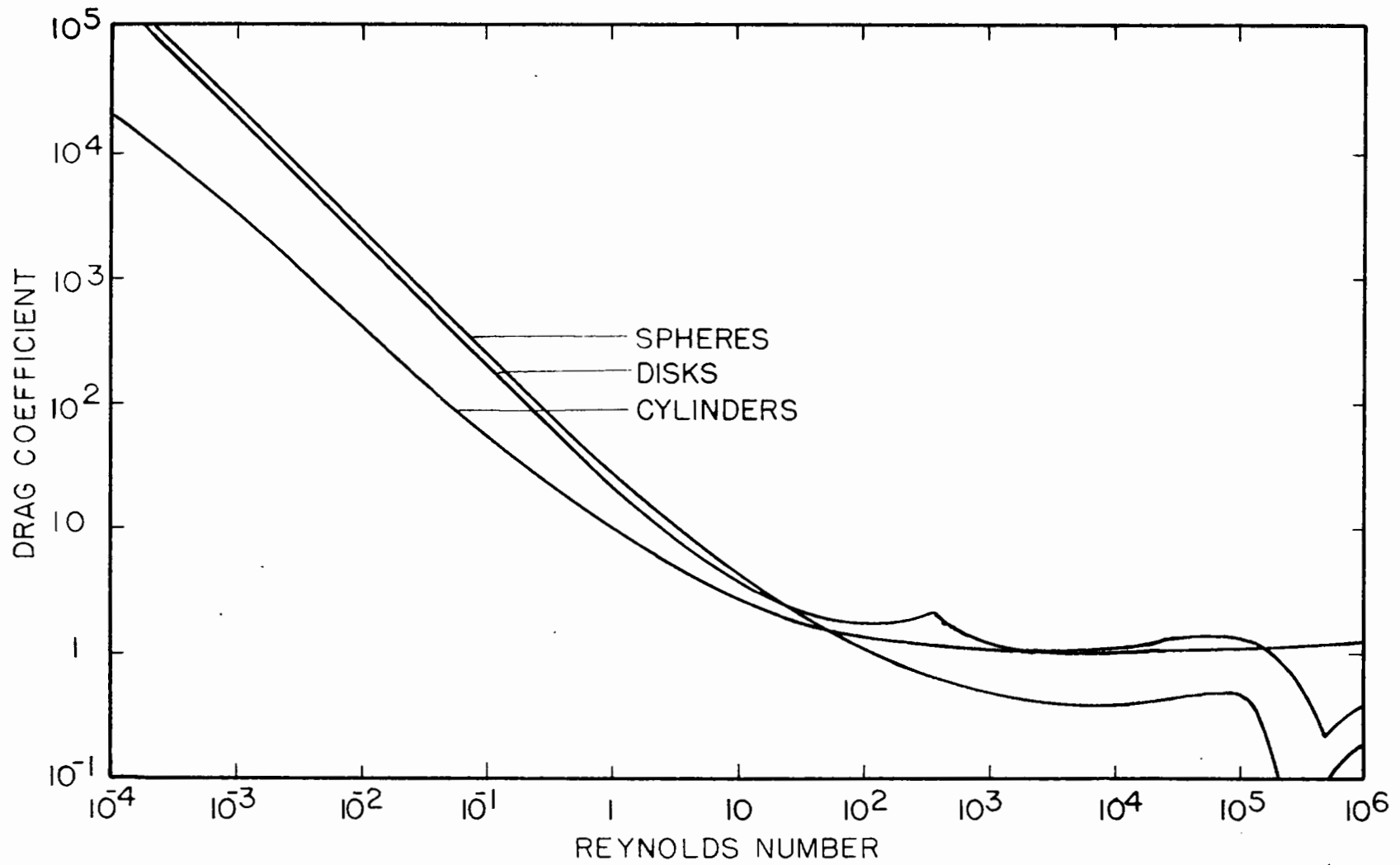


Fig. 1. Drag Coefficients for Spheres, Disks, and Cylinders

then the calculation had to be subdivided into separate parts;

3 - Rearrangement and integration to obtain an expression correlating the time and change in Reynolds Number.

c) Application to Sprays

Several complications arise when the theory just outlined is applied to sprays. These complications include the turbulence of the drying air stream, the effect of particle concentration on the fluid properties, the rotation of drops and the possibility of droplet deformation occurring.

(i) Turbulence

The effect of turbulence on the drag coefficient was critically reviewed by Torobin and Gauvin (246) who noted the conflicting reports mentioned in the literature.

Burke and Plummer suspended fixed spheres in turbulent air flow and recorded resistances up to 60% higher than those given by the standard curve (20). They attributed this increase to the fact that the velocities of the fluid eddies meeting the particle are greater than the observed mean translational velocity of the fluid. Since the square of the statistical sum of such velocity terms is less than the statistical sum of the squares of these terms it is evident that the kinetic energy of the fluid, and therefore the resistance to flow about the solid may be greater than that indicated by the product of the mass and the square of its mean

translational velocity. A more valid explanation of this increase, if correctly indicated, would be one which involved a microscopic appraisal of the interaction of the ambient fluid around the particle with the turbulent field existing in their equipment. Wilhelm and Valentine (264) obtained high drag coefficient values for spherical particles suspended in an upward current of air. Bouvard (17) presented a mathematical analysis for the effect of velocity fluctuations and arrived at the conclusion that the fall velocity in a turbulent stream is less than that in a laminar field.

On the other hand, Lunnon (140) obtained the drag coefficients of spheres by dropping them down mine shafts. He found that slight air disturbances produced a decrease in the drag coefficients and this was attributed to the presence of turbulence. Miller and McInally (160) obtained data of the suspension velocity of solids in water and found that an upward current could increase the suspension velocity by as much as 47%. These two findings are in direct opposition to the data of Wilhelm and Valentine (264). Miller and McInally suggested that the turbulent action tended to decrease the influence of the fluid viscosity and thereby reduced the drag force.

(ii) The Effect of Particle Concentration

Studies of the effect of particle concentration may be divided into two categories: those in closed vessels and those in an infinite fluid. Einstein (48) showed that in the former case the fluid velocity appeared to decrease and this has been expressed in terms of the particle

concentration. Due to extremely high voidages of sprays (0.995 - 0.999) this decrease is unlikely to become appreciable. A second complicating factor is that the particles tend to drag fluid with them through the fluid and a back flow occurs to offset this motion. The net result is an increase in the relative velocity and consequently in the Reynolds Number.

Studies in infinite systems have shown that a decrease in the resistance to flow and hence in the drag coefficient occurs, due to the effect of one sphere on the adjacent one. This effect can be significant and Stimson and Jeffrey (227) showed that it amounted to 7% at interspatial distances of 10 diameters (voidage 0.999) and 11% at interspatial distances of 6 diameters (voidage 0.995).

(iii) Drop Rotation

Rotation effects on drag coefficients can be divided into two classes depending on whether the axis of rotation is parallel or perpendicular to the main direction of flow. In the former case, a marked influence of rotation on the drag was found by Wieselsberger (263) and Luthander and Rydberg (142). The effect was correlated in terms of a rotation factor,  $2V_R/d\omega$ . The drag coefficient was found to increase with decrease in the rotation factor (95, 209, 247). Also the critical Reynolds Number was lowered by rotation (142, 263). An explanation can be found by considering the effect of rotation on the boundary layer. The centrifugal force on the fluid in boundary layer promotes an earlier separation. This increases the drag force, since both the angle of the

wake and its cross-sectional area are increased.

When the axis of rotation is perpendicular to the main direction of flow, an interesting distortion of the boundary layer occurs. The rotation of the sphere has the effect of supplementing the flow lines past the sphere where the direction of flow and rotation coincide. The result is the elimination of separation, a reduction of the boundary layer and a decrease in the fluid pressure. On the opposite side, where the flow direction is opposite to the rotation, a turbulent boundary layer is formed and separation is developed. There is a marked increase in the fluid pressure and the wake becomes high unsymmetrical. Consequently the stream exerts a considerable force on the sphere at right angles to the mean flow direction and this is known as the Magnus effect.

#### (iv) Droplet Deformation

Calderbank and Korchinski (21) have shown that drops can be considered to be perfectly spherical and rigid provided that the Reynolds Number is less than 200. Hu and Kintner (93) felt that the Reynolds Number can be as high as 300 and this is in agreement with Garner (64). As spray drops seldom have Reynolds Numbers exceeding fifty, it is very unlikely that there will be any change in the drag coefficient due to droplet deformation. This means that the internal drop circulation which undoubtedly occurs has no effect on the drag coefficient. Hence it may be concluded that liquid sprays will behave in the same manner as solid sprays and this has been experimentally verified (102, 104). Klee and

Treybal (111) observed a departure of the drag coefficient from the standard curve for Reynolds Numbers below 200, for a liquid-liquid system, but this can be attributed to the high interfacial tension between the two liquid phases. However, it should be realized that the above work was performed under conditions in which the acceleration contribution is of a minor nature, whereas decelerations as high as 32,000 ft./sec.<sup>2</sup> have occurred in sprays (99).

d) The Effect of Acceleration on the Drag Coefficient

Few workers have considered the possibility of a modification of the drag coefficient due to particle acceleration or deceleration. The usual procedures for calculating particle trajectories are based on the assumption that the drag coefficient can be expressed in terms of the Reynolds Numbers alone (44, 129, 175, 184, 217) in spite of the fact that there is considerable literature indicating the existence of an increase of the drag coefficient due to acceleration. However, the explanations for this increase and the methods of correlation have varied widely.

The first exhaustive study was due to Lunnon (140) who recognized the existence of a dependence of the drag coefficient on the particle velocity and acceleration. His experimental work consisted in measuring the time of fall of metal spheres of diameters 0.2 to 10.2 cm. through distances amounting to 528 metres in mine shafts. As the time of fall was measured and recorded electrically, the precision and accuracy were excellent. All attempts at correlation failed and the only resort was

empirical curve fitting, i.e., the representation of the drag coefficient in terms of the Reynolds Number by individual graphs for different acceleration rates. The increase in drag coefficient due to acceleration was considerable, e.g., 200% increase for acceleration of 781 cm/sec.<sup>2</sup>.

Iverson and Balent (100) have summarized the literature on the widely used method of correlation involving the added mass concept. According to this theory the body is considered to possess an added mass which is a function of:

- 1 - the size and shape of the body;
- 2 - the direction in which it is moved through the fluid with respect to an axis in the body;
- 3 - the density and viscosity of the fluid.

The equation of unidirectional accelerated motion in which this concept is used is:

$$F = ma = (1/2)C_D \rho_G V_G^2 A_f = k' m_f a \quad \dots(155)$$

- where m - mass of particle;  
 a - particle acceleration;  
 k' - added mass factor;  
 m<sub>f</sub> - mass of fluid displaced.

Values of k' from 0.03 to 2.0 have been reported for spheres, (115, 141, 155, 177). This method has proved to be unsatisfactory as it fails to account for the observed dependence of the drag coefficient on

the particle acceleration.

Iverson and Balent (100) suggested that the coefficient of drag is a function of an acceleration modulus as well as the Reynolds Number. This modulus is defined as  $(aL'/V_R^2)$  and may be seen to depend on both the velocity and acceleration.  $L'$  is a characteristic length of the particle. Iverson and Balent found that this modulus could be used to correlate data obtained from accelerating disks.

The effect of deceleration of liquid drops with respect to the surrounding medium on the drag coefficient appears to be opposite to that of acceleration. Hanson (79) and Ingebo (99) both obtained drag coefficients for spray drops that are considerably below those indicated by the standard curve. Hanson studied the evaporation of fuel sprays injected into and accelerated by a high velocity, horizontal air stream. The rate of evaporation with distance from the nozzle, air velocity and drop size distribution were determined experimentally. His analysis was based on the assumptions that the spray characteristics can be represented by the mean volume diameter and that Froessling's equation for the evaporation rate of fuel drops is valid.

Hanson (79) assumed that the spray could be represented by the mean volume diameter,  $d_v$ , which is considered to have weight,  $m$ , at any given instant. If this drop were originally of mass,  $m_0$ , i.e., before any evaporation occurred, then the evaporation fraction of the spray,  $E_f$ , is given by:

$$E_f = (m_0 - m)/m_0 \quad \dots(156)$$

$$\text{and} \quad dm/d\theta = -m_o V_D (dE_f/dx) \quad \dots(157)$$

where  $V_D$  - velocity of the drop of diameter  $d_v$ .

As the evaporation fraction was determined experimentally at different distances from the nozzle,  $dm/d\theta$  can be evaluated. Assuming that Froessling's equation for the evaporation rate can be applied we obtain:

$$dm/d\theta = -m_o V_D (dE_f/dx) = -(2 D_v M p_s d_v / RT)(1 + 0.276(Re)^{1/2}(Sc)^{1/3}) \dots(158)$$

$$\text{Here } Re = d_v V_R \rho / \mu_G \quad \dots(159)$$

$V_R$  - velocity of drop of diameter  $d_v$  with respect to the air.

Equations 158 and 159 enable the relation between the drop velocity and distance from the nozzle to be calculated.

The following force balance was then established by Hanson, who neglected the effect of gravity and considered only unidirectional horizontal motion.

$$R_D = m(dV_D/d\theta) = mV_D(dV_D/dx) = C_D V_R^2 \rho_G A_f / 2 \quad \dots(160)$$

Equation 160 was used in calculating the drag coefficients for the fuel spray drops and these are shown in Fig. 2. The dependence which Hanson observed on the air velocity is not apparent on a log-log plot; and the drag coefficients were considerably lower than those indicated by the standard curve for Reynolds Numbers of 20 to 100.

Ingebo (99) used a droplet camera, i.e., a device especially designed for measuring the velocity and diameter of spray drops to obtain

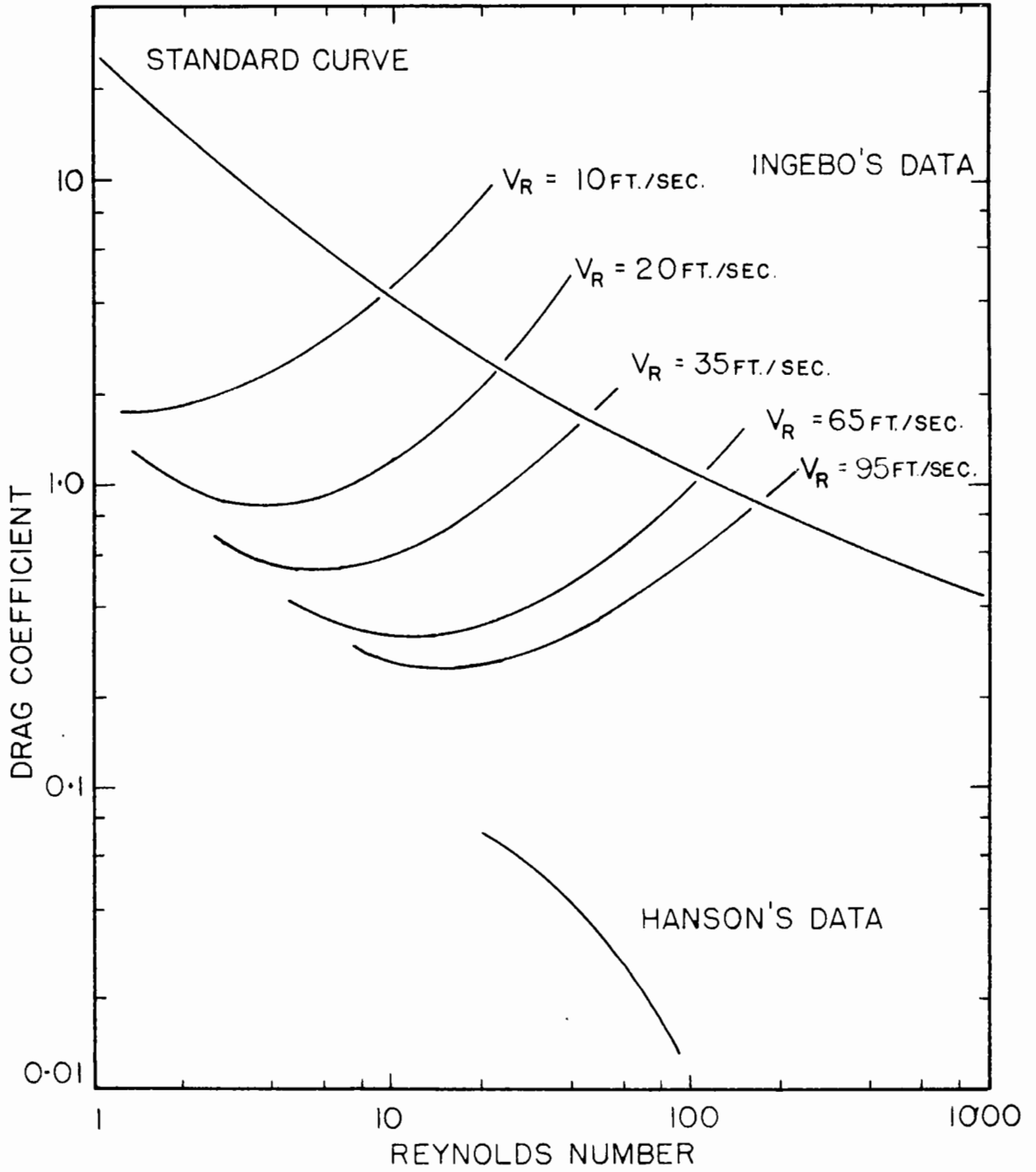


Fig. 2. Comparison of the Data of Hanson and Ingebo

the drop size distribution and drop velocity of iso-octane sprays injected from a simple orifice into a turbulent air stream. From this data and wet-bulb temperature measurements, vaporization rates and drag coefficients were calculated for the spray drops as they were accelerating and evaporating in horizontal air streams of velocity 140 to 180 ft./sec. Ingebo's analysis is based on the change in momentum. Consider a drop of mass  $m + \Delta m$  travelling at an instantaneous velocity,  $V_D$ , in an air stream of constant velocity,  $V_G$ . After time  $\Delta \theta$  has elapsed, the drop has a mass  $m$  and an increased velocity  $V_D + \Delta V_D$ , while the vaporized element of mass  $\Delta m$  has assumed the velocity of the stream. The change in momentum is given by:

$$\Delta M = m \Delta V_D + \Delta m (V_G - V_D) \quad \dots(161)$$

The instantaneous force  $R_D$ , acting on the drop is the time derivative of the momentum:

$$R_D = dM/d\theta = m(dV_D/d\theta) + (V_G - V_D)(dm/d\theta) \quad \dots(162)$$

$$\text{and } (dm/d\theta)h_{fg} = hA \Delta t = \tilde{h} dk_f \Delta t \text{Nu} \quad \dots(163)$$

Combination of equations 161, 162 and 163 yields:

$$C_D = 4 \rho_L a d / 3 \rho_G (V_G - V_D)^2 + 8k_f \Delta t \text{Nu} / h_{fg} \rho_G d (V_G - V_D) \quad \dots(164)$$

Equation 94 was used to evaluate the Nusselt Number of the evaporating iso-octane drop and thereby enabled the drag coefficients to be computed.

Ingebo presented his data in the form of a family of curves of  $C_D$  versus Reynolds Numbers, with air velocity as a parameter. For low

Reynolds Numbers the drag coefficient was much less than the value given by the standard curve, but it increased with the Reynolds Number and on occasions intersected the standard curve. A comparison of his results with those of Hanson is given in Fig. 2.

B. EXPERIMENTAL SECTION

## INTRODUCTION

From the foregoing literature survey, it is apparent that the work performed on the evaporation of sprays can be divided into three classes:

1 - Purely analytical approaches based on drastic assumptions which have been later disproved (46, 217).

2 - Determinations of the rates of evaporation from sprays under conditions where the relative velocity between the spray drops and the surrounding gaseous medium is negligible (40, 108, 110, 147, 175).

3 - Investigation of the evaporation occurring from sprays accelerated by high velocity air streams (28, 30, 31, 51, 79, 99).

The majority of the work performed in the last class was devoted to the measurement of heat, mass and momentum fluxes in the drying gases without specific consideration of the liquid phase (28, 30, 31). The main difficulty lies in the determination of the spray velocity. Photography of the individual spray drops requires elaborate equipment due to the small drop sizes and high velocities encountered.

An analytical approach applying Froessling's equation to obtain a correlation between the spray evaporation and the drop velocities relative to the drying gas has been used to calculate the drag coefficients of the spray drops (51, 79). Only Ingebo (99) has succeeded in measuring the evaporation rate and the drop diameters and velocities of iso-octane sprays injected into high-velocity horizontal, turbulent air streams. The method of atomization and choice of flow conditions were totally different from

those usually encountered in commercial spray dryers. Hence it is evident that there is a distinct need for accurate data on the heat and mass transfer rates to decelerating spray drops produced by typical, industrial, atomizing nozzles.

The present work constitutes the first attempt to measure the heat and mass transfer coefficients of decelerating, spray drops produced in internal-mixing, pneumatic and hollow-cone, pressure nozzles. Also the effect of two flow patterns which so far have received little consideration was investigated.

Before the rates of heat and mass transfer to the spray drops can be obtained the physical properties of the liquid and gaseous phases must be determined. The evaluation of these physical properties presents many problems not the least of which was involved in the sampling methods. Consequently, the development and evaluation of the experimental techniques used to measure the average drop size and size distribution and also the drop velocity, temperature and evaporation as well as the velocity, temperature and humidity of the drying air are presented in the first part of the Experimental Section. The data obtained for the velocity of the spray drops at different distances from the atomizing nozzle enabled the drag coefficients of these drops to be calculated.

In the experimental determination of the evaporation rates of the spray, two different flow patterns were studied: cross-current flow, where the direction of the drying air path is perpendicular to the axis of the spray, and co-current flow, where the air path is in the same direction as the axis of the spray. The second chapter of the Experimental Section is

devoted to the determination of the heat and mass transfer coefficients and the Nusselt Number of the spray drops for cross-current flow. The equipment consisted of a trapezoidal chamber containing six horizontal sections through which the drying air was passed at right angles to the vertical spray. Finally the equipment and results for co-current flow are presented in the third chapter. In this case, a vertical cylindrical drying chamber was used with downward flow of the spray and drying air.

## I. MEASUREMENTS OF SPRAY PROPERTIES

As was previously mentioned, the complexity of the phenomena occurring in the nozzle zone of a spray presents considerable difficulty in determining the physical properties of the spray components. The presence of liquid drops renders the conventional methods of measuring the drying air temperature, humidity and velocity completely useless. Special techniques had to be developed before accurate values of these variables could be obtained. The high rate of evaporation of small drops produces rapid changes in the physical properties of the spray and drying air, thus making the sampling method of paramount importance. The latter was in turn markedly affected by the flow pattern under study; thus the most suitable procedure for both flow patterns had to be determined separately.

### 1. SPRAY DROP SIZE DISTRIBUTION

The available techniques for determining the size of spray drops have been reviewed in the literature survey, and the method finally chosen involved direct sampling of the spray with a small immersion cell, and photography under a microscope. Subsequently the photographs were examined and the drop sizes measured with a microscope, thus enabling the drop size distribution to be obtained.

#### a) Equipment

The immersion cell consisted of a hollow, aluminum, cylindrical tube, 0.25 in. external diameter, 0.20 in. internal diameter, and 0.20 in.

deep. The cell holder was made from a brass ring, 0.1 in. thick, which surrounded the cell and to which was attached a 1/8-in. welding rod. The bottom edge was grooved so that a thin disk of optical glass could be glued into position. A film of General Electric SC-87 anti-wetting agent was applied to this disk so that the spray drops would not flatten on contact with the glass. The selection of the immersion liquid for the cell presented considerable difficulties as the surface tension and viscosity had to be low so as to permit the spray drops to settle freely and quickly, while the density had to be comparable with that of water so as to minimize the flattening of the drops due to gravitational forces. From a chemical point of view, complete inertness towards water was a prerequisite. Varsol - a mixture of hydrocarbons - was found to possess the desired physical properties and was accordingly selected.

Owing to the relatively high velocities of the spray drops in the nozzle zone, good impaction efficiencies were obtained. This improved the accuracy of the method but presented some sampling difficulties as the cell could only be exposed to the spray for a fraction of a second to minimize droplet coagulation which might result from too high a droplet concentration in the sample. To achieve the necessary degree of control during sampling a hollow cylindrical shield of outside diameter 0.50 in., internal diameter 0.45 in. and length 2.0 in. was machined. This was attached to a 1/8-in. welding rod. This shield was used to cover and protect the immersion cell before and after sampling. The arrangement was such that the cell and holder could be inserted into the shield and the whole assembly passed through a 1/2-in. standard brass nipple mounted in the side of the spray chamber. A sketch of the holder and shield with the

cell in place, is shown in Fig. 3.

b) Procedure

The path traversed by the immersion cell during sampling had to be carefully controlled especially when cross-current flow conditions were investigated. Displacement of the spray by the drying air occurred, resulting in a displacement of the smaller spray drops in the direction of the air flow. To eliminate errors due to this displacement, the sample path must be in a direction opposite to that of the drying air.

A few drops of Varsol were placed in the immersion cell which was then covered with the cylindrical shield. In the case of the cross-current flow chamber the whole assembly was inserted through the exit brass nipple of the section under investigation and moved near to the spray. Accurate control of the sampling time was achieved by varying the rate at which the immersion cell was pushed out of the shield and through the spray. Recovery of the cell without further interference from the spray was effected by pushing the cylindrical shield through the spray and over the cell, and then withdrawing the whole assembly.

The sampling technique for the co-current drying air flow pattern was much simpler due to the radial symmetry of the air flow. Two traversing paths were used: a direct path along a diameter through the spray and an angular sweep through the centre of the spray. For the first few inches of the spray, the former method was used due to the extremely short time needed to obtain a suitable sample.

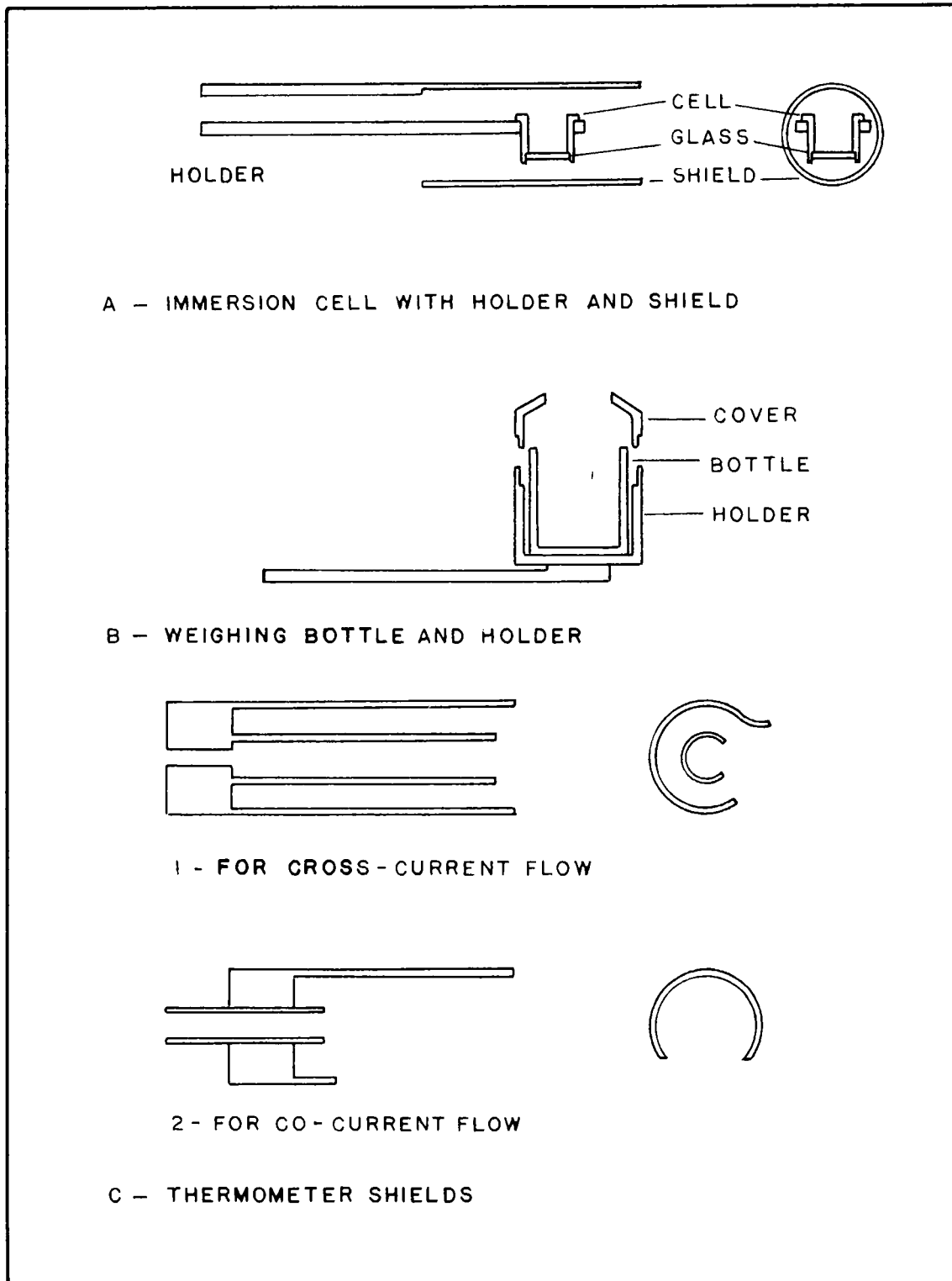


Fig. 3. Sampling Devices and Thermometer Shields

After the spray sample had been obtained the cell was placed on the stage holder of a Bausch and Lomb microscope. In order to avoid errors due to the uneven liquid surfaces, the cell was filled with more Varsol and covered with a glass slide. Photographs of the spray drops were then taken with a single lens Asahiflex reflex camera fitted onto the microscope. A parallel light beam from a 200-watt microscope lamp was used and exposure times of  $1/25$  second were found to give the best results. Adox KB 14 film was used as its fine grain makes any errors due to resolution negligible. As the spray drops produced by pneumatic nozzles were much smaller than those from pressure nozzles, different magnifications had to be used. A 16-mm. focal length objective and 12.5X eyepiece were used for the small drops, giving a total magnification of 54.3X; while a 32-mm. focal length objective and 7.5X eyepiece with overall magnification of 12.6X was used for the larger drops. The presence of a ground-glass screen on the camera facilitated the focusing. A calibration of the drop sizes was established by photographing a Fisher Scientific microscope stage micrometer graduated in 10- and 100-micron divisions under identical optical conditions.

Counting of the drops was performed using the same microscope with a 32-mm. objective and a micrometer eyepiece. Approximately 150 to 250 drops were counted for each determination of the drop size distribution and Sauter mean diameter. The selection of size groups for the counting procedure was carefully considered. For the smaller drop sizes (pneumatic nozzles) drop size increments of 3.5 and 6.0 microns were found to be satisfactory. However as drop sizes of 200 microns were encountered with the pressure nozzle, increments of 15 to 25 microns had to be used.

c) Sources of Error

As the design of the immersion cell was such that no evaporation could occur during the measurement of the drop size distribution, the main sources of error are coagulation of the drops during settling and unrepresentative sampling during collection. The former can be reduced to a minimum by obtaining samples of such low drop concentration as to eliminate statistically the possibility of coagulation. The latter, however, constitutes a more complex problem.

Curves for the impaction efficiencies of various shapes in a particle-laden gas stream were presented by Langmuir and Blodgett (172). Unfortunately a shape similar to that of the sample cell and holder was not investigated. However, they reported a marked dependence of the drop diameter on the impaction efficiency. This indicated that the more numerous the particles of small diameter impacted, the larger was the efficiency. Since numerous drops with diameters as low as one micron were collected in the immersion cell, it can be inferred that the sampling efficiency for the larger drops was excellent. In fact, the method has been used widely with considerable accuracy for conditions of little or no relative velocity between the drops and the sampling medium (40, 71, 145, 201). In the present work, an appreciable relative velocity was at all times maintained. Hence it may be concluded that the accuracy of this method for obtaining drop size distributions in decelerating sprays is more than satisfactory.

## 2. SPRAY DROP VELOCITIES

Few attempts at measuring the velocity of spray drops have appeared in the literature, and the only extensive experimental study was due to York and Stubbs (268). Working with a hollow-cone pressure nozzle, they reported a marked dependence on the radial position in the spray. This is to be expected as the centrifugal forces occurring during spray formation introduce radial gradients in the latter. Accordingly, a method of measuring the spray drop velocity by means of direct photography with a high speed motion picture camera was developed.

### a) Photography of Spray Drops

The physical arrangement of the cross-current flow equipment was such that photography of the spray in the drying chamber was impossible. Consequently, equipment permitting the spray velocities to be determined under roughly similar evaporation conditions was constructed. This equipment consisted of an 8-in. outside diameter lucite cylindrical column, 5 ft. long and with a wall thickness of  $1/8$  in. The spray nozzle was fitted at the top of the column in such a manner that the axis of the spray coincided with that of the column. Circular holes were cut in the column wall at distances from the nozzle corresponding to the distances of the midpoints of the horizontal sections of the cross-flow equipment. Thin optical glass disks were glued into these holes and the window so produced eliminated errors in focusing through the curved lucite column wall.

The camera used was a 16-mm. Fastax High-Speed Motion Picture Camera No. WF-3, manufactured by the Wollensak Optical Company. Camera speeds of 8000 frames per second were obtained and this permitted drop velocities of up to 200 ft./sec. to be measured. A small depth of focus is essential as otherwise the measurement of drop diameters would be impossible. This was accomplished by means of a 101-mm., f/3.5 lens with suitable extension tubes. Illumination of the spray was achieved by a 1000-watt flood lamp. Black cardboard screens with slits were used to provide a parallel beam of light as well as the most favourable background. The optimum angle between the camera and the illuminating beam of light was experimentally determined to be 135 degrees.

The main difference between the conditions existing in the lucite column and those in the cross-current spray chamber is the air flow pattern. For the cross-current flow the spray is deformed and flattened, while in the lucite column the air entrained by the jet action of the pneumatic nozzle enforces the spray drop velocities. A correction for this difference was made by subtracting the air velocity from the measured drop velocities.

Control of the camera voltage and illuminating light was obtained with a Wollensak Goose Control Unit. This device regulates the voltage and consequently the speed of the camera, the duration of the supplied voltage, and the illuminating flood lamp switch. Also a timing-light generator was incorporated into the circuit. This is a square wave generator, and it was used to activate the timing pulse of the camera which flashed a light for the duration of a few microseconds every 1/100 or 1/1000

of a second. By means of this arrangement the time which elapsed between successive pictures could be measured. A photograph showing the layout of the equipment is given in Fig. 4.

The first step in the experimental procedure was to adjust the position of the high speed camera until it was focused on a point on the axis of the spray. This was achieved by suspending a plumb line from the nozzle orifice and focusing on the line. Incidentally this served as an excellent check on the alignment of the lucite column. The light beam was also adjusted so that the plumb line was brightly illuminated. The flow rates, temperatures, and pressures of the fluid streams to the nozzle were regulated to correspond with the values used during the evaporation tests in the cross-current equipment. A suitable camera voltage - and consequently speed - was selected in order that the spray drops would appear on at least three consecutive frames. This selection procedure resulted from trial and error tests. One 100-ft. reel of Wollensak Fastax safety motion picture film type 931 was taken for each spray velocity determination. When developed, these films showed the drops as black streaks on a light background, indicating that refracted light from the drops was recorded on the film.

A similar procedure was used to photograph the spray drops in the co-current flow drying air chamber. Here the cylindrical drying chamber was fitted with glass windows, and so could be considered as being optically analogous to the lucite column. Thus photography of the spray drops under actual experimental conditions, i.e., measured evaporation rates, drop size distributions, drying air flow and temperatures, and spray temperatures, was

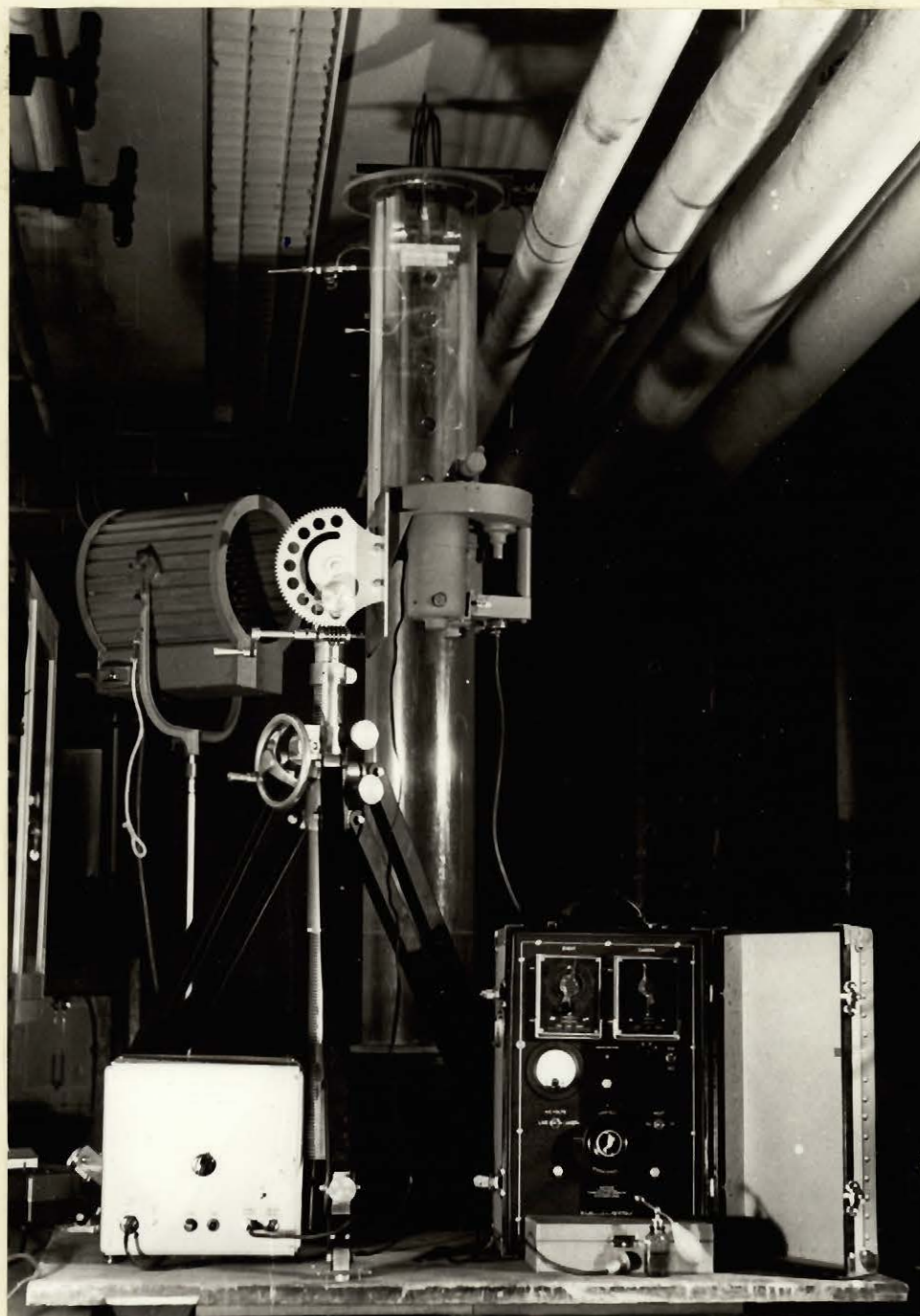


Fig. 4. Equipment for Determining Drop Velocities

achieved.

b) Determination of Drop Velocities

Analysis of the Fastax high speed films was accomplished by means of a 16-mm. Craig Projecto-Editor. This viewer projected the film onto a ground-glass screen. The Fastax camera was operated with a magnification of 0.862X and the film viewer enlarged the image by a factor of 11.1X, thus producing an overall magnification of 9.7X. Visual detection of drops of diameter less than 10 microns was therefore impossible. The grain of the Fastax high speed film was 54 lines per mm. and thus the resolution would not permit drops smaller than 10 microns to be photographed clearly. Accordingly the measurement of velocities for the very small drops had to be abandoned. An increase in the magnification of the picture taken by the Fastax camera would reduce the field of view and consequently the number of frames on which a particular drop appeared. As the larger drops travelled at velocities of over 100 ft./sec. near the nozzle and the field of view was 0.70 cm., a camera speed of 8000 frames/sec. was required to obtain a picture of the same drop on two successive frames.

The sharpness and intensity of colour of the streak observed on the ground-glass screen served as an indication of the accuracy of focusing on a particular drop. Measurements were taken only on drops that appeared as a sharp dark mark on the screen. A cathetometer was used to measure the thickness of the streaks. The instrument was fitted with a moving cross hair and a vernier scale, and the magnification so produced

enabled drop sizes to be measured within 2 or 3 microns. Corresponding velocities were easily calculated from measurements of the distance travelled between successive frames. The time elapsed between successive frames was obtained by counting the frames between successive timing light marks on the film.

Tables of the drop velocities and diameters measured for both pneumatic and pressure nozzles under the various operating conditions given in Table III appear in Appendix I. These results are presented graphically in Fig. 5 to 13. The air velocity in the column,  $V_G$ , is shown as a dotted line. The effect of drop diameter on the velocity is clearly shown to be of great significance. This can be attributed to the greater kinetic energy retention of large drops. Considerable scatter appears, but it should be remembered that the factors influencing the velocity of the spray drops are many and complex. The mechanism of atomization is such that spray drops of the same size but occupying different radial positions in the spray can easily have different initial velocities. Also the high levels of turbulence intensity (circa 20%) can lead to marked differences in the fluid resistance to the motion of the spray drops. In view of these considerations, it would appear that the fluctuations in the experimental observations were probably not excessive.

Fig. 5 to 13 illustrate the effects of the atomizing variables and evaporation on the drop velocities. Thus much higher drop velocities are obtained from pneumatic nozzles than from pressure nozzles, and an increase in the flow rate or pressure of either fluid stream results in an increase of the drop velocities. The effect of evaporation is more complex.

TABLE III  
NOZZLE OPERATING CONDITIONS

Nozzle	Pressure Range	Run No.	Spray Angle degree	Water Stream			Atomizing Air Stream		
				$q_L$ lb./hr.	$P_L$ p.s.i.g.	$T_L$ °F.	$q_A$ lb./hr.	$P_A$ p.s.i.g.	$t_A$ °F.
Pneumatic (1/4) JN No. 12	low pressures	1-12; 21-24	12	2.00	14.9	76-92	5.45	25.0	65-100
Pneumatic (1/4) JN No. 12	mixed pressures	-	14	2.00	20.3	76-92	7.20	35.0	65-100
Pneumatic (1/4) JN No. 12	high pressures	25-30	15	4.40	25.0	62-75	7.20	35.0	65-100
Pneumatic (1/4) JN No.22B	-	31-34	20	6.00	6.0	62-81	20.5	25.0	65-100
Pressure (1/4)LNNS No.1	-	13-20	60	5.01	99	76-90	-	-	-
Pressure (1/4) LN No. 1	-	35-43	60	12.00	95	90-250	-	-	-

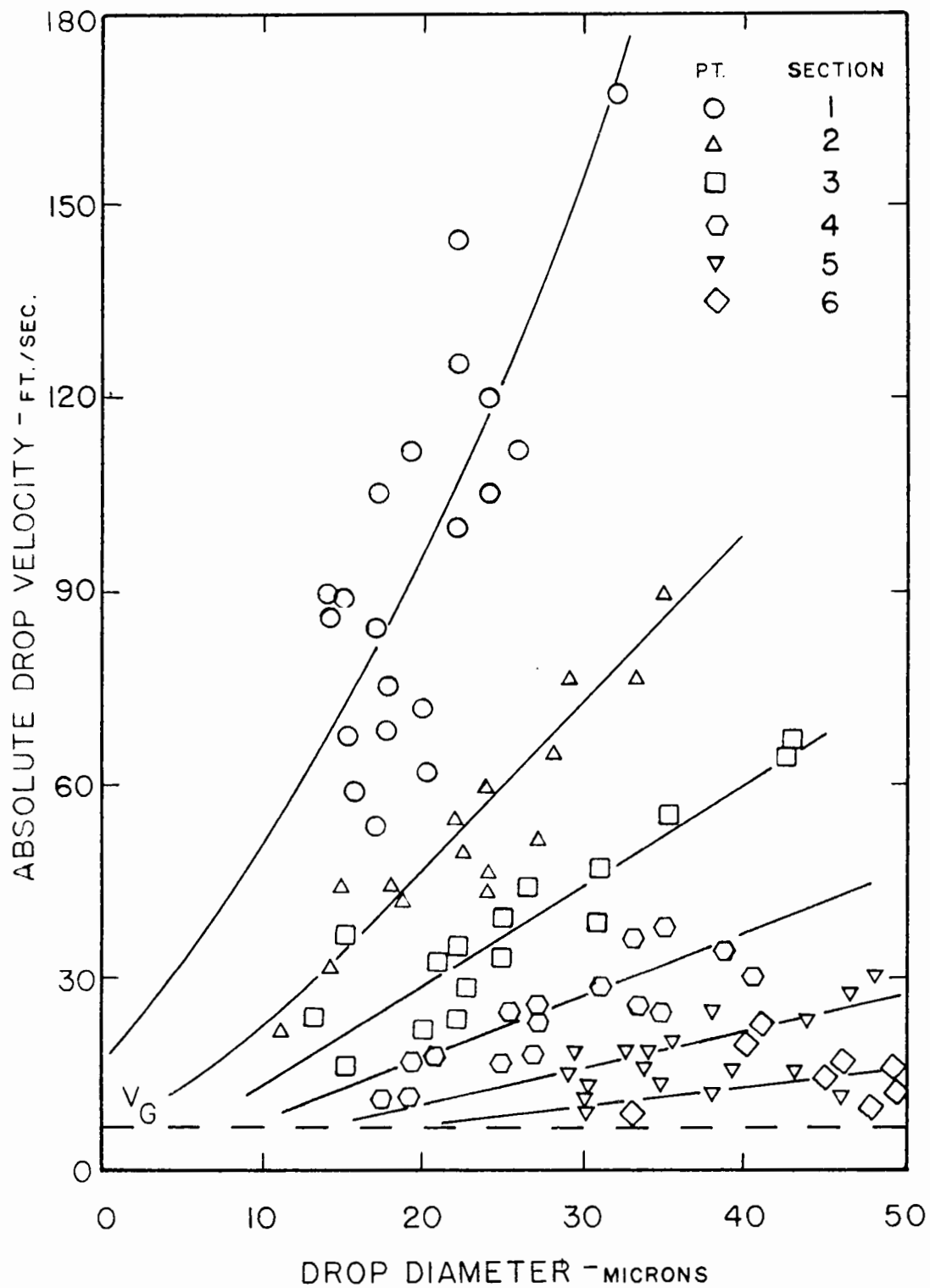


Fig. 5. Drop Velocities for Pneumatic Nozzle 1/4JN No. 12  
(Low Atomizing Pressures - Negligible Evaporation)

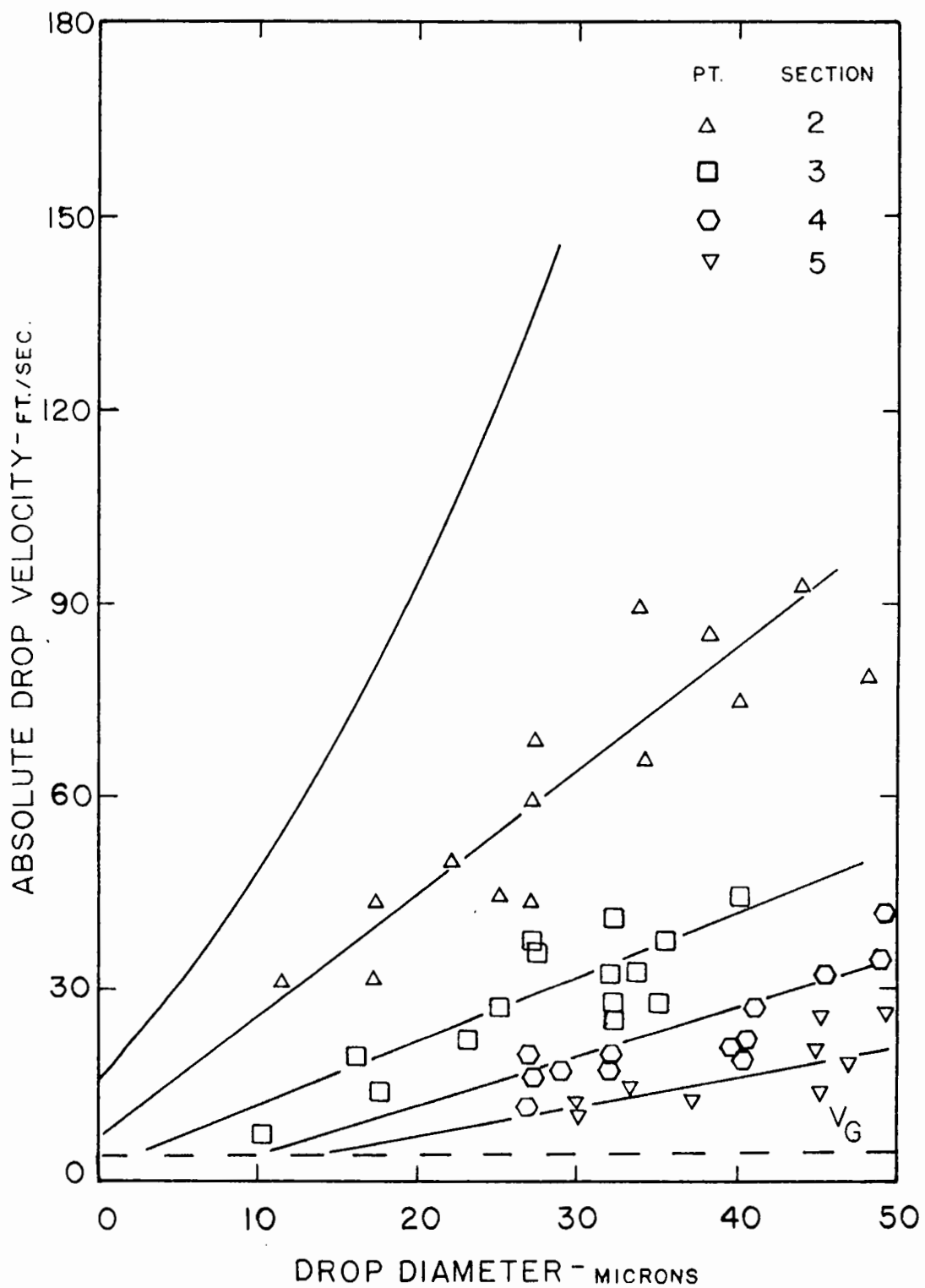


Fig. 6. Drop Velocities for Pneumatic Nozzle 1/4WJN No. 12  
(Low Atomizing Pressures - Considerable Evaporation)

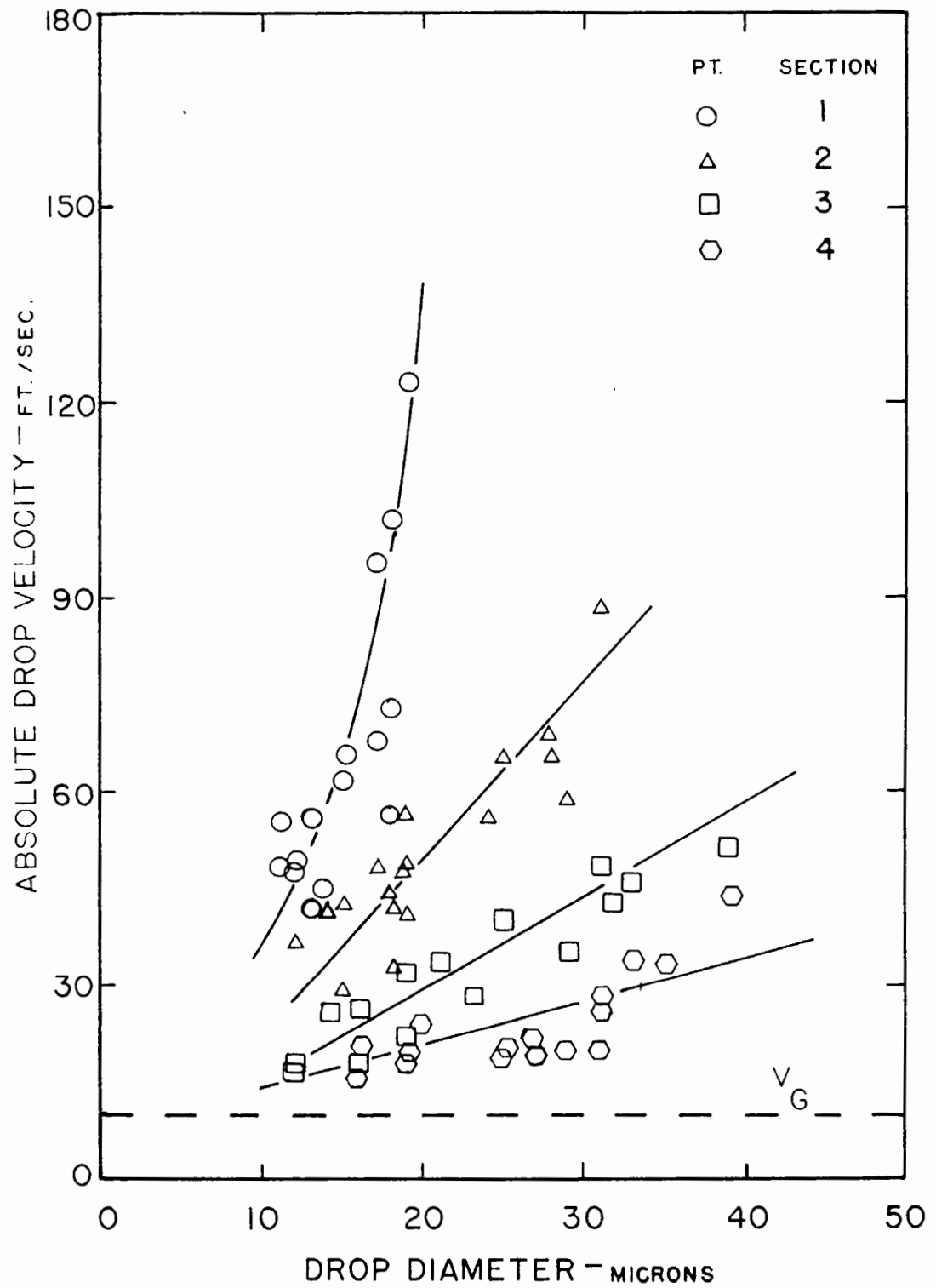


Fig. 7. Drop Velocities for Pneumatic Nozzle 1/4JN No. 12  
(Mixed Atomizing Pressures - Negligible Evaporation)

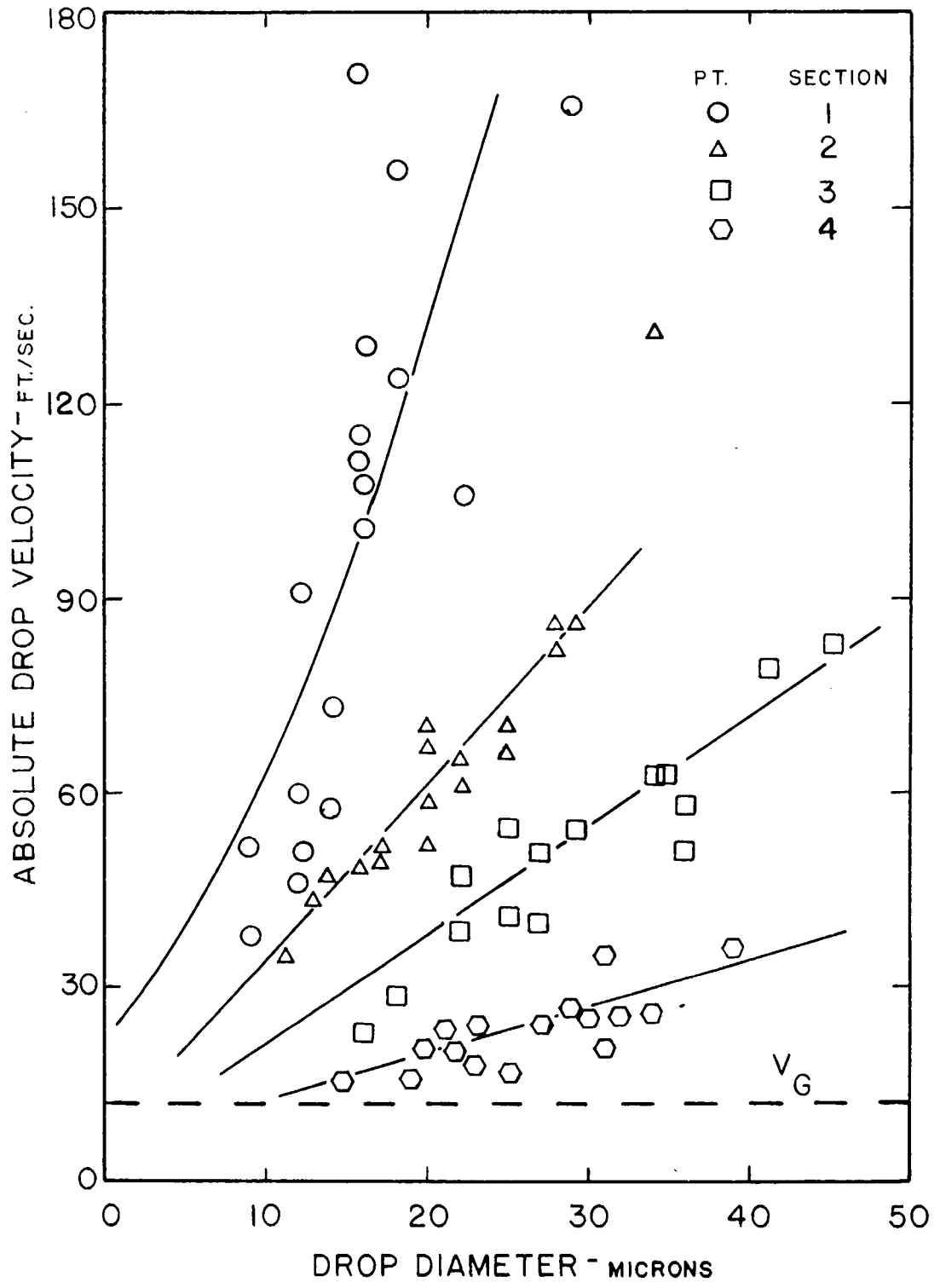


Fig. 8. Drop Velocities for Pneumatic Nozzle 1/4JN No. 12  
(High Atomizing Pressures - Negligible Evaporation)



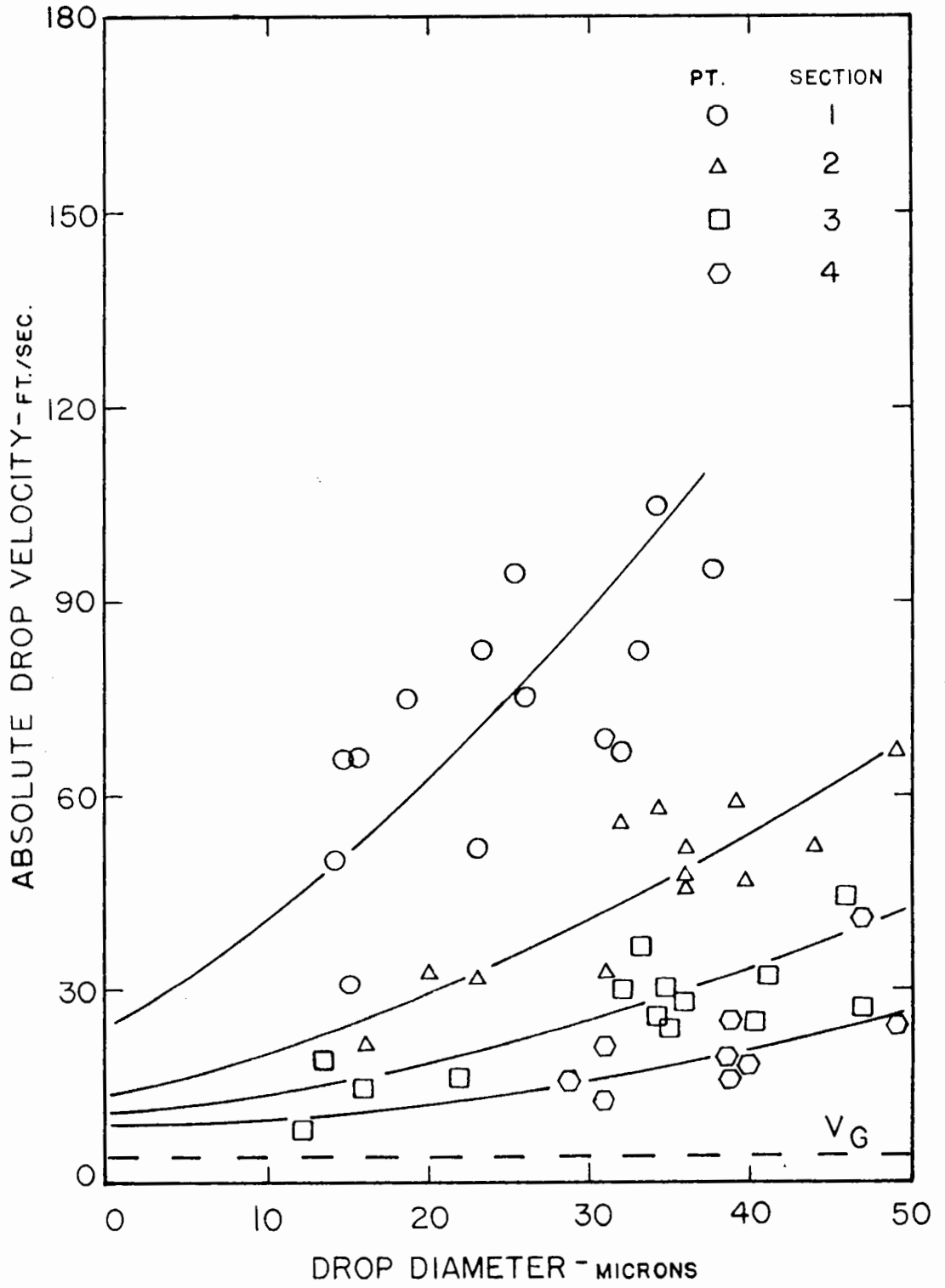


Fig. 10. Drop Velocities for Pneumatic Nozzle 1/4JN No. 22B.  
(Considerable Evaporation)

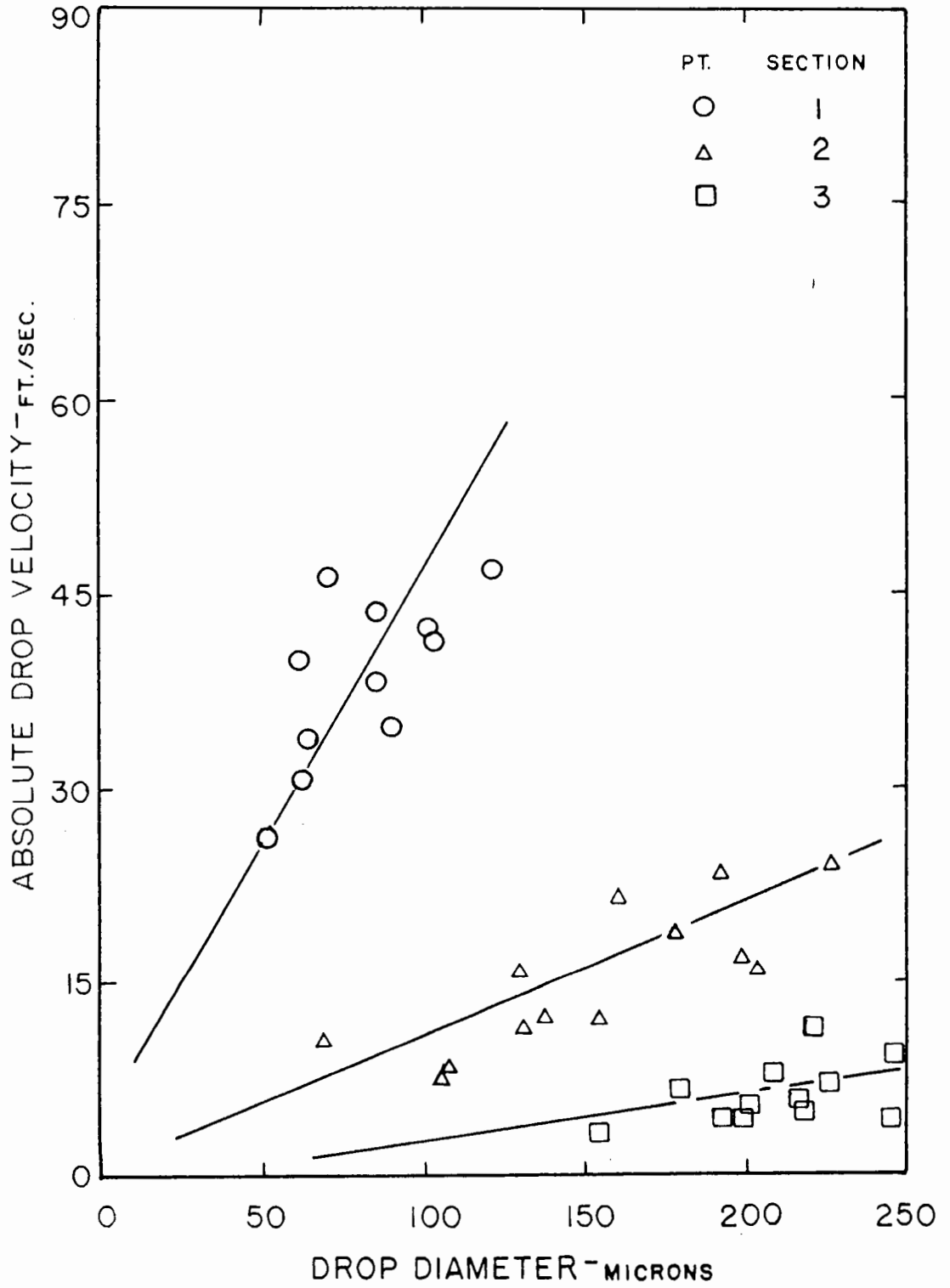


Fig. 11. Drop Velocities for Pressure Nozzle 1/4LNSS No.1  
(Negligible Evaporation)

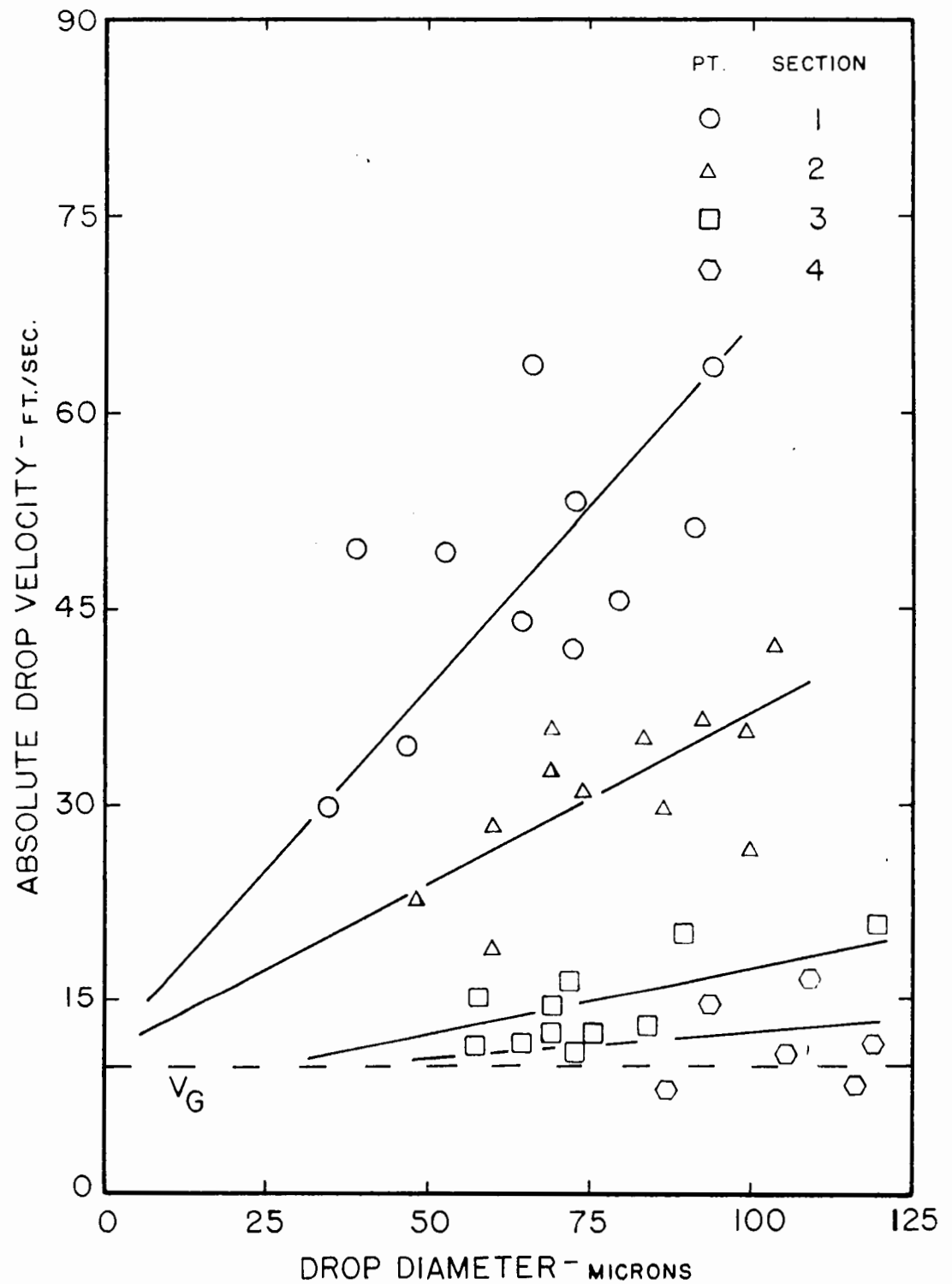


Fig. 12. Drop Velocities for Pressure Nozzle 1/4LN No. 1  
(Considerable Evaporation)

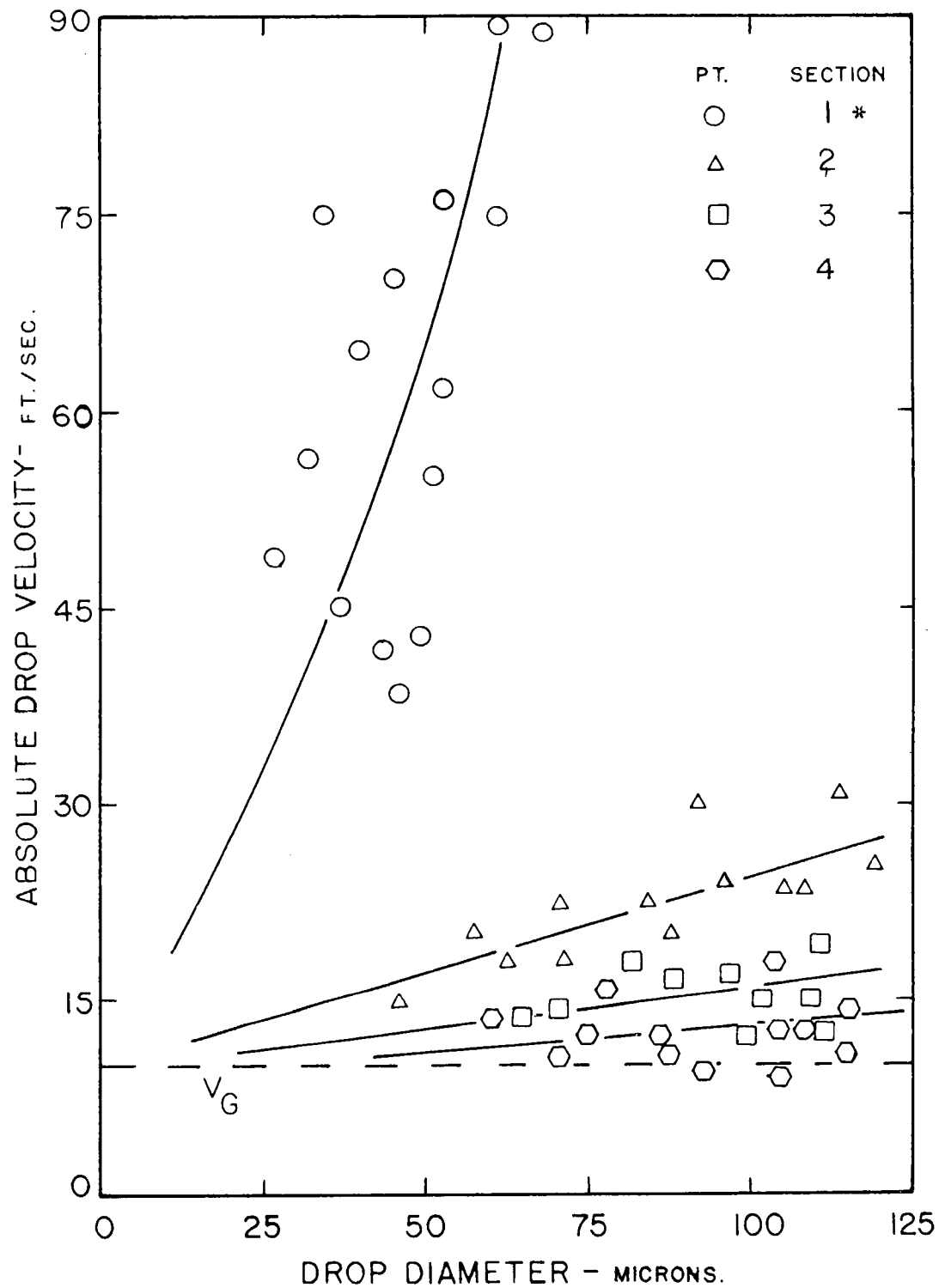


Fig. 13. Drop Velocities for Pressure Nozzle 1/4LN No. 1  
(Considerable Evaporation - Superheated Feed)

\* Section 1 -  $x = 0.5$  in.

There is little effect close to the nozzle, but when a considerable fraction of the spray has evaporated, lower spray velocities are obtained. This appears to be a combination of two opposite effects caused by evaporation:

1 - A reduction in the mass of the spray with decrease in the kinetic energy available for penetration of the surrounding air;

2 - Since the rate of evaporation in a spray controls the rate of change in the size of the drops, the greater the evaporation rate, the larger will be the initial drop diameter required to produce a drop of given size at a fixed point in the spray. But the velocity of any given drop is governed by the velocity with which it leaves the nozzle, and as this initial velocity increases with particle size, the velocity of the drop at the given point in the spray tends to increase with increasing evaporation rate.

### c) Calculation of Drag Coefficients

The measurements of drop velocities in the lucite column were made under conditions of negligible evaporation. Consequently the data so obtained were used to compute drag coefficients. Values of the relative drop velocity with respect to the surrounding air were required for these calculations. The various methods of determining the air velocity in a spray are discussed in detail in a subsequent chapter; only the result of the method which was finally selected will be given here. Briefly, this method consists of extrapolating the drop velocity - drop diameter graphs to zero diameter and of taking the value of the intercept on the velocity axis as the air velocity.

An analysis of the forces acting on a drop falling under the influence of gravity yields the expression:

$$mg(\rho_L - \rho_G)/\rho_L - C_{Df} A V_R^2 \rho_G/2 = m(dV_D/d\theta) \quad \dots(165)$$

Since  $\rho_G$  may be neglected in comparison with  $\rho_L$ , this equation may be put into incremental form as follows:

$$\Delta V_D/\Delta\theta = g - (3C_{Df} \rho_G V_R^2/4d\rho_L) \quad \dots(166)$$

Substitution of the change in the relative velocity at different distances from the nozzle for a drop of constant diameter enabled the drag coefficients to be evaluated. Tables of the drag coefficients with the corresponding Reynolds Numbers are given in Appendix II. A graphical comparison with the data of Hanson (79) and Ingebo (99) is given in Fig. 14.

The values of the drag coefficients obtained are lower than those indicated by the standard curve by a factor of approximately 10. This conforms with the data of Hanson and Ingebo. A trend for the larger drop sizes to have higher drag coefficients was noted and this indicates the possibility of the size of the particle having an influence on the drag coefficient.

### 3. SPRAY DROP TEMPERATURE

There is considerable evidence in the literature indicating that evaporating sprays remain at the wet-bulb temperature of the drying air (28, 40, 79, 99, 110, 112, 147, 175, 184, 188). In particular the work of Kinzer and Gunn (110) is most impressive. They collected samples of the

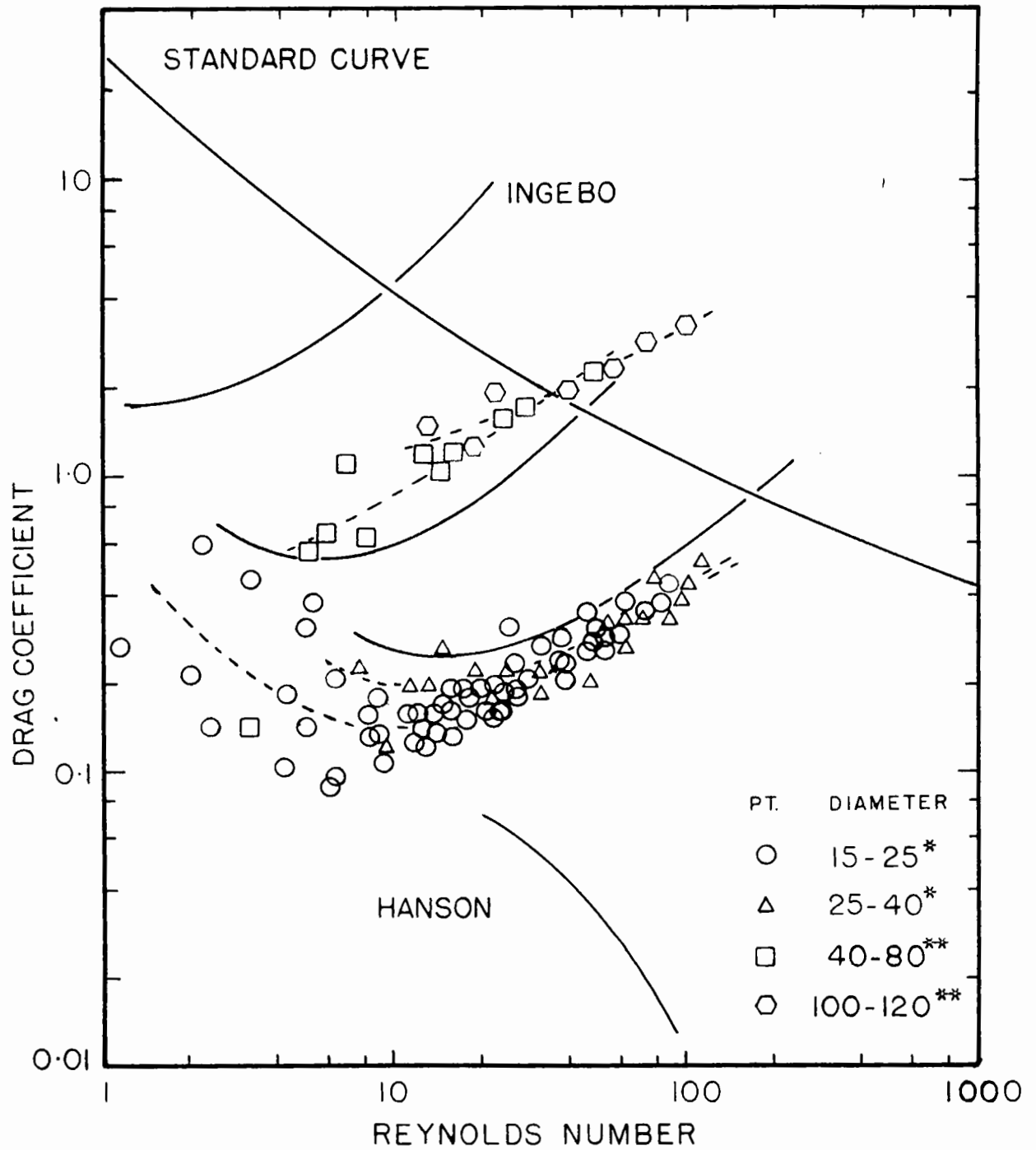


Fig. 14. Drag Coefficients for Decelerating Spray Drops

(\* Pneumatic Nozzle 1/4 JN No. 12)  
 (\*\* Pressure Nozzle 1/4 LNNS No. 1)

spray in a water bath, the temperature of which was thermostatically controlled. Differences in the temperature of the spray and the water bath were detected by means of the scattering of light beams. This scattering was produced by differences in the refractive index and density of the water due to a temperature gradient. This method proved to be extremely sensitive and by varying the temperature of the water bath the spray drops were shown to be within  $0.2^{\circ}\text{F.}$  of the wet-bulb temperature.

Accordingly, a thermocouple probe was constructed for use in measuring the spray temperature. This device consisted of a copper-constantan thermocouple mounted inside a No. 16 hypodermic needle. The end of the thermocouple protruded about  $3/4$  in. beyond the needle tip and a soldered junction was made at the very end. The head of the hypodermic needle was fitted to a suitable plug for the sample port of the drying chamber. In order to prevent excessive accumulation of spray drops, the tip of the thermocouple was bent slightly downwards. When the device was inserted into the spray, the liquid drops would accumulate and then fall off under the effect of gravity. This continual flow of liquid drops kept the tip at the spray temperature. The thermocouple leads were connected to a Leeds and Northrup potentiometer capable of measuring temperatures to  $0.3^{\circ}\text{F.}$  The spray temperature so determined agreed closely (within  $1.0^{\circ}\text{F.}$ ) with the wet-bulb temperature of the drying air.

This probe was also used to determine the spread of the spray; as when placed outside of the spray, the temperature of the drying air was recorded. The line of demarcation between the dry-bulb and wet-bulb temperature enabled the boundaries of the spray to be determined.

#### 4. EVAPORATION FROM SPRAYS

An accurate method of measuring the evaporation from the spray is essential for the determination of the rates of heat and mass transfer. A very convenient solution to this problem was found, which consisted of adding a dilute solution of a highly coloured dye to the water prior to spraying and of measuring colourimetrically the change in concentration of the dye as evaporation proceeded. A strawberry-red vegetable dye proved to be ideal for this purpose, as colour changes corresponding to one part in ten million could be detected. This permits the use of very low dye concentrations in the feed solution, of the order of one part per ten thousand. Changes in the physical properties of the spray due to the presence of the dye were negligible as the mole fraction of the dye was extremely small, in view of its high molecular weight. Also no surface active properties were imparted, such as a depression of the surface tension.

##### a) Determination of Colour Intensity

Samples of the spray were collected under a silicone oil in 5-ml. weighing bottles which were introduced into the spray by means of an aluminum holder. The design of the holder, shown in Fig. 3, was such that the weighing bottle was completely protected from the spray and no evaporation of the drops could occur after collection. A careful survey of the commercially available silicone oils was made and Dow Corning Silicone Oil No. 200 was chosen because of its low surface tension, low viscosity, very low vapour pressure (0.5 mm. Hg at 200°F.), and its

complete immiscibility with water and with the vegetable dye. The weight of the sample was obtained on a semimicro-balance capable of accurate detection of weight changes of one-tenth of a milligram. Exposure times in the spray were controlled so that approximately 100 to 1000 mg.-samples were obtained.

The contents of the weighing bottle were then transferred to a 25-ml. volumetric flask and diluted with distilled water. As the silicone oil was immiscible and floated to the surface, most of it could be removed with a syringe before the flask was made up to the mark.

A Fisher Scientific Neofluoro-Photometer was used to measure the colour intensity of the solutions. The most suitable filter was found to have a wavelength of 525 millimicrons. For all analyses the standard comparison cell contained distilled water. The calibration curve shown in Fig. 15 was obtained from measurements on prepared samples of known concentration, with and without silicone oil. The oil was found to have no noticeable effect on the colour intensity. The linear relation between the logarithm of the light absorption and the concentration of the strawberry-red dye demonstrates the applicability of the Beer-Lambert Law over a range of 1 part per  $10^5$  to 1 part per  $10^7$ .

#### b) Sources of Error

The major source of error is the deflection of the smaller spray drops due to the separation of the air-stream flow patterns around the sampling device. The size of the bottle and holder is appreciable and must cause some disturbance of the spray flow. In order to test the

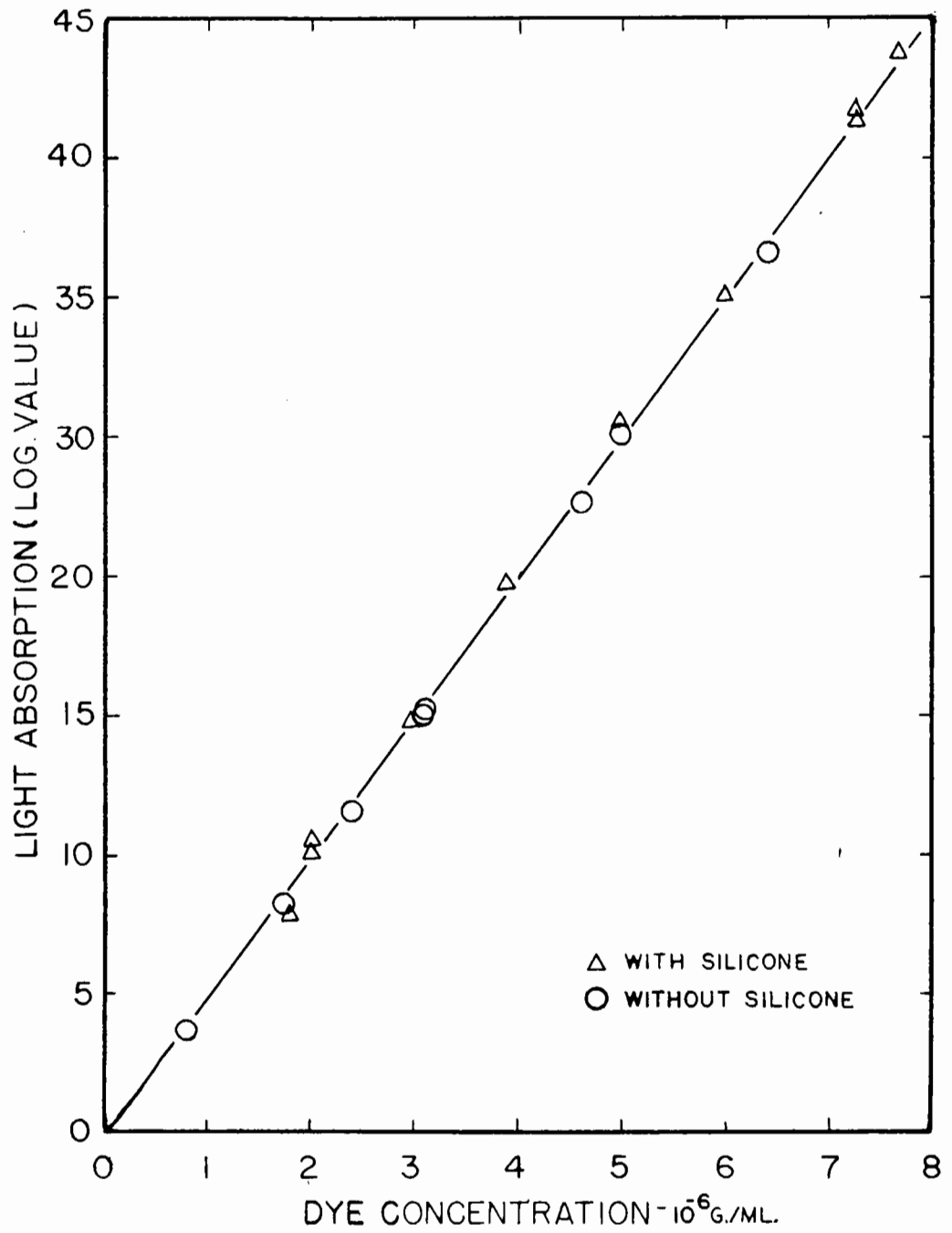


Fig. 15. Calibration Curve for Dye Concentration

accuracy of the method a one inch microscope slide was oiled and inserted into the spray. Examination under a microscope revealed the presence of an appreciable number of drops under five microns diameter, even though the work of Geist et al. (67a) predicts low impaction efficiencies. As previously mentioned the presence of these small drops indicates that the collection efficiency of the larger drops was good. Due to the fact that the total weight of the spray contained by the smaller drops is negligibly small, the error incurred in sampling is insignificant. It should be noted that coagulation of the spray drops under the silicone oil is not undesirable and must occur in order to obtain an appreciable sample.

Throughout the experimental procedure, extensive care was taken to obtain accurate results, and duplicate analyses agreed to within 3%, on an evaporation basis.

##### 5. AIR VELOCITY IN SPRAYS

The determination of the air velocity in a droplet-laden system is extremely difficult. Since there is no known method of direct measurement, the pertinent indirect approaches were considered.

Venezian (254) reported that the air velocity profile upstream of a centrally located pneumatic nozzle in a cylindrical spray column remained unchanged when low water flow rates were used with certain nozzles (Spraying Systems Co., 1/4 JN No. 12 and 22B). In other words, the presence of a low water feed rate had no effect on the upstream, air-velocity pattern. This suggested that air velocities which were determined with the

discharge of only atomizing air from the nozzle could be applied to actual spray conditions. A standard pitot tube and a special wedge-shaped probe developed by Stachiewicz (224) were used to measure the air velocities under conditions of no water flow. (Photographs of these probes are shown in Fig. 16. The velocity profiles obtained were similar to those reported in the literature (4, 6, 28)).

However, these results were obtained during unrealistic operation of the pneumatic nozzles. Small drops are considered to be excellent tracers for air velocities in turbulent systems (44, 246). Consequently a better method of estimating the air velocities in the spray is the determination of the intercept on the velocity axis of the drop diameter-drop velocity graphs (Fig. 5-13). The main source of error is the actual determination of the drop velocities in this range. As the terminal settling velocity of spray drops is extremely low (172, 175), the absolute drop velocities approach that of the air stream at appreciable distances from the nozzle. The air-velocity profiles obtained nearer the nozzle are in agreement with those presented in the literature (4, 6, 28).

## 6. AIR TEMPERATURE IN SPRAY

The measurement of the drying air temperature is very important as the driving force, i.e., temperature difference, for heat transfer, must be known accurately. Different methods of obtaining the correct air temperatures were used for cross-current and co-current air flow.

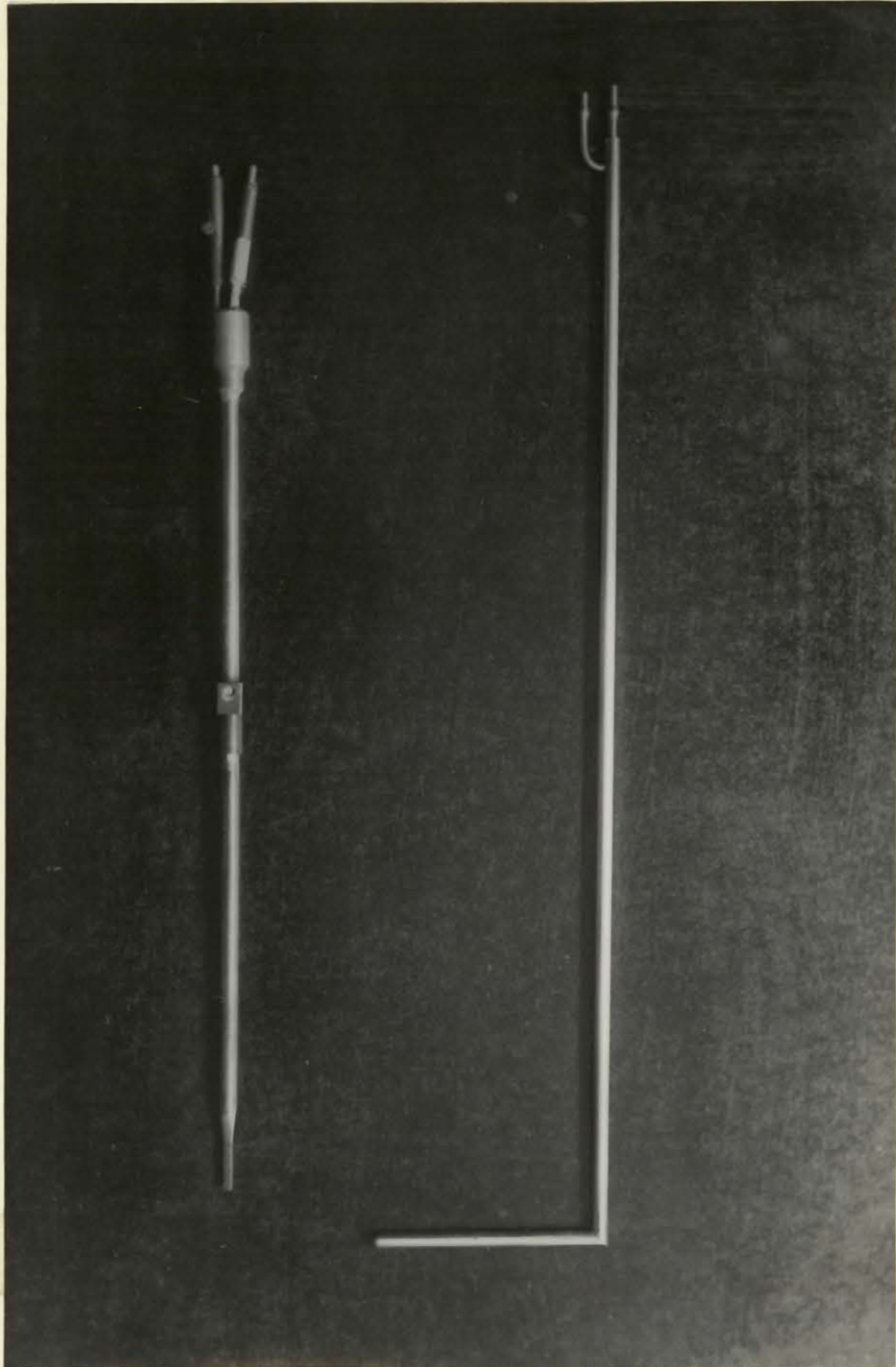


Fig. 16. Probes for Measuring Air Velocities

a) Cross-Current Air Flow

No difficulty was experienced in measuring the temperature of the drying air entering the horizontal sections of the drying chamber. Standard recalibrated mercury thermometers of range 0 to 150°C, in 1 C.°-divisions were used. However, the determination of the exit air stream temperature was complicated by the entrainment of the smaller spray drops. The very low relative velocity between the drops and the air, combined with a low absolute air velocity (circa 5 to 10 ft./sec.) made the protection of the thermometer bulb very difficult. Two concentric aluminum foil shields proved to constitute the most successful design. The inner shield was of 0.4 in. diameter and was designed to reduce radiation effects from the cold surface of the outer shield. This shield was considerably larger (diameter 0.9 in.) and extended 1 in. beyond the bulb of the thermometer. The curved lip of the top edge was designed to prevent the water drops from accumulating and falling past the unprotected side of the thermometer. A sketch of the shield is given in Fig. 3. Mercury thermometers of range 0°C. to 110°C. calibrated in 1 C.°-divisions were used.

The possibility of using a thermocouple instead of the thermometer was investigated, since it would have offered the advantage of reaching equilibrium within a very short time. However the results obtained with thermocouples showed wide fluctuations and inconsistencies, which were attributed to the periodic wetting of the thermocouple junction by small spray drops. The thermal inertia of the mercury thermometer bulb was large enough to eliminate such transient effects.

### b) Co-Current Drying Air Flow

The technique used to measure the air temperatures for this type of flow was very similar to that used by Dlouhy (40). A somewhat larger aluminum foil shield of diameter 0.8 in. and length 2.5 in. was used (Fig. 3). Also the insulation of the thermometer stem was improved by means of a double-jacketed glass cover. The whole device was attached to a transite plug designed to fit the sample port and the arrangement was such that the movement required to obtain a temperature traverse was possible. An accurate 0 to 100°C. mercury thermometer, calibrated in 0.1 C.-divisions was used for most of the temperature readings but for higher temperatures, a standard 0 to 150°C. mercury thermometer was used.

### c) Sources of Error

In order to ascertain the effect of the shield on the thermometer reading, calibration tests were performed using droplet-free air streams. The results indicated that the thermometer recorded temperatures to within 1°F. of the actual value. The extension of this to actual spray conditions is much more difficult. A quantitative mathematical analysis is impossible but conduction losses to the stem are very low. The criterion by which the usefulness of the shields should be evaluated is the ability to obtain reproducible results, while the accuracy of the results can be deduced from heat balances.

It should be noted that the formation of a wake or eddy by the shielded thermometer promotes an air flow pattern which greatly increases

the heat transfer to the thermometer bulb. In this wake a region of low pressure occurs on the down-stream side of the shield with the point of lowest pressure at the open end. The drying air flows around the shield to the thermometer and discharges at the open end. The reversal in the flow direction of the air separates the spray drops due to their kinetic inertia.

#### 7. DETERMINATION OF THE AIR HUMIDITY

The change in the absolute humidity of the air during the drying of a spray is usually small (circa 0.005 to 0.015 lb. water/lb. dry air in this work) and so considerable accuracy was required in measuring the absolute humidities.

There are several experimental methods of measuring the air humidity, and these can be conveniently divided into three classes. Firstly, there are those methods that depend on a change in the physical properties of substances in contact with wet air. The various types of hygrometers, thermal conductivity measuring devices for wet air, conductance cells made of palladium wires coated with lithium chloride are examples of this class. Secondly, there are absolute methods whereby the water vapour in the air sample is removed by a chemical reagent and the water present is determined either gravimetrically or by recording a change in volume. Thirdly, the possible equilibrium conditions between water and air provide two widely used techniques, known as the dew-point and wet- and dry-bulb methods, respectively.

The accuracy with which the air humidity can be determined using hygrometers was inadequate for the present study. Similarly, the more refined techniques based on physical changes suffer from the additional disadvantages of a narrow range of application and necessity of frequent calibration.

Both of the remaining classes held distinct promise, and so were thoroughly investigated. Volumetric and gravimetric absolute methods were developed and tested against the dew-point and wet-and-dry bulb methods.

a) The Gravimetric Method

In this method the weight of water vapour in an air sample was measured by means of absorption by molecular sieve pellets which were suspended from a quartz spiral. The mass of dry air remaining was then calculated from temperature and pressure measurements. Unfortunately, the molecular sieve pellets absorbed carbon dioxide gas as well as the water vapour in the air sample, and so the gravimetric method could only be applied to air samples from which the carbon dioxide had been previously removed.

(i) Equipment

The apparatus consisted of a 1.5-in. internal diameter glass tube, 50 in. long, fitted with ground-glass joints at both ends. A cross bar was sealed into the top joint so that the quartz spiral could be suspended. This spiral had been previously calibrated and had a sensitivity of 0.08

cm./mg. with a total load capacity of 400 mg. Fourteen 1/16-in. pellets (350 mg.) of molecular sieve type 4A were suspended in a kite-tail arrangement from the bottom of the spiral by means of a very fine copper wire. Changes in the length of the spiral were measured by means of a cathetometer which enabled the weight of the pellets to be determined to 0.1 mg. A mercury manometer made from capillary tubing was attached to the main glass column. The temperature of the air in the column was measured by a mercury thermometer of range 0 to 150°C., calibrated in 1 C.-divisions. This thermometer was suspended from a steel spring which fitted into the bulge of the upper ground glass joint. To provide hot air for the regeneration of the molecular sieve pellets, a nichrome heating wire was wrapped around the lower part of the column. Stainless steel wool was placed inside the bottom part of the column to promote the rapid transfer of heat from the hot wire to the air in the column. A schematic diagram of the equipment is shown in Fig. 17.

(ii) Procedure

Before each adsorption test, the water vapour remaining in the molecular sieve pellets from the previous test had to be removed. In order to achieve this, clean air was passed through a tube containing calcium chloride and into the bottom of the sampling column. The air was heated to approximately 200°C. as it rose slowly through the steel wool. Complete regeneration of the molecular sieve pellets was achieved in about half an hour. The column was then completely evacuated by means of a Cenco-Hyvac vacuum pump capable of reducing the pressure in the vessel to 0.1 mm. Hg

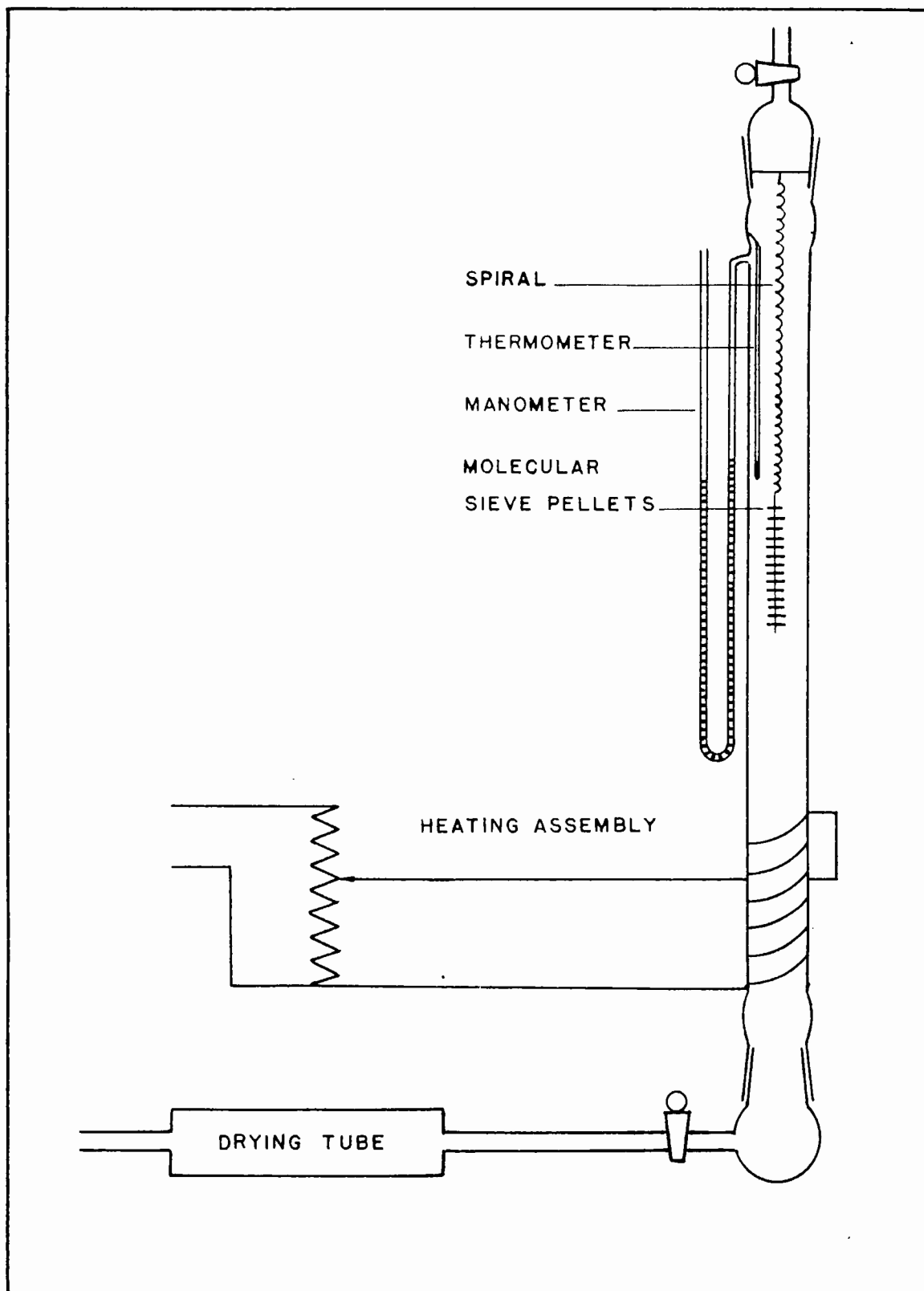


Fig. 17. Schematic Diagram of the Gravimetric Method of Humidity Measurements

abs., and allowed to cool to room temperature. The length of the quartz spiral was read to within 0.01 mm. with a cathetometer. Due to rotational effects, both ends of the spiral had to be read to obtain the correct length.

The sample of air was then admitted by opening the top stopcock. It was found that at least eight hours were required for complete adsorption of the water vapour in the air. When no further extension of the spiral was noted over a period of four hours, the length of the spiral was again read. The temperature and pressure of the dry air remaining in the column were also recorded. Atmospheric pressure was measured with a Welch Scientific barometer installed in the laboratory. The absolute humidity of the air sample is simply the ratio of increase in weight of the molecular sieve pellets to the weight of drying air remaining in the vessel. The latter weight was calculated from the ideal gas law.

#### b) The Volumetric Method

The principle of this method and that of an Orsat Gas analyzer are identical. The water vapour in a sample of air was removed by contact with magnesium perchlorate and the operation followed volumetrically in a gas burette.

##### (i) Equipment

Measurement of the air sample was accomplished in a precision Mine Air Gas burette (Fisher Scientific Company No. 10-60062). The

lowest and narrowest section (94 to 100 ml.) was graduated in 0.05 ml. divisions and so volume changes of 0.01 ml. could be detected. The burette was surrounded by a water jacket in which a comparison tube was also installed. This comparison tube was connected through a check valve and levelling tube to the burette. From the burette the air could be passed by raising the levelling bulb through a U-tube containing magnesium perchlorate into a self-sealing mercury reservoir. This mercury seal consisted of two chambers so constructed that the air could be passed into the lower compartment and so force the mercury into the upper section. When the air was sucked back into the burette, the mercury flowed back into the lower chamber. A fixed level of mercury in the lower chamber was obtained by means of a pilot light circuit with contacts sealed into the mercury chamber. Magnesium perchlorate was chosen as the dehydrating agent in the U-tube as it does not absorb carbon dioxide or any gas other than water vapour. It also possesses a high drying capacity.

The U-tube and mercury seal were immersed in a constant temperature water bath. Water from the bath was circulated rapidly through the water jacket surrounding the burette by means of an 1/100-h.p. Eastern Industries Midget centrifugal pump. The temperature control was found to be better than 0.5°F. The comparison tube placed in the water bath served as a safeguard against a change in atmospheric pressure or water bath temperature, as any change in these variables affects both the gas in the burette and comparison tube equally. A photograph of the equipment is shown in Fig. 18.

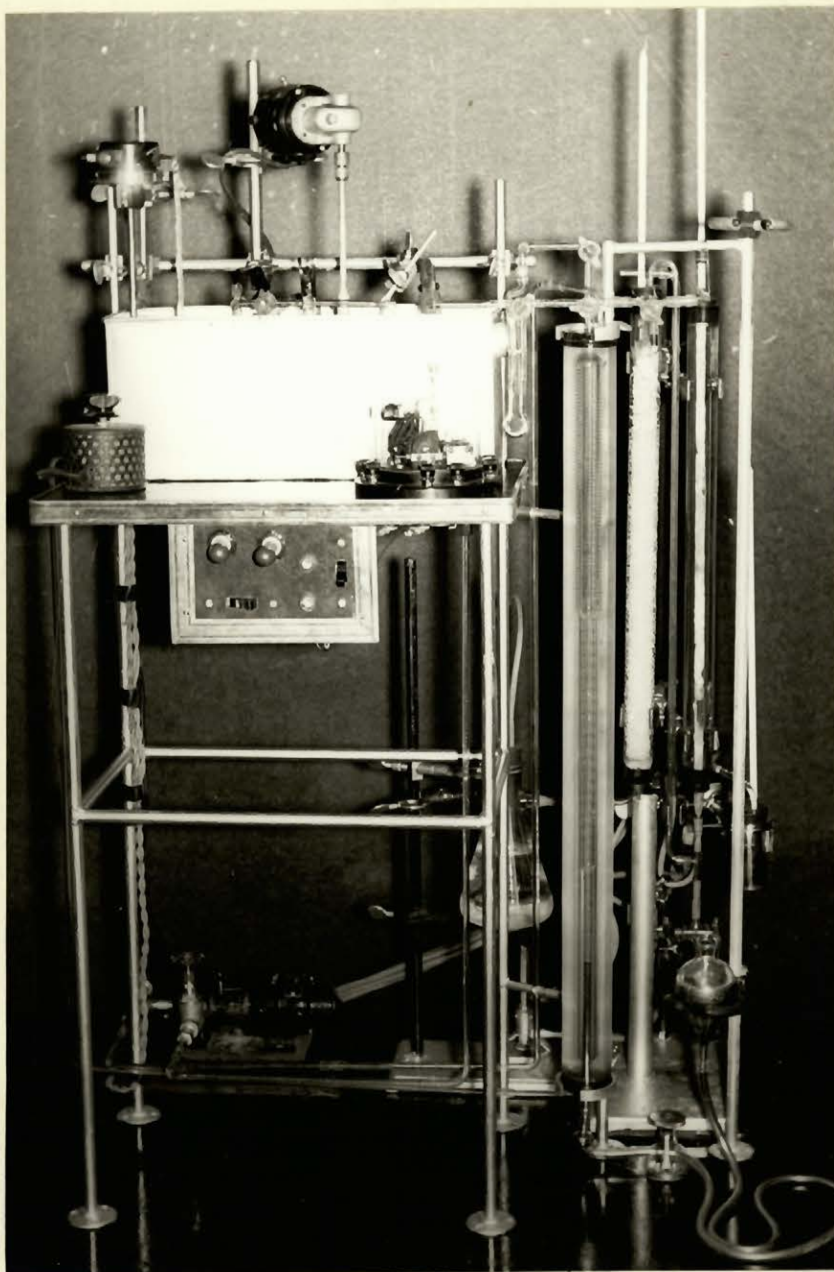


Fig. 18. The Volumetric Method of Humidity Measurements

(ii) Procedure

The water bath was first brought up to a temperature above the dew point of the air sample and fifteen minutes allowed for steady conditions to be reached. During this time, the water was circulated through the jacket so the burette and comparison tube would be at the same temperature as the water bath, and a check on the level of mercury in the mercury seal made. The pressure of the air in the comparison tube and U-tube were equalized to that of the atmosphere. As soon as this condition was achieved, the levelling tube was connected to the comparison tube for the remainder of the test.

Any residual air in the gas burette was expelled and the sample of air was drawn in slowly from the collection bottle with the mercury levelling bulb. The sample was allowed to reach constant temperature before its pressure was balanced with that in the comparison tube, and the volume read. The air was then passed slowly at about 1 ml./sec., through the U-tube into the mercury seal chamber and drawn back to the burette at approximately the same rate. Control of the level of the mercury seal was effected through the pilot light. After the pressure of the air sample in the burette had been readjusted to that in the comparison tube the new volume was recorded. Two or three passes through the magnesium perchlorate U-tube were found to be adequate. The absolute humidity of the air was then obtained from the following formula:

$$H = (\text{change in volume}/\text{final volume})(18/29) \quad \dots(167).$$

c) The Dew Point Method

A 400-ml. round lipped beaker served as the sample container. This beaker was sealed with a rubber stopper through which a thimble and two tubes were inserted (Fig. 19). The tubes served as inlet and exit sampling ports while the thimble provided the polished surface. Good heat transfer to the thimble and a bright surface are essential and so the thimble was made of copper and chrome-plated.

Control of the temperature of the thimble was accomplished by circulating water through it at a high flow rate. A precision mercury thermometer 0 to 100°C. with 0.1 C.°-subdivisions was used to measure the water temperature. Two copper coils immersed in large beakers were included in the water circuit together with a 1-litre Florence flask serving as a reservoir. By filling the beakers with melting ice or hot water the temperature of the water in the thimble could be regulated as desired.

The residual air in the instrument was displaced by flushing for about five minutes before admitting the sample of air. The temperature of the thimble was then reduced at the rate of about 1°C./minute. As soon as the first signs of moisture appeared on the thimble the cooling was stopped and the temperature recorded. A low-power cathetometer microscope was used to observe the highly-polished surface and the appearance of moisture was easily detected. The temperature of the circulating water was then slowly raised, and when the deposited moisture disappeared the temperature was again recorded. The dew point was taken as the mean of



Fig. 19. The Dew Point Method of Humidity Measurements

the two temperatures and the humidity of the sample calculated from the formula:

$$H = p_s / (P - p_s) \quad (18/29) \quad \dots(168)$$

where  $p_s$  - the vapour pressure of water at the dew point in mm. Hg;

$P$  - total pressure of air sample in mm. Hg.

d) The Wet and Dry Bulb Method

The U-tube arrangement shown in Fig. 20 was used and the air entered in one of the arms where the dry-bulb temperature was measured with a mercury thermometer. Another thermometer with its bulb wrapped in a cloth wick was placed in the second arm. The other end of the wick dipped through a hole in the bottom of the U-tube into a 100-ml. Erlenmeyer flask containing distilled water. This enabled the wet-bulb temperature to be recorded.

The air was passed through the U-tube at a constant rate for as long as possible, the limiting factor being the size of the air sample. However five to ten minutes were found to be satisfactory. The equipment was usually connected in series with the dew point apparatus so that the same air used in flushing the sample beaker could be used in obtaining equilibrium conditions. When steady state conditions were obtained, both thermometers were read and the absolute humidity determined from a water - air humidity chart (152, 171, 257).

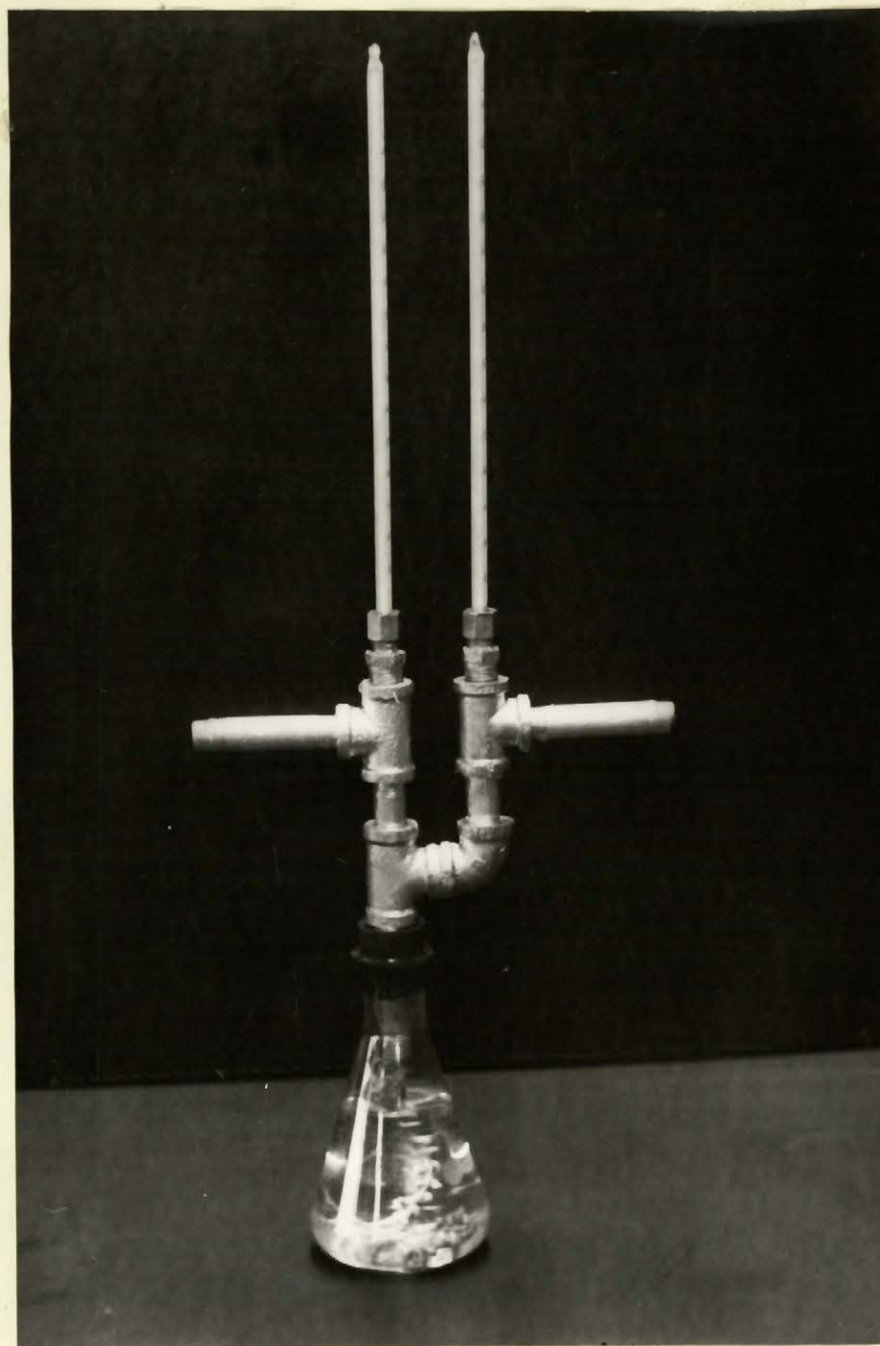


Fig. 20. The Wet- and Dry-Bulb Method of Humidity Measurements

e) Comparison of Methods

To test the accuracy and precision of the various methods of humidity measurement, air of known humidity was prepared by several different methods. These included addition of water to bone-dry air made from bottled oxygen and nitrogen, and saturation of room air after carbon dioxide removal. Removal of carbon dioxide was required if the gravimetric method was to be used as the molecular sieve pellets adsorbed carbon dioxide. Tests using partially saturated room air were also performed.

The synthetic air was prepared in a 20-litre glass jar. This jar was flushed thoroughly with nitrogen from a gas cylinder and then evacuated to 79% of the original pressure. Oxygen was then admitted until the pressure was the same as it was originally. This technique enabled absolutely dry air (without carbon dioxide and the minor gases) to be prepared. A small glass capsule was used to introduce a known weight of water into the vessel. The glass capsule was weighed, distilled water added from a microsyringe and then sealed and reweighed. The capsule was placed in the glass jar before the dry air was prepared. Release of the water contained by the capsule could be effected by shaking the glass jar until the thin glass capsule broke. Tests showed that all of the water evaporated within one hour. Expulsion of the air from the glass jar was effected by inflating a thin rubber balloon which was suspended in the vessel.

The carbon dioxide-free, saturated air was prepared by bubbling

air from the laboratory compressor through packed towers containing warm potassium hydroxide solutions. The air was then passed counter-currently to cold distilled water through an absorption column. At this point, the final adjustment in the humidity was made by passing the air through a column packed with glass wool and surrounded by a water jacket. A mercury thermometer graduated in  $0.1^{\circ}\text{F}$ .-divisions was used to measure the temperature of this jacket. The air so prepared was stored over oil in an aluminum gasometer or sucked into the glass jar used in the previous method.

Partially saturated room air was obtained by drawing air through a water bubbler into the glass jar. The humidity of the air so produced could be varied by changing the rate and time of bubbling as well as the temperature of the water in the bubbler.

The results of the tests performed using the prepared samples of air described above are given in Appendix III. It should be noted that the most accurately prepared air was the synthetic air as all the required measurements could be made with accuracies of  $0.1\%$  or better.

On the other hand, a change in the temperature of one Centigrade degree in the water jacket used for the preparation of the air samples corresponded to a change of  $6\%$  in the humidity of the air. Hence the accuracy of the methods is assessed primarily from the tests performed using the synthetic air. The comparison of the four methods given in Table IV clearly indicates why the volumetric method was selected.

TABLE IV  
COMPARISON OF HUMIDITY-MEASUREMENT METHODS

<u>Method</u>	<u>Gravimetric</u>	<u>Volumetric</u>	<u>Dew Point</u>	<u>Wet- and Dry-Bulb</u>
Humidity range obtainable	0.000 to 0.025	0.000 to 0.040	0.005 to 0.030	0.005 to 0.030
Humidity change detectable	0.0002	0.0002	0.0004	0.0010
Time required for test	6 to 24 hr.	20 min.	20 min.	10 min.
Sample used	1000 ml.	150 ml.	1500 ml.	several litres
Ease of operation	Time consuming	Very easy	Hard on eyes	Very easy
Main source of error	Measurement of spiral extension	Balance of pressures in burette and comparison tube	Detection of the deposition of moisture	Establishment of equilibrium conditions

f) Sampling Techniques

One of the most important and difficult operations is the collection of a representative sample of the air from the drying chamber. Again, the method of sample collection varied with the flow patterns of the drying air.

(i) Cross-Current Drying Air Flow

Due to the extremely fine mist encountered in this type of flow an impact separator was used to remove the spray drops from the air. The sampling device consisted of a small 1-in. diameter glass bottle filled to a depth of one inch with a non-volatile silicone oil (Fig. 21). An empty glass tube, the end of which was attached to a Weatherhead compression fitting, was inserted through the rubber stopper in the bottle. The end of the tube dipped below the silicone oil and a small pad of glass wool was inserted into the Weatherhead cap. When the air from the spraying chamber was drawn rapidly through the inlet tube into the bottle the water drops were impacted on the glass wool and thus separated from the air. An exit tube was also inserted into the rubber stopper and this was connected to a sample bottle of the desired size. The effectiveness of this method depends to a large extent on the velocity of the air entering the tube and the samples were therefore taken as quickly as possible.

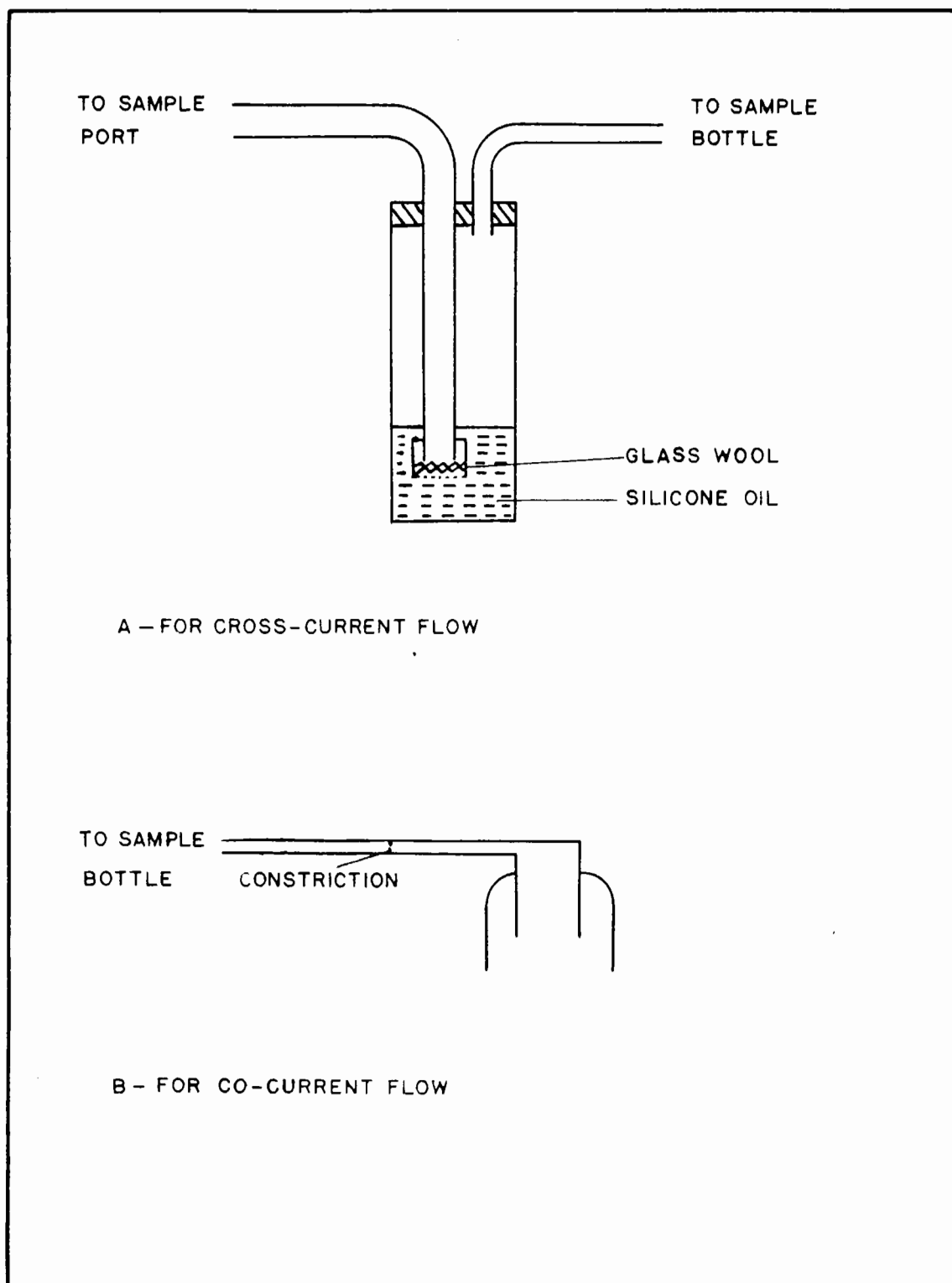


Fig. 21. Sampling Devices for Humidity Measurements

(ii) Co-Current Drying Air Flow

For this case it was found to be possible to obtain a representative sample by withdrawing the drying air counter-currently to the direction of the air flow. The design of the sampling device is shown in the sketch in Fig. 21. The outer tube surrounding the sample tube prevented the spray drops from wetting the surface of the sampler. A marked decrease in the sample air velocity was achieved by using an expanded section at the sample point. Control of the flow rate was maintained by means of a constriction incorporated into the sampling tube. An evacuated sample bottle was connected to the exit of the sample tube.

## II. EVAPORATION WITH CROSS-CURRENT FLOW

The use of a cross-current flow of drying air to measure the evaporation rates from a spray at small distances from the nozzle appeared to offer many advantages. By guiding the air at right angles to the vertical spray through horizontal compartments, in a specially constructed drying chamber, it was expected that better contact and more rapid penetration of the spray by the drying air could be achieved than in conventional co-current flow. The increase in the humidity of the drying air from each compartment would provide an accurate and simple method of determining the rate of evaporation at various distances from the nozzle. Undue deformation of the spray could be avoided or minimized by using drying air flow rates considerably less than those usually encountered in co-current drying systems. Finally, it was expected that by working at low evaporation rates, experimental spray drop velocity data obtained separately under conditions of negligible evaporation in a lucite column, could be used for the calculation of the heat and mass transfer rates occurring in the actual equipment.

### 1. EQUIPMENT

To promote good contact between the drying air and the spray, the cross-sectional area available for the air flow had to conform with the shape of the spray. As the initial spray shape is conical, a trapezoidal drying chamber consisting of six horizontal sections was constructed. The spray passed vertically downward through openings cut in

the partitions between the sections and was collected in a cylindrical air-tight tank under the spray chamber. A better understanding of the arrangement of the equipment can be obtained by consulting the accompanying photograph and drawing given in Fig. 22 and 23. The control panel accommodated most of the control valves and metering instruments, thus greatly facilitating the operation of the equipment. It also permitted the immediate detection of any change in the operating conditions which occurred during a test.

a) The Spray Chamber

As was previously mentioned, the spray chamber was constructed in the form of a trapezoidal box, with the cross-sectional area available for the flow of the drying air in the shape of a trapezium with parallel sides of 2 and 12 inches, spaced 36 in. apart. The overall length of the box was 30 in. These measurements refer to the internal dimensions of the chamber. Adequate insulation was provided by covering the  $\frac{1}{2}$ -in. plywood used for the construction of the box with layers of  $\frac{1}{4}$ -in. transite and  $\frac{1}{8}$ -in. arborite on the inside and outside respectively. These layers were glued together with Sauereisen cement and fastened with  $\frac{1}{8}$ -in. steel bolts, thus producing a rigid wall with the excellent insulating properties of transite, which is a compressed asbestos board.

Dividing partitions of transite were fitted into the chamber so that six horizontal sections of height 3 in., 3 in., 4 in., 4 in., 4 in., and 6 in. respectively, were formed. All crevices and corners were made water-tight with Gasket-Goo, and several coats of high temperature aluminum



Fig. 22. The Cross-Current Flow Equipment

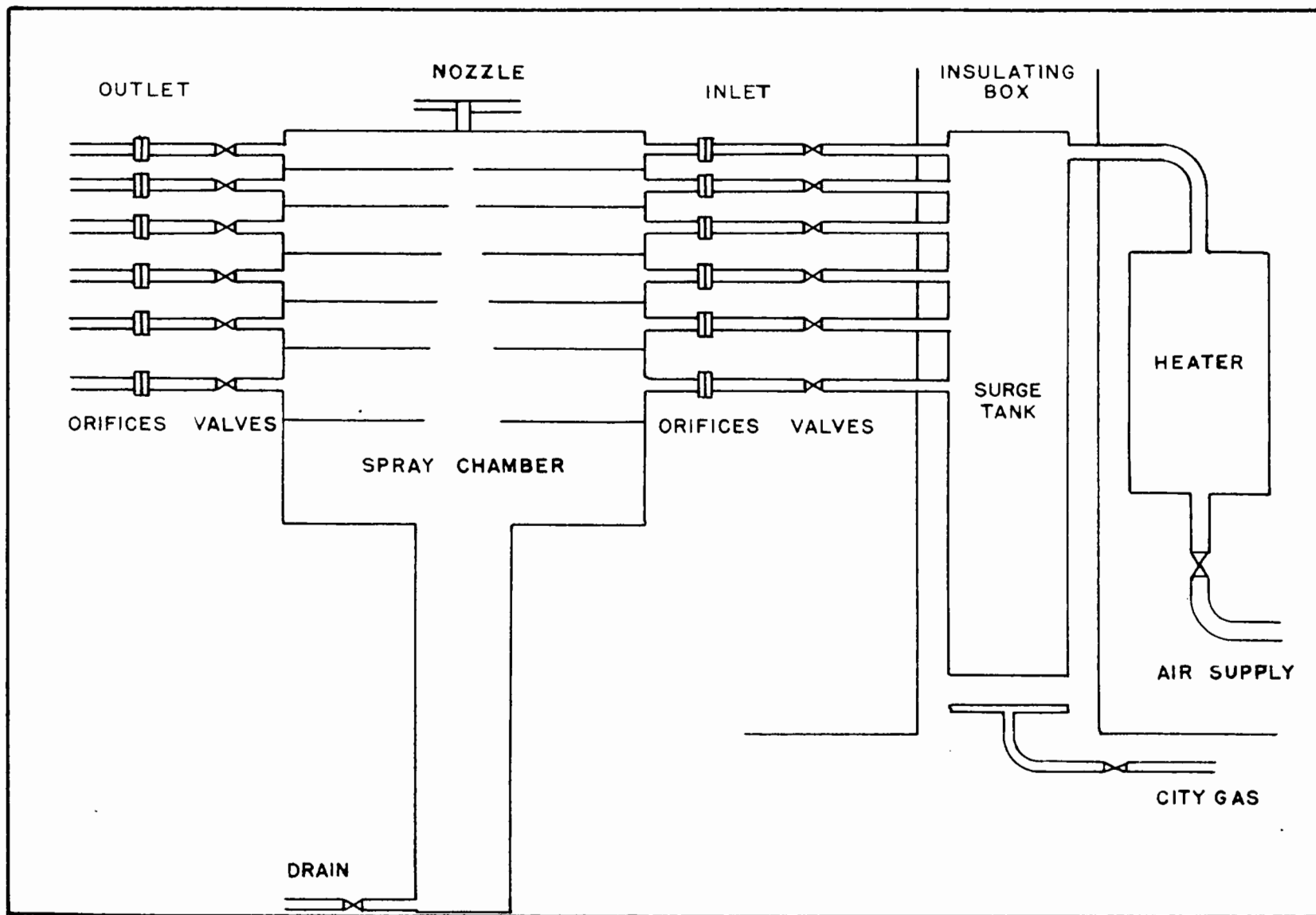


Fig. 23. Schematic Diagram of the Cross-Current Flow Equipment

paint were applied until the transite became impervious to water. Circular holes were cut in these partitions so as to permit the spray to pass downward from the nozzle which was installed in the centre of the top surface of the chamber. The cylindrical drainage tank was fastened into the bottom of the chamber and this served as a reservoir for the unevaporated water which accumulated during a test.

Visual observation of the spray was achieved by installing a 9-in. x 30-in. x  $\frac{3}{4}$ -in. pyrex glass plate in the front sloping side of the spray chamber. This was sealed into position by means of a supporting frame and a rubber gasket. Inlet and outlet drying air ports were cut in the centre of the ends of each of the horizontal sections. Standard  $\frac{1}{2}$ -in. brass nipples were fastened into these ports with locknuts and rubber gaskets. Another pair of ports was cut in the front side of each horizontal section to permit the insertion of thermometers for measuring the drying air temperature. Finally, six more ports were cut in the back of the chamber in the centre of the horizontal section to permit the entry of the thermocouple probes used for measuring the spray temperatures. The physical measurements of the six horizontal sections comprising the drying chamber are presented in Table V, together with the corresponding data for the drying chamber used in the co-current flow tests which are described later.

#### b) Drying Air Circuit

A Nash Hytor Compressor type L3, driven by a 15-H.P. Tamper motor, was used to supply the drying air. In this type of compressor, the cooling

TABLE V  
COMPARISON OF SPRAY CHAMBERS

Section	Distance from Nozzle in.	Cross-Sectional Area Available for Flow		Location of Sampling Ports (in. from Nozzle)		
		Cross-Current Equipment - ft. <sup>2</sup>	Co-Current Equipment - ft. <sup>2</sup>	Cross-Current Equipment	Co-Current Equipment	
					Pneumatic Nozzles	Pressure Nozzles
1	0-3	0.050	0.350	1.5	-	0.5
2	3-6	0.066	0.350	4.5	4.0	4.5
3	6-10	0.115	0.350	8.0	8.0	8.5
4	10-14	0.0147	0.350	12.0	12.0	12.5
5	14-18	0.0175	0.350	16.0	16.0	16.5
6	18-24	0.304	0.350	21.0	20.0	20.5

water comes into direct contact with the compressed air. Due to the low water temperature available, the humidity of the drying air seldom exceeded 0.012 lb. water/lb. dry air. Control of the air flow rate was achieved by means of a 2-in. globe valve installed on the by-pass line across the compressor. The compressed air was metered by means of a Schutte and Koerting rotameter No. 7A-25, and passed through an electric heater. This heater was constructed in the laboratory and contained six 1000-watt elements. A wide range of air temperatures was obtained by incorporating individual switches on the heaters, while automatic control was provided by means of a United Electric thermoregulator type E8N installed on the last element.

From the heater, the air was passed to a 20-gallon surge tank in which the flow and temperature fluctuations could easily be removed. This tank was maintained at any desired temperature up to 300°F. by two gas ring burners located beneath it. The hot flue gases from these burners rose slowly in a transite box which was built around the surge tank.

Separate feed lines of  $\frac{1}{2}$ -in. brass pipe were installed to convey the hot air from the tank to each of the six sections in the drying chamber. A globe valve, a calibrated orifice connected to vertical water manometers, and a thermometer were included in each of the feed lines for the purpose of controlling and metering the air flow. The exit air flow from the horizontal sections of the drying chamber was similarly controlled and metered. Here the measuring procedure was simplified by the fact that the downstream pressure was always atmospheric. Brass piping and fittings

were used in all of the lines. Insulation of the feed lines was accomplished by building a box around the lines and filling the box with vermiculite.

c) Atomizing Nozzle Circuits

Two types of atomizing nozzles were used in this investigation: an internal-mixing, pneumatic nozzle - (1/4) JN No. 12 - and a hollow-cone pressure nozzle - (1/4) LNN SS No. 1 - both supplied by Spraying Systems Co., Chicago. The operating characteristics and capacity for these two nozzles were shown in Table III. The feed to the nozzle was usually tap water but a feed tank was incorporated, from which a dilute solution of the red dye could be sprayed. Two strainers were installed in the feed line so as to remove any solid particles that might plug the narrow passages in these nozzles. Control of the feed stream was established by means of a 1/4-in. globe valve. A Schutte and Koerting rotameter No. 2R was used to meter the flow while the pressure acting on the nozzle was measured with a 0 to 100 p.s.i.g. Bourdon gauge.

The air used for atomization with the pneumatic nozzle was supplied by an Ingersoll Rand compressor. Control of the atomizing air pressure on the nozzle was effected by a 1/4-in. Taylor reducing valve. The air stream was metered similarly to the liquid stream and a strainer was included in the line to ensure good operation of the nozzle. The pressure acting on the nozzle was measured with a 0 to 60 p.s.i.g. Bourdon gauge. Mercury thermometers were installed in the respective feed lines, close to the nozzle.

## 2. PROCEDURE

The operating procedure may be divided into two steps: the adjustment of the operating conditions, and the collection of the experimental data used in the calculation of the heat and mass transfer coefficients.

### a) Adjustment of the Operating Conditions

The first step in the operation of the cross-current flow dryer was the regulation of the air streams in the horizontal sections. Consequently, the Nash Hytor compressor was started and the thermoregulator on the electrical heater set to the desired temperature. The gas ring burners under the surge tank were lighted. The control valves installed in the flow lines between the surge tank and the drying chamber were adjusted so that the flow rate of air to the individual horizontal sections would be approximately proportional to the cross-sectional area available for flow in each section. Also the valves in the exit pipes from the sections were adjusted so that the same mass of air left each section as entered it. In this way flow of uniform velocity was established in all the sections of the drying chamber. Any leak that developed at one of the many sampling ports in the equipment could be immediately detected by a discrepancy in the overall inlet and outlet flow rates.

Readings of the thermometers installed in the horizontal sections of the drying chamber were also taken. These data enabled the heat losses to be calculated. At high temperatures the heat losses assumed significant

proportions (circa 15%). As these losses were measured, the required corrections could be made.

b) Collection of the Experimental Data

Following adjustment of the drying air flow, the atomizing nozzle was put in operation. The controlling factor for both nozzles was the liquid feed rate; in the case of the pneumatic nozzle, the pressure of the atomizing air stream also required very close control, as it governs both the average droplet size and the size distribution of the spray. Whereas fine atomization can be obtained from a pneumatic nozzle at any feed rate by proper adjustment of the air pressure, no such control can be obtained from a pressure nozzle, which must be operated very close to its rated capacity (which automatically sets the pressure) if good atomization is expected.

Care was exercised in choosing the operating conditions of the nozzle so as to obtain as narrow a spray angle as possible. This reduced the possibility of the spray touching the walls of the spray chamber, and could be verified by visual observation through the pyrex glass window. Usually, there was no contact between the spray and the spray chamber for the first few sections when the pneumatic nozzle was used. Some wetting occurred after the fourth and fifth sections, and data taken in a section where wetting was observed were discarded. The pressure nozzle had a wide spray angle and consequently accurate data could only be recorded in the first three sections.

Half an hour was allowed for steady state to be established, based on the criterion that all the temperatures and flow rates remained constant for a period of 15 minutes. The following measurements of the spray and drying air properties were then taken:

### 1. Atomizing and Drying Air Streams

- liquid feed flow rate,  $q_L = W_L$  (section 1);
- liquid feed temperature,  $T_L = T_1$  (section 1);
- liquid feed pressure at nozzle,  $P_L$ ;
- concentration of red dye in feed,  $c_1$  (section 1);
- atomizing air flow rate,  $q_A = w_{a1}$  (section 1);
- atomizing air temperature,  $t_A = t_{a1}$  (section 1);
- atomizing air pressure at nozzle,  $P_A$ ;
- atomizing air humidity,  $H_{a1}$  (section 1);
- overall drying air flow rate;
- overall drying air temperature;
- overall drying air humidity.

### 2. Drying Chamber Data for each Section

- inlet drying air flow rate,  $w_{d1}$ ;
- inlet drying air temperature,  $t_{d1}$ ;
- inlet drying air humidity,  $H_{d1}$ ;
- inlet drying air pressure;
- outlet drying air flow rate,  $w_{d2}$ ;
- outlet drying air temperature,  $t_{d2}$ ;
- outlet drying air humidity,  $H_{d2}$ ;
- wet-bulb temperature of outlet drying air;

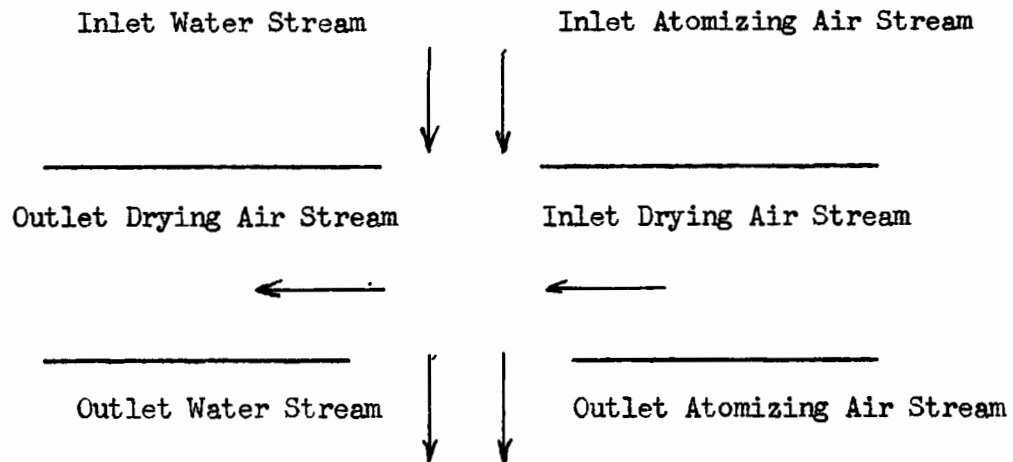
- drop size distribution of spray, and hence  $d_{vs}$ ;
- concentration of red dye in spray,  $c$ ;
- inlet spray temperature,  $T_1$ ;
- outlet spray temperature,  $T_2$ .

### 3. CALCULATIONS

#### a) Analysis of Flow Pattern

The careful adjustment of the drying air flow streams prior to spraying enabled the effect of the atomizing streams on the flow pattern to be determined. Fig. 24 illustrates the various flow streams entering and leaving each of the horizontal sections of the drying chamber. The outlet drying air flow rates measured by the calibrated orifices had to be corrected for the entrainment of the spray drops by the drying air. The effect of entrainment is to increase the density of the fluid and this causes an increase in the pressure drop across the metering orifice. The correction procedure consisted of changing the measured exit flow rates by a correction factor which was simply the ratio of the overall measured exit flow rates to the overall inlet flow rates.

For the runs with the pneumatic nozzle, it was observed that the outlet drying air stream,  $w_{d2}$  (cor.), was nearly always greater than the corresponding inlet stream,  $w_{d1}$ . This was attributed to the redistribution of the atomizing air stream ( $w_{a1}$  for Section 1). There was practically no change in the drying air streams for the pressure nozzle tests.



Legend

Inlet Water Stream -  $W_1$  lb./hr.  
 $T_1$  °F.

Inlet Atomizing Air Stream -  $w_{a1}$  lb./hr.  
 $H_{a1}$  lb.  $H_2O$ /lb. air  
 $t_{a1}$  °F.

Inlet Drying Air Stream -  $w_{d1}$  lb./hr.  
 $H_{d1}$  lb.  $H_2O$ /lb. air  
 $t_{d1}$  °F.

Outlet Drying Air Stream -  $w_{d2}$  lb./hr.  
 $H_{d2}$  lb.  $H_2O$ /lb. air  
 $t_{d2}$  °F.

Outlet Water Stream -  $W_2$  lb./hr.  
 $T_2$  °F.

Outlet Atomizing Air Stream -  $w_{a2}$  lb./hr.  
 $H_{a2}$  lb.  $H_2O$ /lb. air  
 $t_{a2}$  °F.

FIG. 24. Schematic Diagram of Flow Pattern in Any Section of Cross-Current Spray Chamber

Before any material or heat balances can be made, several average temperatures must first be defined:

$$t_1' = (w_{d1}t_{d1} + w_{a1}t_{a1})/(w_{d1} + w_{a1}) \quad \dots(169)$$

$$t_2' = (w_{d2}(\text{cor.})t_{d2} + w_{a2}t_{a2})/(w_{d2}(\text{cor.}) + w_{a2}) \quad \dots(170)$$

$$t_{av} = (t_1' + t_2')/2 \quad \dots(171)$$

$$T_s = (W_1T_1 + W_2T_2)/(W_1 + W_2) \quad \dots(172)$$

For the pneumatic nozzle runs, the atomizing air was at approximately 85°F. and usually of humidity 0.01 lb. water per lb. dry air, and was considered to be adiabatically cooled to saturation at 71°F. and humidity of 0.014 lb. water per lb. dry air in the first section. This operation and the establishment of the spray at the wet-bulb temperature of the drying air stream were assumed to occur simultaneously. It should be noted that the mass of water evaporated by this process was negligible compared to that occurring during the subsequent drying.

The determination of the spray drop velocities by means of high speed cinematography of the drops was not possible in the drying chamber proper. However, drop velocity data obtained under conditions of practically no evaporation in a separate lucite column appeared to apply validly to the cross-flow tests as the evaporation occurring in the latter was relatively low. A correction for the different flow patterns in the lucite column and the cross-current flow dryer was required, as the downward flow of air in the lucite column was appreciable. The most logical approach was to consider that the spray drops penetrated the cross-current

drying air stream at an absolute velocity equal to the difference between the measured velocities and the overall downward air velocity in the lucite column. Consequently in all calculations involving the spray drop velocities in the cross-flow equipment, the air velocity was deducted from the drop velocities determined in the lucite column.

b) Material and Enthalpy Balances

A material balance on any section of the drying chamber yields:

$$W_1 - W_2 = w_{d2}(\text{cor.})H_{d2} + w_{a2}H_{a2} - w_{d1}H_{d1} - w_{a1}H_{a1} \dots(173)$$

Similarly a complete enthalpy balance can be written using a temperature datum of 32°F. for liquid water:

$$\begin{aligned} & w_{d1} \int_{32}^{t_{d1}} (C_p) dt + w_{d1} H_{d1} (h_g)_{t_{d1}} + w_{a1} \int_{32}^{t_{a1}} (C_p) dt + w_{a1} H_{a1} (h_g)_{t_{a1}} + \\ & W_1 (h_f)_{T_1} = w_{d2}(\text{cor.}) \int_{32}^{t_{d2}} (C_p) dt + w_{d2}(\text{cor.}) H_{d2} (h_g)_{t_{d2}} + \\ & w_{a2} \int_{32}^{t_{a2}} (C_p) dt + w_{a2} H_{a2} (h_g)_{t_{a2}} + W_2 (h_f)_{T_2} + \text{heat losses} \quad \dots(174) \end{aligned}$$

where  $h_f$  - enthalpy of liquid water with datum of water at 32°F., (B.t.u./lb.);

$h_g$  - enthalpy of water vapour with datum of water at 32°F., (B.t.u./lb.).

From the above equations it is evident that the heat,  $Q$ , transferred to the spray by the air may be calculated by the following equation:

$$Q = (W_1 - W_2)(h_g)_{t_{av}} + W_2(h_f)_{t_2} - W_1(h_f)_{t_1} \quad \dots(175)$$

The transfer of heat calculated by this equation was used for the subsequent calculation of the heat and mass transfer coefficients, while the change in mass of the spray for a given section was calculated from the increase in humidity of the drying air in that particular section, i.e., equation 173.

### c) Heat Transfer Coefficients and Nusselt Numbers

As the properties of the drying air were known only at the inlet and outlet of each section, it was impossible to obtain the rate of change of its temperature or humidity in the spray. However the average values of these properties can be determined and used in the calculation of the heat and mass transfer coefficients.

The average surface area of the spray drops,  $A_s$ , in a given section of the drying chamber is a function of the mean diameter of the drops, the height of the section, the average absolute velocity of the drops and the average weight of unevaporated water.

$$A_s = [(W_1 + W_2)/2] S_w \Delta x / 3600 V_D \quad \dots(176)$$

where  $\Delta x$  - height of section, (ft.);

$V_D$  - average absolute velocity of drop of same size as Sauter mean diameter, (ft.)/(sec.).

The average absolute drop velocity was obtained from the graphs expressing the drop velocity in terms of the drop diameter for the appropriate evaporation conditions and the appropriate  $d_{vs}$ . Here the

specific surface area,  $S_w$ , was obtained from the particle count by substitution in the following formula:

$$S_w = \frac{\sum nd^2}{(\rho_L \sum nd^3/6)} = 29,400/d_{vs} \quad \dots(177)$$

where  $d_{vs}$  - Sauter mean diameter in microns.

The driving force for heat transfer is the temperature difference between the drying air and the evaporating spray and this can be calculated from the equation:

$$\Delta T = t_{av} - T_s \quad \dots(178)$$

The heat transfer coefficient for a drop of diameter,  $d_{vs}$ , was calculated by combining equations 175, 176 and 178 with the following expression:

$$h = Q/A_s \Delta T \quad \dots(179)$$

The Nusselt Number was calculated from its definition:

$$Nu = hd_{vs}/k_f \quad \dots(180)$$

Due to the small content of water vapour in the surrounding gas film, the thermal conductivity,  $k_f$ , was taken as that of air alone at the arithmetic average temperature of the drying air and the drop surface (147), i.e.,  $(t_{av} + T_s)/2$ .

#### d) Mass Transfer Coefficients and Modified Nusselt Numbers

Owing to the analogy existing between heat and mass transfer and the unique physical properties of the air-water system, the wet-bulb temperature curves on the humidity chart and the adiabatic saturation curves

have been shown experimentally to coincide when the heat transfer contribution due to radiation is negligible compared with that due to convection (152, 178, 257). This fact can be used to derive the well known Lewis relation between the heat transfer coefficient and the mass transfer coefficient (152).

$$h = k_g' s \quad \dots(181)$$

where  $k_g'$  - mass transfer coefficient, (lb.)/(hr.)(ft.<sup>2</sup>)( $\Delta H$ );  
 $s$  - average humid heat of the gas film, (B.t.u.)/(lb. dry air)  
 (°F.)

The mass transfer coefficients  $k_G$ ,  $k_g$  and  $k_g'$  are interrelated:

$$k_g = k_G M = k_g' M / M_m p_f \quad \dots(182)$$

$$\text{as } k_g' \Delta H = k_g' (p_s - p_a) M / p_f M_m = k_g (p_s - p_a) \quad \dots(183)$$

where  $\Delta H$  - humidity difference across gas film corresponding to  $\Delta T$

$$\text{and } (p_s - p_a), = H_s - H_a \quad \dots(184)$$

$H_s$  - humidity of saturated air at spray temperature  $T_s$ ,  
 (lb. of water)/(lb. of dry air);

The modified Nusselt Number for mass transfer (equation 66) can be rewritten by means of equations 181 and 182 in the form:

$$\text{Nu}^t = h d_{vs} / s D_v \rho_f \quad \dots(185)$$

This expression can be rewritten in terms of the Nusselt Number.

$$\text{Nu}^t = \text{Nu}(k_f / s D_v \rho_f) \quad \dots(186)$$

e) Incremental Drop Size Analysis

The stepwise calculations, performed by Marshall (147) and by Dlouhy (40) were not designed for systems where the relative velocity between the spray drops and drying air is changing, and are consequently inapplicable to the present system. In fact, the terminal velocity of spray drops are often negligible when compared with the velocity of the drying air stream. In the nozzle zone the spray drops travel considerably faster than the surrounding air, and the stepwise procedure developed for these conditions is summarized below.

1 - Classification of the spray drop size distribution into six to ten suitable drop size groups. The mass per cent of the spray contained in each group was calculated from the average diameter of the drop size group and the number of drops in that size group.

$$\text{Mass per cent of spray} = n_i m_i / \sum_i n_i m_i \quad \dots(187)$$

where  $n_i$  - number of drops in the  $i$ th size group;

$m_i$  - mass of single average drop in the  $i$ th size group,

$$\text{lb.} = \pi \rho_L d^3 / 6 \quad \dots(188)$$

$d_i$  - diameter of average drop in  $i$ th size group, ft.

2 - The drop velocity of the average diameter drop was obtained from the appropriate drop velocity - drop diameter graph (Fig. 5 to 13) and was used to determine the Reynolds Number and the residence time,  $\Delta \theta_i$ , of the drop in the section:

$$\text{Re} = d_i V_{Ri} \rho_G / \mu_G \quad \dots(189)$$

where  $V_{Ri}$  - velocity of average drop relative to the surrounding fluid, (ft.)/(sec.).

$$\Delta \theta_i = \Delta x / v_{Di} \quad \dots(190)$$

where  $v_{Di}$  - absolute velocity of average drop, (ft.)/(sec.).

3 - Using the above Reynolds Number, the Nusselt Number was calculated from the equation proposed by Ranz and Marshall (188). This in turn permitted the heat transfer coefficient,  $h_i$ , to be calculated:

$$Nu = 2.0 + 0.6(Re)^{1/2}(Pr)^{1/3} \quad \dots(96)$$

$$h_i = (Nu)k_f/d_i \quad \dots(191)$$

4 - Since the temperature difference between the drying air and the drop was known, the heat,  $Q_i$ , transferred to a single drop could be calculated:

$$Q_i = h_i A_i \Delta T \quad \dots(192)$$

where  $A_i$  - surface area of average drop in  $i$ th size group,

$$\text{ft.}^2 = \pi d_i^2 \quad \dots(193)$$

The evaporation occurring could be expressed in terms of the initial mass of the drop:

$$E_{fi} = Q_i / \left[ (h_g)_{t_{av}} - (h_f)_{T_s} \right] m_i \quad \dots(194)$$

where  $E_{fi}$  - fraction of drop of mass  $m_i$  evaporated.

5 - This fractional evaporation was calculated for the  $i$ th drop size group, and the overall evaporation from the spray  $E_f$  is obtained from the equation:

$$E_f = \sum_i \left[ E_{fi} (n_i m_i) / \sum_i (n_i m_i) \right] \quad \dots(195)$$

#### 4. RESULTS

Twelve runs were performed using the internal mixing pneumatic nozzle - (1/4) JN No. 12 - Spraying System Co., Chicago. The range of operating conditions investigated was:

- total drying air flow rate, 42 to 81 lb./hr.;
- inlet drying air temperatures, 138 to 214°F.;
- inlet drying air humidities, 0.0066 to 0.0122 lb. H<sub>2</sub>O/lb. air;
- liquid flow rate to nozzle, 2.0 lb./hr.;
- atomizing air flow rate, 5.45 lb./hr.;
- total evaporation from spray, 19 to 55%;
- Sauter mean diameter of spray, 14.1 to 35 microns.

Eight runs were performed using the hollow-cone pressure nozzle - (1/4) LNN SS No. 1 - Spraying System Co., Chicago. Similar experimental conditions were used and the limits encountered are given below:

- total drying air flow rate, 25 to 46 lb./hr.;
- inlet drying air temperatures, 144 to 220°F.;
- inlet drying air humidity, 0.0124 to 0.0170 lb. H<sub>2</sub>O/lb. air;
- liquid flow rate to nozzle, 5.10 lb./hr.;
- total evaporation from spray, 2 to 7%;
- Sauter mean diameter of spray, 65 to 169 microns.

The experimental evaporation data for both nozzles are given in Appendix IV together with the calculated values of the heat and mass transfer coefficients and the Nusselt Numbers, which are shown in terms of

the dimensionless groups  $(Re)^{1/2}(Pr)^{1/3}$  and  $(Re)^{1/2}(Sc)^{1/3}$  in Fig. 25 to 28. Typical microphotographs of the spray drops are presented in Fig. 29, while the changes in the Sauter mean diameter, spray mass and temperature that occurred with evaporation are illustrated in Fig. 30 and 31 for both the pneumatic and pressure nozzles.

Stepwise calculations were performed for four runs using the pneumatic nozzle and for one run using the pressure nozzle. Tables of the measured and calculated evaporation are given in Appendix VI together with a table indicating the method of calculation. These results are expressed graphically in Fig. 32.

## 5. DISCUSSION OF RESULTS

As expected, humidity measurements of the individual drying air streams proved to be the most suitable and accurate method of determining the spray evaporation, as considerable difficulty was experienced in obtaining samples of the spray near the nozzle for colourimetric analysis of the red dye concentration. However at greater distances from the nozzle (i.e., sections 3, 4, and 5) excellent agreement was obtained between the spray evaporation calculated from the humidity measurements and that computed from changes in the dye concentration.

The main disadvantage of the cross-flow equipment was the complexity of the air flow patterns generated in the spray chamber. Control of the air streams in the horizontal sections entailed the simultaneous adjustment of twelve valves. A slight change in the static pressure in the

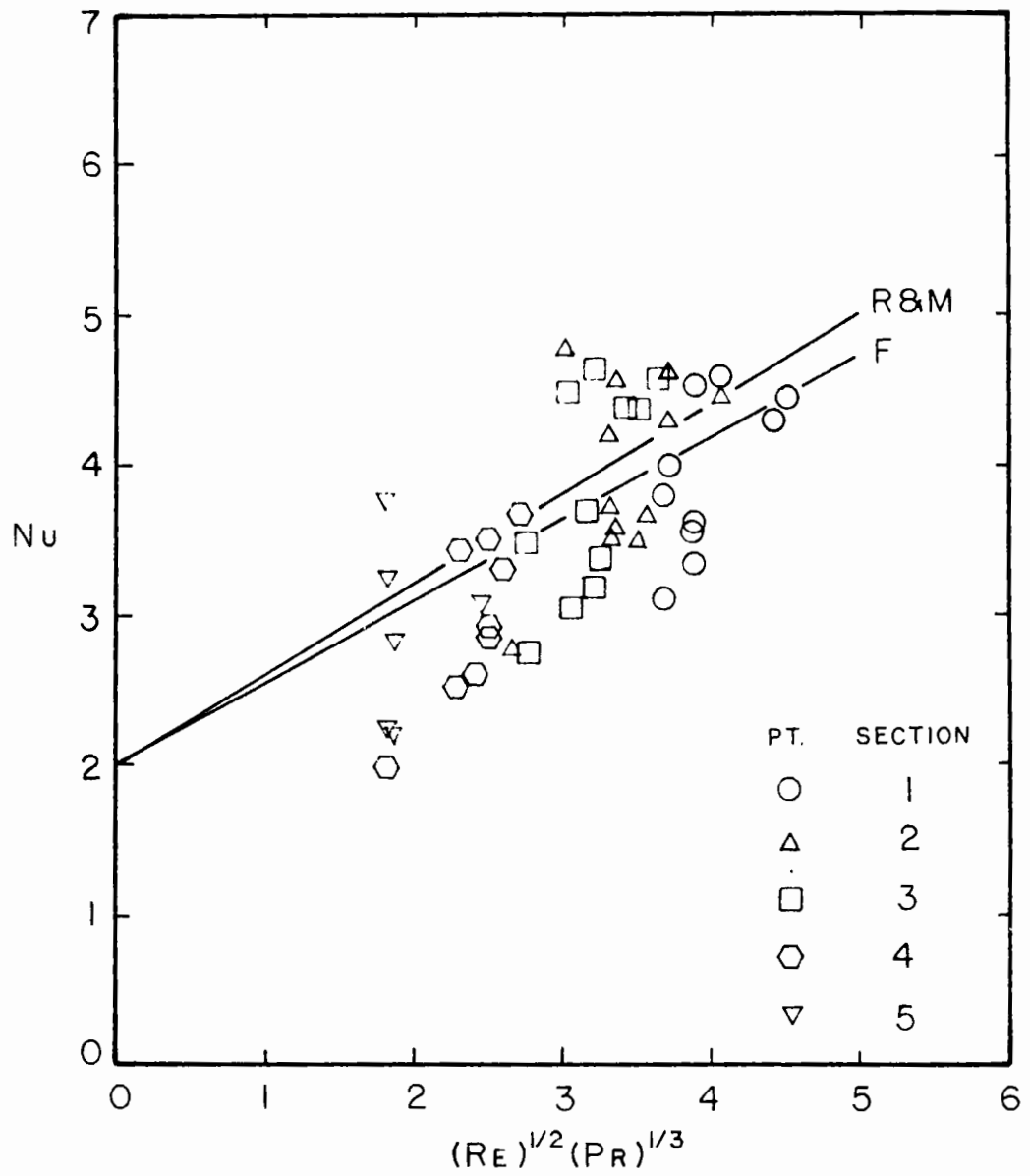


Fig. 25. Heat Transfer Data for Runs 1 - 12

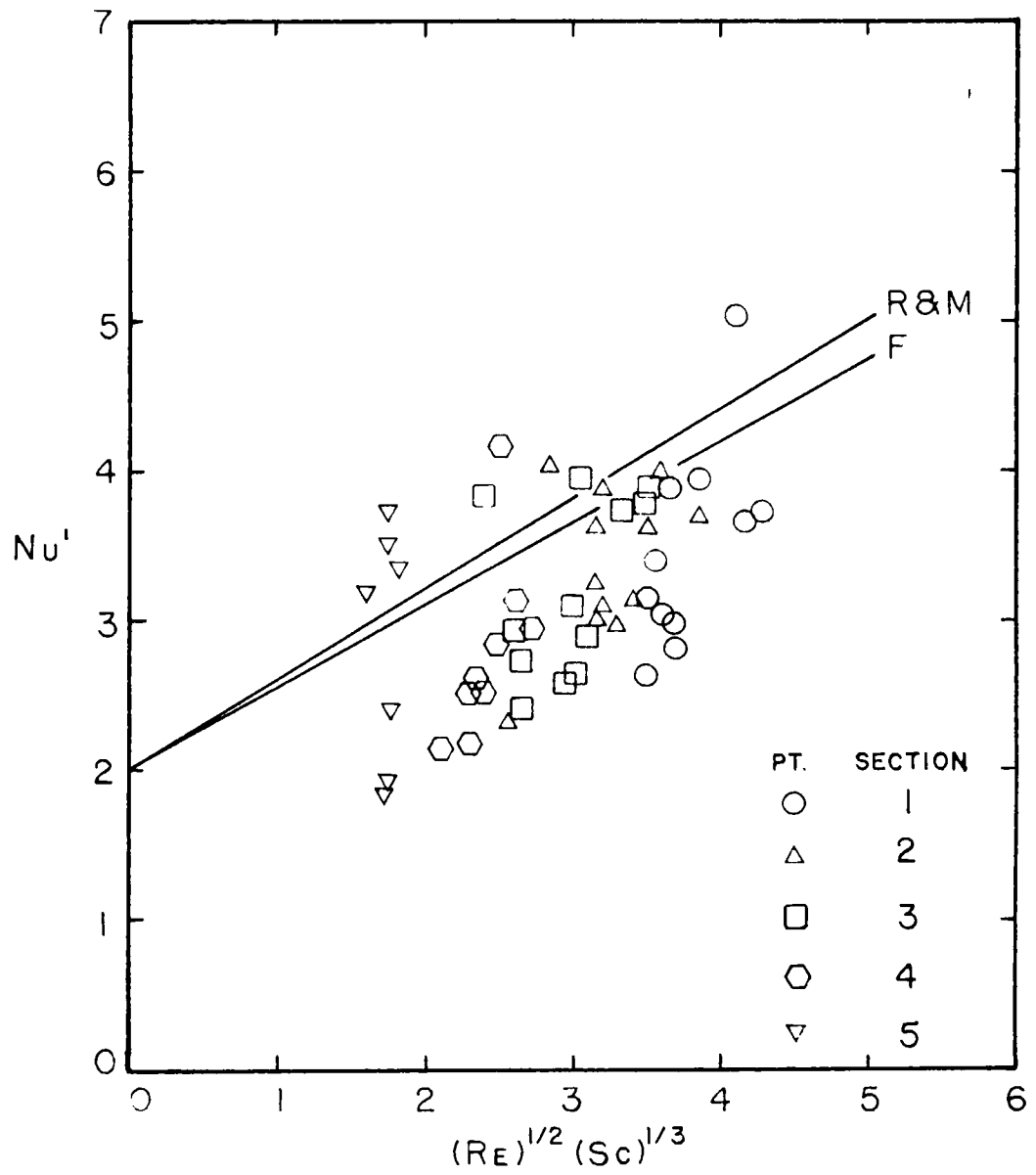


Fig. 26. Mass Transfer Data for Runs 1 - 12

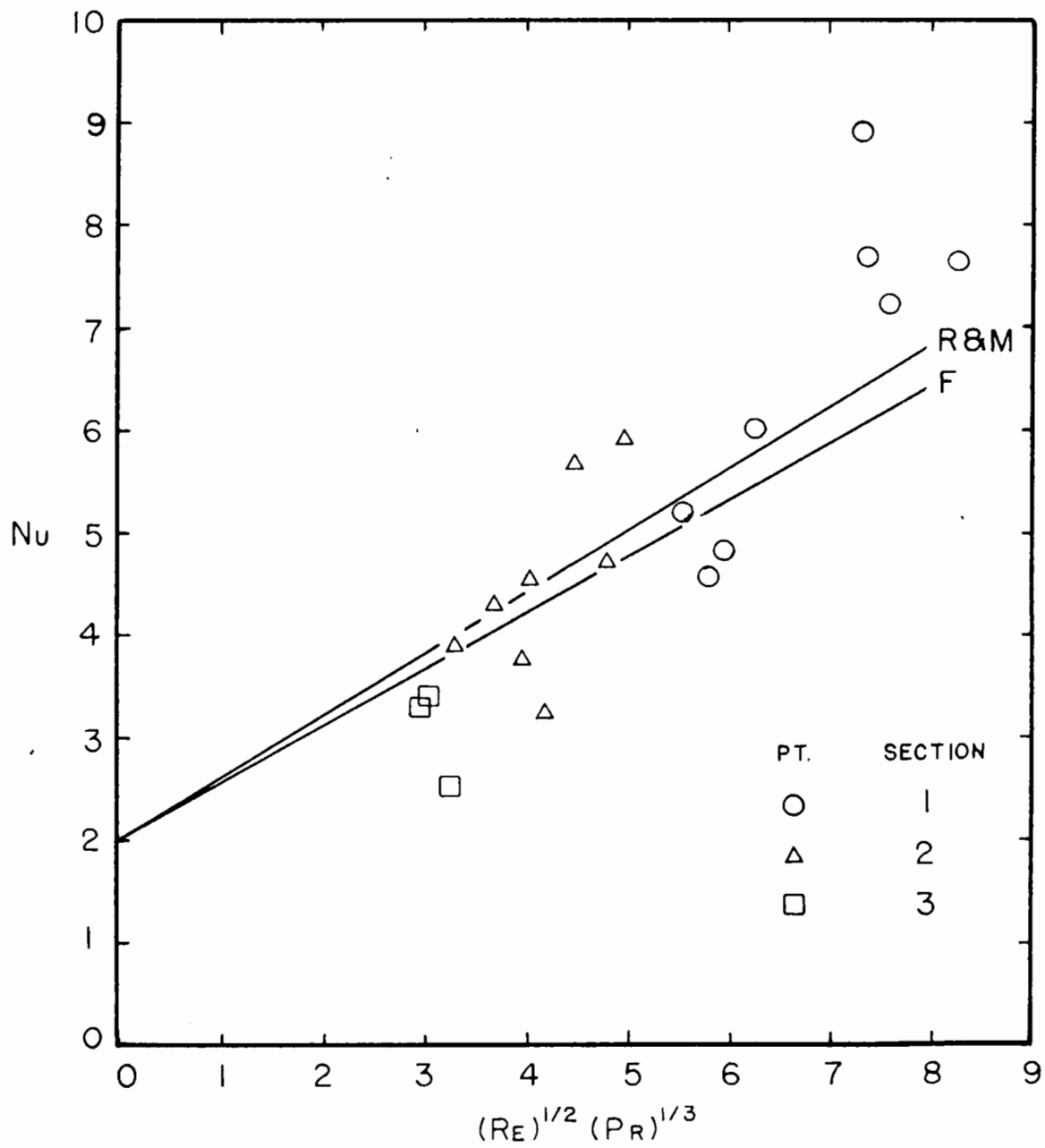


Fig. 27. Heat Transfer Data for Runs 13 - 20

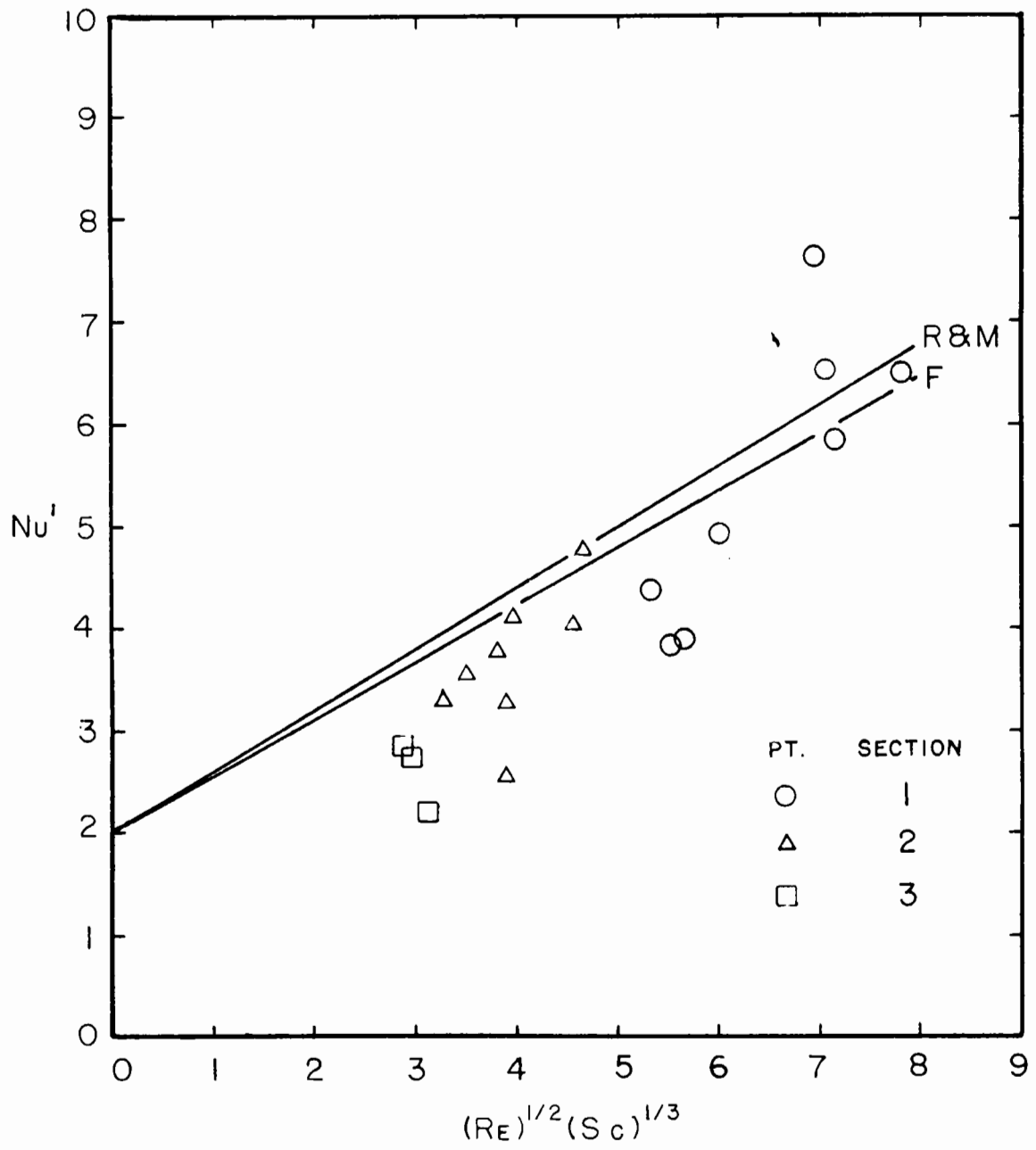


Fig. 28. Mass Transfer Data for Runs 13 - 20

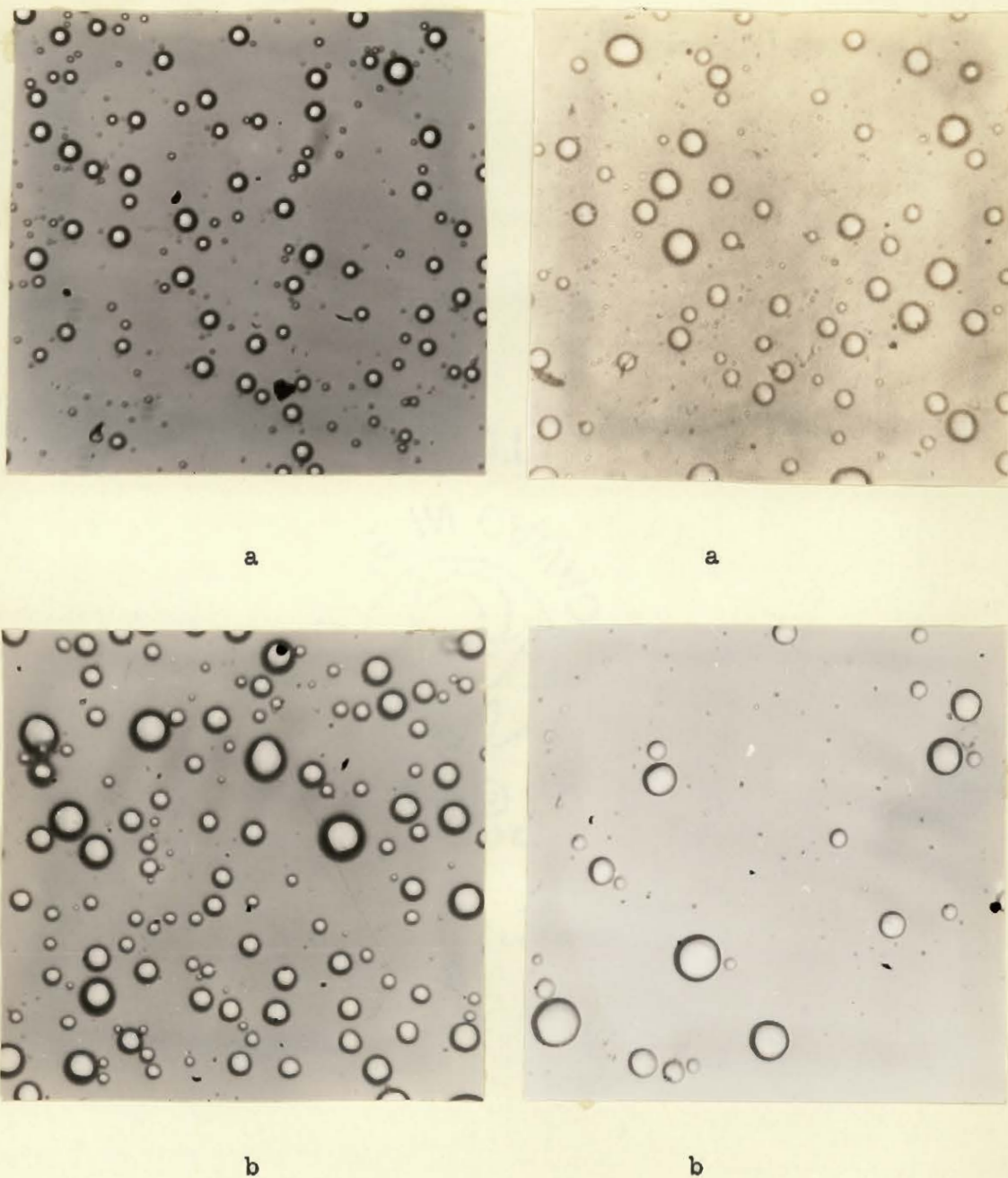


Fig. 29. Typical Microphotographs of the Spray Drops in the Cross-Current Flow Equipment

- a) Pneumatic Nozzle 1/4JN No. 12 Low Atomizing Pressures (Mag. 175X)
- b) Pressure Nozzle 1/4LNNSS No. 1 (Mag. 40X)

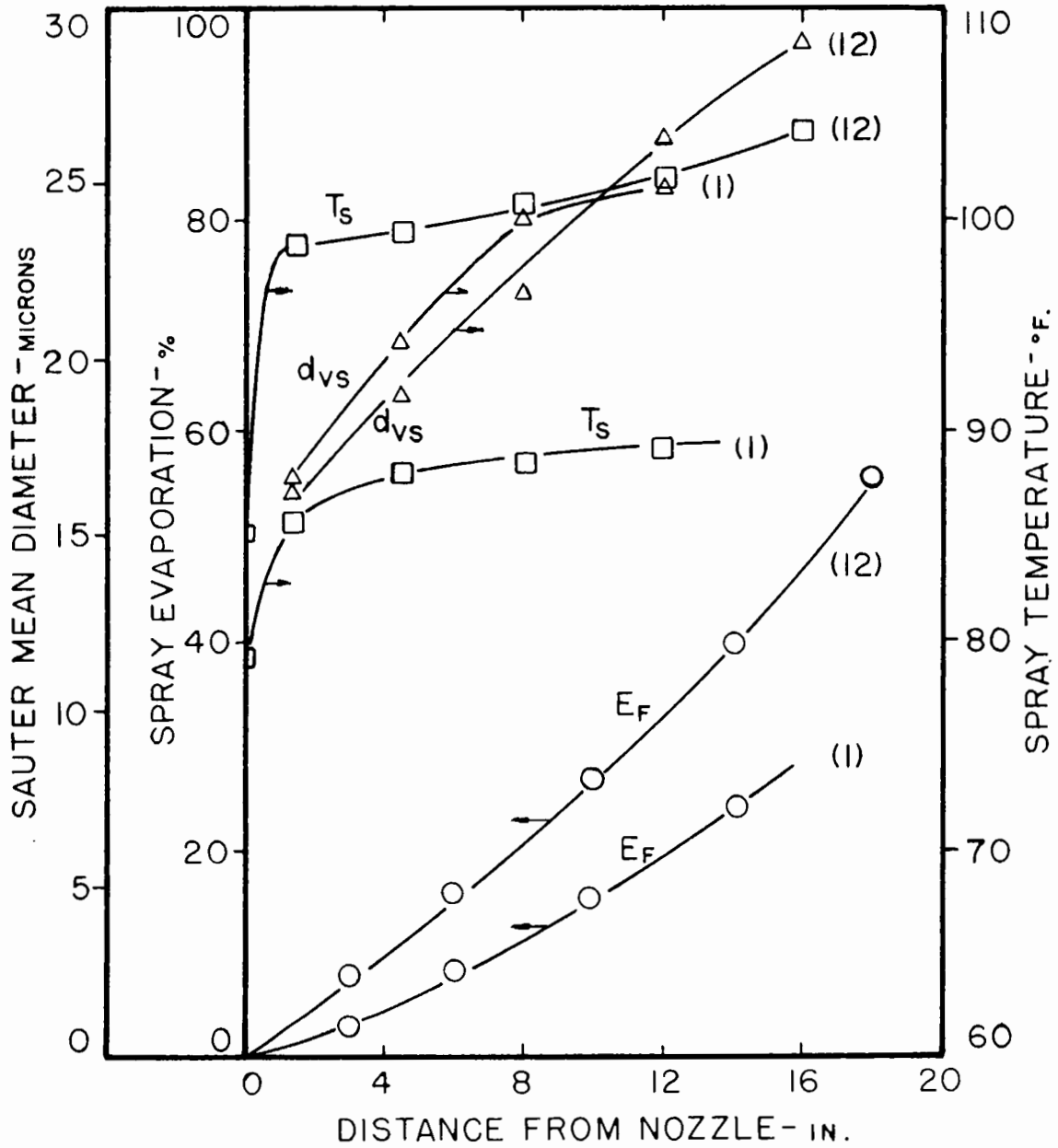


Fig. 30. Changes in Spray Properties for Pneumatic Nozzle Runs

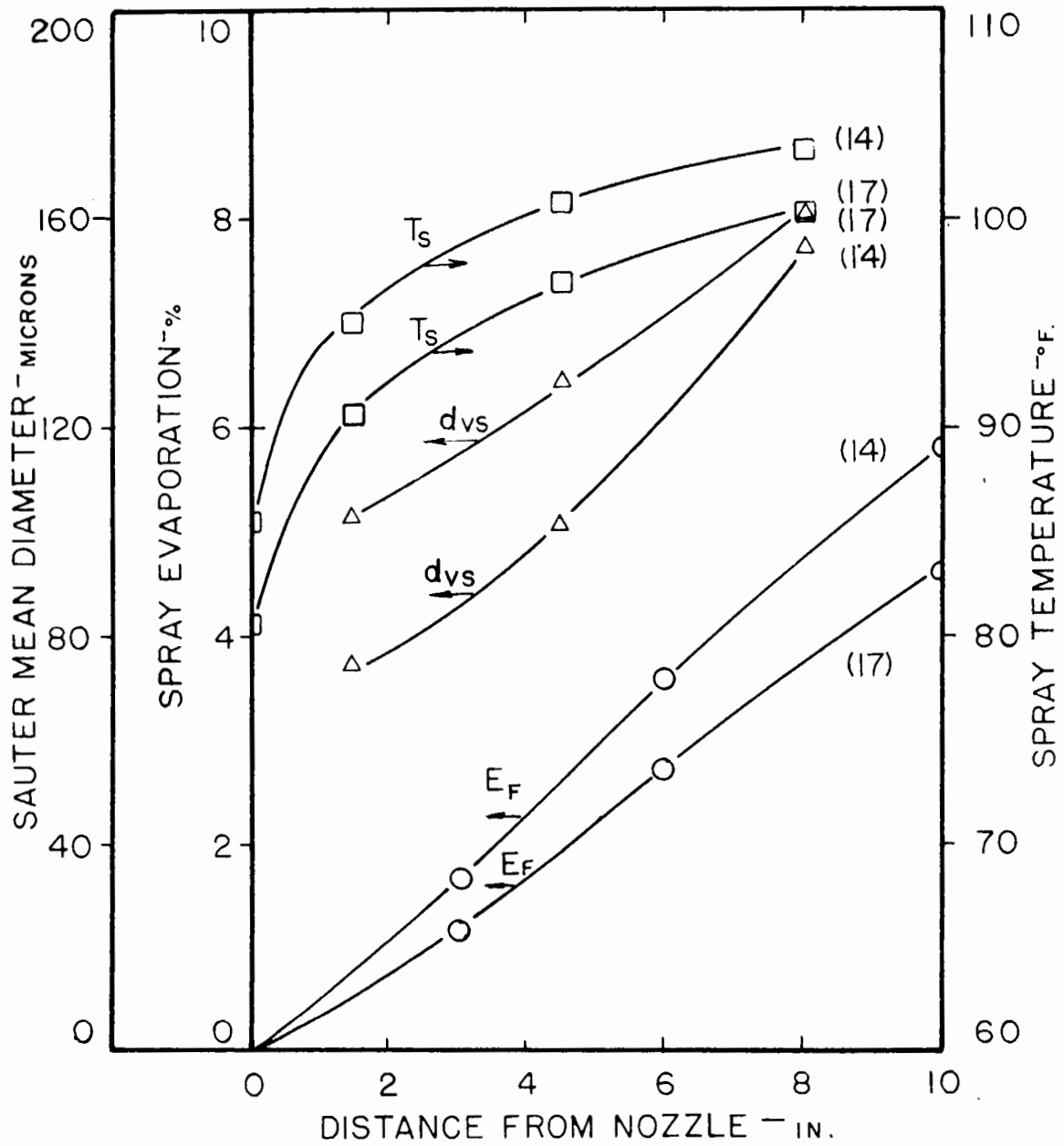


Fig. 31. Changes in Spray Properties for Pressure Nozzle Runs

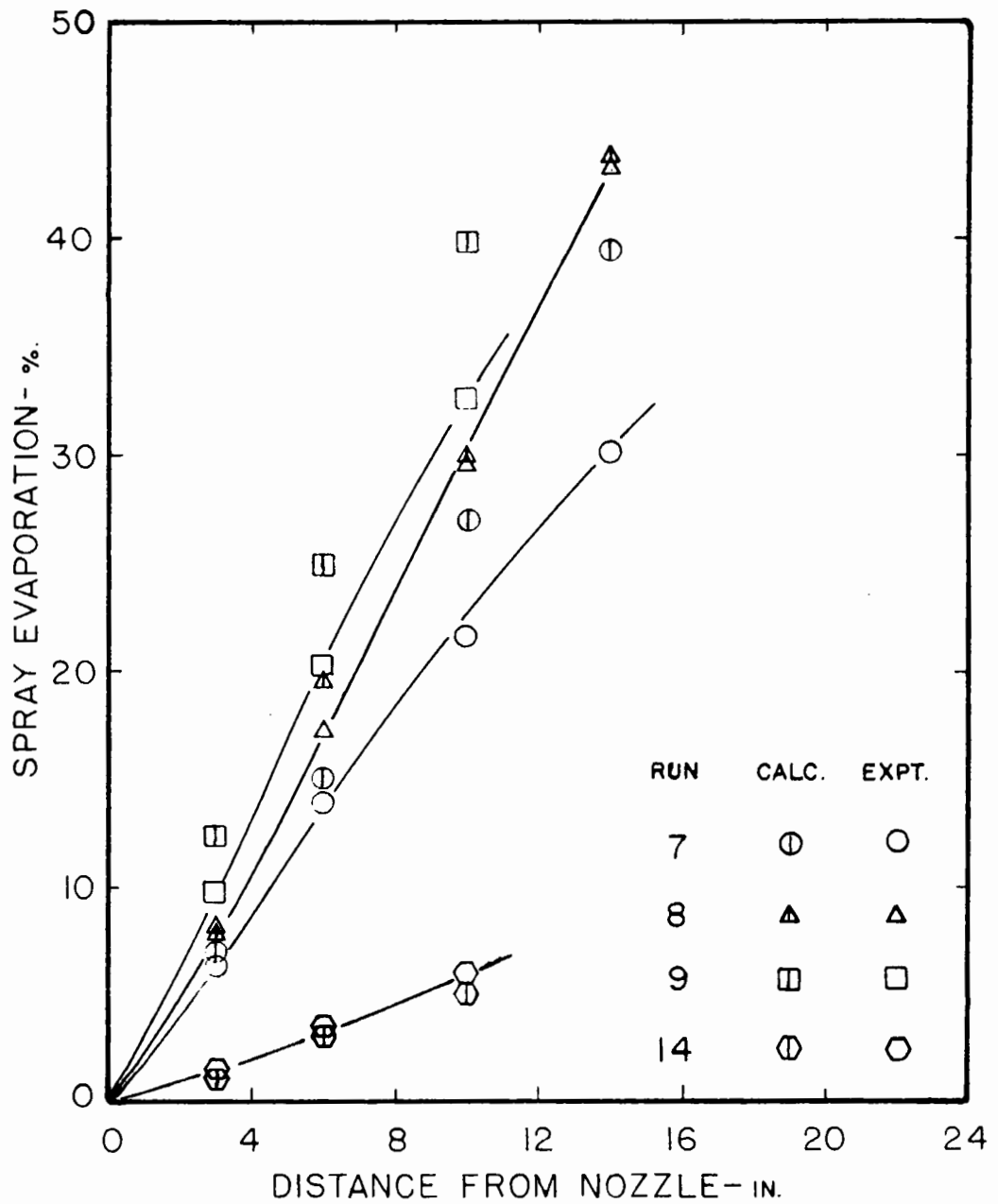


Fig. 32. Application of Incremental Analysis to Cross-Current Flow Runs

chamber, which could be caused by increasing the inlet drying air flow rate to any section, had the effect of altering the outlet flow rates of the drying air streams. This in turn changed the distribution of the atomizing air stream among the various sections and could produce appreciable changes in the drying air temperatures and evaporation rates.

a) Heat and Material Balances

The heat and material balances performed on the spray chamber during the adjustment of the operating conditions prior to an evaporation run led to the following conclusions:

1. Air leaks from the chamber were negligible. Measurements of the inlet and outlet air flow rates when the nozzle was not in use agreed to within 3%. However, with the nozzle in operation, the entrainment of the spray drops by the drying air had the effect of increasing the overall density of the outlet flow streams, and thus produced larger differential pressures across the metering orifices. The correction procedure has been previously outlined.

2. Heat losses were usually very small, except at low flow rates of the drying air and high temperatures, where they amounted to approximately 15%. As the heat transferred from the drying air to the spray was calculated from the increase in the air humidity and change in spray temperature, rather than from the change in temperature of the drying air, this source of error was eliminated from the calculations. The net effect of heat losses was to reduce the temperature of the drying air, and consequently the temperature difference between the air and the spray.

### b) Nozzle Characteristics

Marked differences in the operating characteristics of the two atomizing nozzles (pneumatic (1/4) JN No. 12 and pressure (1/4) LNN SS No. 1) were observed. The spray drops produced by the pneumatic nozzle ( $d_{vs}$  in the range 14.1 to 35 microns) were much smaller than those obtained from the pressure nozzle ( $d_{vs}$  in the range 65 to 169 microns).

Differences in the spray drop velocities and the spray angles were also observed. As may be seen in Fig. 5 to 13, much greater drop velocities were recorded in the nozzle zone of the sprays produced by the pneumatic nozzle than those from the pressure nozzle.

The pressure nozzle exhibited a considerably wider spray angle, and contact of the spray with the chamber walls consequently occurred nearer to the atomizer. Differences in the deformation of the spray by the drying air were also observed. For the pressure nozzle, the spray drops tended to be entrained, or displaced in the direction of the air velocity. With the pneumatic nozzle, an additional flattening of the spray in a direction at right angles to the main air velocity was observed. No measurements were taken in any section where appreciable contact between the spray and walls was observed.

### c) Heat and Mass Transfer

Comparison of the temperature and humidity of the inlet and outlet drying air streams showed that in most cases the path traced on a humidity chart followed an adiabatic cooling curve, confirming the fact that the

heat losses were insignificant.

The temperature of the spray as determined by the thermocouple probe was essentially the same as the wet-bulb temperature of the drying air in contact with it. Changes in the spray temperature from section to section were noted, and attributed to changes in the wet-bulb temperatures of the drying air streams. Although all the drying air streams came originally from the same source and were heated to the same temperature, heat losses in the feed lines from the surge tank to the spray chamber and the drop in temperature during expansion from the feed line into the drying chamber accounted for the difference in the various wet-bulb temperatures. In addition, the atomizing air stream tended to reduce the wet-bulb temperature; as this effect was largest near the nozzle, the spray temperatures increased with an increase in distance from the nozzle.

The Sauter mean diameter,  $d_{vs}$ , of the spray was found to increase initially with distance from the nozzle, i.e., as evaporation proceeded. This behaviour - which may at first appear unusual - is actually to be expected with a wide distribution in drop sizes, since the smaller spray drops evaporate much more quickly than the larger ones (on which the value of the Sauter mean diameter depends to a great extent). The rate of this increase diminished rapidly to an almost constant value of the Sauter mean diameter in Sections 3, 4 and 5.

The heat transfer coefficient for the Sauter mean diameter drop size was calculated using equation 179. This coefficient was used to calculate the Nusselt Number for heat transfer which was correlated in

terms of the Reynolds and Prandtl Numbers. Although an appreciable scatter was exhibited, the experimental data verified the following correlation, which was proposed by Ranz and Marshall (188), for Reynolds Numbers from 2 to 80.

$$\text{Nu} = 2.0 + 0.6(\text{Re})^{1/2}(\text{Pr})^{1/3} \quad \dots(96)$$

When an attempt was made to extend these results to mass transfer, the modified Nusselt Numbers were approximately 10% lower than those predicted by the equation.

$$\text{Nu}' = 2.0 + 0.6(\text{Re})^{1/2}(\text{Sc})^{1/3} \quad \dots(97)$$

Modified Nusselt Number values lower than the corresponding Nusselt Number have been reported for spray drying evaporating under conditions of no spray drop deceleration (40). A possible explanation may be the assumption that the gas film properties should be evaluated at the arithmetic average of the drop temperature and that of the drying gases.

The effect of changes in the atomization conditions on the evaporation rate from the spray can be predicted from the correlations of Ranz and Marshall. A decrease in the Sauter mean drop diameter results in an increase in the heat and mass transfer coefficients as the Nusselt Number and the Modified Nusselt Number are directly proportional to the drop diameter and the transfer coefficient. There is a counteracting effect due to a decrease in the Nusselt Number which is produced as the Reynolds Number is proportional to the drop diameter. However, this effect is considerably smaller than the direct effect as the Reynolds Number appears

to 0.5 power with a coefficient of 0.60 in equations 96 and 97. Also a decrease in the Sauter mean diameter increases the specific area of the spray, and the overall result is a sharp rise in the evaporation rate.

An increase in the drop velocities may be similarly analyzed. The first effect is an increase in the Reynolds Number and consequently in the Nusselt Number and the transfer coefficients. The magnitude of this change is given by equations 96 and 97. However the time that the drops take to travel a given distance along the spray axis is proportional to the reciprocal of the drop velocity. Consequently, even though the evaporation rate is increased by an increase in the drop velocity, the evaporation occurring in a given distance along the spray axis is reduced.

#### d) Drag Coefficients

The drop velocity - drop diameter data obtained at different distances from the nozzle in the lucite column under conditions of practically no evaporation enabled the drag coefficients to be calculated. These coefficients were presented graphically in Fig. 14, together with the data of Hanson (79) and Ingebo (99).

A marked dependence on the drop diameter was observed. The smaller drop sizes (15 to 25, and 25 to 40 microns) were obtained using the pneumatic nozzle - (1/4) JN No. 12. The drag coefficients calculated for these drops were lower than those indicated by the standard curve by a factor of 3 to 10. High drag coefficients were obtained for the larger drops (60 to 120 microns) produced by the pressure nozzle - (1/4) LNN SS

No. 1. Here the ratio between the calculated drag coefficients and those indicated by the standard curve was 1/10 to 3.0.

It should be noted that deceleration rates as high as 100,000 ft./sec.<sup>2</sup> were recorded for drops 1.5 in. from the pneumatic nozzle. As the deceleration rates increase rapidly with proximity to the nozzle, it is logical to assume that even higher deceleration rates occurred closer to the nozzle.

The effect of the drop diameter on the drag coefficients of the decelerating drops indicates that the scale of turbulence in the surrounding gas is a factor in the decrease in the drag coefficient. Further evidence in support of the effect of turbulence was the fact that the drag coefficients for 40 micron drops produced by the pneumatic nozzle were lower than those obtained for similar drops produced by the pressure nozzle.

e) Incremental Analysis of Evaporation Rates

Fig. 32 shows the agreement between the evaporation based on the validity of the correlation of Ranz and Marshall and using the method outlined previously with that determined experimentally. The calculated evaporation from the spray appears to be somewhat higher than the measured values but the deviations are of the same order of magnitude as those exhibited by the experimentally determined Nusselt Numbers.

The incremental drop size procedure is a more logical and exact method of testing the applicability of the correlations of Ranz and Marshall.

However, it suffers from the weakness that most of the spray evaporation occurs from the smaller drop sizes and the velocity of these drops had to be determined by extrapolation of the drop velocity - drop diameter curves. As the drop velocities of the smaller drop sizes are relatively low, appreciable errors can occur in the estimation of the drop velocities.

### III EVAPORATION WITH CO-CURRENT FLOW

The most important factor to be considered in the design of the drying chamber of a spray dryer is the particle trajectory. When the flow pattern is very complex, knowledge of the exact trajectory of the droplets or particles is very difficult, if not impossible to obtain. As is evident from the previous section, the entraining action exerted by a high-velocity jet on the slower moving surrounding fluid makes the prediction of the flow pattern in the vicinity of the atomizing nozzle even more uncertain.

To provide better control of the spray pattern and of the flow lines in the drying air, a downward, co-current design was adopted for this part of the investigation. High speed cinematography of the spray in the drying section itself was used to measure the drop velocities. This enabled the residence time of the spray in any given section to be calculated, and so permitted accurate values of the heat and mass transfer coefficient to be determined. Since flow was co-current, relatively large quantities of the drying air could be used without producing any appreciable deformation of the spray. This large flow rate of drying air together with the fact that higher drying air temperatures could be obtained, produced larger evaporation rates than those found in the cross-current flow equipment.

## 1. EQUIPMENT

The equipment used was essentially a prototype of a commercial, co-current spray dryer, and contained all of the latter's fundamental components, except that no separator was installed for the collection of the product. To minimize back-mixing and other forms of irregular flow, which would alter the trajectories of the spray drops, no expanded section was incorporated. Instead, the entire co-current equipment consisting of the air heating unit, spray chamber and exhaust system was constructed in the form of a continuous 8-in. diameter duct. The arrangement of the equipment is shown by the accompanying sketches and photographs in Fig. 33 to 36. The problem of regulating the flow streams and adjusting the operating conditions was greatly reduced by installing all the control valves and metering devices on a central control panel (Fig. 37). This panel was divided into two sections so that the electrical instruments would be separate from the instrumentation for the atomizing streams.

### a) The Spray Chamber

This part of the spray dryer consisted of three separate cylindrical sections - the approach section, the nozzle zone section and the drying section. These sections were mounted co-axially so that the drying air and spray passed vertically downward in co-current flow.

In the approach section, the drying air was passed through a straightening plate in order to produce a uniform velocity profile. Insulation of this section was accomplished by covering the duct with a

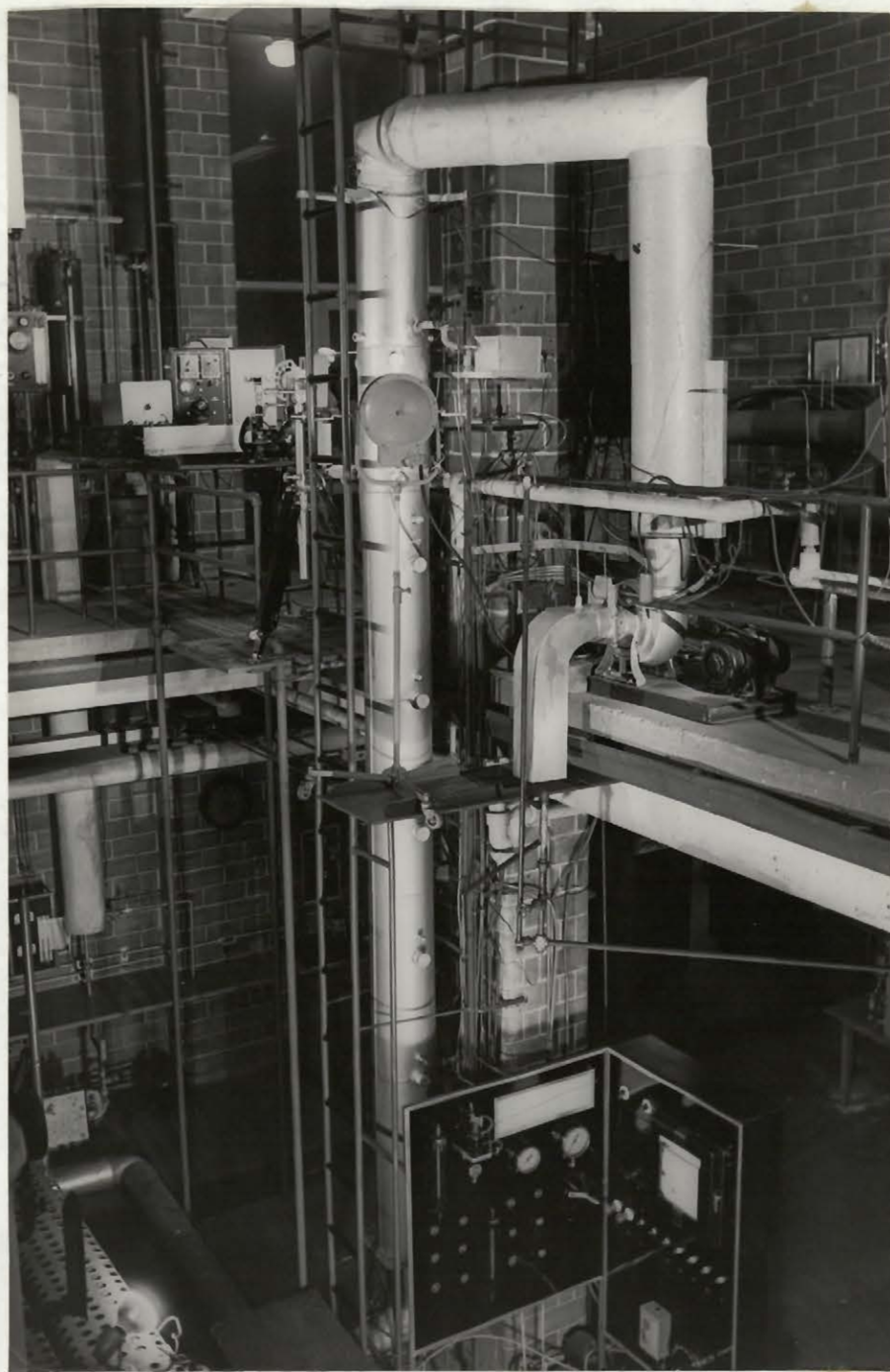


Fig. 33. The Co-Current Flow Equipment

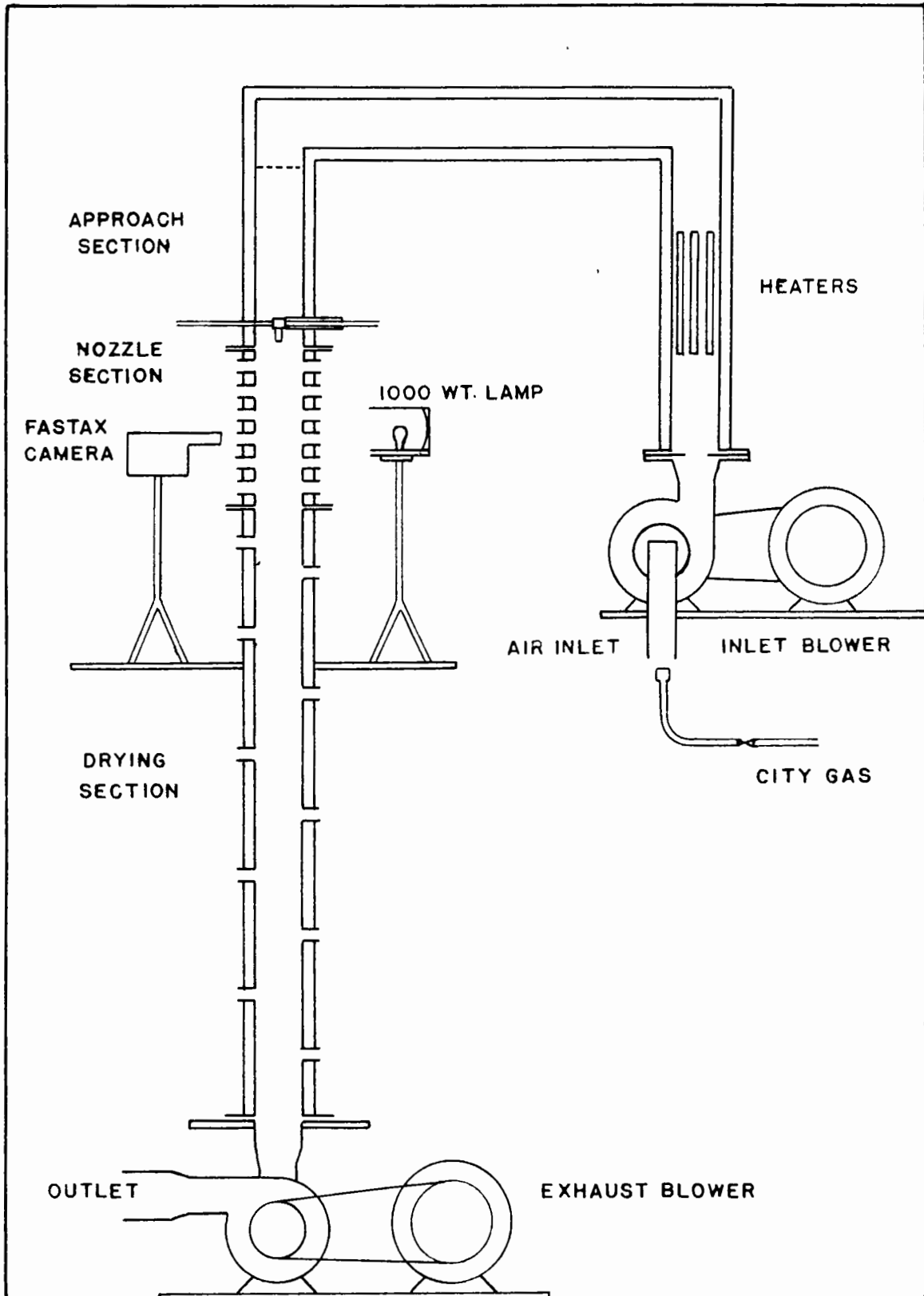


Fig. 34. Schematic Diagram of the Co-Current Flow Equipment

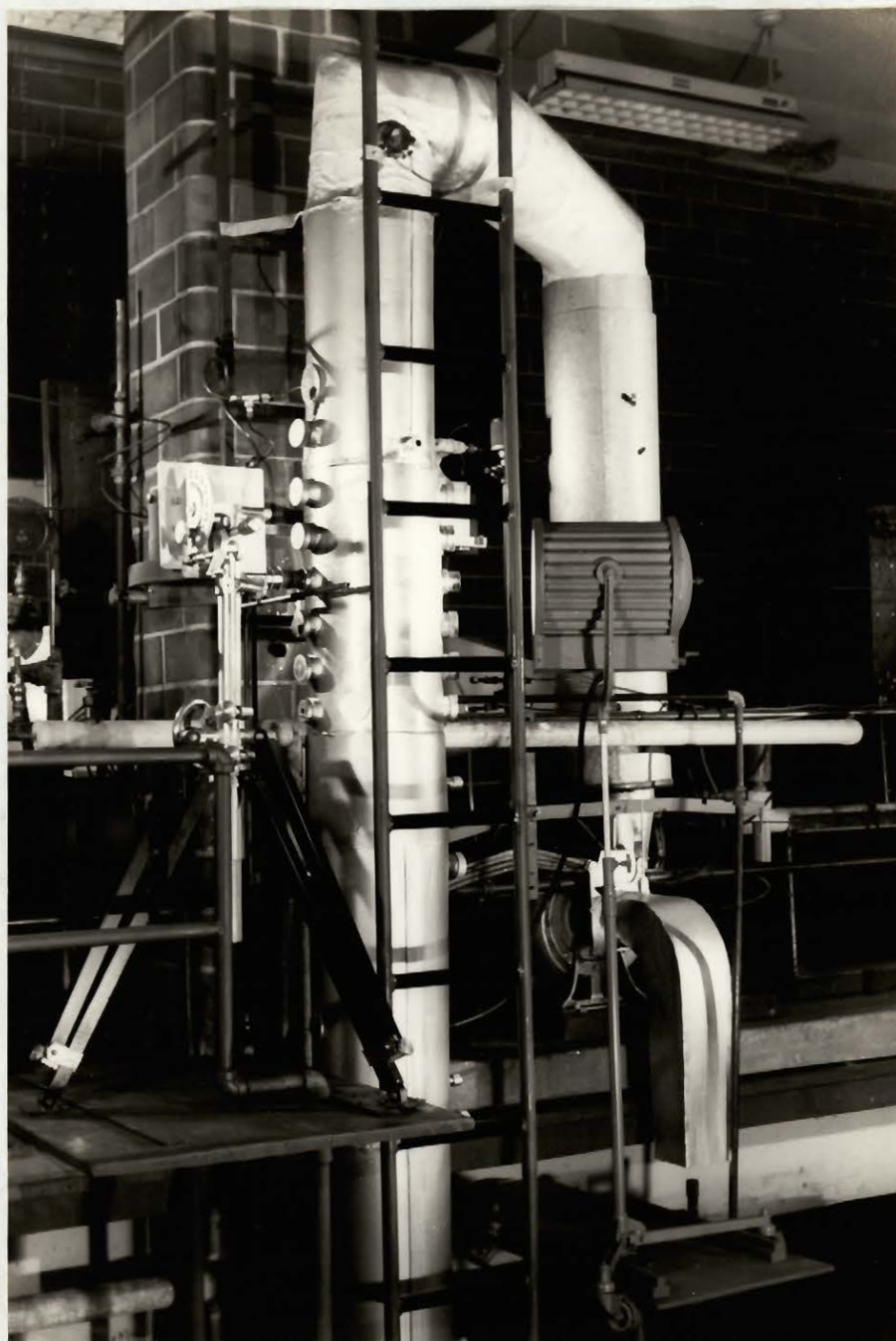


Fig. 35. The Co-Current Flow Equipment (Nozzle Section)

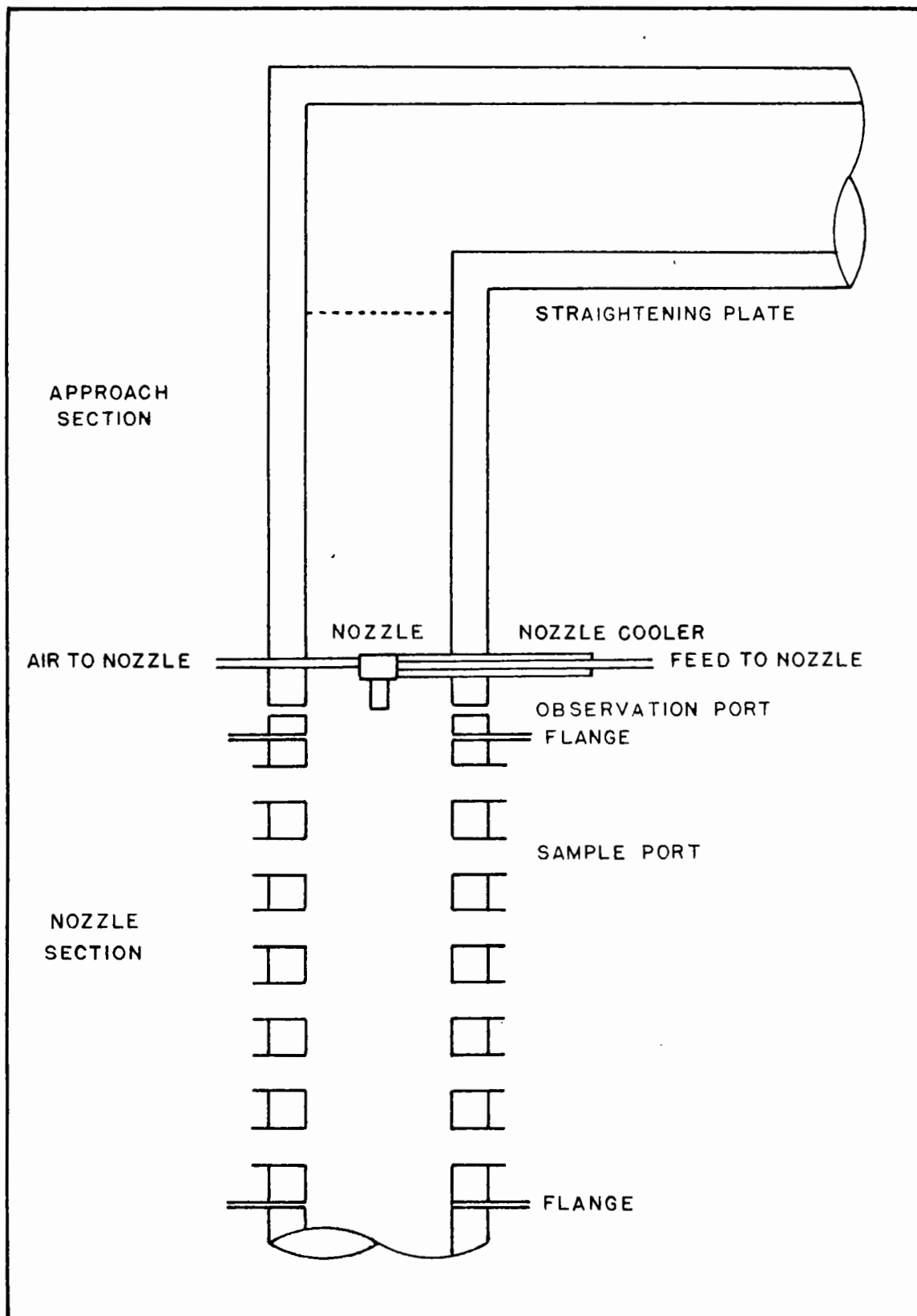


Fig. 36. Schematic Diagram of the Co-Current Flow Equipment (Nozzle Section)



Fig. 37. The Control Panel of the Co-Current Flow Equipment

2-in. layer of magnesia insulation. The nozzle was installed at the end of the approach section and care was taken to ensure that the nozzle axis and that of the vertical duct coincided. Two observation ports were provided so that the position and operation of the nozzle could be assessed at any time.

From the approach section the drying air entered the nozzle section which was constructed from 16-gauge cold-rolled steel. This section was 2 ft. long and was fitted with six pairs of sampling ports spaced at 4-in. intervals. A surrounding galvanized jacket one foot in diameter was provided and two inches of insulation was obtained by filling the annular space with vermiculite. The sample ports were constructed from standard 2-in. steel nipples 3-in. long, welded to the steel chamber. These ports were used for photographing the spray, and consequently the angle between a pair of ports was made 135 deg., as previously established. Ordinarily the ports were sealed with transite plugs, but special plugs with optical glass windows were made to permit spray photography.

The drying section was 12-ft. long, and was similarly insulated. However the sample ports were spaced further apart. The inside surface of the whole duct was covered with several coats of high-temperature aluminum paint. Copper - constantan thermocouples were soldered onto the inner wall and these were connected to a Speedomax Leeds and Northrup 12-point temperature recorder. This served as an indication of the operation of the whole equipment, as a change in drying air temperature or wetting of the walls by the spray could be immediately detected. The temperature recorder was equipped with a selection switch so that the

readings obtained could be checked by a Leeds and Northrup potentiometer.

Access to the sample ports was achieved by installing a vertical ladder running along the full height of the spray dryer. Platforms on which the Fastax camera and accompanying equipment could be assembled were also constructed. One of these platforms served as an operating station to make the required measurements in the nozzle zone of the spray.

Due to the different nozzle holders used for pneumatic and pressure nozzles, the position of these nozzles in the tower was different. The distance of the centre of the sample ports from the nozzle for both types of atomizers was presented in Table V.

#### b) The Drying Air Circuit

A Canadian Blower and Forge Co. blower type No. 22 driven by a 1.5-H.P. Electric Tamper motor was used to supply the drying air. To overcome the pressure drop in the exhaust duct another blower - of the same size and make - was installed between the spray chamber and the exhaust system. This arrangement had the effect of maintaining a zero static pressure in the equipment, thereby eliminating the possibility of leaks from the sample ports. Adequate control of the drying air flow was achieved by installing a 6-in. slide valve near the intake of the inlet blower. Operation of this valve from the control panel was accomplished by means of a system of pulleys.

The drying air flow through the equipment was measured by a 4-in.

orifice which was installed about two feet from the inlet air blower. The pressure drop across the orifice was measured with a 1:10 inclined water manometer located on the control panel. A calibration of this orifice was required, because of its location, and this was obtained by temporarily installing a standard orifice at the outlet of the spray chamber.

Electrical heaters were used to heat the drying air, but an auxiliary gas burner located just below the intake of the inlet blower was required for the production of high air temperatures. The electrical heating system consisted of three heaters of capacity 1.0, 2.0 and 3.25 K.W., respectively, and was installed just after the 4-in. orifice. The first heater was connected to an Aminco bimetallic thermoregulator, the sensing element of which was installed just before the straightening plate in the approach section of the spray chamber. This ensured a constant drying air temperature. The voltage to the second heater was regulated by means of a General Radio Co. Variac, thus providing a wide range of temperatures. A copper - constantan thermocouple located after the heaters was used to measure the air temperatures. All switches, pilot lights as well as the variac were mounted on the control panel.

The heating section and connecting duct to the spray column were covered with 2 in. of magnesia insulation to reduce heat losses.

#### c) The Atomizing Stream Circuits

Two internal-mixing, pneumatic nozzles type (1/4) JN No. 12 and

22B and one pressure nozzle type (1/4) LN No. 1 manufactured by Spraying Systems Co., Chicago, were used to atomize the dilute solution of the red dye used as liquid feed. The feed was stored in a 5-gallon tank and was forced by means of compressed air through a 1/4-in. globe valve and a Schutte and Koerting rotameter No. 2R in series. The control of the flow rate was excellent as the pressure of the compressed air above the liquid in the feed tank was regulated by means of a 1/4-in. Taylor reducing valve. A strainer and provision for the calibration of the rotameter were included in the feed line. The pressure of the feed at the nozzle was measured with a 0 to 100-p.s.i.g. Bourdon gauge.

A cooling system consisting of two heat exchangers was used to regulate the temperature of the feed to the nozzle. The first was located outside of the column while the second was constructed around the feed line to the nozzle in the chamber. The temperature of the feed was measured by means of a copper - constantan thermocouple probe located in the feed line about one inch from the nozzle. An alternative system was used for high feed temperatures, i.e., feed temperatures above the wet-bulb temperature of the drying air stream. Here a stainless steel coil heater surrounded by a fire brick furnace was installed in the feed line near the nozzle. A bunsen burner, placed under the furnace, provided the heat. Heat losses in the line from the heating coil to the nozzle were compensated for by an asbestos-covered, nichrome, heating wire which was wrapped around this portion of the feed line. The assembly was covered with asbestos tape. Control of the feed temperature was achieved by varying the voltage applied to the nichrome wire heater by means of a rheostat which was connected as

a potential divider across the 110 volt mains and also by adjusting a 1/4-in. globe valve installed in the city gas line to the burner.

The compressed air required for pneumatic atomization was obtained from the Ingersol Rand compressor used in the cross-current flow equipment. Similar instrumentation consisting of a 1/4-in. Taylor reducing valve, a Schutte Koerting rotameter No. 2R and a 0 to 100 p.s.i.g. Bourdon gauge were used. Brass pipe and fittings were used exclusively for the construction of all the atomizing stream lines.

## 2. PROCEDURE

As in the cross-current flow runs, a standard test procedure which is described below was used. The operating procedure was divided into two steps which together with the variations required for high feed temperature tests are outlined below.

### a) Adjustment of Equipment

To test the adjustment of the nozzle in the spray chamber, velocity profiles were taken prior to spraying water. The blowers were started and the drying air flow regulated by means of the 6-in. slide valve in the air intake duct. The equipment was brought up to the required temperature by turning on all the heaters to their maximum capacity. For very high drying-air temperatures the gas burner below the air intake duct was also used. The desired air temperature was achieved by adjusting the thermoregulator connected to the 1-K.W. heater and the variac which

controlled the voltage applied to the 2-K.W. heater.

The atomizing air stream to the pneumatic nozzle as well as the cooling water to the heat exchangers controlling the feed temperature were turned on, and half an hour was allowed for steady state conditions to be established. Air velocity traverses were made using a standard pitot tube and a wedge-shaped probe developed by Stachiewicz (224). These instruments were previously described on page 137 and correct values of the air velocities were obtained due to the absence of water drops. Examination of the velocity traverses permitted an accurate alignment of the nozzle axis to be made. When the pressure nozzle was used, visual observation of the nozzle position and the spray cone had to be relied upon to adjust the nozzle position.

The temperatures recorded by the Speedomax recorder along the spray chamber, indicated that heat losses from the equipment were negligible. In fact, the heat losses from the entire drying chamber never resulted in a temperature drop of more than 5°F. However the cooling effect of the atomizing air produced a temperature drop in the drying air which varied from 5 to 12°F. depending on the relative magnitude of the air streams.

b) Collection of Experimental Data

When the operation of the equipment was proved to be satisfactory, the liquid feed to the nozzle was adjusted to the desired value. The controlling factors were the liquid flow rate and the air atomizing pressure for the pneumatic nozzles, while the feed rate sufficed for the pressure

nozzle. The danger of the spray touching the wall of the spray chamber was far less than in the cross-current system, nevertheless the operating conditions of the nozzles chosen were the same as in the cross-current system. Measurements of the spray properties could therefore be taken as far away from the nozzle as desired.

Half an hour was usually required for steady state to be established, as indicated by constancy of temperatures throughout the equipment.

The following measurements of the spray and drying air properties were then taken.

#### 1. Atomizing and Drying air Streams

- liquid feed flow rate,  $q_L = W$  (at nozzle);
- liquid feed temperature,  $T_L$  (at nozzle);
- liquid feed pressure at nozzle,  $P_L$ ;
- concentration of vegetable dye in feed,  $c$  (at nozzle);
- atomizing air flow rate,  $q_A$ ;
- atomizing air temperature,  $t_A$ ;
- atomizing air pressure at nozzle,  $P_A$ ;
- overall drying air flow rate,  $w$ ;
- initial drying air temperature.

#### 2. Drying Chamber Data for each Section

- drying air temperature,  $t$ ;
- humidity of drying air,  $H$ ;

- drop size distribution of spray and hence  $d_{vs}$ ;
- concentration of red dye in spray,  $c$ ;
- spray temperature,  $T_s$ .

### c) Spray Drop Velocities

The spray drop velocities were measured during the actual runs by the high speed cinematography method described in detail previously. Drop velocity determinations were not required for each test as the effect of changing the drying air temperature and consequently the evaporation rate, was not sufficiently great. However the drop velocities had to be determined whenever the atomizing streams were changed. Consequently measurements were taken for all of the nozzles when the atomizing conditions were changed. As measurements of the drop velocities closer than 4 in. to the pneumatic nozzles were not possible, the data obtained previously from the lucite column were used. Errors due to differences in drying air flow rates and temperatures are negligible so close to the nozzle, as data obtained 4.5 in. from the nozzle for both systems agreed closely.

### d) Flashing Tests

For some runs using the pressure nozzle, the liquid feed was heated above the wet-bulb temperature of the drying air. The preliminary tests on the operating conditions of the spray dryer were identical, but minor modifications in the test procedure were required. The water-cooled heat exchangers surrounding the liquid feed line were removed, and the gas-

fired stainless steel heating coil together with the asbestos covered nichrome heating coil were installed. The desired feed temperature was obtained by adjusting the voltage applied to the heating coil and the gas flow rate to the burner. For greater accuracy in the determination of the feed temperature, the thermocouple reading was taken with a separate Leeds and Northrup potentiometer. The remainder of the test procedure and the measurements taken conformed with the procedure previously described.

### 3. CALCULATIONS

#### a) Analysis of the Flow Pattern

For a co-current flow pattern, the analysis of the spray drop trajectories is considerably simpler. For all extents and purposes, the drop velocity vector and that of the drying air can be considered to have the same direction, since the radial velocity component causing expansion of the spray is very much smaller than the vertical component. Direct cinematography of the spray drops was possible and the air velocity in the nozzle zone was obtained by extrapolation of the drop velocity - drop diameter graphs.

During the adjustment of the spray axis for the pneumatic nozzle, temperature profiles were taken at various cross-sections. These were found to be practically uniform across the column for all distances greater than two inches from the nozzle. This meant that the turbulent mixing of the drying air and atomizing air streams was sufficiently rapid for the

production of a single temperature-valued system. This permitted one air temperature to be used in the analysis of the system. However when water was sprayed, the evaporation occurring in the spray cone produced air temperatures considerably lower than those prevailing in the surrounding annulus.

b) Material and Enthalpy Balances

The following material balance can be established between any two cross-sectional areas (1 and 2) in the nozzle zone. Average properties of the liquid and gas phases across the cross-sections are used.

$$W_1 - W_2 = w(H_2 - H_1) \quad \dots(196)$$

Due to the fact that the heat losses from the spray chamber were negligible and the atomizing air flow rate is negligible compared to that of the drying air, the following enthalpy balance based on a datum of 32°F can be written:

$$w \int_{32}^{t_1} (C_p) dt + wH_1(h_g)_{t_1} + W_1(h_f)_{T_1} = w \int_{32}^{t_2} (C_p) dt + wH_2(h_g)_{t_2} + W_2(h_f)_{T_2} \quad \dots(197)$$

Equation (197) may be simplified as:

1 - The enthalpy of water vapour does not change significantly with temperature. A one per cent change in the numerical value corresponds to a change in the vapour temperature of 25°F.;

2 - The spray temperature remains constant at the wet-bulb temperature of the drying air.

$$wC_p(t_1 - t_2) = (W_1 - W_2) (h_g)_{t_{av}} + W_2(h_f)_{T_2} - W_1(h_f)_{T_1} \quad \dots(198)$$

Equation (198) may be used to determine the heat transferred to the spray from the drying air.

$$Q = (W_1 - W_2) (h_g)_{t_{av}} + W_2(h_f)_{T_2} - W_1(h_f)_{T_1} \quad \dots(199)$$

For co-current flow it was found to be more convenient and accurate to obtain the evaporation rate of the spray in the column by means of the change in concentration of the dye with distance from the nozzle. The fraction of the spray evaporated in a given section of the spray chamber,  $E_f$ , may be expressed in terms of the initial and final concentrations of the dye  $c_1$  and  $c_2$  respectively.

$$E_f = (c_2 - c_1)/c_2 \quad \dots(200)$$

### c) Transfer Coefficients and Nusselt Numbers

As the spray drop properties and the drying air conditions are known at various distances from the nozzle, two methods are available for calculating the heat transfer coefficients. The first method consists of converting equation (199) into a differential form and determining the rate of change of the variables at certain points (40). The second method is to divide the nozzle zone into small sections and to calculate average values of the spray and drying air properties for each of these sections (175). Due to the lengthy procedure required for drawing tangents to curves accurately, or for calculating the slopes of the curves (10, 214), a modification of the second method was used.

Values of the drying air temperature, spray evaporation, Sauter mean diameter and the velocity of a spray drop of the same size as the Sauter mean diameter were plotted against the distance from the nozzle as the abscissa. Average values of these quantities from section to section were obtained by graphically integrating the area under the curve and dividing the values so obtained by the distance over which the integration was performed. These values were used in the calculation of the heat transfer coefficients and, subsequently, of the Nusselt Numbers. The procedure used was analogous to that described previously. Stepwise calculations were also performed as indicated for the cross-current runs.

#### 4. RESULTS

Fourteen runs were performed using the pneumatic nozzles: 4 runs with the (1/4)JN No. 12 nozzle at low atomizing pressures, 6 runs with the same nozzle at high atomizing pressures and 4 runs with the (1/4)JN No. 22B nozzle. The range of operating conditions investigated was:

- drying air flow rate, 300 lb./hr.;
- initial drying air temperature, 145 to 230°F.;
- feed flow rate to nozzle, 2 to 6 lb./hr.;
- feed temperature, 62 to 87°F.;
- atomizing air flow rate to nozzle, 5.45 to 20.5 lb./hr.;
- Sauter mean diameter of spray 13.5 to 28.8 microns;
- evaporation from spray, 40 to 85%.

Four runs were also performed using the pressure nozzle - (1/4) LN No. 1 - with feed temperatures near the wet-bulb temperature of the

drying air stream. Five more runs were performed with the same nozzle for higher feed temperatures. The range of operating conditions investigated was:

- drying air flow rate, 750 lb./hr.;
- initial drying air temperature, 150 - 250°F.;
- feed flow rate to nozzle, 12.0 lb./hr.;
- Sauter mean diameter of spray 40 to 82 microns;
- evaporation from the spray 9 to 63%.

The experimental data obtained together with the calculated values of the heat and mass transfer coefficients and the Nusselt Numbers are given in Appendix V.

Microphotographs of the spray drops produced by the pneumatic and pressure nozzles are given in Fig. 38. Fig. 39 illustrates typical simultaneous changes in the evaporation rate, air and spray temperatures, Sauter mean drop diameter and the velocity of a drop of the same size as the Sauter mean diameter which occurred with change in distance from the nozzle, i.e., as evaporation proceeded. Graphs recording the changes in the spray evaporation, spray temperature, drying air temperature and Sauter mean diameter with distance from the nozzle are given for the various operating conditions of the pneumatic nozzles, and the pressure nozzle in Fig. 40 to 42. The effect of feed temperature on the evaporation rate is shown in Fig. 43.

The Nusselt Numbers for heat and mass transfer are plotted with respect to the dimensionless groups,  $(Re)^{1/2}(Pr)^{1/3}$  and  $(Re)^{1/2}(Pr)^{1/3}$  in

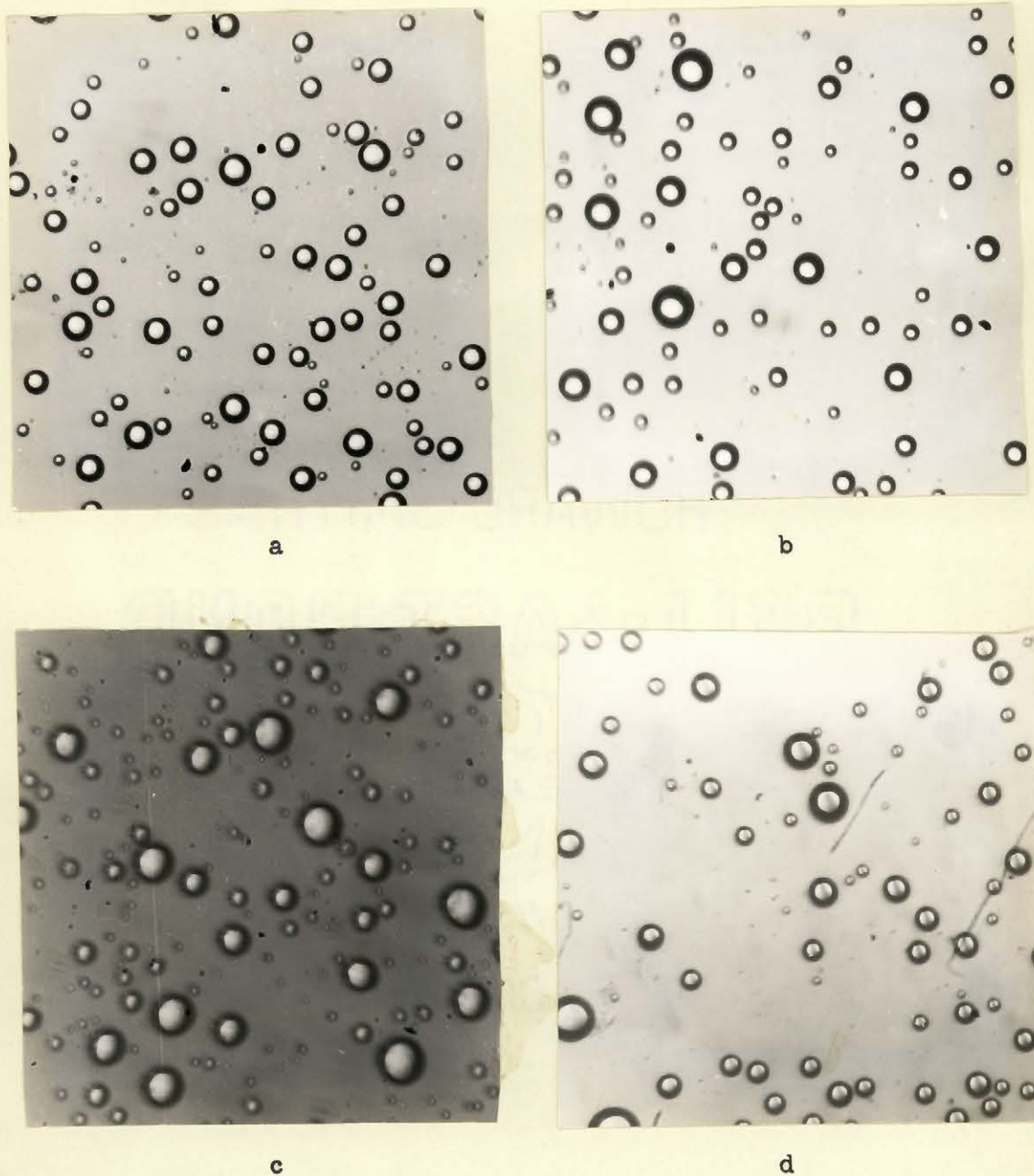


Fig. 38. Typical Microphotographs of the Spray Drops in the CO-Current Flow Equipment

- a) Pneumatic Nozzle 1/4JN No. 12 High Atomizing Pressures (Mag. 175X)
- b) Pneumatic Nozzle 1/4JN No. 22B (Mag. 175X)
- c) Pressure Nozzle 1/4LN No. 1 (Mag. 40X)
- d) Pressure Nozzle 1/4LN No. 1 Superheated Feed (Mag. 40X)

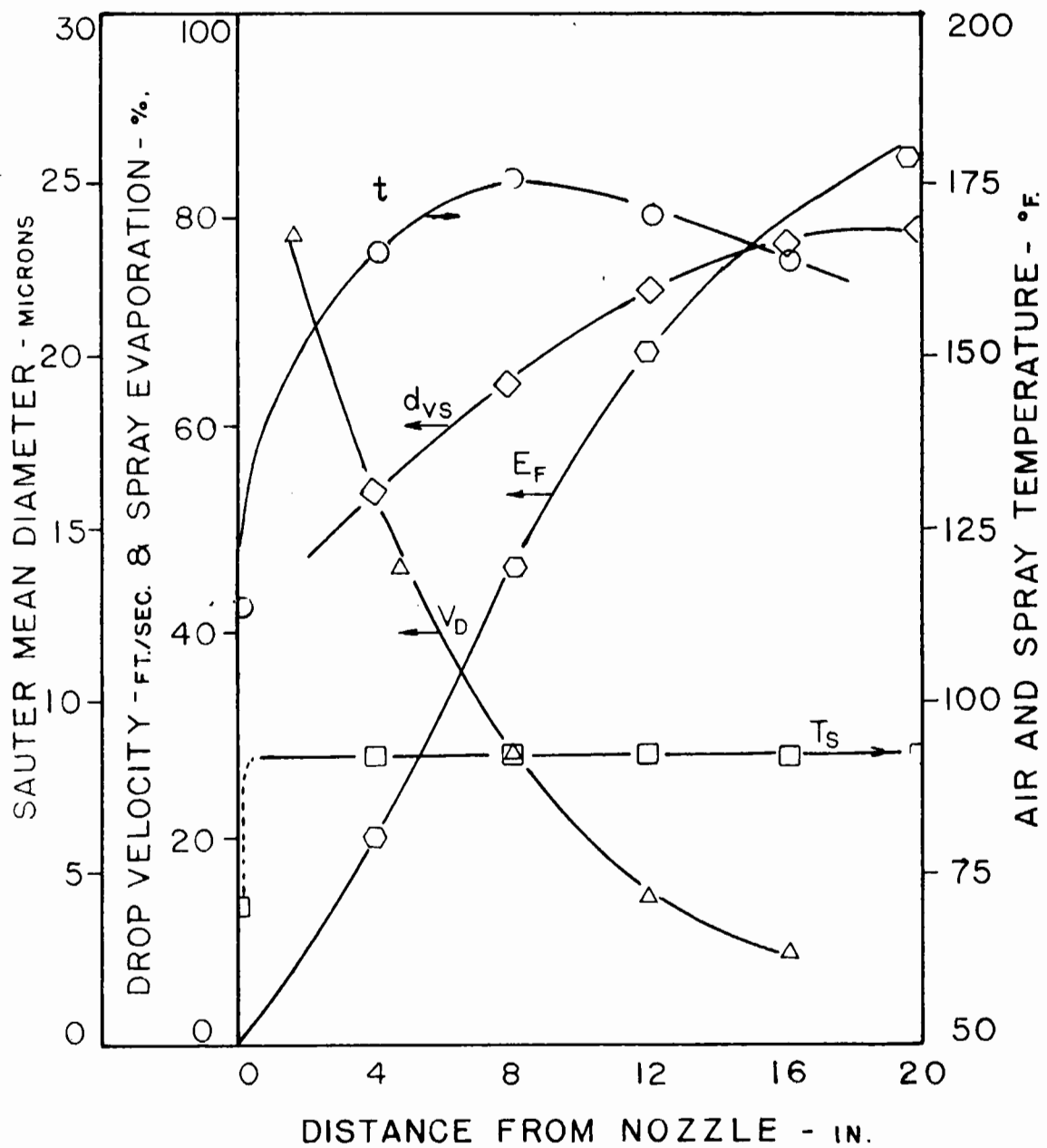


Fig. 39. Changes in Spray and Air Properties for Run 29

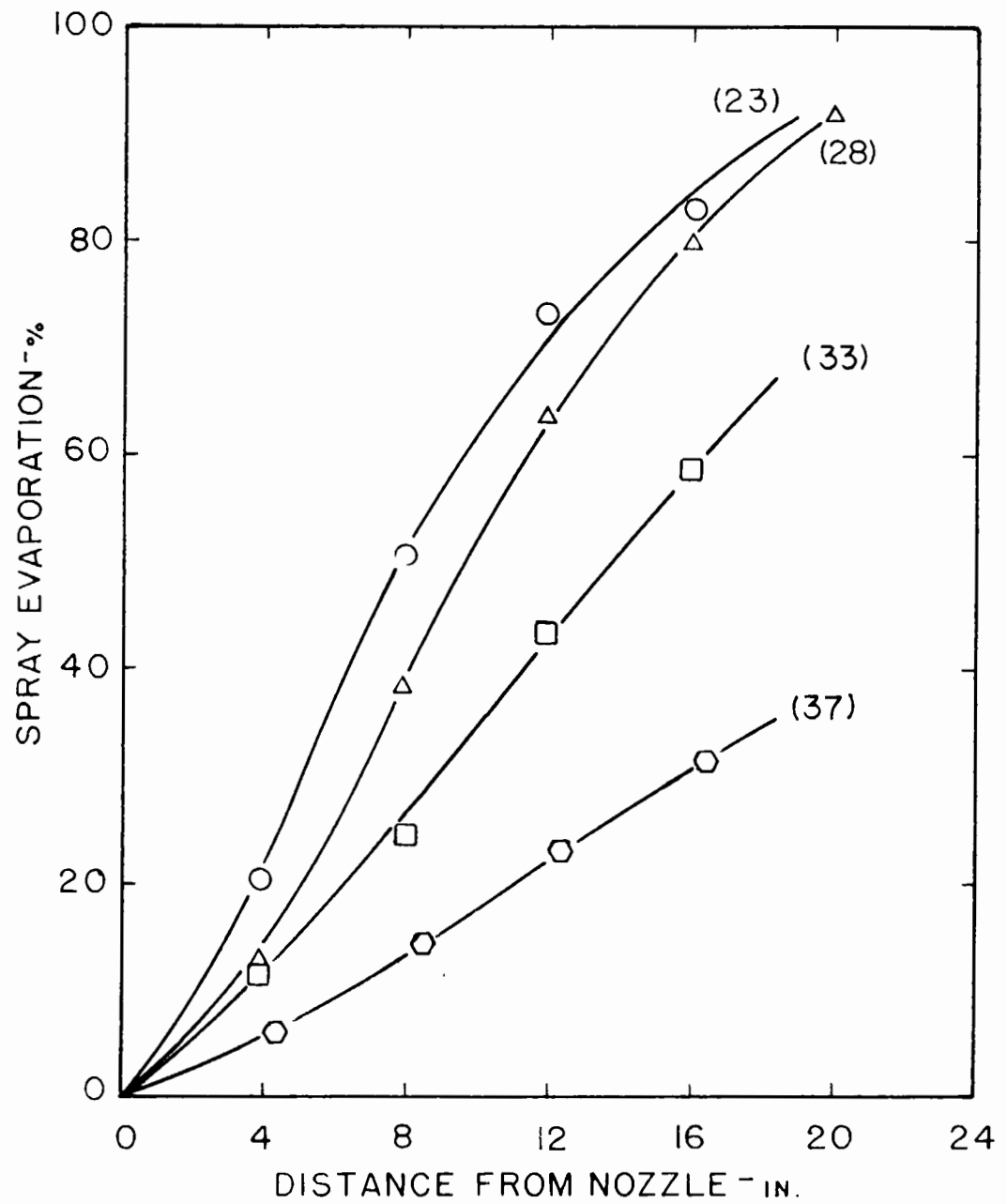


Fig. 40. Spray Evaporation - Distance from Nozzle Data

(Numbers in parentheses denote run number )

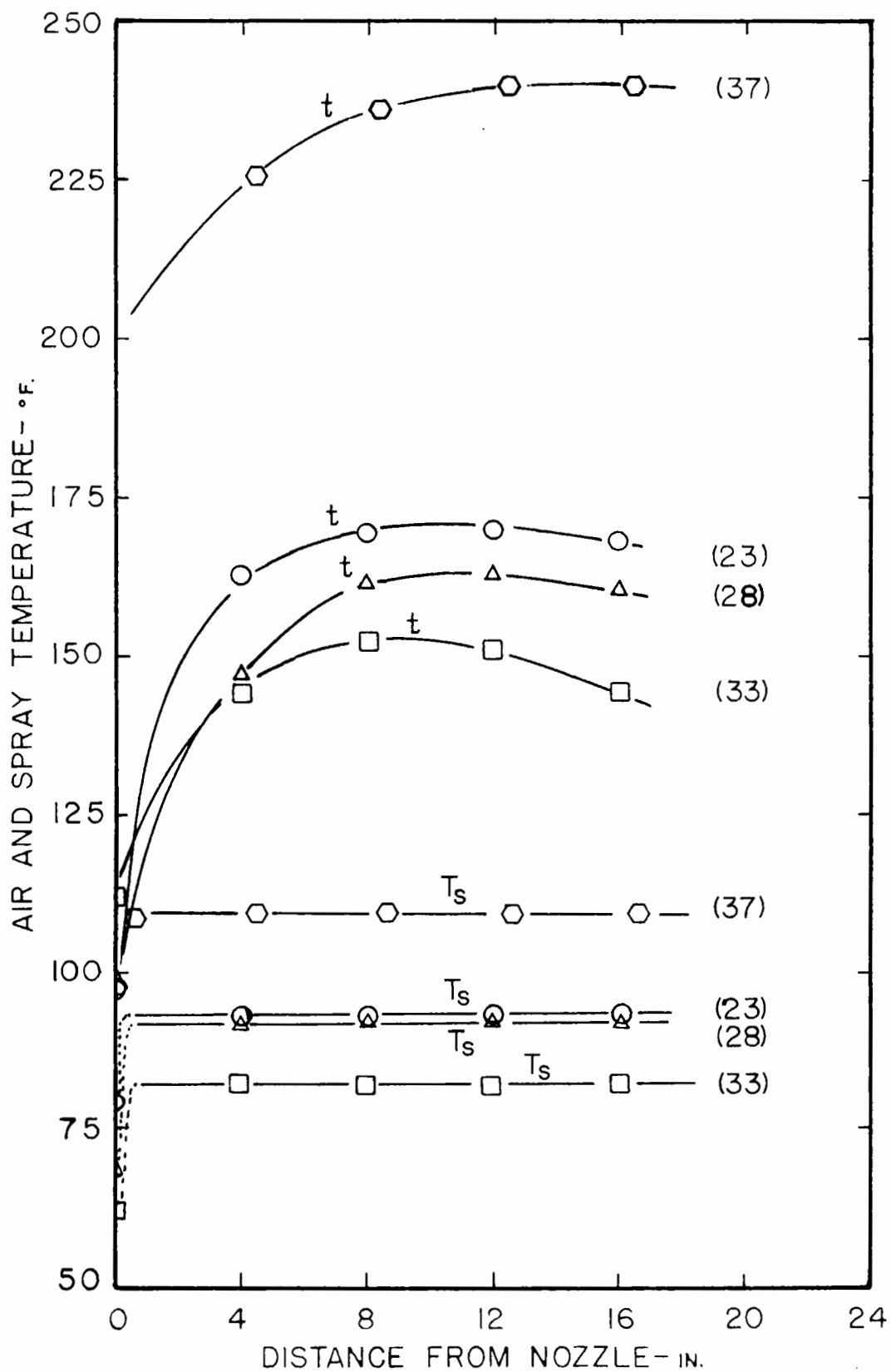


Fig. 41. Air and Spray Temperature - Distance from Nozzle Data  
(Numbers in parentheses denote run number)

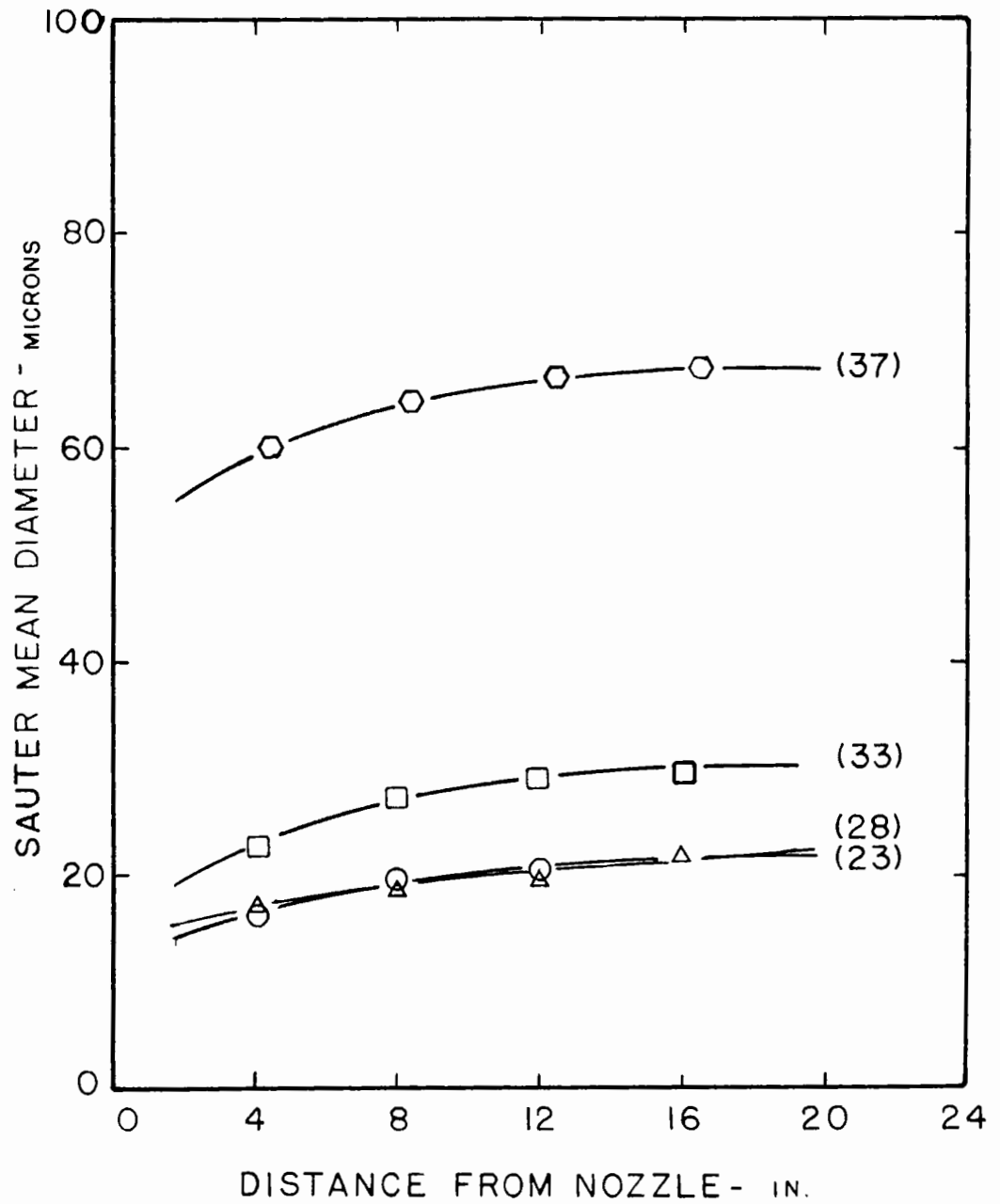


Fig. 42. Sauter Mean Drop Diameter - Distance from Nozzle Data  
(Numbers in parentheses denote run number)

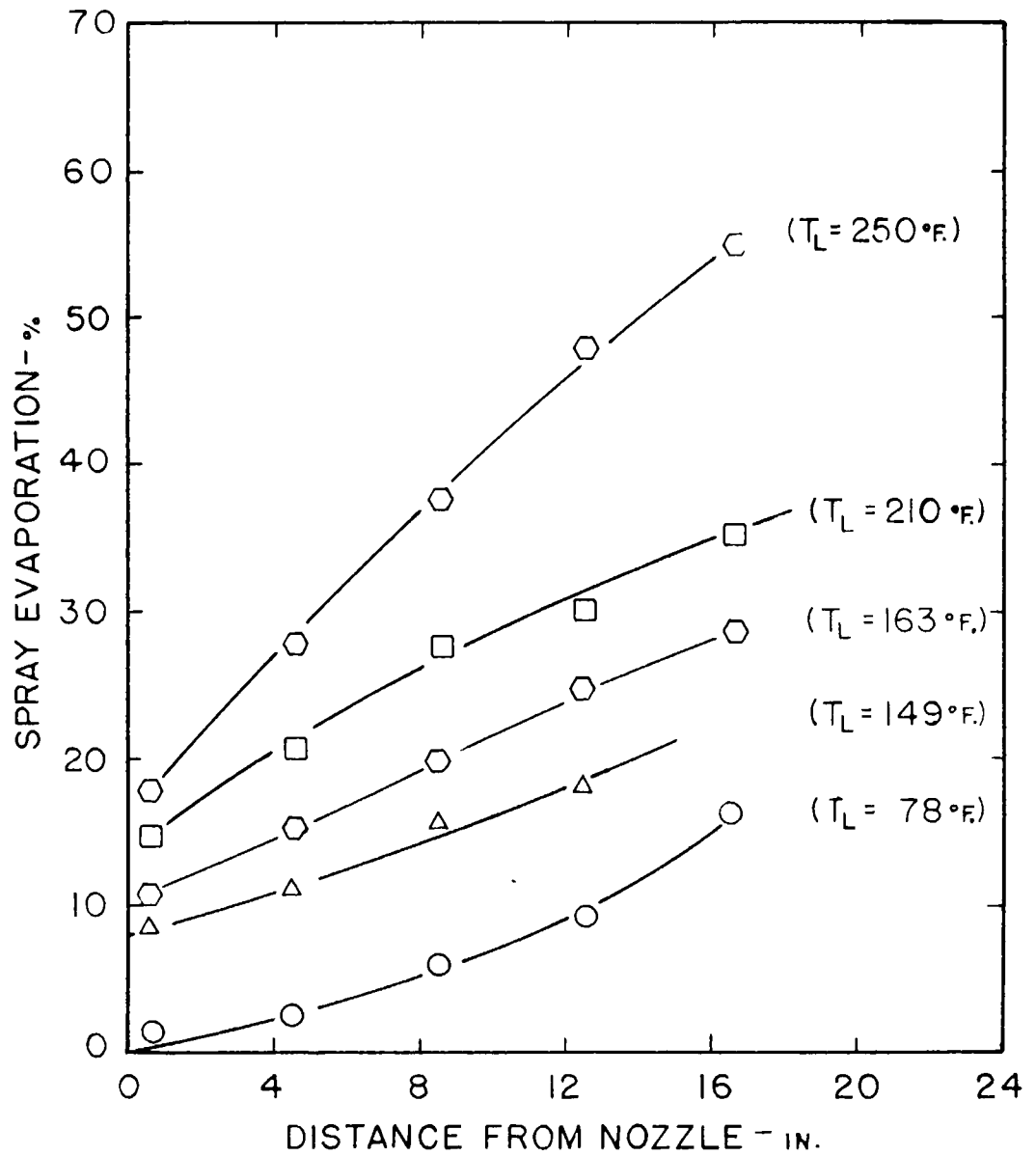


Fig. 43. Effect of Feed Temperature on Evaporation

Fig. 44 - 47. A typical air velocity profile in the nozzle section of the spray chamber is shown in Fig. 48 under conditions of no water flow from the nozzle, i.e., discharge of atomizing air only.

Finally Fig. 49 presents a comparison of the measured evaporation and that calculated by the stepwise procedure previously outlined. The tabulated data for the incremental calculation are given in Appendix VI.

## 5. DISCUSSION OF RESULTS

The flow patterns obtained in the co-current drying chamber were much simpler than those encountered in the cross-current drying chamber and so more accurate data were obtained.

Evaporation from the spray was followed by means of changes in the concentration of the red vegetable dye. The fact that the sample bottle was moved radially through the spray during the collection of the spray removed the necessity of traversing. Humidity changes in the drying air would be meaningless unless accompanied by extensive traversing and air-velocity determination. The latter measurements are exceedingly difficult and prone to error.

### a) Heat and Material Balance

The heat and material balances in the co-current equipment were excellent. The outlet blower which was located between the spray chamber and the exhaust system enabled the static pressure in the spray chamber to be regulated. By adjusting the static pressure in the spray chamber to

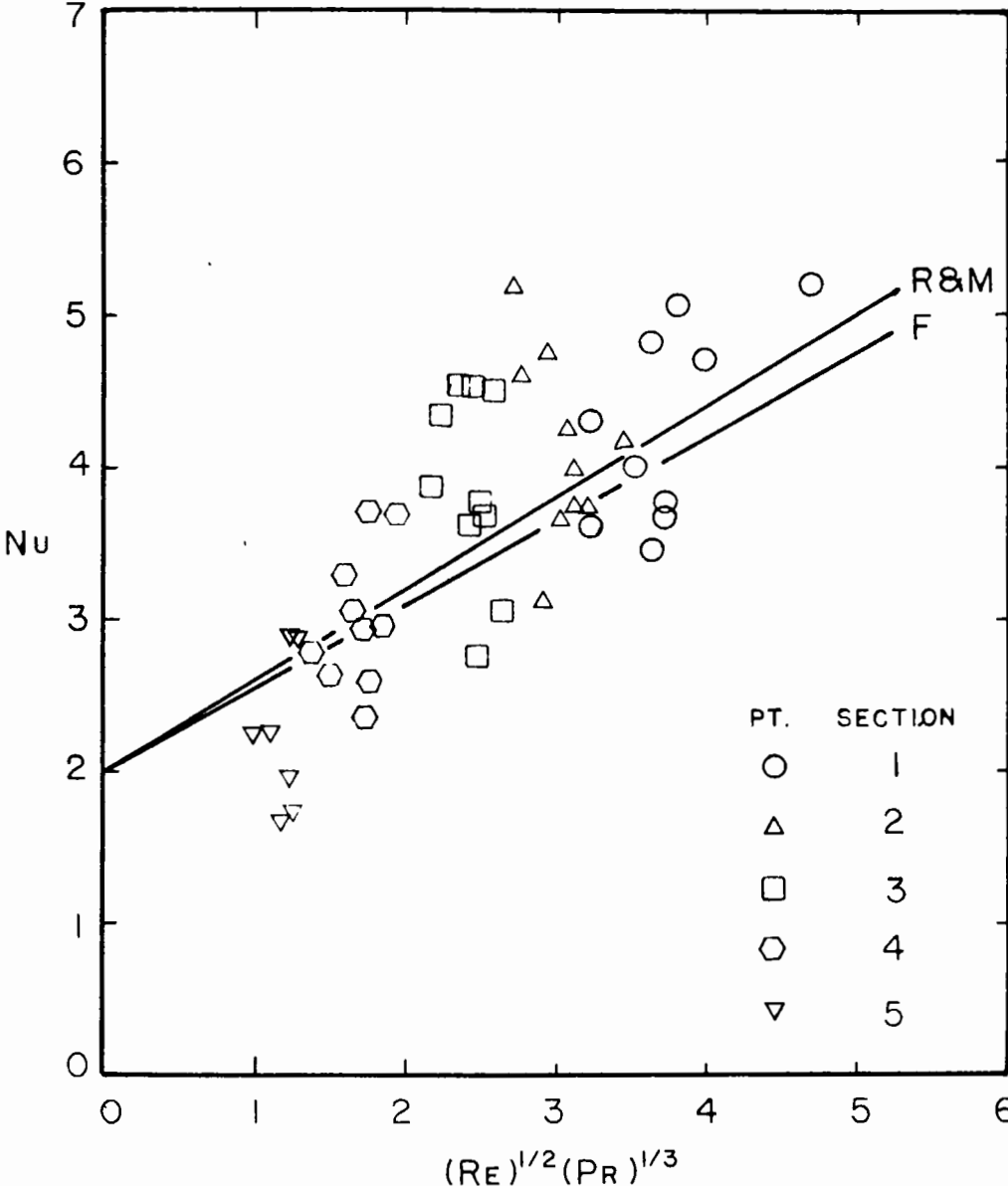


Fig. 44. Heat Transfer Data for Runs 21 - 30

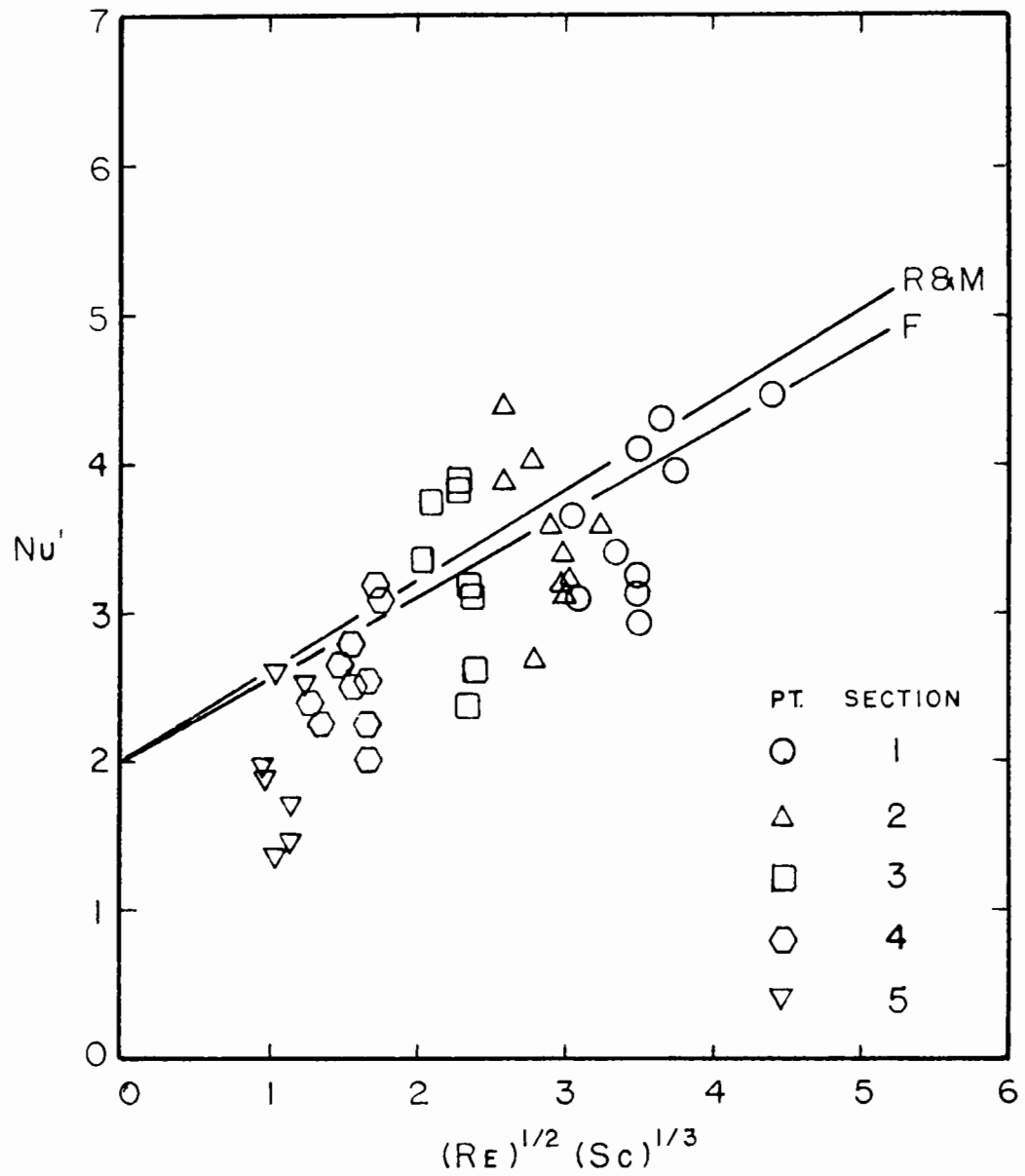


Fig. 45. Mass Transfer Data for Runs 21 - 30

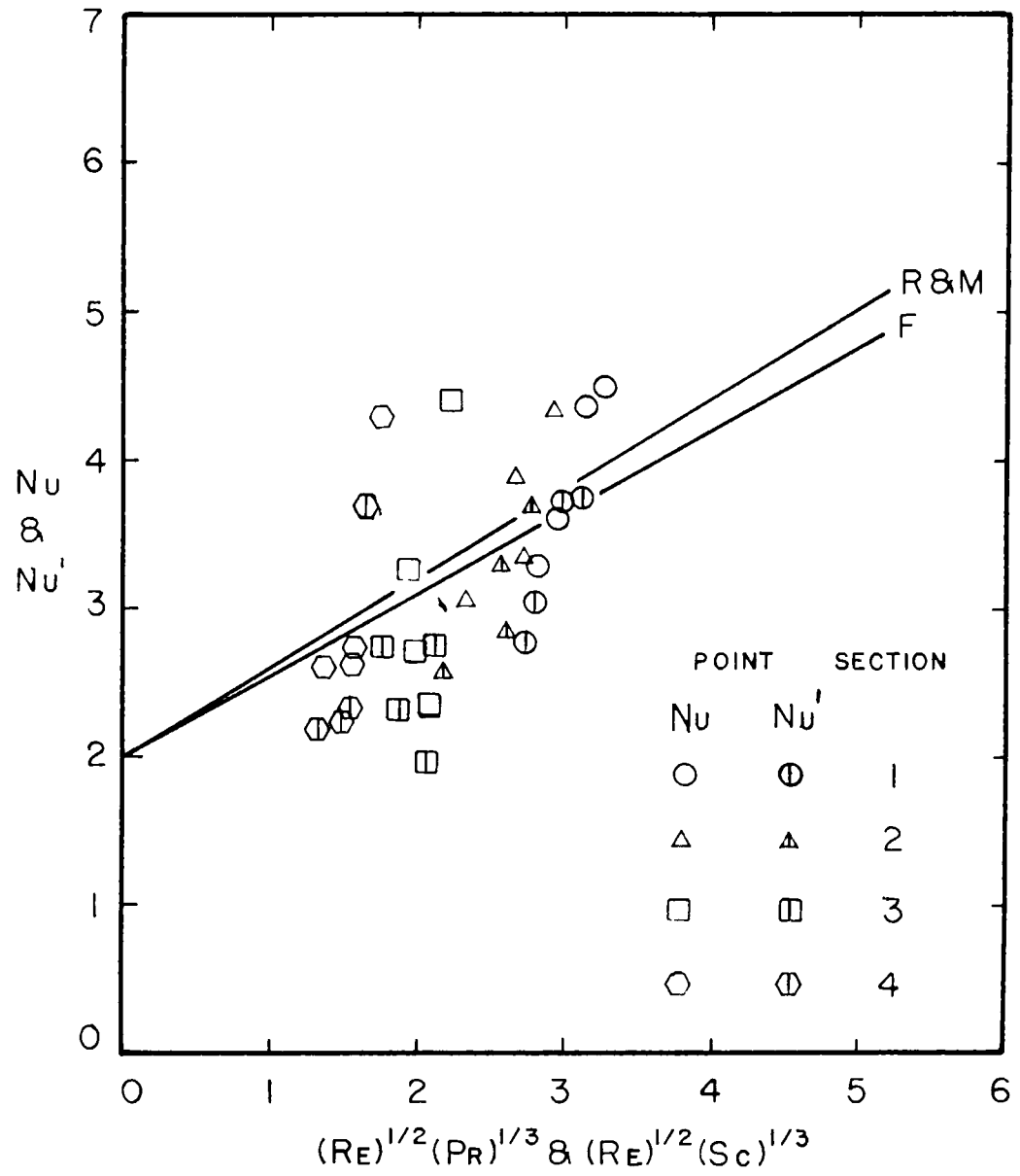


Fig. 46. Heat and Mass Transfer Data for Runs 31 - 34

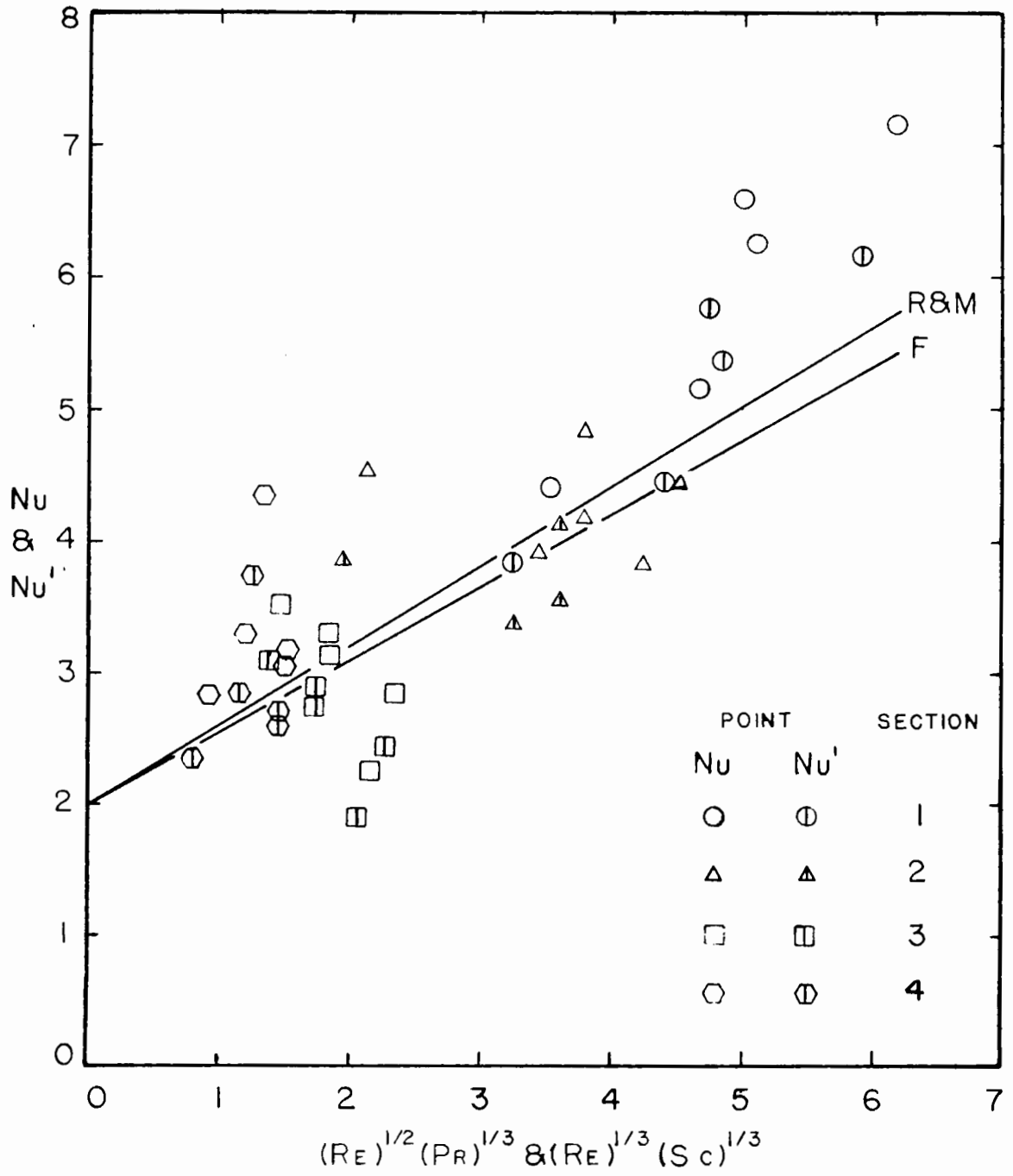


Fig. 47. Heat and Mass Transfer Data for Runs 35 - 39

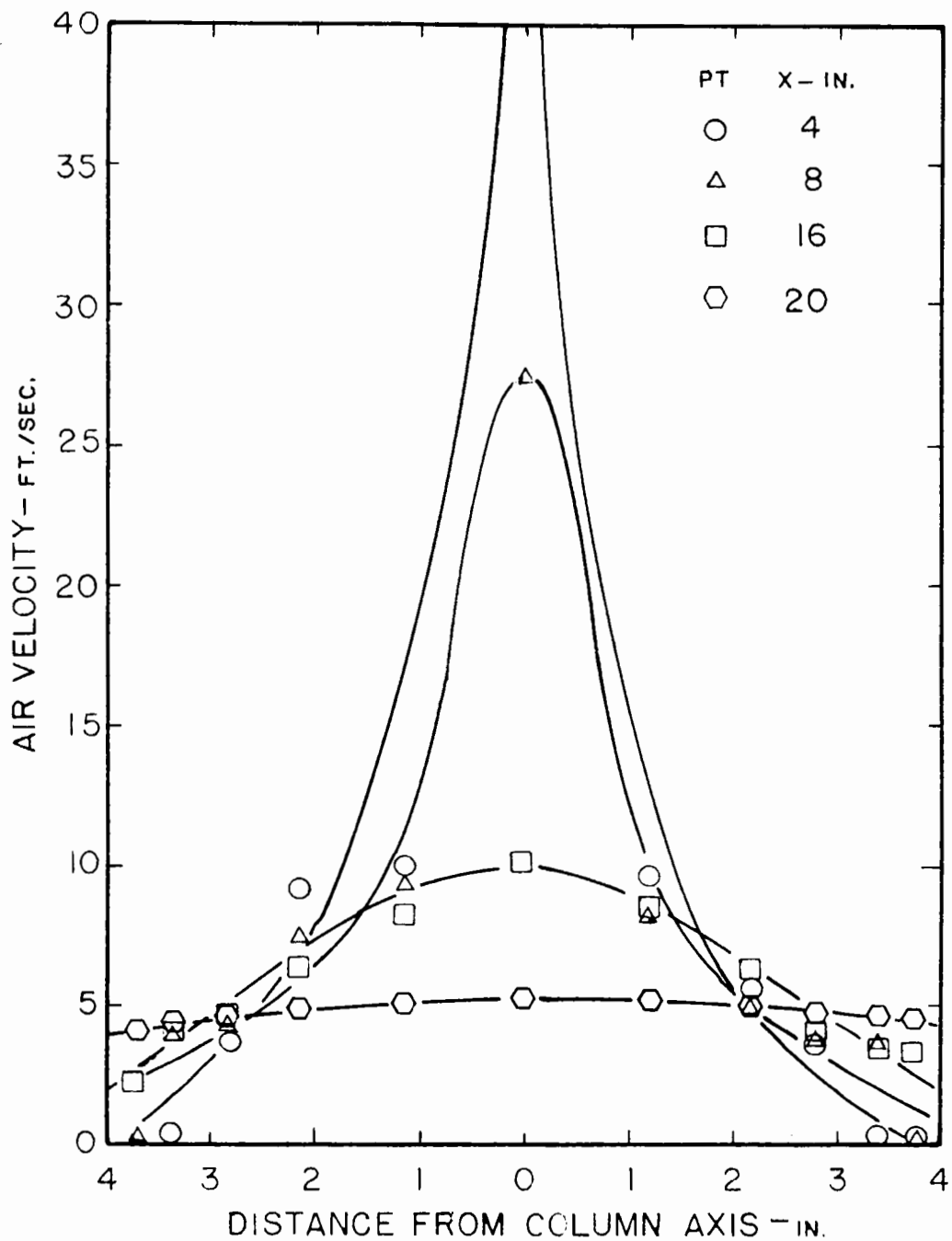


Fig. 48. Initial Air Velocity Profile in Nozzle Section  
(Pneumatic Nozzle 1/4JN No. 12 - Low Atomizing Pressures)

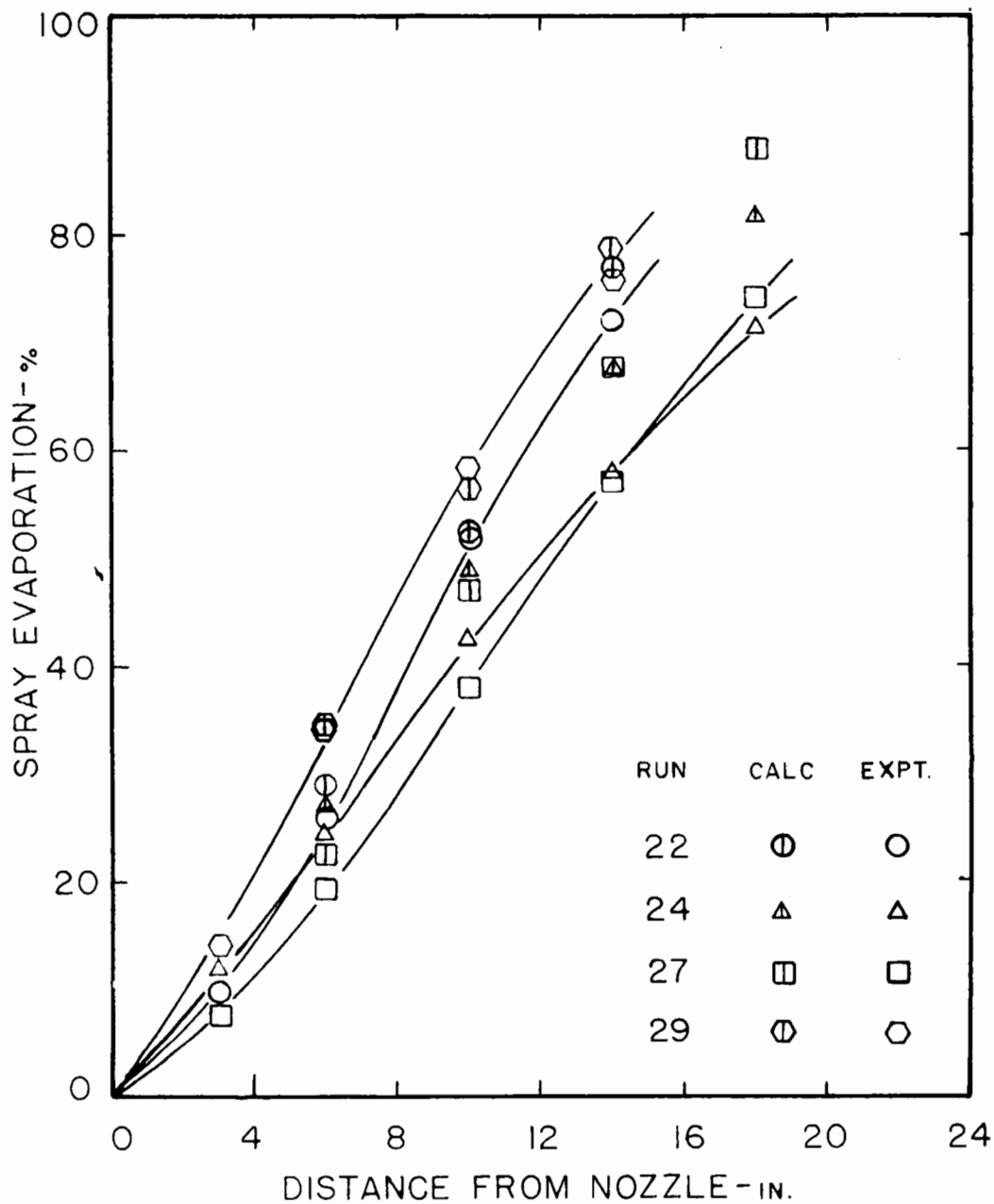


Fig. 49. Application of Incremental Analysis to Co-Current Flow Runs

zero, the possibility of leaks was eliminated.

The loss of heat from the spray chamber could be determined by recording the temperature of the drying air in the spray chamber when the atomizing nozzle was not in use. As a temperature drop greater than 4°F. was not obtained for the entire spray chamber, it can be concluded that the loss of heat in the nozzle section is negligible.

#### b) Nozzle Characteristics

A fairly wide range of drop sizes, drop velocities and atomizing air velocities was obtained with the two pneumatic nozzles and the pressure nozzle investigated. As in the cross-flow runs, larger drop sizes and lower drop velocities were obtained with the pressure nozzle than with the pneumatic nozzles. A comparison of the two pneumatic nozzles revealed that almost identical drop sizes were obtained, but that the No. 12 nozzle produced sprays with higher drop velocities at lower atomizing air velocities (Fig. 6, 9 and 10). These figures also demonstrate that the smaller spray drops decelerate to the overall air velocity in the column much more rapidly than the larger drops.

Examination of Fig. 48 indicates that the air velocities measured with the impact probes under conditions of no water flow are higher than those indicated by the intercepts of the drop velocity - drop diameter curves on the velocity axis in Fig. 5. This is to be expected as a considerable part of the energy of the atomizing air is consumed during the production of the spray.

It should be noted that almost complete radial symmetry in the air velocities was obtained, especially when the pneumatic nozzles were used. This may be attributed to the fact that the thrust and entraining action of the atomizing air jet completely masked any flow irregularities in the drying air stream.

c) Heat and Mass Transfer

Fig. 39 to 42 represent the changes in the drying air temperature, spray temperature, spray mass and Sauter mean diameter that occurred in the nozzle section as evaporation proceeded. The temperature of the drying air within the spray was observed to increase initially with increase in the distance from the nozzle. This is due to localized cooling of the drying air in contact with the evaporating spray close to the nozzle. An additional factor is the annulus of hotter drying air which, passing initially outside the spray, mixes progressively with the atomizing gas stream as the spray expands. However a maximum value was reached when the atomizing gas stream had mixed completely with the surrounding drying gas stream and also when the localized cooling effect was negligible. After this point the decrease in the air temperature corresponded to the heat required for the evaporation of the spray. In contrast to the cross-current flow chamber the spray temperature invariably remained constant at the wet-bulb temperature of the drying air stream.

As in the cross-current flow tests, the Sauter mean diameter increased initially with increase in the distance from the nozzle. This behaviour may be attributed to the rapid evaporation of very small sizes

which may be expected for the case of a wide drop size distribution. However, the rate of increase in the Sauter mean diameter soon decreased and in some cases smaller values were reported in Section 5.

The spray evaporation - distance from the nozzle graph consistently exhibited an initial gradual increase in the rate of evaporation followed by a point of inflection and finally a decrease in the evaporation rate. The initial increase is due to the increase in the temperature of the air in contact with the spray with distance from the nozzle, and the fact that the spray drop velocities decrease very rapidly with distance from the nozzle. The latter phenomenon has the effect of increasing the spray drop residence time and so increased the evaporation. The initial increase in the drop diameter undoubtedly opposes the above effects and consequently must be of lesser significance. As evaporation proceeds, the evaporation rate decreases due to a decreasing drying air temperature, increasing Sauter mean drop diameter and a decrease in the spray remaining. Here the effect of spray evaporation (increase in the drying air humidity and decrease in temperature) begins to play an important role. The above effects due to evaporation were common to all of the nozzles tested.

The Nusselt Numbers calculated were correlated in terms of the Reynolds and Prandtl Numbers and verified the validity of the correlation proposed by Ranz and Marshall (188) for the heat transfer (equation 96). The modified Nusselt Numbers were again found to be 10 to 15% lower than would be predicted using the corresponding equation for mass transfer (equation 97).

The validity of the correlation of Ranz and Marshall was also tested using the stepwise calculation procedure where the different drop size groups were considered separately. Considerably better agreement was obtained between the measured and calculated evaporation increments in the various sections. This can be attributed to the more accurate measurement of the drop velocities for the smaller drop sizes made possible by the simpler air flow patterns which existed in the co-current equipment.

d) Effect of Feed Temperature

An increase in the temperature of the feed pumped to the pressure nozzle was found to result in a considerable increase in the evaporation rate (Fig. 43). This phenomenon may be attributed to the following factors:

- 1 - Increase in initial evaporation due to release of thermal energy stored in the liquid as the spray temperature suddenly drops to the wet-bulb temperature of the drying air stream; this is the well-known phenomenon of flash evaporation;
- 2 - An increase in the feed temperature results in a decrease in the liquid viscosity and surface tension. Both of these factors tend to reduce the average spray drop size, as shown by equations 31 to 35, and this has been previously shown to have a considerable effect on the evaporation rate;
- 3 - The drop velocities were observed to decrease with increase in the feed temperature. The result is an increase in the residence time of the spray in any given section along the spray axis and an increase in the evaporation rate.

Once the spray drops have attained the wet-bulb temperature of the drying air stream, the evaporation proceeded according to the correlations of Ranz and Marshall. The attainment of the wet-bulb temperature was shown to occur almost immediately, i.e., within one inch from the nozzle. From the above, it is evident that considerable increases in the evaporation rates of sprays from pressure nozzles can be accomplished by preheating the feed.

## CONCLUSIONS

The development of suitable methods for measuring the physical properties of the two phases of a drop-laden air jet constituted an important phase of the work reported in this investigation. The presence of both phases renders the usual techniques for the determination of the air velocity, temperature and humidity useless. Also the small terminal velocity of the drops and the high level of turbulence encountered in the spray - from 20 to 3% downstream (36) - made the collection of a representative spray sample difficult. However, techniques for measuring the spray properties were developed, which appeared to overcome these difficulties.

The well-known fact that the spray drops remain at the wet-bulb temperature of the drying air stream (28, 79, 110, 112, 147, 175, 184, 188) was applied in designing a thermocouple for measuring the temperature of the spray drops. The design was original and the results obtained verified that the spray remained at the wet-bulb temperature.

Measurements of the evaporation from sprays by means of a change in concentration of a dissolved solid have been reported (40). However such methods usually involve high concentrations of the dissolved solid. The present technique employed a highly coloured strawberry red vegetable dye and the concentrations of the solution sprayed (1 part per ten thousand) produced no change in the liquid surface tension or viscosity.

The shields used to protect the thermometers for the determination of the drying air temperatures were similar to those developed by Dlouhy (40). However, the design had to be modified, owing to the complexity of the flow patterns and the relatively high turbulence intensities.

A thorough experimental investigation of the available methods of measuring the air humidities was performed, and two absolute methods were developed. When the accuracy of these methods was compared with that obtained by conventional methods (wet- and dry-bulb and dew-point), the volumetric method was shown to be quite superior. Humidity changes of 0.0002 lb. water/lb. dry air were detectable over a range of 0 to 0.05 lb. water/ lb. dry air.

Measurements of the drop velocities in sprays are extremely rare (99, 268) and so far there appears to be no published data on the drop velocities in sprays produced by pneumatic nozzles. The measuring technique developed using high-speed cinematography enabled the drop velocities to be measured as close as 1.5 in. from the pneumatic nozzle and 0.5 in. from the pressure nozzle. Comparison of the velocity data for the two atomizers showed that smaller drops and higher velocities were obtained using the pneumatic nozzles.

The drop velocities were observed to decrease until the velocity of the air stream was reached, since the terminal velocities were extremely low. This can be verified by the fact that drop velocities lower than that of the air stream were almost never observed. Examination of Fig. 5 to 13 shows that the smaller drops decelerate to the overall drying air velocity

before the larger ones. This is in accordance with theory, since small particles require a shorter time than large ones to reach their terminal velocity (129).

A careful analysis of Fig. 5 to 13 permitted the following conclusions to be drawn:

- 1 - An increase in the liquid flow rate - and consequently in the liquid feed pressure - results in an increase in drop velocities (Fig. 7 and 8);
- 2 - An increase in the atomizing air flow rate - and consequently in the atomizing air pressure - results in a slight increase in the drop velocities (Fig. 5 and 7). The effect is accompanied by an increase in the entraining capacity and air velocity of the jet;
- 3 - The influence of evaporation on the drop velocities has been previously discussed, and appears to involve two opposite effects. Firstly, there is a decrease in the drop velocity due to a reduction in the spray mass, with a corresponding diminution of the kinetic energy available for penetration of the surrounding gas. Secondly, as an increase in the evaporation rate increases the initial drop size at the atomizing nozzle corresponding to a particular drop size at any given point in the spray, and as the initial drop velocity increases with drop diameter, there is a tendency for this increased velocity to be retained during the penetration of the surrounding air. Comparison of Fig. 5 and 6, and Fig. 8 and 9 shows that the relative velocity of the drops close to the nozzle tended to be higher at small drop diameters and smaller at large drop diameters where considerable evaporation occurred.

Fig. 5 and 6 indicated that at greater distances from the nozzle lower drop velocities occurred;

4 - An increase in the drying air velocity resulted in an increase in the drop velocity (Fig. 5 and 6, 8 and 9). This is undoubtedly due to a diminution in the drag force which is proportional to the square of the relative velocity.

The air velocity in the spray was evaluated from the intercept on the velocity axis of the drop velocity - drop diameter curves. This method appeared to be more promising than measurements of the air velocity where only air was discharged from the nozzle. The assumption that the velocity distribution would remain the same in the presence of the spray appeared to be unjustified.

Drag coefficients for the decelerating spray drops were calculated from the changes in the drop velocity with distance from the nozzle. The values obtained were considerably lower than those indicated by the standard curve for spheres. A dependence on the drop diameter was indicated as the larger drops exhibited larger drag coefficients. This suggests that the scale of turbulence is a contributing factor. Also the spray drops produced by the pneumatic nozzle exhibited lower drag coefficients than those obtained from pressure nozzles, which can be explained as follows. As the intensity of turbulence in the nozzle zone of sprays from pneumatic nozzles is comparable to that of an expanding jet - about 20% initially (36) - and is therefore considerably greater than that produced by pressure nozzles, an increase in the intensity of turbulence appears to reduce the drag coefficients. There is some

supporting evidence in the literature (140, 160) but the complexity of the phenomena occurring and the limited and conflicting nature of the available data makes the formulation of any definite conclusions extremely difficult. However, the effects of spray drop concentration, rotation and deformation appear to be negligible (21, 93, 102, 104, 111, 132, 227).

It is interesting to note that Ingebo's data, as shown in Fig. 2, appears to indicate an opposite behaviour to that just reported. As the iso-octane spray was injected counter-currently into the high velocity air stream, it can be inferred that the larger drops were probably accelerated more slowly than the smaller ones and so should possess larger relative velocities. Ingebo's data in Fig. 2 clearly shows that an increase in the relative velocity which corresponded to the larger drops produced a decrease in the drag coefficient, which is in direct contradiction to the findings of the present investigation.

The heat and mass transfer rates to the spray drops were measured in the region where deceleration from the initial velocity to that of the drying air occurred. This constituted the first attempt to measure the evaporation rates in the nozzle zone of sprays produced by typical industrial atomizing nozzles. The only similar previous work, which was rather limited in nature, was performed using extremely high drying air velocities and a counter-current method of spray injection (99).

The equations proposed by Froessling (60), and Ranz and Marshall (188) for stationary drops suspended in moving air streams were found to be

generally applicable for correlating the Nusselt Numbers in terms of the dimensionless groups,  $(Re)^{1/2}(Pr)^{1/3}$ ,  $(Re)^{1/2}(Sc)^{1/3}$ , (Fig. 25, 26, 27, 28, 44, 45, 46, 47), in the range of Reynolds Numbers investigated.

The Nusselt Numbers obtained for the decelerating drops (Fig. 25, 27, 44, 46, 47) were consistently higher than the corresponding Modified Nusselt Numbers (Fig. 26, 28, 45, 46, 47). Similar results were reported for freely falling spray drops (40). However, this is still rather difficult to explain but could possibly be attributed to inaccuracies in the mass diffusivity values. The scatter of the experimental data may appear to be considerable, but may be ascribed to the fluctuations inherent to the system: by this, it is meant that in any part of the nozzle zone, drops of a given diameter can have different velocities depending on the effect of the turbulent velocity fluctuations during deceleration. This view is confirmed by the fact that larger deviations were obtained for the No. 22B pneumatic nozzle (Fig. 46) than for the No. 12 nozzle (Fig. 44, 45). The former nozzle has a much higher atomizing air flow rate and therefore must produce considerably greater turbulent fluctuations in the co-current drying air stream. It might be expected that the intensity of turbulence encountered might result in an increase in the heat and mass transfer rates, (51,144) but such effects are relatively small and are thus not likely to be apparent in the range of Reynolds Numbers investigated.

The data obtained using the pressure nozzle in the cross-current equipment were presented in Fig. 27 and 28. At first sight it may appear that there is a marked tendency for the Nusselt Numbers obtained at the

lower Reynolds Numbers in the lower sections of the chamber to be significantly lower than that indicated by the equations of Froessling (61) and Ranz and Marshall (188). However, any such conclusions would be premature as the extremely wide spray angle of the pressure nozzle could conceivably have produced some contact with the spray chamber walls in those sections which would produce lower evaporation rates.

The step-wise calculations in which the incremental drop-size groups were considered separately, predicted evaporation rates which were considerably higher than those actually measured. This may be attributed to the difficulty of obtaining accurate values of the velocities of the smaller drop sizes from which most of the evaporation occurred. The data obtained for the co-current flow runs (Fig. 49) agreed more closely with the measured evaporation rates than that obtained for the cross-current flow runs, thus indicating that the smaller drop velocities were determined more accurately.

The effect of increasing the feed temperature on the evaporation rate was determined (Fig. 43). Marked increases in the evaporation rates were observed, and this was attributed to three separate factors. Firstly, there is an instantaneous flashing as the drop temperature decreases to the wet-bulb temperature of the surrounding gas. Secondly, the decrease in the liquid surface tension and viscosity produces a decrease in the spray drop sizes (Equations 31 to 35). This results in an increase in the specific surface available for heat and mass transfer and consequently increases the evaporation rate. Thirdly, there is a decrease in the drop velocities (Fig. 12 and 13), and this has the effect of increasing the

residence time of the spray drops and consequently the evaporation in any given distance along the spray axis.

It is realized that much additional experimental work will have to be carried out before the effects resulting from preheating the feed can be fully assessed. From the preliminary study which has been presented, it appears that this approach might offer many practical advantages.

In closing, it can be said that this study has clearly indicated that the rates of heat and mass transfer to spray drops can be predicted with good accuracy, once the drop size distribution for the given atomizing nozzle under the given operating conditions is known. This latter can be obtained from the nozzle manufacturer's data, or alternatively, from experimental determinations.

Before the evaporation rate can be predicted, however, the drop velocity must be ascertained. This is a problem of considerably greater complexity. The present work has amply demonstrated that the oversimplified approach used by Sjenitzer (217) and Edeling (46) based on conventional values of the coefficients of drag of spheres falling in still fluids, is hopelessly inadequate. It is obvious that considerably more work will have to be done on the momentum transfer aspects of an expanding spray of droplets before working correlations capable of predicting the droplet velocities at any distance from the nozzle can be established. Since the latter are themselves functions of the evaporation rate, which is the unknown in the problem, the complicated nature of the situation can be visualized.

It is realized of course that the present study has only served to give a better appreciation of the importance of drop velocity estimations, and of their order of magnitude for a few specific cases. It cannot be pretended that it is anything more than an introduction to this field. It is hoped, however, that the results of this investigation, limited as they are, will stimulate continued interest in this topic.

## SUMMARY AND CONTRIBUTION TO KNOWLEDGE

Due to the lack of data available on the rates of heat and mass transfer to spray drops while decelerating with respect to the surrounding air, a fundamental investigation of the evaporation rates to sprays produced by typical industrial atomizing nozzles was performed. The following conclusions were drawn from the results of this investigation:

- 1 - The conventional methods of measuring air humidities were inadequate for this investigation and an absolute method capable of detecting humidity changes of 0.0002 lb. water/lb. dry air was developed;
- 2 - A method of measuring the spray drop velocities using high-speed cinematography was developed;
- 3 - Smaller drops and high drop velocities were obtained using the pneumatic nozzles as compared with pressure nozzles;
- 4 - An increase in the liquid flow rate, the atomizing gas flow rate, or the air velocity in the spray chamber tended to increase the drop velocities;
- 5 - The effect of evaporation on the drop velocities was of a minor nature;
- 6 - The air velocities in the spray were estimated from the intercept of the drop velocity - drop diameter graphs on the drop velocity axis;
- 7 - The drag coefficients of the decelerating spray drops were considerably lower than those indicated for the standard curve for spheres;

- 8 - A dependence of the drag coefficient on the drop diameter was observed thus indicating that the scale of turbulence is probably a contributing factor;
- 9 - Spray drops from the pneumatic nozzles appeared to have lower drag coefficients than those of the same diameter produced by the pressure nozzle, thus suggesting that an increase in the intensity of turbulence reduces the drag coefficient;
- 10 - As the relative velocity of the spray drops decreases to a very low value, the eddy diffusivities of the spray drops and the drying air become almost equal;
- 11 - Considerable evaporation of the spray can occur in the nozzle zone;
- 12 - The Nusselt Numbers of the decelerating spray drops were correlated in terms of the equations of Froessling (61) and Ranz and Marshall (188).
- 13 - Values of the modified Nusselt Number were consistently 10 to 15% lower than those indicated by the equation of Ranz and Marshall (188);
- 14 - An increase in the velocity of the spray drops increases the heat and mass transfer rates but the evaporation occurring per unit distance along the spray axis is reduced;
- 15 - An increase in the feed temperature decreases the average spray drop size and velocity, thus increasing the evaporation rate.

## NOMENCLATURE

### a) Roman Symbols

- A - surface area of drop (ft.<sup>2</sup>);
- A<sub>D</sub> - cross-sectional area of drying duct, (ft.<sup>2</sup>);
- A<sub>f</sub> - cross-sectional area opposed to flow, (ft.<sup>2</sup>);
- A<sub>n</sub> - arbitrary coefficient of nth term in series of J<sub>0</sub>;
- A<sub>s</sub> - average total surface area of the spray drops, (equation 176), (ft.<sup>2</sup>);
- a - particle acceleration, (ft.)/(sec.)<sup>2</sup>;
- a<sub>n</sub> - nth root of J<sub>1</sub>;
- B - function of evaporation rate, (equation 102);
- b - vane height of disk, (in.), also distribution parameter, (equation 53), and function of x, (equation 142);
- C<sub>D</sub> - drag coefficient, (equation 152);
- C<sub>m</sub> - spreading coefficient - 0.075;
- C<sub>P</sub> - specific heat at constant pressure of gas film surrounding drop, (B.t.u.)/(lb.)(°F.);
- c - concentration of diffusing vapour in the boundary layer, (lb. diffusing vapour)/(ft.<sup>3</sup>), also conc. of red dye in feed, (gm.)/(ml.);
- $\bar{c}$  - root mean square velocity of diffusing molecules, (ft.)/(sec.);
- c<sub>m</sub> - concentration of diffusing vapour at the drop surface, (lb. diffusing vapour)/(ft.<sup>3</sup>);
- D - diameter of gas film surrounding drop, (ft.), also generalized molecular diffusion constant;
- D<sub>D</sub> - diameter of spray chamber, (ft.);
- D<sub>d</sub> - diameter of spinning disk, (cm.);
- D<sub>v</sub> - diffusivity of surrounding gas film, (ft.<sup>2</sup>)/(hr.);

- $d$  - diameter of drop, microns;  
 $\bar{d}$  - size parameter, (equation 50);  
 $d_a$  - arithmetic mean diameter, microns;  
 $d_g$  - geometric mean diameter of spray drops, microns;  
 $d_M$  - diameter of main drop formed, (equation 40), microns;  
 $d_m$  - diameter of largest drop in spray, microns;  
 $d_{nm}$  - number median diameter of spray drops, microns;  
 $d_o$  - diameter of smallest drop in spray, microns;  
 $d_{or}$  - orifice diameter, of atomizing nozzle, (cm.);  
 $d_s$  - surface mean diameter of spray drops, microns;  
 $d_{sd}$  - surface-diameter mean diameter of spray drops, microns;  
 $d_{qp}$  - generalized mean statistical diameter, microns;  
 $d_v$  - volume mean diameter of spray drops, microns;  
 $d_{vm}$  - volume median diameter of spray drops, microns;  
 $d_{vs}$  - Sauter mean diameter of spray drops, microns;  
 $d_{99.99}$  - diameter of drop such that 99.99% of spray drops have diameter less than it, (cm.);  
 $E_A$  - energy required for atomization, (ft.-lb. force);  
 $E_P$  - potential energy of the unstable liquid jet configuration, (ft.-lb. force);  
 $E_f$  - fraction of spray evaporated;  
 $F$  - force, (lb.-force), also function of Reynolds Number, (equation 95);  
 $F(d)$  - cumulative distribution function;  
 $f$  - Froessling's friction or wind factor (equation 70);  
 $f_F$  - Fanning friction factor;  
 $g$  - acceleration due to gravity, (ft.)/sec.<sup>2</sup>);  
 $g_c$  - dimensional constant, to convert the absolute system of dimensions to the gravitational system, 32.2 (lb.)(ft.)/ (ft.-lb. force)(sec.<sup>2</sup>);

- $H$  - absolute humidity of the air, (lb.  $H_2O$ )/(lb. dry air);  
 $H_a$  - humidity of the drying air, (lb.  $H_2O$ )/(lb. dry air);  
 $H_s$  - humidity of air in contact with drop surface, (lb.  $H_2O$ )/(lb. dry air);  
 $h$  - heat transfer coefficient, (B.t.u.)/(hr.)(ft.<sup>2</sup>)(°F.);  
 $h_f$  - enthalpy of liquid water with datum at 32°F., (B.t.u.)/(lb.)  
 $h_g$  - enthalpy of water vapour with datum at 32°F., (B.t.u.)/(lb.);  
 $h_{fg}$  - heat of vapourization, (B.t.u.)/(lb.);  
 $i$  - imaginary unit;  
 $J_0$  - Bessel function of the first kind and zero order;  
 $J'_0$  - derivative of  $J_0$  with respect to the argument;  
 $J_1$  - Bessel function of the first kind and first order;  
 $k$  - constant;  
 $k'$  - added mass factor, (equation 155);  
 $k_a$  - thermal conductivity of air, (B.t.u.)/(hr.)(ft.)(°F.);  
 $k_f$  - average thermal conductivity of the gas film, surrounding drop, (B.t.u.)/(hr.)(ft.)(°F.);  
 $k_G$  - mass transfer coefficient, (lb.-moles)/(hr.)(ft.<sup>2</sup>)( $\Delta p$ );  
 $k_g$  - mass transfer coefficient, (lb.)/(hr.)(ft.<sup>2</sup>)( $\Delta p$ );  
 $k'_g$  - mass transfer coefficient, (lb.)/(hr.)(ft.<sup>2</sup>)( $\Delta H$ );  
 $L$  - break-up length of the liquid jet, ft.;  
 $L'$  - characteristic length of the particle;  
 $L_u$  - vector mixing length;  
 $L_V$  - wetted periphery of spinning disk, (ft.);  
 $L_\psi$  - mixing length applied to generalized concentration variable;  
 $l$  - mean free path of diffusing molecules, (ft.);  
 $l_p, l_T$ , correlations coefficients (equation 137, 140);

- $l_x, l_r, l_\phi$  components of vector mixing length,  $L_u$ ;
- $M$  - average molecular weight of diffusing vapour, (lb.)/(lb.-mol.), also total momentum flux, (equation 119);
- $M_m$  - average molecular weight of gases in the surrounding film, (lb.)/(lb.-mol.);
- $m$  - mass of a drop, (lb.);
- $m'$  - mass of a drop, (lb.-mol.);
- $m_f$  - mass of fluid displaced, (lb.);
- $m_o$  - original mass of drop, (lb.);
- $N$  - unit vector directed outward normal to surface;
- $N_f$  - frequency of formation of drops from the jet;
- $n$  - distance from surface of drop along normal, also no. of drops;
- $n_d$  - number of drops with diameters between zero and  $d$  in the entire sample;
- $n_v$  - number of drops per unit volume;
- $n_v$  - number of vanes for a disk;
- $P$  - total pressure of air, (lb. force)/(ft.<sup>2</sup>);
- $P_A$  - atomizing pressure of gas stream, (p.s.i.a.);
- $P_L$  - liquid feed pressure at nozzle, (p.s.i.a.);
- $p, q$  - integers characteristic of the statistical mean diameters;
- $p_a$  - partial pressure of diffusing component in the surrounding medium, (lb. force)/(ft.<sup>2</sup>);
- $p_f$  - average partial pressure of the surrounding medium in the gas film, (lb. force)/(ft.<sup>2</sup>);
- $p_s$  - saturated vapour pressure of liquid, (lb. force)/(ft.<sup>2</sup>);
- $Q$  - rate of generation per unit volume of heat, mass or momentum;
- $Q_h$  - local rate of generation of sensible heat, (B.t.u.)/(unit volume)(hr.);
- $q_A$  - atomizing air flow rate, (lb.)/(hr.);

- $q_L$  - liquid flow rate, (lb.)/(hr.);  
 $R$  - gas constant 1543 (ft.-lb. force)/(lb. mol.)(°R.);  
 $R_D$  - radius of the column, (ft.), also drag force resistance, (lb. force);  
 $R_d$  - radius of the atomizing disk, (ft.);  
 $R(y)$ - correlation coefficient, (equation 115);  
 $r$  - distance from drop centre to point in gas film, (ft.);  
 $r_0$  - initial radius of the jet, (ft.);  
 $r_{1/2}$ - radial distance at which flow momentum is one half the value at the axis, (equation 142);  
 $S$  - unit vector in any given direction;  
 $S_f$  - shape factor, (equation 62);  
 $S_w$  - specific surface area of spray drops, (ft.<sup>2</sup>)/(lb.);  
 $s$  - average humid heat of the gas film, (B.t.u.)/(lb. dry air)(°F.);  
 $T$  - absolute temperature of a drop, (°R.);  
 $T_f$  - average absolute temperature of gas film surrounding drop, (°R.);  
 $T_L$  - liquid feed temperature, (°F.);  
 $T_s$  - temperature of spray, (°F.);  
 $t$  - temperature of drying air, (°F.);  
 $t_A$  - atomizing air temperature, (°F.);  
 $t_1^i$  - average inlet drying gas temperature, (°F.);  
 $t_2^i$  - average outlet drying gas temperature, (°F.);  
 $u, v, w$ . velocity components of velocity  $V$  in direction  $x, y, z$ ;  
 $V_D$  - absolute velocity of drop, (ft.)/(sec.);  
 $V_f$  - cumulative volume fraction, i.e., volume fraction of spray drops with diameter less than  $d$ ;  
 $V_L$  - velocity of liquid jet, (ft.)/(sec.);  
 $V_R$  - velocity of drop relative to the surrounding fluid, (ft.)/(sec.);

- $V_T$  - tangential component of the liquid velocity,  $V_L$ , (ft.)/(sec.);  
 $V_V$  - vertical component of the liquid velocity,  $V_L$ , (ft.)/(sec.);  
 $W$  - mass flow rate of the spray in any section, (lb.)/(hr.);  
 $W_A$  - work of surface formation, (ft.-lb. force);  
 $w$  - drying air flow rate, (lb. dry air)/(hr.);  
 $x$  - axial distance from the source of the jet, (in.);  
 $x, y, z$ , Cartesian coordinates;  
 $x, r, \phi$  cylindrical coordinates  
 $Y$  - any fluctuating variable;  
 $y$  - ordinate value on the probability plot; also function of  $d$ , (equations 57, 60);

b) Greek Symbols

- $\alpha$  - rate of growth of the amplitude on the liquid jet;  
 $\beta$  - dimensionless diffusion coefficient, (equation 116); also coefficient of volume expansion of gas film, ( $^{\circ}R.$ );  
 $\Gamma$  - gamma function;  
 $\gamma$  - amplitude of the disturbance on the liquid jet;  
 $\delta$  - distribution parameter;  
 $\epsilon$  - eddy diffusivity, (equation 117, 129, 135), (ft.<sup>2</sup>)(hr.);  
 $\zeta$  - number of waves per foot of jet circumference;  
 $\theta$  - angle of spray, (radians); also time, (sec.);  
 $\theta_0$  - arbitrary reference time;  
 $\Lambda$  - parameter in Reichardt's Theory, (equation 144, 145);  
 $\lambda$  - wavelength of the disturbance on liquid jet, (also defined by equation 107);  
 $\mu_L$  - absolute viscosity of the liquid, (lb.)/(ft.)(sec.);

- $\rho_G$  - absolute viscosity of the gas, (lb.)/(ft.)(sec.);  
 $\nu$  - dimensionless rate of growth, (equation 5);  
 $\pi$  - ratio of circumference of circle to diameter, 3.14;  
 $\rho_G$  - density of surrounding air, (lb.)/(ft.<sup>3</sup>);  
 $\rho_f$  - average density of the gas film surrounding drop, (lb.)/(ft.<sup>3</sup>);  
 $\rho_L$  - density of liquid feed, (lb.)/(ft.<sup>3</sup>);  
 $\rho_V$  - density of diffusion vapour, (lb.)/(ft.<sup>3</sup>);  
 $\sigma$  - enclosing surface area of volume,  $\tau$ ;  
 $\sigma_L$  - surface tension of liquid, (dynes)/(cm.);  
 $\tau$  - element of volume;  
 $\phi$  - generalized molecular transport potential;  
 $\chi$  - defined by equation 105;  
 $\psi$  - generalized variable of the concentration of heat, mass or momentum;  
 $\omega$  - mean angular velocity, (radian/sec.);

c) Subscripts

- - time-mean average, (equation 109);  
 ' - fluctuating component, (equation 108);  
 av - average conditions;  
 a1, a2 initial and final atomizing air stream in any section of cross-current flow equipment;  
 d1, d2 initial and final drying air flow streams in any section of cross-current flow equipment;  
 i - ith component or size group;  
 x, y, z, x, r, , components or values in direction of axis;  
 0 - arbitrary reference or initial point;

1, 2 - initial and final conditions over a given increment or section.

d) Dimensionless Numbers

- Gr - Grashof Number,  $d^3 \rho_f^2 g_c \beta \Delta T / \mu_f^2$ ;
- Nu - Nusselt Number,  $h d_{vs} / k_f$ ;
- Nu' - Modified Nusselt Number,  $k_{Gm} d_{vs} \rho_f / D v_f$ ;
- Pr - Prandtl Number,  $C_p \mu_f / k_f$ ;
- Re - Reynolds Number -  $d_{vs} V_R \rho_f / \mu_f$  (equations 14, 78, 150);
- Sc - Schmidt Number -  $\mu_f / \rho_f D_v$ ;
- We - Weber Number -  $V_L (2 \rho_L r_o / \sigma_L)^{1/2}$ ;
- Z - Ohnesorge Number -  $\mu_L / (2 \rho_L r_o \sigma_L)^{1/2}$ .

## BIBLIOGRAPHY

1. Adler, C.R., Mark, A.M., Marshall, W.R., Jr., and Parent, R.J., Chem. Eng. Progr., 47: 515, 601 (1951).
2. Adler, C.R., and Marshall, W.R., Jr., Chem. Eng. Progr., 47: 515, 601 (1951).
3. Albertson, M.L., Dai, Y.B., Jensen, R.A., and Rouse, H., Proc. Am. Soc. Civil Eng., 74: 1571 (1948).
4. Alexander, L.G., Baron, T., Comings, E.W., Univ. of Ill. Eng. Expt. Station, Bull. 413 (1953).
5. Alexander, L.G., and Coldren, C.L., Ind. Eng. Chem., 43: 1325 (1951).
6. Alexander, L.G., Comings, E.W., Grimmett, H.L., and White, E.W., Chem. Eng. Progr. Symposium Series No. 10, 50: 93 (1954).
7. Alexander, L.G., Kivnick, A., Comings, E.W., and Henze, E.D., Am. Inst. Chem. Engrs. J., 1: 55 (1955).
8. Allen, H.S., Phil. Mag., 50: 323, 519 (1900).
9. Anson, D., Fuel, 32: 39 (1953).
10. Avakian, A.S., Sc.D. Thesis, Mass. Inst. Technol. (1933).
11. Bahr, D.W., Nat. Adv. Comm. Aero., RME53114 (1953).
12. Baron, T., Univ. of Illinois Tech. Rept., 4 (1949).
13. Baron, T., and Alexander, L.G., Chem. Eng. Progr., 47: 181 (1951).
14. Bevans, R.S., Conference on Fuel Sprays, Univ. of Michigan (1949).
15. Boltze, Diss., Gottingen (1908).
16. Boussinesq, J., Memoirs presentes par divers savants a l'Academie des Sciences, 23 (1877).
17. Bouvard, M., Houille Blanche, 6: 862 (1951).
18. Bradley, R.S., Evans, M.G., and Whytlaw-Gray, R.W., Proc. Roy. Soc. (London), 186A: 368 (1946).
19. Briton, M.D., Ind. Eng. Chem., 47: 23 (1955).
20. Burke, S.P., and Plummer, W.S., Ind. Eng. Chem., 20: 1200 (1928).

21. Calderbank, P.H., and Korchinski, I.J.O., Chem. Eng. Sci., 6: 65 (1956).
22. Callaghan, E.E., and Ruggeri, R.S., Nat. Adv. Comm. Aero. Tech. Note 1615 (1948).
23. Carrier, W.H., and Mackey, C.O., Trans. Am. Soc. Mech. Engrs., 59: 33 (1937).
24. Castleman, R.A., Jr., Nat. Adv. Comm. Aero. Tech. Note 231 (1926).
25. Castleman, R.A., Jr., J. Research Nat. Bur. Stand., 6 RP 281369 (1931).
26. Chaloud, J.H., Martin, J.B., and Baker, J.S., Chem. Eng. Progr., 53: 593 (1957).
27. Cleeves, V., and Boelter, L.M.K., Chem. Eng. Progr., 43: 123 (1947).
28. Coldren, C.L., Ph.D. Thesis, Univ. of Illinois (1954).
29. Coldren, C.L., and Comings, E.W., "Pneumatic Thermometer and Hygrometer", Univ. of Illinois (1956).
30. Coldren, C.L., and Comings, E.W., Chem. Eng. Progr., 53: 403 (1957).
31. Comings, E.W., and Coldren, C.L., Chem. Eng. Progr., 53: 231 (1957).
32. Consiglio, J.A., and Sliepcevich, C.M., Am. Inst. Chem. Engrs. J., 3: 418 (1957).
33. Coolidge, J.L., "Introduction of Mathematical Probability", Oxford Univ. Press (1925).
34. Corrsin, S., Nat. Adv. Comm. Aero., A.C.R. 3L23 (1943).
35. Corrsin, S., Am. Soc. Civil Engrs., 75: 901 (1949).
36. Corrsin, S., and Uberoi, M.S., Nat. Adv. Comm. Aero. Tech. Note 1864 (1949).
37. Crosby, E.J., and Marshall, W.R., Jr., Chem. Eng. Progr., 53: 347 (1957).
38. De Juhasz, K.J., and Meyers, W.E., "Bibliography of Sprays", The Texas Co., N.Y. (1953).
39. De Juhasz, K.J., Zahn, O.F., and Schweitzer, P.H., Penn. State Coll. Bull., 40 (1932).
40. Dlouhy, J., Ph.D. Thesis, McGill University (1957).

41. Doble, S.M., *Engineering*, 159: 21, 61, 103 (1945).
42. Dorman, R.G., *Brit. J. App. Phys.*, 3: 189 (1952).
43. Dumas, M., and Laster, R., *Chem. Eng. Progr.*, 49: 518 (1953).
44. Doussard, J.L., Sc.D. Thesis, Mass. Inst. Technol. (1954).
45. Duffie, J.A., and Marshall, W.R., Jr., *Chem. Eng. Progr.*, 49: 417, 480 (1953).
46. Edeling, C., *Beihefte, angew. Chem.*, No. 57 (1949).
47. Ehrich, F.F., *J. Aero. Sci.*, 2: 99 (1953).
48. Einstein, A., *Ann. Phys.*, 19: 289 (1906), 34: 591 (1911).
49. Elembass, W., *Physica*, 9: 285 (1942).
50. Erdmenger, R., *Chem. Ing. Tech.*, 28: 513 (1956).
51. Fledderman, R.G., and Hanson, A.R., Univ. of Michigan, Eng. Research Dept., CM667 (1951).
52. Flugel, G., *Nat. Adv. Comm. Aero. Tech. Memo* 982 (1941).
53. Fraser, J.P., M. Aero. Eng. Thesis, Cornell Univ. (1949).
54. Fraser, R.P., and Eisenklam, P., *Trans. Inst. Chem. Engrs. (London)*, 34: 294 (1956).
55. Fraser, R.P., Eisenklam, P., and Dombrowski, N., *Brit. Chem. Eng.*, 2: 414, 496, 536, 610 (1957).
56. Friedlander, S.K., *Am. Inst. Chem. Eng. J.*, 3: 43 (1957).
57. *Ibid.*, 381 (1957).
58. Friedlander, S.K., and Johnstone, H.F., *Ind. Eng. Chem.*, 49: 1151 (1957).
59. Friedman, S.J., Gluckert, F.A., and Marshall, W.R., Jr., *Chem. Eng. Progr.*, 48: 181 (1952).
60. Frisch, H.L., *J. Chem. Phys.*, 22: 123 (1954).
61. Froessling, N., *Gerlands Beitr. Geophys.*, 52: 170 (1938).
62. Fuchs, N., *Phys. Z. Sowjetunion*, 6: 224 (1934).
63. Fuchs, N., and Petrojanoff, I., *Nature*, 139: 111 (1937).
64. Garner, F.H., *Trans. Inst. Chem. Engrs. (London)*, 28: 88 (1950).

65. Garner, F.H., Chem. Ing. Tech., 29: 28 (1957).
66. Garner, F.H., and Henny, V.E., Fuel, 32: 151 (1953).
67. Gauvin, W.H., Chem. Can. 7: No. 9, 48 (1955).
- 67a Geist, J.H., York, J.L., and Brown, G.G., Ind. Eng. Chem., 43: 1371 (1951).
68. Giffen, E., and Muraszew, A., "The Atomization of Liquid Fuels", John Wiley and Sons Inc., N.Y. (1953).
69. Godsave, G.A.E., Nat. Gas Turbine Establishment (England), Rept. R 88 (1952).
70. Goldstein, S., "Modern Development in Fluid Dynamics", Oxford Press, London (1938).
71. Golitzine, N., Nat. Research Council (Canada), Rept. ME-177 (1950).
72. Gooden, E.L., and Smith, C.L., Ind. Eng. Chem. Anal. Edit., 12: 479 (1940).
73. Gretzinger, J., Ph.D. Thesis, Univ. of Wisconsin (1956).
74. Gucker, F.T., Jr., Proc. First Nat. Air Pollution Symp., Stanford Research Inst. (1951).
75. Gunn, R., and Kinzer, G.D., J. Met., 6: 243 (1949).
76. Gwyn, J.E., Garver, J.C., and Marshall, W.R., Jr., Paper presented at the A.I.Ch.E. Meeting Boston (1956).
77. Haenlein, A., Nat. Adv. Comm. Aero. Tech. Memo 659 (1932).
78. Hamilton, W.F., Ind. Eng. Chem. Anal. Ed., 2: 234 (1930).
79. Hanson, A.R., "Ohio State Univ. Studies in Eng.", XXI: No. 3, 415 (1952).
80. Happel, J., and Brenner, H., Am. Inst. Chem. Engrs. J., 3: 507 (1957).
81. Harkins, W.D., and Brown, F.F., Am. Chem. Soc. J., 41: 499 (1919).
82. Hausser, F., and Stobl, G., Z. f. Tech. Phys., 5: 159, 624 (1924).
83. Herring, W.M., and Marshall, W.R., Jr., Am. Inst. Chem. Eng. J., 1:200 (1955).
84. Hinze, J.O., App. Sci. Research, 1A: 273 (1949B).

85. Hinze, J.O., *Am. Inst. Chem. Eng. J.*, 1: 289 (1955).
86. Hinze, J.O., and Milborn, H., *J. App. Mech.*, 17: 145 (1950).
87. Hinze, J.O., and van der Hegge Zijnen, B.G., *App. Sci. Res.*, 1A: 435 (1947).
88. Holroyd, H.B., *J. Franklin Inst.*, 215: 93 (1933).
89. Hottel, R.A.F. *Tech. Note* 167 (1943).
90. Houghton, H.G., *Physics*, 4: 419 (1933).
91. Houghton, H.G., and Radford, W.H., *Papers Phys. Oceanog. Met.*, 6: No. 3 (1938).
92. Howarth, L., *Proc. Cambridge Phil. Soc.*, 34: 185 (1938).
93. Hu, S., and Kinter, R.C., *Am. Inst. Chem. Engrs. J.*, 1: 42 (1955).
94. Hughes, R.R., and Gilliland, E.R., *Chem. Eng. Progr.*, 48: 497 (1952).
95. Illingworth, C.R., *Phil. Mag.*, 49: 389 (1953).
96. Ingebo, R.D., *Chem. Eng. Progr.*, 48: 403 (1952).
97. Ingebo, R.D., *Nat. Adv. Comm. Aero. Tech. Note* 2368 (1951).
98. *Ibid.*, 2850 (1953).
99. *Ibid.*, 3265 (1954).
100. Iverson, H.W., and Balent, R., *J. Appl. Phys.*, 22: 324 (1951).
101. Jacob, M., "Heat Transfer", Vol. 1, John Wiley and Sons, N.Y. (1949).
102. Johnstone, H.F., and Kleinschmidt, R.V., *Trans. Am. Inst. Chem. Engrs.*, 34: 181 (1938).
103. Johnstone, H.F., Pigford, R.L., and Chapin, J.H., *Trans. Am. Inst. Chem. Engrs.*, 37: 95 (1941).
104. Johnstone, H.F., and Williams, G.C., *Ind. Eng. Chem.*, 31: 993 (1939).
105. Joyce, J.R., *J. Inst. Fuel*, 22: 150 (1949).
106. Keenan, H.P., and Neumann, E.P., *Trans. Am. Soc. Mech. Engrs.*, 64A: 75 (1942).
107. Keenan, J.H., Neumann, E.P., and Lustwerk, F., *J. App. Mech.*, 17: 299 (1950).
108. Kesler, G.H., *Sc.D. Thesis*, Mass. Inst. Technol. (1952).

109. Keyer, J.J., Am. Inst. Chem. Engrs. J., 1: 305 (1955).
110. Kinzer, G.D., and Gunn, R., J. Met., 8: 71 (1951).
111. Klee, A.J., and Treybal, R.E., Am. Inst. Chem. Eng. J., 2: 444 (1956).
112. Knelman, F.H., M. Eng. Thesis, McGill University (1950).
113. Kramers, H., Physica, 12: 61 (1946).
114. Kravath, F.F., Heat and Vent., 37: 17 (1940).
115. Krishnaiyar, N.C., Phil. Mag., 6: 1049 (1923).
116. Kroll, H.E., Chem. Eng. Progr., 43: No. 2, 21 (1947).
117. Kroll, K., Chem. Ing. Tech., 26: 132 (1954).
118. Kronig, R., and Bruijsten, J., J. App. Sci. Research, 2A: 439 (1950).
119. Kronjiline, Tech. Phys. (U.S.S.R.), 3: 311 (1936).
120. Kuehn, R., Nat. Adv. Comm. Aero. Tech. Memo 329, 330, 331 (1925).
121. Kuethe, A.M., J. App. Mech., 2A: 87 (1935).
122. Kyte, J.R., Madden, A.J., and Piret, E.L., Chem. Eng. Progr., 49: 653 (1953).
123. Lane, W.R., Ind. Eng. Chem., 43: 1312 (1951).
124. Lange, N.A., "Handbook of Chemistry", 7th Ed. Handbook Publishers, Sandusky, Ohio (1949).
125. Langmuir, I., Phys. Rev., 12: No. 2, 368 (1918).
126. Langmuir, I., and Blodgett, K.B., U.S. Army Air Force Tech. Rept. 5418 (1946).
127. Lapple, C.E., "Fluid and Particle Mechanics", Univ. of Delaware (1951).
128. Lapple, C.E., Chem. Eng. Progr., 50: 283 (1954).
129. Lapple, C.E., and Shepherd, C.B., Ind. Eng. Chem., 32: 605 (1940).
130. Lee, D.W., Nat. Adv. Comm. Aero. Tech. Rept. 425 (1932).
131. Lewis, H.C., Edwards, D.G., Goglia, H.J., Rice, R.I., and Smith, L.W., Ind. Eng. Chem., 40: 67 (1948).
132. Licht, W., and Narasimhamurty, J.R.S., Am. Inst. Chem. Engrs. J., 1: 367 (1955).

133. Lin, V.E., Dept. U.S.A.F., Project 2160 (1955).
134. Littaye, G., Comptes Rendues, 218: 440 (1944).
135. Ljachowski, D.N., J. Tech. Phys. (Leningrad), 10: 999 (1940).
136. Lloyd, P., Proc. Inst. Mech. Engrs. (London), 15: 462 (1945).
137. Longwell, J.P., Sc.D. Thesis, Mass. Inst. Technol. (1943).
138. Longwell, J.P., and Weiss, M.A., Ind. Eng. Chem., 45: 667 (1953).
139. Luchak, G., and Langstroth, G.O., Can. J. Research, 28A: 574 (1950).
140. Lunnon, R.G., Proc. Roy. Soc. (London), 110A: 302 (1926).
141. Lunnon, R.G., Proc. Roy. Soc. (London), 112A: 680 (1928).
142. Lutlander, S., and Rydberg, A., Physik, Z., 36: 552 (1935).
143. Lyons, D.B., M. Eng. Thesis, McGill University (1951).
144. Maisel, D.S., and Sherwood, T.K., Chem. Eng. Progr., 46: 131 (1950).
145. Marshall, W.R., Jr., Chem. Eng. Progr., Monograph Series, 50: No. 2 (1954).
146. Marshall, W.R., Jr., Chem. Can., 7: No. 11, 62 (1955).
147. Marshall, W.R., Trans. Am. Soc. Mech. Engrs., 77: 1377 (1955).
148. Maxwell, J.C., "Diffusion", Sci. Papers, 2: Cambridge Univ. Press (1890).
149. May, K.R., J. Scientific Instruments, 17: 144 (1932).
150. May, K.R., J. Appl. Phys., 20: 932 (1949).
151. McAdams, W.H., "Heat Transmission", p. 171, McGraw-Hill Book Co. Inc., N.Y. 1942.
152. McCabe, W.L., and Smith, J.C., "Unit Operations of Chem. Eng.", p. 848, McGraw-Hill Book Co. Inc., 1956.
153. McCullough, S., and Perkins, P.J., Nat. Adv. Comm. Aero., RME 50K01 (1951).
154. McElroy, G.E., U.S. Bur. Mines Tech. Paper 678 (1945).
155. McEwen, G.F., Phys. Rev., 33: 429 (1911).

156. Merrington, A.C., and Richardson, E.G., Proc. Phys. Soc., 59: 1 (1947).
157. Meyer, P., Trans. Inst. Chem. Engrs., 15: 127 (1937).
158. Mickelson, W.R., Nat. Adv. Comm. Aero. Tech. Note 3570 (1955).
159. Miesse, C.C., Ind. Eng. Chem., 47: 1690 (1955).
160. Miller, W., and McInally, T.W., J. Roy. Tech. College (Glasgow), 3: 682 (1936).
161. Mirsky, W., Ph.D. Thesis, Univ. of Michigan (1956).
162. Morse, H.W., Proc. Am. Acad. Arts. Sci., 45: 363 (1910).
163. Mugele, R.A., and Evans, H.D., Ind. Eng. Chem., 43: 1317 (1951).
164. Nisi, H., and Porter, A.W., Phil. Mag., 46: 754 (1923).
165. Nukiyama, S., and Tanasawa, Y., Trans. Soc. Mech. Engrs. (Japan), 4: No. 14, 5-13 (1938). 4: No. 15, 5-24 (1938). 5: No. 18, 5-14 (1939). 5: No. 18, 5-15 (1939). 6: No. 22, 5-7 (1940). 6: No. 23, 5-18 (1940).
166. Ohnesorge, W. von, Z. angew. Math. u. Mech., 16: 355 (1936).
167. Oktay, C.M., Ph.D. Thesis, Univ. of Florida (1955).
168. Ostwald, W., Autotechnik, 8: Book 3 (1919).
169. Page, L., "Introduction to Theoretical Physics", D. Van Nostrand Co. Inc., N.Y. (1928).
170. Perry, J.H., "Chem. Engrs. Handbook", 3rd Edition, p. 757, 1298, McGraw-Hill Book Co. Inc. N.Y. 1950.
171. Ibid., p. 811.
172. Ibid., p. 1021-22.
173. Ibid., p. 1170.
174. Pigford, R.L., and Pyle, C., Ind. Eng. Chem., 43: 1646 (1951).
175. Pinder, K.L., M. Eng. Thesis, McGill University (1952).
176. Pohlhausen, Z. angew. Math. u. Mech., 1: 115 (1925).
177. Poisson, S.D., Mem. de l'Institute, 11: 521 (1832).
178. Porter, R.W., and Considine, D.M., Chem. Engrs. Handbook, Edit. 3rd. p. 1298 (1950).

179. Prandtl, L., Proc. Third Intern. Math Congr. (Heidelberg), (1904).
180. Prandtl, L., Z. angew. Math. u. Mech., 5: 136 (1925).
181. Prandtl, L., and Tietjens, O.G., (Trans. by Den Hartog, J.P.)  
"Applied Hydro and Aeromechanics", Chap. 5, McGraw-Hill Book Co.  
Inc., New York, 1934.
182. Probert, R.P., Phil. Mag., 37: 94 (1946).
183. Ranz, W.E., Ind. Eng. Chem., 49: 288 (1951).
184. Ranz, W.E., Bulletin No. 65, Dept. Eng. Res., Penn. State Univ. (1956).
185. Ranz, W.E., Trans. Am. Soc. Mech. Engrs., 78: 909 (1956).
186. Ranz, W.E., Chem. Eng. Education, 1: 24 (1957).
187. Ranz, W.E., and Hofelt, C., Jr., Ind. Eng. Chem., 49: 288 (1957).
188. Ranz, W.E., and Marshall, W.R., Jr., Chem. Eng. Progr., 48: 141, 173  
(1952).
189. Ranz, W.E., and Wong, J.B., Ind. Eng. Chem., 44: 1371 (1952).
190. Rasbash, D.J., J. Sci. Instrum., 30: 189 (1953).
191. Rayleigh, E., Phil. Mag., 5B4: 59 (1892).
192. Rayleigh, Lord, Proc. Roy. Math. Soc. (London), 10 (1878).
193. Rayleigh, Lord, Phil. Mag., 34: 153 (1892).
194. Reichardt, H., VDI-Forschungsheft 414 (1942).
195. Reichardt, H., Roy. Aero. Soc. J., 47: 167 (1943).
196. Reichardt, H., Z. angew. Math. u. Mech., 24: 268 (1944).
197. Richardson, E.G., "Flow Properties of Disperse Systems", p. 266,  
N. Holland Pub. Co. Amsterdam (1953).
198. Rosin, P., and Rammler, E., J. Inst. Fuel, 7: 29 (1933).
199. Rouse, H., "Fluid Mechanics for Hydraulic Engineers", McGraw-Hill  
Book Co., N.Y. 1938.
200. Ruden, P., Die Naturwissenschaft, 21: 375 (1933).
201. Rupe, J., Third Symposium on Combustion and Flame and Explosion  
Phenomena, The Williams and Wilkins Co., Baltimore (1949).

202. Saad, M.A., Ph.D. Thesis, Univ. of Michigan (1956).
203. Sauter, J., Forsch. Gebiete Ing., No. 297 (1926).
204. Sauter, J., Nat. Adv. Comm. Aero. Tech. Memo 518 (1929).
205. Savart, F., Ann. Chim., 53: 337 (1833).
206. Schmidt, F.S., Ann. Phys., 61: 633 (1920).
207. Schmidt, J.M., Jet Prop. Lab., Calif. Inst. Technol. Prog. Rept., No. 3-18 (1948).
208. Schmidt, W., Probleme der Kormischer Physik, Jensen and Schwassman Publications, Hamburg (1925).
209. Schlichting, H., Ing. Arch., 21:227 (1953).
210. Schuebel, Nat. Adv. Comm. Aero, Tech. Memo 644 (1931).
211. Shapiro, A.H., and Erickson, A.J., Trans. Am. Soc. Mech. Engr., 79: 775 (1957).
212. Shepherd, C.B., and Lapple, C.E., Ind. Eng. Chem., 31: 972 (1938).
213. Shereshefsky, J.L., and Steckler, S., J. Chem. Phys., 41: 108 (1936).
214. Sherwood, T.K., and Reed, C.E., "Applied Mathematics in Chemical Engineering", McGraw-Hill Book Co. Inc., N.Y. (1939).
215. Sherwood, T.K., and Woertz, B.B., Ind. Eng. Chem., 31: 1034 (1939).
216. Sinclair, D., "Handbook on Aerosols", Atomic Energy Comm. (1950).
217. Sjenitzer, F., Chem. Eng. Sci., 1: 101 (1952).
218. Sleicker, C.A., Jr., and Churchill, S.W., Ind. Eng. Chem., 48: 1819 (1956).
219. Sliepceovich, C.M., Final Prog. Rept., Contract W36-039-Sc-32307, Eng. Research Inst., Univ. of Michigan (1949).
220. Smith, R.H., J. Aero Sci., 3: 26 (1935).
221. Smith, S.W., and Moss, H., Proc. Roy. Soc. (London), 93: 373 (1917).
222. Soo, S.L., Chem. Eng. Sci., 5: 57 (1956).
223. Squires, L., and Squires, W., Trans. Am. Inst. Chem. Engrs., 33: 1 (1937).

224. Stachiewicz, J.W., Gas Dynamics Lab. Rept. R 41, McGill Univ. (1954).
225. Stanford Research Institute, News Bull., 5: No. 5, 4 (1953).
226. Stefan, Wier. Ber., 65: 323 (1872). 68: 385 (1874). 83: 343 (1881).
227. Stimson, M., and Jeffrey, C.B., Proc. Roy. Soc., 111A, 110 (1926).
228. Stoker, R.L., J. App. Phys., 17: 243 (1946).
229. Stokes, G.G., Trans. Cambridge Phil. Soc., 9: 8 (1850).
230. Stokes, G.G., Trans. Cambridge Phil. Soc., 9: Part 2, 51 (1851).
231. Straus, R., Ph.D. Thesis, London University (1949).
232. Strazhewski, L., Tech. Phys. (U.S.S.R.), 4: No. 11, 978 (1937).
233. Takahasi, Y., Geophys. Mag. (Tokyo), 10: 321 (1936).
234. Tang, Y.S., Ph.D. Thesis, Univ. of Florida (1952).
235. Tate, R.W., and Marshall, W.R., Jr., Chem. Eng. Progr., 49: 161, 226 (1953).
236. Taylor, E.H., and Harmon, D.B., Jr., Ind. Eng. Chem., 46: 1455 (1954).
237. Taylor, G.I., Proc. Roy. Soc. (London), 120A: 13 (1928).
238. Taylor, G.I., Proc. Roy. Soc. (London), 135A: 685 (1932).
239. Taylor, J.F., Ph.D. Thesis, Univ. of Ill. (1950).
240. Tichacek, L.J., Barkelaw, C.H., and Baron, T., Am. Inst. Chem. Engrs. J., 3: 439 (1957).
241. Tolman, R.C., Gerke, R.H., Brooks, A.P., Herman, A.G., Mulliken, R.S., and Dew-Smyth, H., J. Am. Chem. Soc., 41: 575 (1919).
242. Tollmien, W., Z. angew. Math. u. Mech., 6: 468 (1926).
243. Tomotika, S., Proc. Roy. Soc. (London), 150A: 322 (1935).
244. Tomotika, S., Proc. Roy. Soc. (London), 153A: 302 (1935).
245. Topley, B., and Whytlaw-Gray, R.W., Phil. Mag., 4: 873 (1927).
246. Torobin, L.B., and Gauvin, W.H., "The Fundamental Properties of Solid-Gas Flow", P.P.R.I.C. Rept. (1956).
247. Truckenbrodt, E., Ing. Arch., 22: 21 (1954).

248. Turner, G.M., and Moulton, R.W., Chem. Eng. Progr., 49: 185 (1953).
249. Tuve, Priestler, and Wright, Heat, Piping and Air Conditioning, 13: 708 (1941).
250. Tyler, E., Phil. Mag., 16: 504 (1933).
251. Tyler, E., and Richardson, E.G., Proc. Roy. Soc. (London), 37: 297 (1925).
252. Tyler, E., and Watkin, F., Phil. Mag., 14: 849 (1932).
253. Uberoi, M.S., and Corrsin, S., Nat. Adv. Comm. Aero. Tech. Rept. 1192 (1953).
254. Venezian, E.C., Turbulence and Entrainment Characteristics of Some Atomizing Nozzles, Summer Essay, McGill University (1957).
255. Victorein, K., Forsch. Gebiete Ing., 12: 1, 16 (1941).
256. Voorheis, T.S., M.Sc. Thesis, Univ. of California (1939).
257. Walker, W.H., Lewis, W.K., McAdams, W.H., and Gilliland, E.R., "Principles of Chemical Engineering", p. 582, McGraw-Hill Book Co. Inc., New York (1937).
258. Walton, W.H., and Prewett, W.C., Proc. Phys. Soc. (London), 62B: 341 (1949).
259. Weber, C., Z. angew. Math. u. Mech., 11: 136 (1931).
260. Wetzel, R.H., Ph.D. Thesis, Univ. of Wisconsin (1952).
261. Wetzel, R.H., and Marshall, W.R., Jr., Paper Presented at Washington D.C. National Meeting, Am. Inst. Chem. Engrs. (1954).
262. Wieselberger, C., Physik, Z., 23: 219 (1922).
263. Wieselberger, C., Physik, Z., 28: 84 (1927).
264. Wilhelm, R.H., and Valentine, S., Ind. Eng. Chem., 43: 1199 (1951).
265. Williams, G.C., Sc.D. Thesis, Mass. Inst. Technol. (1942).
266. Williams, G.C., and Schmitt, R.O., Ind. Eng. Chem., 38: 967 (1946).
267. Woeltjen, A., "Über die Feinheit der Brennstoffzerstanbung in Olmaschinen", Technische Hochschule, Darmstadt (1925).
268. York, J.L., and Stubbs, H.E., Trans. Am. Soc. Mech. Engrs., 74: 1157 (1952).
269. Zahm, A.F., Nat. Adv. Comm. Aero. Rept. 253 (1927).

C APPENDICES

APPENDIX I

SPRAY DROP VELOCITIES

TABLE VI

DROP VELOCITY - DROP DIAMETER DATA

Pneumatic Nozzle (1/4) JN No. 12      Low Atomizing Pressures

Negligible Evaporation in Lucite Column       $V_G = 7.0$  ft./sec.

<u>Section 1</u> (x = 1.5 in.)		<u>Section 2</u> (x = 4.5 in.)		<u>Section 3</u> (x = 8.0 in.)	
<u>d</u>	<u><math>V_D</math></u>	<u>d</u>	<u><math>V_D</math></u>	<u>d</u>	<u><math>V_D</math></u>
<u>microns</u>	<u>ft./sec.</u>	<u>microns</u>	<u>ft./sec.</u>	<u>microns</u>	<u>ft./sec.</u>
14	89	11	22.3	23	28.5
14	89	14	32.4	20	22.5
22	144	28	65	23	18.4
14	105	22.3	50	23	18.4
17	84	19.3	45	18	43.2
17	52	22	55	27	47.8
14	87	19	42	25.4	56.7
19	112	24	59	15	37.4
15	44	29	77	25	40.5
15	68	24	44	43	67
20	71	33	77	15.5	17
15.5	59	26.5	44	13	23.8
22	125	35	90	35.5	55.5
17.5	75	26.5	51	43	65.5
20	62	24	47.5	23	41
24	105	31	47.5	20.5	33
17.5	68			22	24
15	89			25	32.9
24	120			30.6	39.5
26	112			22	35
22	100				
32	167				
14	86				

TABLE VI (CTD.)DROP VELOCITY - DROP DIAMETER DATAPneumatic Nozzle (1/4) JN No. 12      Low Atomizing PressuresNegligible Evaporation in Lucite Column  $V_G = 7.0$  ft./sec.Section 4  
( $x = 12$  in.)Section 5  
( $x = 16$  in.)Section 6  
( $x = 21$  in.)

<u>d</u>	<u><math>V_D</math></u>	<u>d</u>	<u><math>V_D</math></u>	<u>d</u>	<u><math>V_D</math></u>
<u>microns</u>	<u>ft./sec.</u>	<u>microns</u>	<u>ft./sec.</u>	<u>microns</u>	<u>ft./sec.</u>
25	15.7	29	15	45	14.8
19	11.3	34.5	19.6	52	18
17.5	11.3	34.5	18	48	10
27	18	38	24.8	46	16.5
17.5	11	46.4	28.3	40	21
27	26	38	11	59	19.5
19.3	17.5	35	13.2	49	12
23	30	58	19.7	49	12.7
31	37.5	48	30	49	12.7
27	23	43	15	33	9
27	26	35	19.7		
25	25.4	46	11		
21	18	39	16		
33	36.8	29	10.8		
35	33	29	12.8		
31	29.2	29	9		
35	24	32.5	18.8		
40.5	30.5	29	19		
39	34	42.6	22.7		
33	26.5				

TABLE VII

DROP VELOCITY - DROP DIAMETER DATA

Section 2 (x = 4.0 in.)		Section 3 (x = 8.0 in.)		Section 4 (x = 12.0 in.)		Section 5 (x = 16.0 in.)	
d	V <sub>D</sub>	d	V <sub>D</sub>	d	V <sub>D</sub>	d	V <sub>D</sub>
microns	ft./sec.	microns	ft./sec.	microns	ft./sec.	microns	ft./sec.
48	79	32	41.5	29	17.5	55	26.6
33.5	90	32	26	49	42	30	12.2
11.5	32	27	36	57	48	30	11.4
22	50	48	80	49	35	45	25.5
27	69	16	19.4	32	18	37.2	26.2
34	66	27	20	32	19.6	48	26.4
27	44	27	38	40.6	22	52	24.5
43.5	94	40	45	45.5	32	47	18.4
38	85	35	28	52	24.5	45	21.7
24.5	45	27	20	40.6	19	52	24.6
17	44	32	29	27.2	16.6	60	30.6
17	32	33.6	32.5	57	38.2	33	14.2
39.5	75	32	33	40.7	27.3	37	13.3
27	60	10	7	24.5	27.3	74	41.0
		17.6	14	27	10.5	67	37.0
		40	43	73	45.1	45	14.2
		35.5	38	40	21.0		
		33.6	33.3	66	42.0		

TABLE VIII

DROP VELOCITY - DROP DIAMETER DATA

Pneumatic Nozzle (1/4) JN No. 12 Mixed Atomizing Pressures

Negligible Evaporation in Lucite Column  $V_G = 10$  ft./sec.

<u>Section 1</u> (x = 1.5 in.)		<u>Section 2</u> (x = 4.5 in.)		<u>Section 3</u> (x = 8.0 in.)		<u>Section 4</u> (x = 12.0 in.)	
d	$V_D$	d	$V_D$	d	$V_D$	d	$V_D$
<u>microns</u>	<u>ft./sec.</u>	<u>microns</u>	<u>ft./sec.</u>	<u>microns</u>	<u>ft./sec.</u>	<u>microns</u>	<u>ft./sec.</u>
17.5	56	15	29	12	16.6	29	20.4
15.3	70	28	64	13.5	26	31	20.4
19.3	123	19	56	12	18	25	21
20.0	35	15	42	25	40	27	19.5
17.5	102	17	48	16	27	15.5	16
13	56	19.3	56	16	18.5	15.5	15
15	63	19	48	21	34	15.5	19.5
11	55	28	69	31	47.5	19.3	19
11	39.2	31	89	29	36.5	35	34
13	42	19.3	50	39	57	39	44
11	47	23.5	56	32	43	19.3	23.8
15	66	15	42	19	32	31	28.7
17	68	14	42	19	20.5	31	21
12	50	17.5	43	33	46	27	21.7
12	48	17.5	33	19	18.5	31	27
17.5	73	19	41.5	23	38.8	25	19
13	48	29	59			33	34
17	96	17.5	44			19	17.8
13.5	45	11.5	37			31	26.5
		25	64			19.3	19

TABLE IX

DROP VELOCITY - DROP DIAMETER DATA

Pneumatic Nozzle (1/4) JN No. 12 High Atomizing Pressures

Negligible Evaporation in Lucite Column  $V_G = 12$  ft./sec.

<u>Section 1</u> (x = 1.5 in.)		<u>Section 2</u> (x = 4.5 in.)		<u>Section 3</u> (x = 8.0 in.)		<u>Section 4</u> (x = 12.0 in.)	
d	$V_D$	d	$V_D$	d	$V_D$	d	$V_D$
<u>microns</u>	<u>ft./sec.</u>	<u>microns</u>	<u>ft./sec.</u>	<u>microns</u>	<u>ft./sec.</u>	<u>microns</u>	<u>ft./sec.</u>
29	166	20	59	22	38.6	27	24
18	156	25	51	15.8	22.5	29	25.5
27.2	199	13	43.5	18	29	19	20.5
15.5	129	22	47	25	55	31	35
13.5	73	28	82	35.5	58	29	25
12	91	11	35.5	29	55	29	27
15.5	108	22.5	51	25	55	29	26
12	51	25	66	34.6	63	39	36.5
15.5	101	34	13.1	25	41	22.5	20
13.5	55	17	49	34	62	32	26
12	60	25	81	35.5	61	34	26
15.5	115	19.5	52	41	79	25	17.5
14.5	46	22	65	27	40	23	24
15.5	111	29	86	45	83	15.5	15
12	46	28	86	27	51	15.5	16
18	123	22.4	61	27	41	19	16
9	51	17	51.5			23	18
9	38	19.5	71			21	23
15.5	171	19.5	68			31	33.4
22	106	15.5	49			33	21

TABLE X  
DROP VELOCITY - DROP DIAMETER DATA

Pneumatic Nozzle (1/4) JN No. 12      High Atomizing Pressures							
<u>Considerable Evaporation in Co-Current Equipment <math>V_G = 4.0</math> ft./sec.</u>							
<u>Section 2</u> (x = 4.0 in.)		<u>Section 3</u> (x = 8.0 in.)		<u>Section 4</u> (x = 12.0 in.)		<u>Section 5</u> (x = 16.0 in.)	
<u>d</u>	<u><math>V_D</math></u>	<u>d</u>	<u><math>V_D</math></u>	<u>d</u>	<u><math>V_D</math></u>	<u>d</u>	<u><math>V_D</math></u>
<u>microns</u>	<u>ft./sec.</u>	<u>microns</u>	<u>ft./sec.</u>	<u>microns</u>	<u>ft./sec.</u>	<u>microns</u>	<u>ft./sec.</u>
42	92	37	65	46	32	58	19
18.6	46	28	45	52	38	42	9
52	106	65	100	65	48	29	16
18.6	49	46	72	52	38	38	18
28	72	50	87	24	17	47.5	19
23	56	30	40	24	20	55	30
37	106	46	76	24	15.5	20	9
37	86	31	62	48	37	33	19
19	63	43	64	65	43	51	14
29	86	65	100	48	34	51	24
21	79	41	69	66	72	30	9
34	74	37	69	43	39	39.5	19
12	44	46	100	45	31	28	12
		56	62	46	34		
		37	53	48	36		

TABLE XI  
DROP VELOCITY - DROP DIAMETER DATA

---

Pneumatic Nozzle (1/4) JN No. 22B

---

Considerable Evaporation in Co-Current Equipment  $V_G = 4.0$  ft./sec.

---

<u>Section 1</u> (x = 1.5 in.)		<u>Section 2</u> (x = 4.0 in.)		<u>Section 3</u> (x = 8.0 in.)		<u>Section 4</u> (x = 12.0 in.)	
<u>d</u>	<u>V<sub>D</sub></u>	<u>d</u>	<u>V<sub>D</sub></u>	<u>d</u>	<u>V<sub>D</sub></u>	<u>d</u>	<u>V<sub>D</sub></u>
<u>microns</u>	<u>ft./sec.</u>	<u>microns</u>	<u>ft./sec.</u>	<u>microns</u>	<u>ft./sec.</u>	<u>microns</u>	<u>ft./sec.</u>
15	30	16	22	12	8	31	13
14	50	20	33	16	15	31	21
14.5	66	23	32	22	16	39	25
15.5	66	31	33	28	15	38.5	19
18.5	75	32	56	32	30	39.5	16
23	52	35.5	46	33	27	51	25
23	83	36	51.5	34	25	54	43
25	94	34	58	35	24	46	45
26	75	39	59	35	30		
31	69	39.5	47	36	28		
33	82	44.5	52	40	25		
34	105	60	68	40	18		
37.5	95	53	63	41	32		
32	66	53	54	47	27		
				47	41		
				58	53		

---

TABLE XII  
DROP VELOCITY - DROP DIAMETER DATA

---

Pressure Nozzle (1/4) LNNS No. 1

Negligible Evaporation in Lucite Column  $V_G = 0$  ft./sec.

<u>Section 1</u> (x = 1.5 in.)		<u>Section 2</u> (x = 4.5 in.)		<u>Section 3</u> (x = 8.0 in.)	
<u>d</u>	<u>V<sub>D</sub></u>	<u>d</u>	<u>V<sub>D</sub></u>	<u>d</u>	<u>V<sub>D</sub></u>
<u>microns</u>	<u>ft./sec.</u>	<u>microns</u>	<u>ft./sec.</u>	<u>microns</u>	<u>ft./sec.</u>
120	47	225	24	300	11
101	42.5	192	23.5	270	9
101	41	203	16	250	9.5
81	38	198	17	247	4.5
90	35	177	19	224	7.5
70	46.5	160	22	220	4.0
83	44	154	12	215	5.5
61	40	138	12.5	208	7.5
63	34.5	130	11.5	200	4.5
60	31	129	15.5	200	5.5
50	26.5	105	7.5	192	4.0
		70	10.5	180	6.5
				154	3.5

---

TABLE XIIIDROP VELOCITY - DROP DIAMETER DATA


---

 Pressure Nozzle (1/4) LN No. 1 Feed temperature 55-75°C.

 Considerable Evaporation in Co-Current Equipment  $V_G = 10$  ft./sec.
 

---

<u>Section 1</u> (x = 0.5 in.)		<u>Section 2</u> (x = 4.5 in.)		<u>Section 3</u> (x = 8.5 in.)		<u>Section 4</u> (x = 12.5 in.)	
<u>d</u>	<u>V<sub>D</sub></u>	<u>d</u>	<u>V<sub>D</sub></u>	<u>d</u>	<u>V<sub>D</sub></u>	<u>d</u>	<u>V<sub>D</sub></u>
<u>microns</u>	<u>ft./sec.</u>	<u>microns</u>	<u>ft./sec.</u>	<u>microns</u>	<u>ft./sec.</u>	<u>microns</u>	<u>ft./sec.</u>
80	45	100	36	120	21	128	12
48	34	84	35	73	11	119	11
39	49	68	33	65	11	115	8
53	49	60	19	70	13	105	10
71	42	60	29	72	17	150	12
38	30	73	32	58	11	170	15
94	64	93	37	150	17	110	16
65	31	100	26	85	13	87	8
91	51	87	29	85	11	94	14
66	63	103	42	90	20		
72	53	48	21	58	15		
65	44	69	36				

---

TABLE XIV  
DROP VELOCITY - DROP DIAMETER DATA

Pressure Nozzle LN No. 1 superheated feed at 250°F.							
Considerable Evaporation in Co-current Equipment $V_G = 10$ ft./sec.							
<u>Section 1</u> (x = 0.5 in.)		<u>Section 2</u> (x = 4.5 in.)		<u>Section 3</u> (x = 8.5 in.)		<u>Section 4</u> (x = 12.5 in.)	
d	$V_D$	d	$V_D$	d	$V_D$	d	$V_D$
<u>microns</u>	<u>ft./sec.</u>	<u>microns</u>	<u>ft./sec.</u>	<u>microns</u>	<u>ft./sec.</u>	<u>microns</u>	<u>ft./sec.</u>
44	38	85	23	110	19	104	12
44	43	119	26	101	15	92	9
61	90	61	18	71	14	78	13
75	129	71	18	66	13	115	14
52	76	86	14	99	12	140	15
40	65	58	22	89	15	104	8
28	49	91	31	82	16	75	12
42	41	94	23	109	15	72	10
51	55	45	15	112	12	103	17.5
35	75	113	31	95	14	60	13
38	45	87	20			115	11
61	75	108	24				
51	62	105	24				
33	56	70	22				
45	70						
68	88						

APPENDIX II

DRAG COEFFICIENTS OF SPRAY DROPS

TABLE XV

DRAG COEFFICIENT - REYNOLDS NUMBER DATA

Pneumatic Nozzle (1/4) JN No. 12 Low Atomizing Pressures. Negligible Evaporation

<u>d = 15 microns</u>		<u>d = 20 microns</u>		<u>d = 25 microns</u>		<u>d = 30 microns</u>		<u>d = 35 microns</u>		<u>d = 40 microns</u>	
<u>C<sub>D</sub></u>	<u>Re</u>										
0.193	17.5	0.256	32.8	0.325	54.4	0.433	83.1	0.519	124.2	0.252	59.5
0.187	14.7	0.206	27.8	0.274	46.1	0.342	70.2	0.447	102.7	0.271	38.6
0.162	11.5	0.181	25.0	0.207	38.4	0.298	56.9	0.335	89.2	0.241	23.0
0.118	8.77	0.150	17.4	0.216	28.6	0.209	43.1	0.302	61.2	0.272	14.8
0.097	6.30	0.120	12.7	0.159	20.6	0.189	31.7	0.323	43.2		
0.103	4.15	0.132	8.53	0.137	13.9	0.169	21.5	0.203	29.1		
0.139	2.36	0.316	5.13	0.163	8.67	0.192	13.2	0.211	18.0		
0.290	1.12	0.480	2.62	0.415	5.36	0.226	7.69	0.177	10.9		

TABLE XVI

DRAG COEFFICIENT - REYNOLDS NUMBER DATA

Pneumatic Nozzle (1/4) JN No. 12 Mixed and High Atomizing Pressures Negligible Evaporation

<u>Mixed Atomizing Pressures</u>						<u>High Atomizing Pressures</u>					
<u>d = 15 microns</u>		<u>d = 20 microns</u>		<u>d = 25 microns</u>		<u>d = 15 microns</u>		<u>d = 20 microns</u>		<u>d = 25 microns</u>	
<u>C<sub>D</sub></u>	<u>Re</u>	<u>C<sub>D</sub></u>	<u>Re</u>	<u>C<sub>D</sub></u>	<u>Re</u>	<u>C<sub>D</sub></u>	<u>Re</u>	<u>C<sub>D</sub></u>	<u>Re</u>	<u>C<sub>D</sub></u>	<u>Re</u>
0.189	16.45	0.345	42.0	0.481	77.2	0.177	22.7	0.263	45.1	0.386	99.5
0.142	14.15	0.287	36.6	0.383	60.8	0.196	19.6	0.235	38.0	0.331	70.4
0.136	11.80	0.227	26.3	0.301	46.3	0.139	16.2	0.195	30.8	0.268	53.8
0.106	9.15	0.176	18.8	0.241	32.2	0.167	12.3	0.167	22.8	0.223	38.6
0.0973	6.40	0.141	12.9	0.168	21.8	0.123	8.76	0.168	15.8	0.183	26.3
0.191	4.30	0.129	8.32	0.155	13.9	0.142	4.82	0.182	8.73	0.196	15.95
0.62	2.27					0.184	2.09				
						0.209	.645				

TABLE XVII

DRAG COEFFICIENT - REYNOLDS NUMBER DATA

Pressure Nozzle (1/4) LNN SS No. 1 - Negligible Evaporation

<u>d = 40 microns</u>		<u>d = 60 microns</u>		<u>d = 80 microns</u>		<u>d = 100 microns</u>		<u>d = 120 microns</u>	
<u>C<sub>D</sub></u>	<u>Re</u>	<u>C<sub>D</sub></u>	<u>Re</u>	<u>C<sub>D</sub></u>	<u>Re</u>	<u>C<sub>D</sub></u>	<u>Re</u>	<u>C<sub>D</sub></u>	<u>Re</u>
1.03	14.0	1.75	27.7	2.31	47.6	2.76	71.0	3.07	101
0.59	7.80	1.22	13.8	1.60	24.6	1.81	37.5	2.20	52.9
0.62	5.70	1.08	6.76	1.23	12.0	1.17	19.0	1.87	27.6
		0.14	3.01	0.57	5.42	0.95	8.72	1.49	12.8

APPENDIX IIIASSESSMENT OF HUMIDITY MEASUREMENT METHODSTABLE XVIIICOMPARISON TESTS USING SYNTHETIC AIR

<u>Sample No.</u>	<u>Humidity Made Up</u>	<u>Humidity Determined lb. H<sub>2</sub>O/lb. air</u>		
		<u>Gravimetric</u>	<u>Volumetric</u>	<u>Dew Point</u>
1	0.01493	0.01496	0.01506	0.01468
		0.01478	0.01510	0.01496
			0.01512	
2	0.01870	0.01856	0.01848	0.01919
		0.01880	0.01888	0.01897
			0.01852	
3	0.01075	0.01078	0.01076	0.01098
		0.01063	0.01078	0.01105
			0.01058	
4	0.00608	0.00620	0.00600	0.00588
		0.00623	0.00613	0.00590
			0.00610	

TABLE XIX

COMPARISON TESTS USING CO<sub>2</sub>-FREE, SATURATED AIR

Sample No.	Humidity Made Up	Humidity Determined lb H <sub>2</sub> O/lb. air			Wet and Dry Bulb
		Gravimetric	Volumetric	Dew Point	
1	0.0115	0.01124	0.01158	0.01142	-
2	0.0159	0.01614	0.01587	0.01620	0.0142
3	0.0118	0.01205	0.01182	0.01155	0.0117
4	0.0200	0.01980	0.02030	0.02080	0.0195
5	0.0180	0.01930	0.01890	0.01890	0.0185

TABLE XX

COMPARISON TESTS USING ROOM AIR

Sample No.	Humidity Determined lb. H <sub>2</sub> O/lb. air		
	Volumetric	Dew Point	Wet and Dry Bulb
1	0.00472	0.0050	0.0045
2	0.01492	0.0152	0.0168
3	0.00883	0.0090	0.0100
4	0.00512	0.0050	0.0054
5	0.01182	0.0142	0.0133
6	0.00991	0.0100	0.0112
7	0.01495	0.0161	0.0170
8	0.01302	0.0125	0.0141
9	0.01230	0.0125	0.0132
10	0.00721	0.0067	0.0080

CROSS-CURRENT EVAPORATION RUNSTABLE XXIRUN NO. 1 - TABLE OF RESULTS

<u>Pneumatic Nozzle (1/4) JN No. 12 Low Atomizing Pressures</u>				
	<u>Section 1</u>	<u>Section 2</u>	<u>Section 3</u>	<u>Section 4</u>
$w_{d1}$ lb./hr.	6.31	8.53	12.82	15.39
$H_{d1}$ lb.H <sub>2</sub> O/lb.air	0.0120	0.0120	0.0120	0.0120
$t_{d1}$ °F.	170	168	176	162
$w_{d2}$ lb./hr.	6.31	9.02	14.61	19.54
$w_{d2}$ (cor.) lb./hr.	6.19	8.85	14.36	19.10
$H_{d2}$ lb.H <sub>2</sub> O/lb.air	0.0197	0.0204	0.0208	0.0208
$t_{d2}$ °F.	91	91	90	89
$w_{a1}$ lb./hr.	5.45	5.57	5.25	3.71
$t_{a1}$ °F.	76	68	68	68
$w_{a2}$ lb./hr.	5.57	5.25	3.71	0.00
$t_{a2}$ °F.	68	68	68	68
$t_{av}$ °F.	103.5	105.1	114.7	116.2
$T_s$ °F. ( $T_L=78$ °F.)	85.0	87.0	87.0	88.0
$\Delta T$ °F.	18.5	18.1	27.7	28.2
$W$ lb./hr.	1.97	1.91	1.80	1.68
$Q$ B.t.u./hr.	76	82	132	178
$E_f$ %	3.6	3.9	6.2	8.4
$d_{vs}$ microns	16.6	20.8	24.1	24.8
$V_D$ ft./sec.	73	41	27	15
$V_R$ ft./sec.	73	41	27	15
$S_w$ 10 <sup>3</sup> ft. <sup>2</sup> /lb.	1.77	1.41	1.22	1.18
$A_s$ 10 <sup>-3</sup> ft. <sup>2</sup>	3.31	4.57	7.55	12.3
$h$ Eng. units	1240	994	632	513
$Nu$	4.28	4.32	3.13	2.60
$Re$	23.8	16.7	12.5	7.18
$(Re)^{1/2}(Pr)^{1/3}$	4.38	3.68	3.18	2.41
$Nu'$	3.64	3.66	2.66	2.22
$(Re)^{1/2}(Sc)^{1/3}$	4.14	3.50	3.02	2.29

TABLE XXII

## RUN NO. 2 - TABLE OF RESULTS

Pneumatic Nozzle (1/4) JN No. 12 Low Atomizing Pressures				
	<u>Section 1</u>	<u>Section 2</u>	<u>Section 3</u>	<u>Section 4</u>
$w_{d1}$ lb./hr.	6.25	6.76	11.50	12.30
$H_{d1}$ lb.H <sub>2</sub> O/lb.air	0.0122	0.0122	0.0122	0.0122
$t_{d1}$ °F.	165	167	167	155
$w_{d2}$ lb./hr.	6.27	7.31	13.61	15.07
$w_{d2}$ (cor.) lb./hr.	6.27	7.31	13.61	15.07
$H_{d2}$ lb.H <sub>2</sub> O/lb.air	0.0201	0.0212	0.0216	0.0218
$t_{d2}$ °F.	93	91	90	89
$w_{a1}$ lb./hr.	5.45	5.43	4.88	2.77
$t_{a1}$ °F.	80	68	68	68
$w_{a2}$ lb./hr.	5.43	4.88	2.77	0.00
$t_{a2}$ °F.	68	68	68	68
$t_{av.}$ °F.	103.5	102.5	111.8	113.5
$T_s$ °F. ( $T_L=79^\circ\text{F.}$ )	86.0	87.0	89.0	91.0
$\Delta T$ °F.	17.5	15.5	22.8	22.5
$W$ lb./hr.	1.97	1.92	1.82	1.68
$Q$ B.t.u./hr.	82	74	136	153
$E_f$ %	3.9	3.5	6.4	7.2
$d_{vs}$ microns	15.1	21.0	23.5	24.2
$V_D$ ft./sec.	63	42	27	14
$V_R$ ft./sec.	63	42	27	14
$S_w$ 10 <sup>3</sup> ft. <sup>2</sup> /lb.	1.95	1.40	1.25	1.21
$A_s$ 10 <sup>-3</sup> ft. <sup>2</sup>	4.23	4.45	7.80	13.4
$h$ Eng. units	1110	1070	761	508
$Nu$	3.55	4.63	3.68	2.54
$Re$	18.2	16.9	12.2	6.52
$(Re)^{1/2}(Pr)^{1/3}$	3.84	3.70	3.14	2.29
$Nu^*$	3.01	3.92	3.10	2.15
$(Re)^{1/2}(Sc)^{1/3}$	3.68	3.54	3.00	2.19

TABLE XXIII  
RUN NO. 3 - TABLE OF RESULTS

<u>Pneumatic Nozzle (1/4) JN No. 12 Low Atomizing Pressures</u>				
	<u>Section 1</u>	<u>Section 2</u>	<u>Section 3</u>	<u>Section 4</u>
$w_{d1}$ lb./hr.	7.70	9.25	13.90	18.66
$H_{d1}$ lb.H <sub>2</sub> O/lb.air	0.0120	0.0120	0.0120	0.0120
$t_{d1}$ °F.	176	176	181	170
$w_{d2}$ lb./hr.	7.60	10.60	16.50	21.90
$w_{d2}$ (cor.) lb./hr.	7.37	10.29	16.00	21.30
$H_{d2}$ lb.H <sub>2</sub> O/lb.air	0.0197	0.0202	0.0209	0.0216
$t_{d2}$ °F.	103	93	91	91
$w_{a1}$ lb./hr.	5.45	5.78	4.74	2.64
$t_{a1}$ °F.	76	64	64	64
$w_{a2}$ lb./hr.	5.78	4.74	2.64	0.00
$t_{a2}$ °F.	64	64	64	64
$t_{av.}$ °F.	110.1	108.5	119.1	120.0
$T_s$ °F. ( $T_L=82$ °F.)	87.0	87.0	87.0	87.0
$\Delta T$ °F.	23.1	21.5	32.1	37.0
$W$ lb./hr.	1.97	1.90	1.79	1.62
$Q$ B.t.u./hr.	86	89	151	216
$E_f$ %	4.1	4.2	7.1	10.2
$d_{vs}$ microns	17.6	20.4	27.0	26.1
$V_D$ ft./sec.	74	40	32	16
$V_R$ ft./sec.	74	40	32	16
$S_w$ 10 <sup>3</sup> ft. <sup>2</sup> /lb.	1.67	1.44	1.09	1.13
$A_s$ 10 <sup>-3</sup> ft. <sup>2</sup>	3.08	4.76	5.65	10.6
$h$ Eng. units	1200	872	831	548
$Nu$	4.43	3.71	4.62	2.96
$Re$	25.0	15.7	16.4	7.81
$(Re)^{1/2}(Pr)^{1/3}$	4.50	3.57	3.63	2.51
$Nu'$	3.73	3.14	3.90	2.50
$(Re)^{1/2}(Sc)^{1/3}$	4.31	3.42	3.47	2.40

TABLE XXIV

## RUN NO. 4 - TABLE OF RESULTS

Pneumatic Nozzle (1/4) JN No. 12 Low Atomizing Pressures				
	Section 1	Section 2	Section 3	Section 4
$w_{d1}$ lb./hr.	7.13	8.26	13.20	14.76
$H_{d1}$ lb. $H_2O$ /lb.air	0.0083	0.0083	0.0083	0.0083
$t_{d1}$ °F.	142	143	147	138
$w_{d2}$ lb./hr.	7.10	8.90	14.65	17.80
$w_{d2}$ (cor.) lb./hr.	7.16	8.98	14.80	17.96
$H_{d2}$ lb. $H_2O$ /lb.air	0.0162	0.0168	0.0174	0.0175
$t_{d2}$ °F.	79	79	77	78
$w_{a1}$ lb./hr.	5.45	5.42	4.80	3.20
$t_{a1}$ °F.	66	57	57	57
$w_{a2}$ lb./hr.	5.42	4.80	3.20	0.00
$t_{a2}$ °F.	57	57	57	57
$t_{av}$ °F.	89.2	89.6	98.3	100.8
$T_s$ °F. ( $T_L=78^\circ\text{F.}$ )	79.0	79.0	79.0	79.0
$\Delta T$ °F.	10.2	10.6	19.3	21.8
$W$ lb./hr.	1.98	1.91	1.81	1.66
$Q$ B.t.u./hr.	66	81	141	174
$E_f$ %	3.1	3.8	6.6	8.2
$d_{vs}$ microns	14.1	15.6	18.2	20.7
$V_D$ ft./sec.	60	28	18	11
$V_R$ ft./sec.	60	28	18	11
$S_w$ $10^3$ ft. $^2$ /lb.	2.09	1.88	1.61	1.42
$A_s$ $10^{-3}$ ft. $^2$	4.80	8.92	15.0	19.8
$h$ Eng. units	1350	859	490	403
$Nu$	4.00	2.81	1.86	1.75
$Re$	16.9	8.88	6.50	4.55
$(Re)^{1/2}(Pr)^{1/3}$	3.68	2.66	2.30	1.91
$Nu^*$	3.38	2.37	1.57	1.48
$(Re)^{1/2}(Sc)^{1/3}$	3.53	2.55	2.21	1.83

TABLE XXV  
RUN NO. 5 - TABLE OF RESULTS

<u>Pneumatic Nozzle (1/4) JN No. 12 Low Atomizing Pressures</u>				
	<u>Section 1</u>	<u>Section 2</u>	<u>Section 3</u>	<u>Section 4</u>
$w_{d1}$ lb./hr.	8.80	9.70	15.16	18.60
$H_{d1}$ lb.H <sub>2</sub> O/lb.air	0.0092	0.0092	0.0092	0.0092
$t_{d1}$ °F.	144	145	145	140
$w_{d2}$ lb./hr.	7.60	10.60	16.22	22.00
$w_{d2}$ (cor.) lb./hr.	7.80	10.85	16.60	22.44
$H_{d2}$ lb.H <sub>2</sub> O/lb.air	0.0189	0.0192	0.0195	0.0199
$t_{d2}$ °F.	83	82	82	81
$w_{a1}$ lb./hr.	5.45	6.45	5.30	3.84
$t_{a1}$ °F.	70	60	60	60
$w_{a2}$ lb./hr.	6.45	5.30	3.84	0.00
$t_{a2}$ °F.	60	60	60	60
$t_{av}$ °F.	99.0	92.8	100.4	103.7
$T_s$ °F. ( $T_L=76^\circ\text{F.}$ )	79.0	79.0	79.0	79.0
$\Delta T$ °F.	20	13.8	21.4	24.7
$W$ lb./hr.	1.96	1.87	1.74	1.69
$Q$ B.t.u./hr.	94	125	180	252
$E_f$ %	4.4	5.9	8.5	11.9
$d_{vs}$ microns	14.7	17.4	20.6	20.5
$V_D$ ft./sec.	62	32	22	10
$V_R$ ft./sec.	62	32	22	10
$S_w$ 10 <sup>3</sup> ft. <sup>2</sup> /lb.	2.00	1.69	1.43	1.43
$A_s$ 10 <sup>-3</sup> ft. <sup>2</sup>	4.40	6.86	10.4	22.4
$h$ Eng. units	1050	1320	810	466
$Nu$	3.34	4.79	3.47	2.00
$Re$	18.2	11.1	9.08	4.10
$(Re)^{1/2}(Pr)^{1/3}$	3.84	2.99	2.72	1.82
$Nu'$	2.84	4.05	2.95	3.48
$(Re)^{1/2}(Sc)^{1/3}$	3.68	2.87	2.60	1.75

TABLE XXVI

## RUN NO. 6 - TABLE OF RESULTS

Pneumatic Nozzle (1/4) JN No. 12 Low Atomizing Pressures					
	Section 1	Section 2	Section 3	Section 4	Section 5
$w_{d1}$ lb./hr.	10.31	13.34	16.60	20.80	21.60
$H_{d1}$ lb.H <sub>2</sub> O/lb.air	0.0095	0.0095	0.0095	0.0095	0.0095
$t_{d1}$ °F.	182	184	180	180	157
$w_{d2}$ lb./hr.	12.90	13.60	17.20	21.00	21.20
$w_{d2}$ (cor.) lb./hr.	13.30	14.05	17.70	21.40	21.60
$H_{d2}$ lb.H <sub>2</sub> O/lb.air	0.0175	0.0180	0.0195	0.0200	0.0205
$t_{d2}$ °F.	104	101	98	96	106
$w_{a1}$ lb./hr.	5.45	2.46	1.75	0.65	0.00
$t_{a1}$ °F.	86	71	71	71	71
$w_{a2}$ lb./hr.	2.46	1.75	0.65	0.00	0.00
$t_{a2}$ °F.	71	71	71	71	71
$t_{av}$ °F.	124.1	131.7	133.4	136.5	131.5
$T_s$ °F. ( $T_L=92$ °F.)	95.0	94.0	93.0	93.0	93.0
$\Delta T$ °F.	29.1	37.7	40.4	43.5	38.5
$W$ lb./hr.	1.95	1.84	1.69	1.49	1.27
$Q$ B.t.u./hr.	132	123	182	232	250
$E_f$ %	6.2	5.8	8.6	10.9	11.3
$d_{vs}$ microns	15.4	23.1	26.5	27.8	35.0
$V_D$ ft./sec.	64	47	31	16	11
$V_R$ ft./sec.	64	47	31	16	11
$S_w$ 10 <sup>3</sup> ft. <sup>2</sup> /lb.	1.91	1.27	1.11	1.06	0.84
$A_s$ 10 <sup>-3</sup> ft. <sup>2</sup>	4.04	3.46	5.58	9.15	8.95
$h$ Eng. units	1120	942	806	583	726
$Nu$	3.57	4.48	4.38	3.33	5.28
$Re$	18.2	20.1	15.2	8.22	7.13
$(Re)^{1/2}(Pr)^{1/3}$	3.83	4.04	3.52	2.58	2.41
$Nu'$	3.04	3.82	3.74	2.84	4.50
$(Re)^{1/2}(Sc)^{1/3}$	3.66	3.86	3.36	2.46	2.30

TABLE XXVII

## RUN NO. 7 - TABLE OF RESULTS

Pneumatic Nozzle (1/4) JN No. 12 Low Atomizing Pressures					
	Section 1	Section 2	Section 3	Section 4	Section 5
$w_{d1}$ lb./hr.	11.20	14.30	15.15	17.50	19.00
$H_{d1}$ lb.H <sub>2</sub> O/lb.air	0.0088	0.0088	0.0088	0.0088	0.0088
$t_{d1}$ °F.	165	172	174	172	145
$w_{d2}$ lb./hr.	13.60	16.20	17.20	19.00	19.90
$w_{d2}$ (cor.) lb./hr.	13.10	15.60	16.55	18.35	19.00
$H_{d2}$ lb.H <sub>2</sub> O/lb.air	0.0160	0.0170	0.0180	0.0185	0.0190
$t_{d2}$ °F.	109	108	107	106	105
$w_{a1}$ lb./hr.	5.45	3.55	2.25	0.85	0.00
$t_{a1}$ °F.	86	71	71	71	71
$w_{a2}$ lb./hr.	3.55	2.35	0.85	0.00	0.00
$t_{a2}$ °F.	71	71	71	71	71
$t_{av.}$ °F.	120.1	127.6	131.1	136.6	125.0
$T_s$ °F. ( $T_L=80$ °F.)	96.0	97.0	97.0	97.0	98.0
$\Delta T$ °F.	24.1	30.6	34.1	39.6	27.0
$W$ lb./hr.	1.95	1.84	1.70	1.54	1.35
$Q$ B.t.u./hr.	150	138	162	188	204
$E_f$ %	7.1	6.5	7.6	8.8	9.6
$d_{vs}$ microns	14.8	19.3	23.0	28.4	29.0
$V_D$ ft./sec.	64	38	27	18	8
$V_R$ ft./sec.	64	38	27	18	8
$S_w$ 10 <sup>3</sup> ft. <sup>2</sup> /lb.	1.98	1.53	1.28	1.03	1.02
$A_s$ 10 <sup>-3</sup> ft. <sup>2</sup>	4.18	5.15	7.45	8.19	15.9
$h$ Eng. units	1490	874	637	584	476
$Nu$	4.57	3.50	3.03	3.43	2.84
$Re$	18.2	13.3	11.9	9.70	4.21
$(Re)^{1/2}(Pr)^{1/3}$	3.84	3.28	3.10	2.80	1.85
$Nu'$	3.90	3.00	2.59	2.93	2.42
$(Re)^{1/2}(Sc)^{1/3}$	3.67	3.13	2.96	2.67	1.76

TABLE XXVIII

## RUN NO. 8 - TABLE OF RESULTS

Pneumatic Nozzle (1/4) JN No. 12 Low Atomizing Pressures					
	Section 1	Section 2	Section 3	Section 4	Section 5
$w_{d1}$ lb./hr.	11.60	12.60	17.50	20.50	21.00
$H_{d1}$ lb.H <sub>2</sub> O/lb.air	0.0090	0.0090	0.0090	0.0090	0.0090
$t_{d1}$ °F.	186	194	194	186	144
$w_{d2}$ lb./hr.	13.00	14.50	19.20	22.80	23.25
$w_{d2}$ (cor.) lb./hr.	12.40	13.80	18.30	21.80	22.25
$H_{d2}$ lb.H <sub>2</sub> O/lb.air	0.0205	0.0215	0.0215	0.0216	0.0220
$t_{d2}$ °F.	107	101	101	104	107
$w_{a1}$ lb./hr.	5.45	4.65	3.45	2.65	1.35
$t_{a1}$ °F.	86	71	71	71	71
$w_{a2}$ lb./hr.	4.65	3.45	2.65	1.35	0.00
$t_{a2}$ °F.	71	71	71	71	71
$t_{av}$ °F.	125.7	127.8	135.0	137.2	123.2
$T_s$ °F. ( $T_L=85^\circ\text{F.}$ )	95.0	95.0	95.0	95.0	95.0
$\Delta T$ °F.	30.7	32.8	41.1	42.2	28.2
$W$ lb./hr.	1.93	1.78	1.58	1.34	1.06
$Q$ B.t.u./hr.	184	181	243	293	308
$E_f$ %	8.7	8.5	11.5	14.0	14.5
$d_{vs}$ microns	16.7	19.4	24.0	27.0	26.8
$V_D$ ft./sec.	73	39	28	17	7
$V_R$ ft./sec.	73	39	28	17	7
$S_w$ 10 <sup>3</sup> ft. <sup>2</sup> /lb.	1.76	1.52	1.22	1.09	1.10
$A_s$ 10 <sup>-3</sup> ft. <sup>2</sup>	3.24	4.82	6.40	8.00	15.6
$h$ Eng. units	1850	1150	922	890	700
$Nu$	6.31	4.59	4.51	4.92	3.80
$Re$	22.7	13.9	11.50	8.51	3.44
$(Re)^{1/2}(Pr)^{1/3}$	4.31	3.34	3.05	2.62	1.70
$Nu^*$	5.40	3.90	3.86	4.20	3.24
$(Re)^{1/2}(Sc)^{1/3}$	4.14	3.20	2.92	2.51	1.62

TABLE XXIX

## RUN No. 9 - TABLE OF RESULTS

Pneumatic Nozzle (1/4) JN No. 12 Low Atomizing Pressures					
	Section 1	Section 2	Section 3	Section 4	Section 5
$w_{d1}$ lb./hr.	12.00	15.30	16.20	21.00	22.00
$H_{d1}$ lb.H <sub>2</sub> O/lb.air	0.0066	0.0066	0.0066	0.0066	0.0066
$t_{d1}$ °F.	193	194	195	194	167
$w_{d2}$ lb./hr.	13.60	17.60	19.40	22.70	24.10
$w_{d2}$ (cor.) lb./hr.	12.80	16.70	18.30	21.40	22.75
$H_{d2}$ lb.H <sub>2</sub> O/lb.air	0.0185	0.0190	0.0195	0.0195	0.0195
$t_{d2}$ °F.	110	111	110	109	119
$w_{a1}$ lb./hr.	5.45	4.65	3.25	1.15	0.75
$t_{a1}$ °F.	90	76	76	76	76
$w_{a2}$ lb./hr.	4.65	3.25	1.15	0.75	0.00
$t_{a2}$ °F.	76	76	76	76	76
$t_{av}$ °F.	131.8	136.8	141.2	148.7	142.2
$T_s$ °F. ( $T_L=78$ °F.)	95.0	95.0	95.0	95.0	95.0
$\Delta T$ °F.	36.8	41.8	46.2	53.7	47.2
$W$ lb./hr.	1.92	1.74	1.52	1.26	0.98
$Q$ B.t.u./hr.	206	219	250	292	311
$E_f$ %	9.7	10.3	11.8	13.8	14.7
$d_{vs}$ microns	16.8	19.3	25.0	26.0	28.5
$V_D$ ft./sec.	72	38	28	16	8
$V_R$ ft./sec.	72	38	28	16	8
$S_w$ 10 <sup>3</sup> ft. <sup>2</sup> /lb.	1.75	1.52	1.17	1.13	1.03
$A_s$ 10 <sup>-3</sup> ft. <sup>2</sup>	3.24	4.82	5.89	8.26	11.7
$h$ Eng. units	1730	1080	923	656	563
$Nu$	5.94	4.25	4.65	3.48	3.29
$Re$	22.5	13.5	12.7	7.46	4.08
$(Re)^{1/2}(Pr)^{1/3}$	4.26	3.31	3.19	2.47	1.82
$Nu'$	5.03	3.63	3.94	6.38	3.50
$(Re)^{1/2}(Sc)^{1/3}$	4.08	3.17	3.06	2.36	1.74

TABLE XXX

## RUN NO. 10 - TABLE OF RESULTS

Pneumatic Nozzle (1/4) JN No. 12 Low Atomizing Pressures					
	Section 1	Section 2	Section 3	Section 4	Section 5
$w_{d1}$ lb./hr.	9.90	12.90	15.50	16.60	17.75
$H_{d1}$ lb.H <sub>2</sub> O/lb.air	0.0083	0.0083	0.0083	0.0083	0.0083
$t_{d1}$ °F.	177	182	188	185	159
$w_{d2}$ lb./hr.	11.35	14.20	15.90	18.70	18.65
$w_{d2}$ (cor.) lb./hr.	11.25	14.10	15.75	18.50	18.45
$H_{d2}$ lb.H <sub>2</sub> O/lb.air	0.0165	0.0177	0.0180	0.0190	0.0190
$t_{d2}$ °F.	104	100	100	104	113
$w_{a1}$ lb./hr.	5.95	4.10	2.90	2.65	0.75
$t_{a1}$ °F.	92	75	75	75	75
$w_{a2}$ lb./hr.	4.10	2.90	2.65	6.75	0.00
$t_{a2}$ °F.	75	75	75	75	75
$t_{av}$ °F.	121.6	126.6	133.1	136.3	134.2
$T_s$ °F. ( $T_L=80$ °F.)	95.0	95.0	95.0	98.0	100.0
$\Delta T$ °F.	26.6	31.6	38.1	38.3	34.2
$W$ lb./hr.	1.95	1.84	1.70	1.53	1.33
$Q$ B.t.u./hr.	145	140	161	212	210
$E_f$ %	6.8	6.6	7.6	10.0	9.9
$d_{vs}$ microns	14.5	19.5	25.4	25.8	28.2
$V_D$ ft./sec.	62	39	28	16	8
$V_R$ ft./sec.	62	39	28	16	8
$S_w$ 10 <sup>3</sup> ft. <sup>2</sup> /lb.	2.03	1.51	1.16	1.14	1.04
$A_s$ 10 <sup>-3</sup> ft. <sup>2</sup>	4.43	4.95	6.50	10.1	16.0
$h$ Eng. units	1230	895	657	556	386
$Nu$	3.71	3.62	3.42	2.96	2.26
$Re$	16.7	13.9	13.1	7.60	4.13
$(Re)^{1/2} (Pr)^{1/3}$	3.67	3.35	3.25	2.47	1.82
$Nu'$	3.17	3.10	2.92	2.53	1.93
$(Re)^{1/2} (Sc)^{1/3}$	3.52	3.21	3.12	2.37	1.74

TABLE XXXI

## RUN NO. 11 - TABLE OF RESULTS

Pneumatic Nozzle (1/4) JN No. 12 Low Atomizing Pressures					
	Section 1	Section 2	Section 3	Section 4	Section 5
$w_{d1}$ lb./hr	10.20	13.00	15.60	16.80	17.00
$H_{d1}$ lb.H <sub>2</sub> O/lb.air	0.0084	0.0084	0.0084	0.0084	0.0084
$t_{d1}$ °F.	203	208	212	208	177
$w_{d2}$ lb./hr.	11.40	14.20	15.90	18.70	18.90
$w_{d2}$ (cor.) lb./hr.	11.25	14.00	15.70	18.50	18.60
$H_{d2}$ lb.H <sub>2</sub> O/lb.air	0.0175	0.0186	0.0190	0.0200	0.0200
$t_{d2}$ °F.	114	108	106	106	118
$w_{a1}$ lb./hr.	5.45	4.40	3.40	3.30	1.60
$t_{a1}$ °F.	92	75	75	75	75
$w_{a2}$ lb./hr.	4.40	3.40	3.30	1.60	0.00
$t_{a2}$ °F.	75	75	75	75	75
$t_{av.}$ °F.	133.6	138.3	144.4	145.2	143.8
$T_s$ °F. ( $T_L=80$ °F.)	97.0	97.0	98.0	99.0	100.0
$\Delta T$ °F.	36.6	41.3	46.4	46.2	43.8
$W$ lb./hr.	1.95	1.83	1.67	1.48	1.26
$Q$ B.t.u./hr.	162	151	178	228	229
$E_f$ %	7.6	7.1	8.4	10.7	10.7
$d_{vs}$ microns	14.7	21.0	28.0	28.8	29.7
$V_D$ ft./sec.	62	40	33	18	8
$V_R$ ft./sec.	62	40	33	18	8
$S_w$ 10 <sup>3</sup> ft. <sup>2</sup> /lb.	2.00	1.40	1.05	1.02	0.99
$A_s$ 10 <sup>-3</sup> ft. <sup>2</sup>	4.37	4.45	4.92	7.80	14.4
$h$ Eng. units	1010	825	780	631	363
$Nu$	3.10	3.59	4.44	3.70	2.18
$Re$	16.8	15.0	16.50	9.22	4.21
$(Re)^{1/2}(Pr)^{1/3}$	3.67	3.48	3.65	2.71	1.85
$Nu'$	2.65	3.00	3.78	3.16	1.86
$(Re)^{1/2}(Sc)^{1/3}$	3.50	3.32	3.48	2.58	1.76

TABLE XXXII

## RUN NO. 12 - TABLE OF RESULTS

Pneumatic Nozzle (1/4) JN No. 12 Low Atomizing Pressures					
	Section 1	Section 2	Section 3	Section 4	Section 5
$w_{d1}$ lb./hr.	11.10	14.80	17.70	20.70	22.95
$H_{d1}$ lb.H <sub>2</sub> O/lb.air	0.0083	0.0083	0.0083	0.0083	0.0083
$t_{d1}$ °F.	192	202	212	214	170
$w_{d2}$ lb./hr.	12.90	16.60	19.90	21.70	24.80
$w_{d2}$ (cor.) lb./hr.	12.45	16.05	19.22	20.95	24.00
$H_{d2}$ lb.H <sub>2</sub> O/lb.air	0.0175	0.0190	0.0200	0.0205	0.0205
$t_{d2}$ °F.	113	110	107	107	119
$w_{a1}$ lb./hr.	5.45	4.10	2.85	1.33	1.06
$t_{a1}$ °F.	92	74	74	74	74
$w_{a2}$ lb./hr.	4.10	2.85	1.33	1.06	0.00
$t_{a2}$ °F.	74	74	74	74	74
$t_{av.}$ °F.	131.6	139.4	148.5	155.2	141.8
$T_s$ °F. ( $T_L = 85$ °F.)	98.0	99.0	100.5	102.0	104.0
$\Delta T$ °F.	33.6	40.4	48.0	53.2	37.8
$W$ lb./hr.	1.94	1.80	1.60	1.36	1.09
$Q$ B.t.u./hr.	166	183	239	271	312
$E_f$ %	7.9	8.7	11.3	12.8	14.7
$d_{vs}$ microns	16.1	19.4	22.0	26.4	29.3
$V_D$ ft./sec.	70	39	24	16	8
$V_R$ ft./sec.	70	39	24	16	8
$S_w$ 10 <sup>3</sup> ft. <sup>2</sup> /lb.	1.83	1.51	1.34	1.11	1.00
$A_s$ 10 <sup>-3</sup> ft. <sup>2</sup>	3.52	4.83	8.28	8.73	12.6
$h$ Eng. units	1400	940	603	584	654
$Nu$	4.60	3.70	2.70	3.12	3.90
$Re$	20.5	13.5	9.41	7.45	4.28
$(Re)^{1/2} (Pr)^{1/3}$	4.07	3.30	2.76	2.45	1.86
$Nu'$	3.94	3.17	2.40	2.67	3.34
$(Re)^{1/2} (Sc)^{1/3}$	3.86	3.14	2.63	2.33	1.77

TABLE XXXIII

## RUNS NO. 13 AND 14 - TABLE OF RESULTS

Pressure Nozzle (1/4) LNN SS No. 1					
	Run No. 13		Run No. 14		
	Section 1	Section 2	Section 1	Section 2	Section 1
$w_{d1}$ lb./hr.	11.10	15.30	11.20	13.88	16.05
$H_{d1}$ lb.H <sub>2</sub> O/lb.air	0.0124	0.0124	0.0117	0.0117	0.0117
$t_{d1}$ °F.	206	220	186	198	193
$w_{d2}$ lb./hr.	12.96	17.05	12.70	15.00	17.22
$w_{d2}$ (cor.) lb./hr.	11.10	15.30	11.20	13.90	16.05
$H_{d2}$ lb.H <sub>2</sub> O/lb.air	0.0145	0.0170	0.0145	0.0167	0.0188
$t_{d2}$ °F.	126	130	122	127	140
$t_{av}$ °F.	160	175	154	162.5	167
$T_s$ °F. ( $T_L=85;85°F.$ )	95	98	95	101	103
$\Delta T$ °F.	71	77	59	61.5	64
$W$ lb./hr.	4.99	4.95	4.99	4.94	4.85
$Q$ B.t.u.	78	90	83	104	131
$E_f$ %	1.4	1.7	1.5	1.9	2.4
$d_{vs}$ microns	91	125	75	101	153
$V_D$ ft./sec.	43	13	36	11	4.5
$V_R$ ft./sec.	43	13	36	11	4.5
$S_w$ 10 <sup>2</sup> ft. <sup>2</sup> /lb.	3.23	2.36	3.92	2.91	1.92
$A_s$ 10 <sup>-3</sup> ft. <sup>2</sup>	2.62	6.23	3.78	9.05	19.6
$h$ Eng. units	418	188	372	186	104
$Nu$	7.61	4.69	5.67	3.79	3.19
$Re$	67.1	27.6	48.2	19.2	11.7
$(Re)^{1/2}(Pr)^{1/3}$	7.36	4.73	6.22	3.94	3.06
$Nu'$	6.51	4.03	4.85	3.30	2.74
$(Re)^{1/2}(Sc)^{1/3}$	7.10	4.56	6.00	3.80	2.95

TABLE XXXIV

## RUNS NO. 15 AND 16 - TABLE OF RESULTS

	Pressure Nozzle (1/4) LNN SS No. 1				
	Run No. 15			Run No. 16	
	Section 1	Section 2	Section 3	Section 1	Section 2
$w_{d1}$ lb./hr.	9.30	13.60	15.50	12.8	12.9
$H_{d1}$ lb.H <sub>2</sub> O/lb.air	0.0130	0.0130	0.0130	0.0160	0.0160
$t_{d1}$ °F.	199	205	208	152	144
$w_{d2}$ lb./hr.	10.8	13.8	16.0	12.9	13.3
$w_{d2}$ (cor.)lb./hr.	10.1	13.1	15.5	12.7	13.0
$H_{d2}$ lb.H <sub>2</sub> O/lb.air	0.0165	0.0206	0.0218	0.0180	0.0196
$t_{d2}$ °F.	126	136	145	102	106
$t_{av}$ °F.	162.5	170.5	176.5	127	125
$T_s$ °F. ( $T_L=90;88^\circ\text{F.}$ )	97	102	105	95	100
$\Delta T$ °F.	65.5	68.5	71.5	32	25
$W$ lb./hr.	4.99	4.93	4.81	5.00	4.96
$Q$ B.t.u./hr.	73	130	160	61	76
$E_f$ %	1.4	2.4	3.0	1.1	1.4
$d_{vs}$ microns	92	103	148	65	84
$V_D$ ft./sec.	43	11	4.5	32	9
$V_R$ ft./sec.	43	11	4.5	32	9
$S_w$ 10 <sup>2</sup> ft. <sup>2</sup> /lb.	3.20	2.85	1.98	4.53	3.50
$A_s$ 10 <sup>-3</sup> ft. <sup>2</sup>	2.57	8.91	19.8	4.95	13.5
$h$ Eng. units	435	213	113	386	226
$Nu$	8.90	4.47	3.36	5.17	3.89
$Re$	67.1	19.3	11.3	38.5	13.7
$(Re)^{1/2}(Pr)^{1/3}$	7.32	3.94	3.02	5.57	3.32
$Nu^*$	7.65	3.84	2.89	4.40	3.31
$(Re)^{1/2}(Sc)^{1/3}$	6.99	3.76	2.88	5.35	3.28

TABLE XXXV

## RUNS NO. 17 AND 18 - TABLE OF RESULTS

	Pressure Nozzle (1/4) LNN SS No. 1				
	Run No. 17			Run No. 18	
	Section 1	Section 2	Section 3	Section 1	Section 2
$w_{d1}$ lb./hr.	12.20	16.00	17.80	12.1	12.9
$H_{d1}$ lb.H <sub>2</sub> O/lb.air	0.0124	0.0124	0.0124	0.0170	0.0170
$t_{d1}$ °F.	195	208	204	158	163
$w_{d2}$ lb./hr.	12.90	16.31	18.00	12.60	14.2
$w_{d2}$ (cor.) lb./hr.	12.22	16.01	17.79	12.10	13.20
$H_{d2}$ lb.H <sub>2</sub> O/lb.air	0.0130	0.0162	0.0170	0.0180	0.0195
$t_{d2}$ °F.	124	130	145	104	105
$t_{av}$ °F.	159.5	169	174.5	131	134
$T_s$ °F. ( $T_L=80:76$ °F.)	91	97	100	82	87
$\Delta T$ °F.	69	72	74.5	49	47
$W$ lb./hr.	5.10	4.97	4.90	5.00	4.98
$Q$ B.t.u./hr.	55	95	100	43	60
$E_f$ %	1.0	1.8	1.9	0.8	1.1
$d_{vs}$ microns	102	128	161	88	104
$V_D$ ft./sec.	47	13.5	5.0	42.5	11.5
$V_R$ ft./sec.	47	13.5	5.0	42.5	11.5
$S_w$ 10 <sup>2</sup> ft. <sup>2</sup> /lb.	2.88	2.30	1.83	3.34	2.82
$A_s$ 10 <sup>-3</sup> ft. <sup>2</sup>	2.18	5.89	16.5	2.33	8.42
$h$ Eng. units	367	225	82	378	151
$Nu$	7.61	5.87	2.51	6.86	3.21
$Re$	84.1	29.4	13.3	69.6	21.6
$(Re)^{1/2}(Pr)^{1/3}$	8.22	4.87	3.28	7.48	4.17
$Nu'$	6.46	5.00	2.15	5.83	2.73
$(Re)^{1/2}(Sc)^{1/3}$	7.83	4.65	3.13	7.15	3.98

TABLE XXXVI

## RUNS NO. 19 AND 20 - TABLE OF RESULTS

	Pressure Nozzle (1/4) LNN SS No. 1			
	Run No. 19		Run No. 20	
	Section 1	Section 2	Section 1	Section 2
$w_{d1}$ lb./hr.	11.50	13.00	13.12	14.98
$H_{d1}$ lb.H <sub>2</sub> O/lb.air	0.0165	0.0165	0.0158	0.0158
$t_{d1}$ °F.	155	163	161	155
$w_{d2}$ lb./hr.	11.90	13.50	13.91	15.51
$w_{d2}$ (cor.) lb./hr.	11.50	13.02	13.10	15.00
$H_{d2}$ lb.H <sub>2</sub> O/lb.air	0.0170	0.0180	0.0178	0.0195
$t_{d2}$ °F.	100	110	106	108
$t_{av}$ °F.	127.5	136.5	133.5	131.5
$T_s$ °F. ( $T_L=80; 84$ °F.)	90	100	90	97
$\Delta T$ °F.	37.5	36.5	43.5	34.5
$W$ lb./hr.	5.01	4.99	5.00	4.95
$Q$ B.t.u./hr.	55	71	63	93
$E_f$ %	1.0	1.3	1.2	1.7
$d_{vs}$ microns	68	110	69	89
$V_D$ ft./sec.	34	12	34	10
$V_R$ ft./sec.	34	12	34	10
$S_w$ 10 <sup>2</sup> ft. <sup>2</sup> /lb.	4.32	2.68	4.26	3.31
$A_s$ 10 <sup>-3</sup> ft. <sup>2</sup>	4.48	7.75	4.34	11.4
$h$ Eng. units	327	252	333	235
$Nu$	4.54	5.62	4.68	4.26
$Re$	42.4	24.8	43.2	16.5
$(Re)^{1/2}(Pr)^{1/3}$	5.82	4.47	5.91	3.63
$Nu^*$	3.86	4.78	3.98	3.62
$(Re)^{1/2}(Sc)^{1/3}$	5.58	4.30	5.68	3.48

APPENDIX VCO-CURRENT EVAPORATION RUNSTABLE XXXVIIRUN NO. 21 - TABLE OF RESULTS

<u>Pneumatic Nozzle (1/4) JN No. 12 Low Atomizing Pressures</u>				
	<u>Section 1</u>	<u>Section 2</u>	<u>Section 3</u>	<u>Section 4</u>
$E_f$ %	10	20	35	19
W lb./hr.	1.90	1.60	1.04	0.50
$t_{av.}$ °F.	166	199	208	211
$T_s$ °F. ( $T_L=87^\circ\text{F.}$ )	101	101	101	101
$\Delta T$ °F.	65	98	107	110
Q B.t.u./hr.	240	425	730	402
$d_{vs}$ microns	16.2	18.5	20.6	22.0
$V_D$ ft./sec.	74	42	22	13
$V_R$ ft./sec.	60	35	18	9
$S_w$ $10^3$ ft. <sup>2</sup> /lb.	1.82	1.59	1.43	1.33
$A_s$ $10^{-3}$ ft. <sup>2</sup>	3.25	4.22	6.28	4.76
h Eng. units	1140	1030	1090	767
Nu	3.78	3.76	4.34	3.25
Re	16.9	12.7	6.00	3.19
$(Re)^{1/2}(Pr)^{1/3}$	3.68	3.20	2.20	1.61
Nu'	3.22	3.24	3.73	2.80
$(Re)^{1/2}(Sc)^{1/3}$	3.48	3.05	2.09	1.53

TABLE XXXVIII  
RUN NO. 22 - TABLE OF RESULTS

<u>Pneumatic Nozzle (1/4) JN No. 12 Low Atomizing Pressures</u>				
	<u>Section 1</u>	<u>Section 2</u>	<u>Section 3</u>	<u>Section 4</u>
$E_f$ %	9	16	27	20
W lb./hr.	1.91	1.66	1.23	0.73
$t_{av.}$ °F.	172	205	215	216
$T_s$ °F. ( $T_L=86^\circ\text{F.}$ )	97	97	97	97
$\Delta T$ °F.	75	108	118	119
Q B.t.u./hr.	215	340	572	424
$d_{vs}$ microns	19.7	22.0	22.9	23.1
$V_D$ ft./sec.	92	48	25	14
$V_R$ ft./sec.	78	41	21	10
$S_w$ $10^3$ ft. <sup>2</sup> /lb.	1.49	1.33	1.28	1.27
$A_s$ $10^{-3}$ ft. <sup>2</sup>	2.15	3.21	5.85	6.15
h Eng. units	1335	980	831	583
Nu	5.21	4.17	3.67	2.59
Re	26.5	14.6	7.75	3.74
$(\text{Re})^{1/2}(\text{Pr})^{1/3}$	4.63	3.44	2.51	1.74
Nu†	4.43	3.60	3.17	2.24
$(\text{Re})^{1/2}(\text{Sc})^{1/3}$	4.41	3.27	2.38	1.65

TABLE XXXIX

## RUN NO. 23 - TABLE OF RESULTS

Pneumatic Nozzle (1/4) JN No. 12 Low Atomizing Pressures				
	<u>Section 1</u>	<u>Section 2</u>	<u>Section 3</u>	<u>Section 4</u>
$E_f$ %	14	25	23	15.5
W lb./hr.	1.87	1.48	0.95	0.58
$t_{av}$ °F.	144	164	169	169
$T_s$ °F. ( $T_L=79^\circ\text{F.}$ )	93	93	93	93
$\Delta T$ °F.	51	71	76	76
Q B.t.u./hr.	325	531	491	329
$d_{vs}$ microns	14.0	16.4	19.2	20.8
$V_D$ ft./sec.	64	38	21	11
$V_R$ ft./sec.	50	31	17	7
$S_w$ $10^3$ ft. <sup>2</sup> /lb.	2.10	1.80	1.53	1.41
$A_s$ $10^{-3}$ ft. <sup>2</sup>	4.25	4.87	6.41	6.86
h Eng. units	1500	1540	1001	631
Nu	4.28	5.14	3.89	2.64
Re	12.6	9.05	5.68	2.52
$(\text{Re})^{1/2}(\text{Pr})^{1/3}$	3.19	2.70	2.14	1.43
$\text{Nu}^\dagger$	3.64	4.40	3.34	2.27
$(\text{Re})^{1/2}(\text{Sc})^{1/3}$	3.06	2.58	2.04	1.36

TABLE XL

## RUN NO. 24 - TABLE OF RESULTS

Pneumatic Nozzle (1/4) JN No. 12 Low Atomizing Pressures					
	<u>Section 1</u>	<u>Section 2</u>	<u>Section 3</u>	<u>Section 4</u>	<u>Section 5</u>
$E_f$ %	11	12	18	19	15
W lb./hr.	1.89	1.66	1.36	0.99	0.65
$t_{av.}$ °F.	132	140	142	142	141
$T_s$ °F. ( $T_L=81°F.$ )	86	86	86	86	86
$\Delta T$ °F.	46	54	56	56	55
Q B.t.u./hr.	245	255	382	403	319
$d_{vs}$ microns	15.6	18.3	20.7	22.8	23.8
$V_D$ ft./sec.	70	42	23	13	8
$V_R$ ft./sec.	56	35	19	9	4
$S_w$ $10^3$ ft. <sup>2</sup> /lb.	1.88	1.61	1.42	1.29	1.24
$A_s$ $10^{-3}$ ft. <sup>2</sup>	3.53	4.42	7.75	9.11	9.35
h Eng. units	1500	1070	882	790	621
Nu	4.81	4.00	3.75	3.69	3.04
Re	16.2	11.9	7.30	3.81	1.76
$(Re)^{1/2}(Pr)^{1/3}$	3.62	3.10	2.43	1.76	1.19
$Nu'$	4.09	3.40	3.19	3.14	2.59
$(Re)^{1/2}(Sc)^{1/3}$	3.47	2.97	2.33	1.69	1.04

TABLE XLI

## RUN NO. 25 - TABLE OF RESULTS

<u>Pneumatic Nozzle (1/4) JN No. 12 High Atomizing Pressures</u>					
	<u>Section 1</u>	<u>Section 2</u>	<u>Section 3</u>	<u>Section 4</u>	<u>Section 5</u>
$E_f$ %	8	13	18	19	14
W lb./hr.	4.23	3.76	3.04	2.14	1.54
$t_{av.}$ °F.	140	151	155	155	152
$T_s$ °F. ( $T_L=62^\circ\text{F.}$ )	90	90	90	90	90
$\Delta T$ °F.	50	61	65	65	62
Q B.t.u./hr.	493	605	839	886	652
$d_{vs}$ microns	14.0	17.2	19.0	20.5	22.0
$V_D$ ft./sec.	80	48	27	13	8
$V_R$ ft./sec.	66	39	23	9	4
$S_w$ $10^3$ ft. <sup>2</sup> /lb.	2.10	1.71	1.55	1.43	1.33
$A_s$ $10^{-3}$ ft. <sup>2</sup>	7.71	9.27	16.2	21.8	23.6
h Eng. units	1280	1070	801	625	446
Nu	3.66	3.74	3.04	2.54	2.02
Re	16.8	12.0	7.80	3.29	1.56
$(\text{Re})^{1/2}(\text{Pr})^{1/3}$	3.68	3.12	2.51	1.63	1.11
$\text{Nu}^*$	3.12	3.18	2.59	2.16	1.33
$(\text{Re})^{1/2}(\text{Sc})^{1/3}$	3.52	2.99	2.40	1.56	1.06

TABLE XLII  
RUN NO. 26 - TABLE OF RESULTS

<u>Pneumatic Nozzle (1/4) JN No. 12 High Atomizing Pressures</u>					
	<u>Section 1</u>	<u>Section 2</u>	<u>Section 3</u>	<u>Section 4</u>	<u>Section 5</u>
$E_f$ %	12	20	26	16	11
W lb./hr.	4.14	3.52	2.41	1.45	0.97
$t_{av}$ °F.	160	180	184	181	175
$T_s$ °F. ( $T_L=63$ °F.)	86	86	86	86	86
$\Delta T$ °F.	74	94	98	95	89
Q B.t.u./hr.	660	936	1210	746	512
$d_{vs}$ microns	14.1	16.6	18.9	21.0	23.0
$V_D$ ft./sec.	80	48	27	14	8.5
$V_R$ ft./sec.	66	39	23	10	4.5
$S_w$ $10^3$ ft. <sup>2</sup> /lb.	2.08	1.77	1.55	1.40	1.28
$A_s$ $10^{-3}$ ft. <sup>2</sup>	7.46	8.99	12.8	13.4	13.5
h Eng. units	1195	1110	967	561	427
Nu	3.44	3.67	3.64	2.35	1.98
Re	16.6	11.2	7.49	3.63	1.81
$(Re)^{1/2}(Pr)^{1/3}$	3.67	3.01	2.46	1.71	1.21
Nu*	2.93	3.14	3.12	2.01	1.69
$(Re)^{1/2}(Sc)^{1/3}$	3.51	2.88	2.35	1.63	1.16

TABLE XLIII

## RUN NO. 27 - TABLE OF RESULTS

Pneumatic Nozzle (1/4) JN No. 12 High Atomizing Pressures					
	<u>Section 1</u>	<u>Section 2</u>	<u>Section 3</u>	<u>Section 4</u>	<u>Section 5</u>
$E_f$ %	7	11	17	20	17
W lb./hr.	4.25	3.86	3.28	2.42	1.61
$t_{av}$ °F.	130	140	144	147	145
$T_s$ °F. ( $T_L=65^\circ\text{F.}$ )	92	92	92	92	92
$\Delta T$ °F.	38	48	52	55	53
Q B.t.u./hr.	426	512	790	928	791
$d_{vs}$ microns	14.6	15.9	17.9	22.0	21.6
$V_D$ ft./sec.	83	45	25	14.5	7
$V_R$ ft./sec.	69	36	21	10.5	3
$S_w$ $10^3$ ft. <sup>2</sup> /lb.	2.01	1.85	1.64	1.34	1.36
$A_s$ $10^{-3}$ ft. <sup>2</sup>	7.19	11.0	19.9	20.7	29.0
h Eng. units	1560	970	764	815	515
Nu	4.68	3.14	2.78	3.64	2.28
Re	18.7	10.4	6.85	4.15	1.18
$(\text{Re})^{1/2}(\text{Pr})^{1/3}$	3.89	2.90	2.45	1.83	0.98
$\text{Nu}^\dagger$	3.98	2.68	2.37	3.11	1.95
$(\text{Re})^{1/2}(\text{Sc})^{1/3}$	3.73	2.78	2.35	1.75	0.93

TABLE XLIV

RUN NO. 28 - TABLE OF RESULTS

<u>Pneumatic Nozzle (1/4) JN No. 12 High Atomizing Pressures</u>					
	<u>Section 1</u>	<u>Section 2</u>	<u>Section 3</u>	<u>Section 4</u>	<u>Section 5</u>
$E_f$ %	8	15	29	20	14
W lb./hr.	4.23	3.88	2.75	1.66	0.93
$t_{av.}$ °F.	129	147	163	162	161
$T_s$ °F. ( $T_L=68^\circ\text{F.}$ )	91	91	91	91	91
$\Delta T$ °F.	38	56	72	71	70
Q B.t.u./hr.	472	698	1346	931	649
$d_{vs}$ microns	14.4	16.8	18.6	20.2	22.3
$V_D$ ft./sec.	82	47	26	13	8
$V_R$ ft./sec.	68	38	22	9	4
$S_w$ $10^3$ ft. <sup>2</sup> /lb.	2.04	1.75	1.58	1.46	1.32
$A_s$ $10^{-3}$ ft. <sup>2</sup>	7.31	10.03	15.5	17.5	14.2
h Eng. units	1701	1242	1204	752	653
Nu	5.05	4.23	4.53	3.07	2.92
Re	18.1	11.4	7.15	3.15	1.74
$(\text{Re})^{1/2}(\text{Pr})^{1/3}$	3.82	3.03	2.40	1.59	1.19
$\text{Nu}'$	4.30	3.59	3.88	2.62	1.49
$(\text{Re})^{1/2}(\text{Sc})^{1/3}$	3.63	2.91	2.30	1.52	1.14

TABLE XLV  
RUN NO. 29 - TABLE OF RESULTS

<u>Pneumatic Nozzle (1/4) JN No. 12 High Atomizing Pressures</u>					
	<u>Section 1</u>	<u>Section 2</u>	<u>Section 3</u>	<u>Section 4</u>	<u>Section 5</u>
$E_f$ %	13	20	25	15	10
W lb./hr.	4.12	3.38	2.40	1.52	0.97
$t_{av.}$ °F.	149	162	174	168	163
$T_s$ °F. ( $T_L=75^\circ\text{F.}$ )	92	92	92	92	92
$\Delta T$ °F.	57	70	82	76	71
Q B.t.u./hr.	680	928	1162	698	468
$d_{vs}$ microns	13.5	16.2	19.2	21.8	23.0
$V_D$ ft./sec.	77	46	28	14	9
$V_R$ ft./sec.	63	37	24	10	5
$S_w$ $10^3$ ft. <sup>2</sup>	2.18	1.81	1.53	1.35	1.28
$A_s$ $10^{-3}$ ft. <sup>2</sup>	8.20	9.25	12.1	13.6	10.5
h Eng. units	1455	1433	1172	677	628
Nu	4.00	4.76	4.51	2.95	2.92
Re	15.2	10.5	7.95	3.76	1.99
$(\text{Re})^{1/2}(\text{Pr})^{1/3}$	3.51	2.91	2.54	1.74	1.27
$\text{Nu}^\dagger$	3.40	4.06	3.86	2.52	2.50
$(\text{Re})^{1/2}(\text{Sc})^{1/3}$	3.36	2.81	2.44	1.67	1.22

TABLE XLVI  
RUN NO. 30 - TABLE OF RESULTS

<u>Pneumatic Nozzle (1/4) JN No. 12 High Atomizing Pressures</u>					
	<u>Section 1</u>	<u>Section 2</u>	<u>Section 3</u>	<u>Section 4</u>	<u>Section 5</u>
$E_f$ %	13	21	27	15	11
W lb./hr.	4.15	3.36	2.33	1.38	0.84
$t_{av.}$ °F.	136	148	159	157	155
$T_s$ °F. ( $T_L=63^\circ\text{F.}$ )	86	86	86	86	86
$\Delta T$ °F.	50	62	73	71	69
Q B.t.u./hr.	700	970	1250	693	512
$d_{vs}$ microns	12.3	15.0	18.1	20.1	21.1
$V_D$ ft./sec.	70	43	25	13	7.5
$V_R$ ft./sec.	56	34	21	9	3.5
$S_w$ $10^3$ ft. <sup>2</sup> /lb.	2.39	1.96	1.62	1.46	1.39
$A_s$ $10^{-3}$ ft. <sup>2</sup>	9.88	10.6	14.0	14.3	14.4
h Eng. units	1422	1480	1222	683	515
Nu	3.62	4.58	4.53	2.80	2.22
Re	12.7	9.21	6.75	2.34	1.32
$(Re)^{1/2}(Pr)^{1/3}$	3.21	2.72	2.34	1.37	1.03
Nu'	3.08	3.90	3.86	2.38	1.89
$(Re)^{1/2}(Sc)^{1/3}$	3.08	2.61	2.24	1.31	.97

TABLE XLVII

## RUN NO. 31 - TABLE OF RESULTS

Pneumatic Nozzle (1/4) JN No. 22B				
	<u>Section 1</u>	<u>Section 2</u>	<u>Section 3</u>	<u>Section 4</u>
$E_f$ %	8	10	14	13
W lb./hr.	5.76	5.22	4.30	3.76
$t_{av.}$ °F.	136	141	150	153
$T_s$ °F. ( $T_L=81^\circ\text{F.}$ )	87	87	87	87
$\Delta T$ °F.	49	54	63	66
Q B.t.u./hr.	603	636	890	826
$d_{vs}$ microns	16.5	21	25	27
$V_D$ ft./sec.	54	30	22	15
$V_R$ ft./sec.	30	16	10	6
$S_w$ $10^3$ ft. <sup>2</sup> /lb.	1.78	1.40	1.18	1.09
$A_s$ $10^{-3}$ ft. <sup>2</sup>	13.1	16.8	22.4	25.2
h Eng. units	940	700	632	500
Nu	3.24	3.03	3.24	2.75
Re	9.18	6.23	4.60	2.91
$(\text{Re})^{1/2}(\text{Pr})^{1/3}$	2.81	2.25	1.91	1.53
$\text{Nu}'$	2.76	2.58	2.76	2.34
$(\text{Re})^{1/2}(\text{Sc})^{1/3}$	2.69	2.16	1.83	1.47

TABLE XLVIII

## RUN NO. 32 - TABLE OF RESULTS

Pneumatic Nozzle (1/4) JN No. 22B				
	<u>Section 1</u>	<u>Section 2</u>	<u>Section 3</u>	<u>Section 4</u>
$E_f$ %	7	9	11	16
W lb./hr.	5.76	5.32	4.70	3.88
$t_{av.}$ °F.	123	146	159	164
$T_s$ °F. ( $T_L = 65^\circ\text{F.}$ )	81	81	81	81
$\Delta T$ °F.	42	65	78	83
Q B.t.u./hr.	546	572	701	101
$d_{vs}$ microns	18	24.5	26.8	27.4
$V_D$ ft./sec.	58	34	23	15
$V_R$ ft./sec.	34	20	11	6
$S_w$ $10^3$ ft. <sup>2</sup> /lb.	1.63	1.20	1.09	1.07
$A_s$ $10^{-3}$ ft. <sup>2</sup>	11.2	13.0	20.6	25.6
h Eng. units	1160	677	438	476
Nu	4.34	3.36	2.38	2.64
Re	11.85	9.08	5.25	2.94
$(\text{Re})^{1/2}(\text{Pr})^{1/3}$	3.08	2.71	2.06	1.54
$\text{Nu}'$	3.68	2.85	2.02	2.25
$(\text{Re})^{1/2}(\text{Sc})^{1/3}$	2.96	2.60	1.97	1.47

TABLE XLIX

## RUN NO. 33 - TABLE OF RESULTS

Pneumatic Nozzle (1/4) JN No. 22B				
	<u>Section 1</u>	<u>Section 2</u>	<u>Section 3</u>	<u>Section 4</u>
$E_f$ %	8	10	16	16
W lb./hr.	5.76	5.23	4.46	3.48
$t_{av.}$ °F.	135	145	155	149
$T_s$ °F. ( $T_L=62^\circ\text{F.}$ )	82	82	82	82
$\Delta T$ °F.	53	63	73	67
Q B.t.u./hr.	624	636	1022	1022
$d_{vs}$ microns	19.0	26.1	27.7	28.8
$V_D$ ft./sec.	60	35	24	16
$V_R$ ft./sec.	36	21	12	7
$S_w$ $10^3$ ft. <sup>2</sup> /lb.	1.55	1.12	1.06	1.02
$A_s$ $10^{-3}$ ft. <sup>2</sup>	10.3	11.6	18.2	20.5
h Eng. units	1140	816	771	743
Nu	4.51	4.34	4.40	4.32
Re	13.2	10.3	6.03	3.81
$(\text{Re})^{1/2}(\text{Pr})^{1/3}$	3.24	2.89	2.21	1.76
$\text{Nu}^*$	3.82	3.68	3.74	3.67
$(\text{Re})^{1/2}(\text{Sc})^{1/3}$	3.11	2.77	2.12	1.69

TABLE L  
RUN NO. 34 - TABLE OF RESULTS

Pneumatic Nozzle (1/4) JN No. 22B				
	<u>Section 1</u>	<u>Section 2</u>	<u>Section 3</u>	<u>Section 4</u>
$E_f$ %	7	9	12	12
W lb./hr.	5.79	5.32	4.68	3.36
$t_{av.}$ °F.	129	139	146	144
$T_s$ °F. ( $T_L=65^\circ\text{F.}$ )	83	83	83	83
$\Delta T$ °F.	46	56	63	61
Q B.t.u./hr.	555	574	764	764
$d_{vs}$ microns	17.5	24.2	25.1	25.3
$V_D$ ft./sec.	56	34	22	14
$V_R$ ft./sec.	32	20	10	5
$S_w$ $10^3$ ft. <sup>2</sup> /lb.	1.68	1.21	1.17	1.16
$A_s$ $10^{-3}$ ft. <sup>2</sup>	12.1	13.1	23.1	25.7
h Eng. units	1000	782	529	488
Nu	3.60	3.88	2.71	2.59
Re	10.3	8.80	4.58	2.30
$(\text{Re})^{1/2}(\text{Pr})^{1/3}$	2.89	2.67	1.93	1.36
$\text{Nu}'$	3.06	3.30	2.31	2.20
$(\text{Re})^{1/2}(\text{Sc})^{1/3}$	2.77	2.56	1.85	1.30

TABLE LI

## RUN NO. 35 - TABLE OF RESULTS

<u>Pressure Nozzle (1/4) LN No. 1</u>				
	<u>Section 1</u>	<u>Section 2</u>	<u>Section 3</u>	<u>Section 4</u>
$E_f$ %	4.0	5.0	8.0	10
W lb./hr.	11.8	11.2	10.5	9.4
$t_{av.}$ °F.	225	239	251	241
$T_s$ °F. ( $T_L=101^\circ\text{F.}$ )	113	113	113	113
$\Delta T$ °F.	112	126	138	128
Q B.t.u./hr.	625	626	1020	1270
$d_{vs}$ microns	59.3	66.1	69.1	72.6
$V_D$ ft./sec.	43	27.5	14	12
$V_R$ ft./sec.	33	17.5	4	2
$S_w$ $10^2$ ft. <sup>2</sup> /lb.	4.96	4.45	4.26	4.06
$A_s$ $10^{-3}$ ft. <sup>2</sup>	9.44	12.6	29.6	30.7
h Eng. units	593	393	250	323
Nu	6.61	4.83	3.18	4.35
Re	30.6	17.8	4.26	2.23
$(\text{Re})^{1/2}(\text{Pr})^{1/3}$	5.00	3.79	1.85	1.34
$\text{Nu}'$	5.72	4.18	2.76	3.77
$(\text{Re})^{1/2}(\text{Sc})^{1/3}$	4.75	3.60	1.76	1.27

TABLE LII

## RUN NO. 36 - TABLE OF RESULTS

Pressure Nozzle (1/4) LN No. 1				
	Section 1	Section 2	Section 3	Section 4
$E_f$ %	1.8	2.0	2.2	3.0
W lb./hr.	11.9	11.7	11.4	11.1
$t_{av}$ °F.	129	140	145	145
$T_s$ °F. ( $T_L=85^\circ\text{F.}$ )	89	89	89	89
$\Delta T$ °F.	46	51	56	56
Q B.t.u./hr.	258	252	278	380
$d_{vs}$ microns	55.9	61.4	69.1	75.8
$V_D$ ft./sec.	41	26	14.5	12.0
$V_R$ ft./sec.	31	16	4.5	2.0
$S_w$ $10^2$ ft. <sup>2</sup> /lb.	5.26	4.80	4.26	3.88
$A_s$ $10^{-3}$ ft. <sup>2</sup>	10.6	14.9	31.0	33.3
h Eng. units	530	332	160	204
Nu	6.29	4.18	2.26	3.16
Re	31.9	17.8	5.63	2.75
$(\text{Re})^{1/2}(\text{Pr})^{1/3}$	5.08	3.79	2.13	1.49
$\text{Nu}'$	5.34	3.56	1.91	2.69
$(\text{Re})^{1/2}(\text{Sc})^{1/3}$	4.86	3.62	2.04	1.43

TABLE LIII

## RUN NO. 37 - TABLE OF RESULTS

Pressure Nozzle (1/4) LN No. 1				
	Section 1	Section 2	Section 3	Section 4
$E_f$ %	3.5	5.0	8.5	9.0
W lb./hr.	11.8	11.3	10.5	9.2
$t_{av.}$ °F.	213	227	235	238
$T_s$ °F. ( $T_L=98^\circ\text{F.}$ )	109	109	109	109
$\Delta T$ °F.	104	118	126	129
Q B.t.u./hr.	581	626	1080	1145
$d_{vs}$ microns	53.4	58.8	65.1	69.1
$V_D$ ft./sec.	40.5	26.0	14.0	11.7
$V_R$ ft./sec.	30.5	16.0	4.0	1.7
$S_w$ $10^2$ ft. <sup>2</sup> /lb.	5.50	5.01	4.52	4.25
$A_s$ $10^{-3}$ ft. <sup>2</sup>	11.1	15.2	31.4	31.2
h Eng. units	505	349	273	254
Nu	5.16	3.94	3.34	3.29
Re	26.6	14.7	4.05	1.83
$(\text{Re})^{1/2}(\text{Pr})^{1/3}$	4.64	3.45	1.81	1.21
$\text{Nu}^\dagger$	4.45	3.39	2.89	2.84
$(\text{Re})^{1/2}(\text{Sc})^{1/3}$	4.41	3.28	1.72	1.15

TABLE LIV  
RUN NO. 38 - TABLE OF RESULTS

<u>Pressure Nozzle (1/4) LN No. 1</u>				
	<u>Section 1</u>	<u>Section 2</u>	<u>Section 3</u>	<u>Section 4</u>
$E_f$ %	2.0	2.2	3.0	3.5
W lb./hr.	11.9	11.6	11.3	10.9
$t_{av.}$ °F.	164	176	173	171
$T_s$ °F ( $T_L=89°F.$ )	93	93	93	93
$\Delta T$ °F.	71	83	80	78
Q B.t.u./hr.	274	279	382	446
$d_{vs}$ microns	68.0	73.2	78.3	81.7
$V_D$ ft./sec.	49	29.5	15	12.1
$V_R$ ft./sec.	39	19.5	5	2.1
$S_w$ $10^2$ ft. <sup>2</sup> /lb.	4.32	4.02	3.76	3.60
$A_s$ $10^{-3}$ ft. <sup>2</sup>	7.3	10.9	26.3	30.0
h Eng. units	528	309	183	191
Nu	7.18	4.46	2.84	3.10
Re	47.1	24.4	6.76	2.95
$(Re)^{1/2}(Pr)^{1/3}$	6.17	4.42	2.34	1.54
Nu*	6.16	3.83	2.44	2.66
$(Re)^{1/2}(Sc)^{1/3}$	5.90	4.22	2.23	1.47

TABLE LV  
RUN NO. 39 - TABLE OF RESULTS

Pressure Nozzle (1/4) LN No.1					
	<u>Flashing</u>	<u>Section 1</u>	<u>Section 2</u>	<u>Section 3</u>	<u>Section 4</u>
$q_L$	12.00	-	-	-	-
$E_f$ %	16.00	8.0	11	10	7
W lb./hr.	-	9.35	8.61	7.40	6.61
$t_{av}$ °F.	-	244	246	240	225
$T_s$ °F. ( $T_L$ 250°F.)	-	115	115	115	115
$\Delta T$ °F.	-	129	131	125	110
Q B.t.u./hr.	-	1020	1406	1265	888
$d_{vs}$ microns	-	40.4	48.7	54.3	57.4
$V_D$ ft./sec.	-	35	17	13	11
$V_R$ ft./sec.	-	25	7	3	1
$S_w$ $10^2$ ft. <sup>2</sup> /lb.	-	7.28	6.06	5.41	5.15
$A_s$ $10^{-3}$ ft. <sup>2</sup>	-	13.4	21.2	28.5	29.0
h Eng. units	-	591	501	358	276
Nu	-	4.42	4.62	3.60	2.90
Re	-	15.2	5.31	2.55	0.89
$(Re)^{1/2}(Pr)^{1/3}$	-	3.51	2.08	1.46	0.85
Nu*	-	3.82	3.96	3.11	2.50
$(Re)^{1/2}(Sc)^{1/3}$	-	3.36	1.99	1.40	0.81

TABLE LVI  
EFFECT OF FEED TEMPERATURE ON EVAPORATION

Pressure Nozzle (1/4) JN No. 1						
Run Number	Feed Temperature °F.	Spray Evaporation - %				
		x = 0.5 in.	x = 4.5 in.	x = 8.5 in.	x = 12.5 in.	x = 16.5 in.
40	78	1.5	2.5	6.0	9.0	16.0
41	149	8.0	11.0	16.0	18.0	-
42	163	11.0	15.0	19.5	24.5	28.0
43	210	14.5	21.0	28.0	30.0	35.0

APPENDIX VIRESULTS OF INCREMENTAL DROP SIZE ANALYSISTABLE LVIISAMPLE CALCULATION FOR RUN NO. 6 SECTION 3

<u>Pneumatic Nozzle (1/4) JN No. 12 Low Atomizing Pressures</u>						
$d_i$ microns	8.9	14.9	20.8	26.8	32.7	38.6
$n_i$	34	48	51	33	22	8
$m_i 10^{-12}$ lb.	0.832	3.82	10.6	22.5	41.0	66.5
$n_i m_i 10^{-12}$ lb.	28	183	542	742	901	532
Wt. % of spray	0.96	6.28	18.5	25.3	30.7	18.1
$V_{Di}$ ft./sec.	7	14	23	32	40	48
$V_{Ri}$ ft./sec.	7	14	23	32	40	48
Re	1.14	3.80	8.72	15.6	23.9	33.6
$(Re)^{1/2} (Pr)^{1/3}$	0.96	1.75	2.65	3.56	4.39	5.21
Nu	2.57	3.05	3.59	4.13	4.63	5.14
$h_i$ Eng. units	1480	1071	890	798	720	690
$A_i 10^{-9}$ ft. <sup>2</sup>	2.69	7.55	14.7	24.0	36.1	51.0
$\Delta\theta_i 10^{-3}$ sec.	47.6	23.7	14.5	10.4	8.32	6.95
$Q_i 10^{-10}$ B.t.u.	21.5	21.6	21.4	22.2	24.0	27.4
$E_{fi}$ %	100	53.0	19.2	9.30	5.50	3.88

TABLE LVIII  
RESULTS FOR CROSS-CURRENT RUNS

Pneumatic Nozzle (1/4) JN No. 12 Low Atomizing Pressures  
Pressure Nozzle (1/4) LNSS No. 1

<u>Run Number</u>	<u>Section</u>	<u>Spray Evaporation - %</u>	
		<u>Calculated</u>	<u>Experimental</u>
6	1	10.4	6.2
	2	9.7	5.8
	3	10.6	8.6
	4	14.2	10.9
7	1	5.9	7.1
	2	10.3	6.5
	3	12.6	7.6
	4	12.9	8.8
8	1	8.1	8.7
	2	10.7	8.5
	3	10.8	11.5
	4	13.7	14.0
9	1	12.1	9.7
	2	13.2	10.3
	3	15.1	11.8
	4	18.0	13.8
14	1	1.3	1.5
	2	1.8	1.9
	3	2.0	2.4

TABLE LIX  
RESULTS FOR CO-CURRENT RUNS

Pneumatic Nozzle (1/4) JN No. 12 Low Atomizing Pressures

Pneumatic Nozzle (1/4) JN No. 12 High Atomizing Pressures

Run Number	Section	Spray Evaporation - %	
		Calculated	Experimental
22	1	-	9
	2	19.3	16
	3	24.2	27
	4	23.9	20
24	1	-	11
	2	15.2	12
	3	22.1	18
	4	18.6	19
	5	16.1	15
27	1	-	7
	2	15.9	11
	3	24.6	17
	4	21.1	20
	5	21.0	17
29	1	-	13
	2	21.2	20
	3	21.9	25
	4	22.0	15
	5	12.1	10